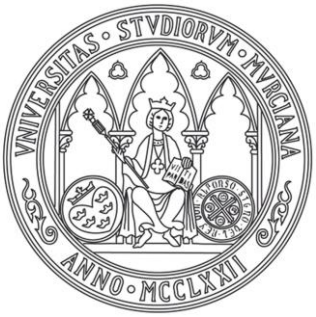

UNIVERSIDAD DE MURCIA

ESCUELA INTERNACIONAL DE DOCTORADO

Escherichia coli acetate metabolism: characterization and regulation

Metabolismo del acetato en *Escherichia coli*: caracterización y regulación

Julia Gallego Jara

2018

UNIVERSIDAD DE MURCIA

Facultad de Química

Departamento de Bioquímica y Biología Molecular B e Inmunología

Metabolismo del acetato en *Escherichia coli*: caracterización y regulación

TESIS DOCTORAL

Julia Gallego Jara

DIRECTORES

Dra. Teresa de Diego Puente Dr. Manuel Cánovas Díaz

Murcia, 2018

During her PhD, Julia Gallego Jara has been recipient of a research training fellowship (FPI Fundación Séneca) and a fellowship for her short stay in Bologna (Fundación Séneca Short Stay Fellowship).

This Thesis has been funded by the projects MCYT BIO2008-04500-C02-01, MICINN BIO2014-54411-C2-1-R and Fundación Séneca-CARM 19236/PI/14.

Acknowledgements

A mis directores de tesis, Teresa de Diego Puente y Manuel Cánovas Díaz, gracias por la ayuda y el apoyo prestados.

Manolo, gracias por acogerme para realizar esta tesis.

Teresa, muchas gracias por haber realizado conmigo cada uno de los pasos de esta tesis, por haberme ayudado siempre y por haberte convertido en mucho más que una directora de tesis.

Arturo, gracias por estar siempre que te necesité.

Ana, gracias por todo; por ayudarme, por escucharme, y por apoyarme siempre. No puedo imaginar cómo hubieran sido estos años sin ti cada día. Gracias por ser la mejor compañera que alguien puede tener.

A todas las personas que han pasado por el laboratorio durante todos estos años. Gracias a Vicente y Sara por ayudarme en mis comienzos. Gracias a José María por escucharme siempre que lo necesité. Gracias a Álvaro, Laura, Sergio, Johana, Yolanda, Ester, Rosalba, María, David, Juana Mari, Celia, Susana, Elena…por hacer del laboratorio un lugar mejor para trabajar. Y por supuesto a Gema, gracias por habernos ayudado tanto. Nuestra etapa final ha sido mucho más fácil gracias a ti.

A mis amigos y a todas las personas que me quieren, gracias por quererme tan bien.

Y sobre todo a mi familia. Gracias mamá, gracias papá y gracias Juan María. Gracias por estar conmigo siempre.

During her PhD, Julia Gallego Jara has contributed to the following publications and congress presentations:

- Bernal V, Castaño-Cerezo S, Gallego-Jara J, Écija-Conesa A, de Diego T, Iborra JL, et al. Regulation of bacterial physiology by lysine acetylation of proteins. N Biotechnol. 2014;31: 586–95. doi:10.1016/j.nbt.2014.03.002

- de Diego T, Gallego-Jara J, Castaño-Cerezo S, Bernal Sánchez V, Fernández Espín V, García de la Torre J, et al. The protein acetyltransferase PatZ from *Escherichia coli* is regulated by autoacetylation-induced oligomerization. J Biol Chem. 2015; 38: 23077–23093 doi: 10.1074/jbc.M115.649806

- Gallego-Jara J, de Diego T, del Real A, Écija-Conesa A, Manjón A., Cánovas M. Lycopene overproduction and *in situ* extraction in organic-aqueous culture systems using a metabolically engineered *Escherichia coli*. AMB Express. 2015; 65. doi: 10.1186/s13568-015-0150-3

-Davis R, Écija-Conesa A, Gallego-Jara J, de Diego T, Filippova E. V, Kuffel G, et al. An acetylatable lysine controls CRP function in *E. coli*. Mol Microbiol. 2017; 107:116-131. doi:10.1111/mmi.13874

-Gallego-Jara J, Écija-Conesa A, de Diego Puente T, Lozano Terol G, Cánovas Díaz M. Characterization of CobB kinetics and inhibition by nicotinamide. PLoS ONE. 2017; 12: e0189689. doi: org/10.1371/journal.pone.0189689

- Gallego-Jara J, Écija-Conesa A, Lozano Terol G, Cánovas Díaz M, de Diego Puente T. Characterization of acetyl-CoA synthetase kinetics and ATP-binding. *Under preparation*.

- Gallego-Jara* J, Écija-Conesa A*, Lozano Terol G, Cánovas Díaz M, de Diego Puente T. Influence of carbon and nitrogen source on acetate metabolism in *E. coli*. *Under preparation*.

- Castaño-Cerezo S, Bernal V, Gallego J, Écija A, Sanchez-Diaz NC, Iborra J.L, et al. Biotecnología de sistemas para la mejora de bioprocesos relacionados con el metabolismo central de *E. coli*: Integración de la regulación transcripcional y post-traduccional (Oral presentation). 2nd Applied Synthetic Biology in Europe. 25th-27th November 2013, Málaga (Spain).

- Gallego J, de Diego T, del Real A, Manjón A, Cánovas M. Overproduction by *E. coli* and *in situ* extraction of lycopene in organic-aqueous systems (Poster). “ANQUE-ICCE-BIOTECH”. 1st-4th July 2014, Madrid (Spain).

- Castaño-Cerezo S, Bernal V, Gallejo J, Ecija A, de Diego T, Manjón A, Cánovas M. Synthetic Biology and Metabolic Engineering of post-translational regulation mechanisms of central metabolism in *E. coli*: New biocatalysts are foreseen. (Oral presentation). V Congreso de Microbiología Industrial y Biotecnología Microbiana. 15-17 Octubre 2014, Oviedo (España).

-Núñez Martín N, Gallego-Jara J, Cánovas Díaz M, Torres N. Optimization of the *E. coli* biosynthesis of lycopene through mathematical modelling (Poster). XXXVII Congreso de la Sociedad Española de Bioquímica y Biología Molecular. 9-12 Septiembre 2014, Granada (España).

-Gallego J, Écija A, Castaño-Cerezo S, Bernal V, de Diego T, Manjón A, e al. Post-translational modifications by N-lysine acetylation: its impact on enzyme activity and transcription factors function in *Escherichia coli* (Poster). 8th Conference on Recombinant Protein Production. 22th-24th April 2015, Palma de Mallorca (Spain).

- Gallego-Jara J, de Diego T, Fernández Espín V, García de la Torre J, Manjón A, Cánovas Díaz M. Characterization of PatZ from *Escherichia coli*, a multimeric protein regulated by auto-acetylation (Oral presentation). I Jornadas doctorales de la Universidad de Murcia. 28-29 Abril 2015, Murcia (España).

-Gallego-Jara J, de Diego T, Écija A, Manjón A and Cánovas M. Kinetic study of the *Escherichia coli* sirtuin enzyme CobB (Oral presentation). II Jornadas doctorales de la Universidad de Murcia. 31 Mayo-2 Junio 2016, Murcia (España).

-Écija Conesa A, Gallego-Jara J, De Diego T, Manjón A and Cánovas M. Structural analysis with DSC and fluorescence in different mutants in lysine 101 of Catabolite Regulator Protein from *Escherichia coli* (Oral presentation). II Jornadas doctorales de la Universidad de Murcia. 31 Mayo-2 Junio 2016, Murcia (España).

- Gallego-Jara. J, Écija Conesa A, De Diego T, Manjón A and Cánovas M. Biochemical and biophysical PatZ characterization (Oral presentation). Bioiberoamérica 2016. 5-8 Junio 2016, Salamanca (España).

-Gallego-Jara. J, Écija Conesa A, De Diego T, Manjón A and Cánovas M. Lycopene production from a continuous aqueous-organic recombinant *Escherichia coli* system (Oral presentation). Bioiberoamérica 2016. 5-8 Junio 2016, Salamanca (España).

-Écija Conesa A, Gallego Jara J, de Diego Puente T, Manjón Rubio A and Cánovas Díaz M. Estudios estructurales del papel de la acetilación de la lisina 101 de la Proteína Reguladora de Catabolito (CRP) de *Escherichia coli*. (Oral presentation). Bioiberoamérica 2016. 5-8 Junio 2016, Salamanca (España).

-Gallego-Jara J, de Diego T, Écija A, Manjón A and Cánovas M. Characterization of the CobB sirtuin acyl-CoA synthase deacetylation in *Escherichia coli* (Oral presentation). III Jornadas doctorales de la Universidad de Murcia. 30 Mayo-1 Junio 2017, Murcia (España).

-Écija Conesa A., Gallego-Jara. J, De Diego T., Manjón A. and Cánovas M. *In vivo* assays lead an acetylable lysine controling CRP function (Oral presentation). III Jornadas doctorales de la Universidad de Murcia. 30 Mayo-1 Junio 2017, Murcia (España).

-Gallego-Jara J, de Diego T, Écija A, Manjón A and Cánovas M. *Escherichia coli* acetylated acetyl-CoA synthetase kinetic characterization (Oral presentation). Biotec 2017. 18-21 Junio 2017, Murcia (España).

-Écija-Conesa A, Gallego-Jara J, De Diego T, Manjón A and Cánovas M. Catabolite Regulator Protein (CRP) acetylation influences in global metabolism of *Escherichia coli* (Oral presentation). Biotec 2017. 18-21 Junio 2017, Murcia (España).

-Lozano-Terol G, Gallego-Jara J, Écija-Conesa A, de Diego T and Cánovas M. PaaK *Escherichia coli* characterization: Insights in the degradation pathway of phenylacetic acid (Oral presentation). Biotec 2017. 18-21 Junio 2017, Murcia (España).

-Lozano-Terol G, Gallego-Jara J, Écija-Conesa A, de Diego T, Manjón A and Cánovas M. Phenylacetic acid metabolism in *E. coli* as a xenobiotic model degradation (Oral presentation). 10th World Congress of Chemical Engineering. 1st-4th October 2017, Barcelona (España).

-Álvarez Vásquez F, González-Alcón C, Gallego-Jara J, Ecija-Conesa A, de Diego T, Cánovas M, et al. Model based optimization of the lycopene biosynthesis in *E. coli* (Poster). 10th World Congress of Chemical Engineering. 1-4 Octubre 2017, Barcelona (España).

Resumen

Escherichia coli (*E.coli*) es una bacteria Gram-negativa que posee una serie de características que la han convertido en el principal modelo procariota en biología y biotecnología. Algunas de estas características son su alta velocidad de crecimiento, su elevada disponibilidad y su facilidad para crecer en diversos medios de cultivo. Estas características, unidas al gran avance que han experimentado en las últimas décadas las técnicas de biología molecular, han hecho que muchos productos de alto interés industrial se obtengan hoy en día empleando cepas de *E. coli* modificadas genéticamente [1,2]. Los terpenos son una amplia familia de compuestos con multitud de aplicaciones farmacológicas, alimenticias o agrícolas [3]. El licopeno es un terpeno de gran interés industrial que posee diversas aplicaciones, aunque hasta el momento no se ha desarrollado un método de producción que pueda competir con la extracción a partir de tomates, la fuente natural en la que es más abundante [4–6]. A pesar de las muchas ventajas que presenta *E. coli* a nivel biotecnológico, también presenta ciertas desventajas. La principal de estas desventajas es la excreción de acetato en cultivos suplementados con glucosa como fuente de carbono. Así, cuando *E. coli* se encuentra creciendo en un medio rico en glucosa excreta al medio grandes cantidades de acetato, lo que conlleva un gasto de energía metabólica y un desperdicio de carbono que limitan el rendimiento de su producción [7,8]. Además, las altas concentraciones de acetato que se alcanzan en cultivos de alta densidad pueden limitar la velocidad de crecimiento de *E. coli*. Por estas razones, existe un gran interés en avanzar en el conocimiento del metabolismo del acetato con el fin de minimizar su excreción y optimizar los procesos biotecnológicos basados en el empleo de esta bacteria.

Por otro lado, las modificaciones post-traduccionales (MPTs), como la N-ε acetilación de lisinas, son esenciales para comprender la regulación metabólica de todos los organismos [9,10]. En *E. coli*, el metabolismo del acetato se encuentra íntimamente ligado a las MPTs por acetilación de lisinas a través de las concentraciones de acetil-CoA y acetil-fosfato [11], y de la regulación de la proteína acetil-CoA sintetasa (Acs). Así, Acs, encargada de catalizar una de las vías de reincorporación metabólica de acetato extracelular, se encuentra regulada por acetilación/desacetilación, siendo las responsables de esta regulación las enzimas PatZ, también llamada YfiQ o Pka, y CobB, principales acetiltransferasa y desacetilasa de *E. coli*, respectivamente [12,13].

El objetivo principal de esta tesis doctoral fue avanzar en el conocimiento del metabolismo del acetato de *E. coli* y en su regulación por acetilación/desacetilación de lisinas. Este objetivo principal ha sido dividido en los siguientes subobjetivos: 1) Diseñar un sistema competitivo de sobrexpresión y extracción de licopeno empleando cepas de *E. coli* modificadas

genéticamente; 2) Llevar a cabo la caracterización bioquímica y biofísica de la enzima PatZ de *E. coli*; 3) Llevar a cabo la caracterización cinética de la sirtuína CobB de *E. coli* y profundizar en el conocimiento de su inhibición por nicotinamida (NAM); 4) Avanzar en el entendimiento del mecanismo catalítico de la proteína Acs de *E. coli* y en su regulación por acetilación y 5) Estudiar la influencia de la fuente de carbono y nitrógeno sobre el metabolismo del acetato, el control del pH intracelular y la acetilación de lisinas en *E. coli*.

A continuación se resumen los principales resultados obtenidos:

En el capítulo 3 de esta tesis se ha llevado a cabo el desarrollo de un método de sobreproducción y extracción continua de licopeno con un sistema bifásico, empleando cepas de *E. coli* modificadas genéticamente. Se han optimizado las condiciones de sobrexpresión y se ha empleado octano como fase orgánica para conseguir la extracción del producto deseado con el menor daño celular, el cual ha sido evaluado mediante citometría de flujo (CF). De esta manera se ha conseguido una producción ampliamente superior a la obtenida con los métodos tradicionales. Por último, los resultados obtenidos en este capítulo corroboran el potencial de *E. coli* en el campo biotecnológico.

El capítulo 4 de esta tesis se ha centrado en la caracterización bioquímica y biofísica de la acetiltransferasa PatZ. Se ha caracterizado cinéticamente la acetilación de la proteína Acs por PatZ por primera vez, observándose una cooperatividad positiva de PatZ hacia su sustrato acetil-CoA e identificándose dieciséis lisinas acetiladas en la secuencia de Acs. Respecto a la caracterización de PatZ, se ha demostrado la autoacetilación reversible de ésta y se han identificado seis lisinas acetiladas a través de este mecanismo. La autoacetilación de PatZ provocó, además, un cambio oligomérico en su estructura, pasando de una estructura tetramérica a una octamérica. Este resultado supone la primera regulación estructural de una proteína por autoacetilación descrita hasta el momento. Finalmente, se ha propuesto un modelo estructural para la conformación tetramérica de PatZ que ha sido desarrollado empleando herramientas bioinformáticas. Este modelo ha sido validado experimentalmente comparando los parámetros estimados para el modelo, calculados con HYDROPRO, con los datos experimentales determinados a partir de la caracterización biofísica.

La sirtuína CobB, principal desacetilasa de *E.coli*, ha sido caracterizada bioquímicamente en el capítulo 5 de esta tesis doctoral. Se ha estudiado cinéticamente la desacetilación de la proteína Acs por CobB. Esta caracterización supone el primer estudio cinético de una sirtuína llevado a cabo empleando como sustrato una proteína acetilada completa en su estado nativo. Los resultados mostraron que CobB es capaz de desacetilar varias lisinas acetiladas de Acs con

una cinética monofásica. Además, se ha demostrado, en contra de lo hasta ahora considerado, que no es necesario que la lisina 609 se encuentre acetilada para que la sirtuína reconozca a Acs. Estos resultados sugieren que la estructura tridimensional proteica es el principal factor que regula la especificidad de las sirtuínas. Además, se ha estudiado la inhibición de CobB por NAM, estableciéndose un mecanismo de inhibición no competitivo. Se han medido las concentraciones de NAM intracelulares en distintos medios de cultivo y fases de crecimiento, demostrándose que las concentraciones son suficientes para regular la actividad de CobB *in vivo*. Finalmente, se ha demostrado que aspectos fisiológicos de *E. coli*, como la excreción de acetato o la expresión de flagelos, pueden estar regulados por los niveles de NAM intracelulares. Los resultados subrayan la importancia de la concentración de NAM y de la enzima nicotinamidasa (PncA) como agentes fundamentales en la regulación de CobB y, por tanto, en el control metabólico por acetilación de lisinas en *E. coli*.

El capítulo 6 de esta tesis se centra en el estudio de la etapa de adenilación del mecanismo catalítico de la proteína Acs. A partir de las estructuras cristalizadas en presencia de ATP de otras enzimas de la superfamilia de proteínas adeniladoras ANL, a la que pertenece Acs, se han construido varios modelos tridimensionales con el fin de predecir la conformación estructural de Acs en la primera etapa de su reacción catalítica. A partir de los dos modelos más robustos se seleccionaron cuatro residuos para estudiar cómo afectaba su mutación a los parámetros catalíticos y a la unión a ATP de la proteína Acs. Se llevó a cabo la caracterización cinética, respecto a los sustratos ATP y acetato, y termodinámica, respecto a la unión a ATP, de las cuatro proteínas mutantes y de la proteína Acs nativa, desacetilada y acetilada, observándose una unión endotérmica entre la proteína Acs y el sustrato ATP. Los resultados para las proteínas nativas demostraron que la acetilación no afecta a la especificidad de la enzima, pero sí a la capacidad catalítica de ésta. Además, la afinidad de las proteínas por ATP estudiada mediante calorimetría isotérmica de titulación (CIT) fue muy similar. Con respecto a las proteínas mutantes estudiadas, los resultados mostraron que la lisina 609 tiene un papel crucial en la unión de Acs a ATP, el cual se vio reflejado también en la caracterización cinética. La mutación de esta lisina llevó a una mayor afinidad de la proteína por el sustrato ATP. La lisina 609, conservada en todas las enzimas de la familia ANL, es la encargada de regular la actividad de Acs *in vivo* mediante su acetilación/desacetilación catalizada por las enzimas PatZ y CobB, respectivamente. Por lo tanto, el estudio de este residuo es fundamental para conocer cómo se regula la actividad de Acs a nivel metabólico. Por otro lado, la mutación de los residuos T264 y D500 condujo a un descenso en la especificidad por los sustratos estudiados y en la capacidad catalítica de Acs y no se observó unión a ATP en las condiciones ensayadas. Finalmente, la mutación de la lisina 270 provocó un

aumento en la capacidad catalítica, aunque la especificidad por los sustratos observada fue muy similar a la de la proteína Acs nativa, al igual que la afinidad por ATP. Los resultados de este capítulo subrayan la importancia de los residuos estudiados en el mecanismo catalítico y en la capacidad de la enzima para unir ATP. Además, suponen un punto de partida en el estudio de la lisina 609 como residuo esencial en el mecanismo catalítico y en la regulación de Acs a nivel metabólico.

En el capítulo 7 se ha estudiado la influencia del tipo de fuente de carbono y nitrógeno sobre distintos aspectos relacionados con el metabolismo del acetato en *E. coli*. Como fuentes de carbono se han evaluado glucosa y glicerol, mientras que como fuente de nitrógeno se escogió amonio inorgánico y una mezcla peptídica (medio complejo). El estudio se ha llevado a cabo sobre la cepa silvestre de *E. coli* y sobre cinco cepas deficientes en genes involucrados en el metabolismo del acetato de *E. coli*. Se han observado importantes diferencias en algunos de los parámetros fisiológicos estudiados, así como en la excreción de acetato, y se ha determinado, por primera vez, el pH intracelular de forma continua para una bacteria en un cultivo. Entre los resultados obtenidos cabe destacar la influencia de la fuente de carbono en el control del pH intracelular, observándose una alcalinización en los cultivos suplementados con glucosa, pero no en los suplementados con glicerol. Para estudiar la influencia de la fuente de carbono y nitrógeno sobre la acetilación de lisinas en *E. coli*, se determinaron las concentraciones intracelulares de acetil-CoA y acetil-fosfato y se evaluó el nivel de acetilación mediante western blot utilizando un anticuerpo anti-acetil Lys. *E. coli* silvestre y las cepas deficientes en los genes *ackA* (codifica la proteína acetato kinasa (AckA)), *patZ* (codifica la proteína PatZ), *cobB* (codifica la proteína CobB) y *acs* (codifica la proteína Acs) mostraron un perfil de acetilación similar en medio mínimo, con un nivel mayor en glicerol que en glucosa. Sin embargo, la cepa Δ*pta* (deficiente en el gen que codifica la proteína fosfotransacetilasa (Pta)) mostró un nivel muy bajo de acetilación y Δ*ackA* un nivel muy alto en el medio complejo estudiado. Por último, no se encontró una relación entre el pH intracelular y el nivel de acetilación, lo que sugiere que la acetilación no enzimática no está directamente relacionada con el pH intracelular en *E. coli*.

Finalmente, las principales conclusiones que podemos extraer de esta tesis doctoral son: 1) Se ha construido un sistema competitivo de producción de licopeno empleando una cepa de *E. coli* modificada genéticamente; 2) La acetiltransferasa PatZ muestra cooperatividad positiva en respuesta a la concentración de acetil-CoA; 3) El estado oligomérico de PatZ está regulado por autoacetilación/desacetilación; 4) Acs es desacetilada por CobB en varias lisinas con una cinética monofásica; 5) CobB es inhibida por NAM siguiendo un mecanismo no competitivo. Además, se ha sugerido un mecanismo de regulación *in vivo* de CobB a través de la

concentración intracelular de NAM; 6) La mutación de la lisina 609 de Acs inhibe su capacidad catalítica y provoca un cambio en la unión de ATP que conlleva un aumento de su afinidad por este sustrato; 7) Los residuos T264 y D500 de la proteína Acs son fundamentales para la capacidad catalítica y para la unión de ATP de la proteína Acs. Por otra parte, el residuo K270 tiene un papel fundamental en la capacidad catalítica de Acs durante su etapa de adenilación, aunque no en la unión de la enzima a ATP; 8) La fuente de carbono y nitrógeno tiene una gran influencia en la fisiología y el control del pH intracelular de *E. coli* y 9) No se ha encontrado una relación entre el pH intracelular y el nivel de acetilación en *E. coli*.

Bibliografía

1. Kamionka M. Engineering of therapeutic proteins production in *Escherichia coli*. Curr Pharm Biotechnol. 2011;12: 268–74. doi:10.2174/138920111794295693

2. Huang C-J, Lin H, Yang X. Industrial production of recombinant therapeutics in *Escherichia coli* and its recent advancements. J Ind Microbiol Biotechnol. 2012;39: 383–399. doi:10.1007/s10295-011-1082-9

3. Ajikumar PK, Tyo K, Carlsen S, Mucha O, Phon TH, Stephanopoulos G. Terpenoids: opportunities for biosynthesis of natural product drugs using engineered microorganisms. Mol Pharm. 2008;5: 167–190. doi:10.1021/mp700151b

4. Sies H, Stahl W. Lycopene: antioxidant and biological effects and its bioavailability in the human. Proc Soc Exp Biol Med. 1998;218: 121–4.

5. Giovannucci E. A review of epidemiologic studies of tomatoes, lycopene, and prostate cancer. Exp Biol Med (Maywood). 2002;227: 852–9. doi:10.1177/153537020222701003

6. Bignotto L, Rocha J, Sepodes B, Eduardo-Figueira M, Pinto R, Chaud M, et al. Anti-inflammatory effect of lycopene on carrageenan-induced paw oedema and hepatic ischaemia–reperfusion in the rat. Br J Nutr. 2009;102: 126–134. doi:10.1017/S0007114508137886

7. Bernal V, Castaño-Cerezo S, Cánovas M. Acetate metabolism regulation in *Escherichia coli*: carbon overflow, pathogenicity, and beyond. Appl Microbiol Biotechnol. 2016;100: 8985–9001. doi:10.1007/s00253-016-7832-x

8. Valgepea K, Adamberg K, Vilu R. Decrease of energy spilling in *Escherichia coli* continuous cultures with rising specific growth rate and carbon wasting. BMC Syst Biol. 2011;5: 1–11. doi:10.1186/1752-0509-5-106

9. Zhao S, Xu W, Jiang W, Yu W, Lin Y, Zhang T, et al. Regulation of cellular metabolism by protein lysine acetylation. Science. 2010;327: 1000–1004. doi:10.1126/science.1179689

10. Castaño-Cerezo S, Bernal V, Post H, Fuhrer T, Cappadona S, Sánchez-Díaz NC, et al. Protein acetylation affects acetate metabolism, motility and acid stress response in *Escherichia coli*. Mol Syst Biol. 2014;10. doi:10.15252/msb.20145227

11. Weinert BT, Iesmantavicius V, Wagner SA, Schölz C, Gummesson B, Beli P, et al. Acetyl-phosphate is a critical determinant of lysine acetylation in *E. coli*. Mol Cell. 2013;51: 265–72. doi:10.1016/j.molcel.2013.06.003

12. Starai VJ, Celic I, Cole RN, Boeke JD, Escalante-Semerena JC. Sir2-dependent activation of acetyl-CoA synthetase by deacetylation of active lysine. Science. 2002;298: 2390–2392. doi:10.1126/science.1077650

13. Starai VJ, Escalante-Semerena JC. Identification of the protein acetyltransferase (Pat) enzyme that acetylates acetyl-CoA synthetase in *Salmonella enterica*. J Mol Biol. 2004;340: 1005–12. doi:10.1016/j.jmb.2004.05.010

Summary

Escherichia coli (*E. coli*) is a Gram-negative bacterium with several characteristics that have made it a global model in biology and biotechnology. Some of these characteristics include fast growth, easy availability and great ability to grow in different culture media. Moreover, the great development of molecular biology tools in last decades has made that several high-value compounds are produced today using genetically modified *E. coli* strains [1,2]. Terpenoids are a large family of compounds with several applications in pharmacological, food and farming industry [3]. Lycopene is an important terpenoid with several applications, although most of lycopene is obtained from tomato, and no competitive biotechnological process exists for its production [4–6]. In spite of the great advantages of *E. coli* in the biotechnology field, it has also some disadvantages. The main *E. coli* biotechnological drawback is the excretion of acetate in cultures supplemented with glucose as carbon source. Thereby, when *E. coli* is growing in a culture with glucose as carbon source, it excretes high amounts of acetate, which leads to a loss of metabolic energy and carbon wasting, limiting production yield [7,8]. Moreover, high acetate concentrations could limit *E. coli* growth rate. For these reasons, much effort has been put into deepening our knowledge of the acetate metabolism with the purpose of minimizing *E. coli* acetate overflow.

By other way, post-translational modifications (PTMs), such as N-ε lysine acetylation, are essential to know metabolism regulation in all the organisms [9,10]. *E. coli* acetate metabolism is closely related to PTMs by lysine acetylation through acetyl-phosphate and acetyl-CoA pools [11] and acetyl-CoA synthetase (Acs) regulation by lysine acetylation. Thus, Acs catalyses one of the acetate reincorporation pathways and is regulated by acetylation/deacetylation catalysed by PatZ acetyltransferase, also known as YfiQ or Pka, and CobB deacetylase enzymes, respectively [12,13].

The main objective of this PhD thesis was to increase our understanding of *E. coli* acetate metabolism and regulation by lysine acetylation/deacetylation. This main objective has been broken down into the following subobjectives: 1) To design a competitive lycopene overexpression and extraction system using genetically modified *E. coli* strains; 2) To carry out a biochemical and biophysical PatZ enzyme characterization; 3) To accomplish a kinetic CobB characterization and to increase our knowledge of nicotinamide (NAM) inhibition; 4) To advance in the knowledge of the Acs *E. coli* enzyme catalytic mechanism and acetylation regulation and 5) To study the influence of carbon and nitrogen sources on acetate metabolism, intracellular pH homeostasis and lysine acetylation in *E. coli*.

The main results of this PhD thesis are summarized below.

In chapter 3 of this thesis a lycopene overproduction and continuous biphasic extraction system employing *E. coli* strains modified by genetic engineering has been developed. Overexpression conditions were optimized and octane was used as the organic phase to extract lycopene with the least cell damage, which was evaluated by flow cytometry (FC). Final production was much higher than those obtained from tomato, which suggests it is a promising strategy for lycopene industrial production. Finally, the results obtained in this chapter corroborate the potential role of *E. coli* in biotechnology field.

Chapter 4 of this dissertation is focused on acetyltransferase PatZ biochemical characterization. The kinetics of Acs acetylation by PatZ have been characterized for the first time, and a PatZ positive cooperativity in response to acetyl-CoA substrate was observed. Sixteen Acs acetylated lysines have been identified in Acs sequence. As regards PatZ characterization, reversible autoacetylation has been described and six PatZ acetylated lysines have been identified. PatZ autoacetylation induced an oligomeric change in protein structure from a tetramer to an octamer. Finally, a structural model for the tetrameric PatZ conformation has been developed employing bioinformatics tools. This model was validated comparing the theoretical model parameters, estimated by HYDROPRO, with the experimental data obtained from PatZ biophysical characterization.

In chapter 5, CobB sirtuin kinetics of Acs deacetylation have been characterized. This is the first sirtuin kinetic study using a whole acetylated native protein as substrate. The results showed that Acs is deacetylated by CobB in several lysines with monophasic kinetics. Moreover it has been demonstrated that acetylation of lysine 609 is not necessary for CobB recognition. These results suggest that structural protein components are the main determinants of sirtuin specificity. CobB inhibition by NAM has been studied and a non-competitive inhibition mechanism has been established. Moreover, intracellular NAM concentrations have been determined for different culture mediums and growth phases and concentrations were high enough to regulate CobB *in vivo*. Finally, it has been demonstrated that several *E. coli* aspects such as acetate excretion or flagella expression could be regulated by NAM levels *in vivo*. The results highlight the importance of NAM concentration and nicotinamidase enzyme (PncA) as essential actors in CobB regulation and *E. coli* metabolic control by lysine acetylation.

Chapter 6 of this dissertation is focused on the study of the adenylating catalytic step of Acs protein. From the crystal structures, in the presence of ATP, of other proteins belonging to the ANL superfamily of adenylating enzymes, several three-dimensional models have been

constructed in order to predict Acs-adenylating catalytic step conformation. Four residues were selected to study the effect of their mutation on catalytic parameters and ATP-binding. Kinetics for ATP and acetate substrates and ATP-binding thermodynamic parameters were determined for the four mutant proteins and for Acs wt protein, in the acetylated and deacetylated state. Acs proteins showed an endothermic ATP-binding. Acs wt results demonstrated that *in vivo* acetylation does not affect enzyme specificity for acetate and ATP substrates, but it has a great effect in catalytic activity. Moreover, acetylated and deacetylated proteins showed a similar affinity when ATP-binding was studied through isothermal titration calorimetry (ITC). As regards mutant proteins, results showed that 609 lysine has an essential role in Acs ATP-binding and catalytic ability. K609, conserved in all ANL proteins, is the responsible for Acs regulation through acetylation/deacetylation catalysed by PatZ and CobB enzymes, respectively. Thus, the study of this residue is essential to understand how Acs activity is regulated *in vivo*. By other way, T264 and D500 residues mutation led to a decrease in specificity for acetate and ATP substrates and in catalytic capability. In agreement, ATP-binding was not observed in the conditions assayed. Finally, lysine 270 mutated protein showed an increase in Acs catalytic activity, although acetate and ATP specificity and ATP-binding affinity was similar to wt enzyme. The results achieved in this chapter highlight the importance of the studied residues in Acs catalytic mechanism and ATP-binding and open a new research field for understanding how lysine 609 mutation induces enzyme inhibition and metabolic regulation.

In chapter 7 of this thesis, the influence of carbon and nitrogen sources on *E. coli* acetate metabolism was evaluated. Glucose and glycerol were selected as carbon sources whereas inorganic ammonium and peptides (complex medium) as nitrogen sources. The *E. coli* acetate metabolism was evaluated for *E. coli* wt and five deficient strains. As regards physiological parameters and acetate excretion determined, several differences were observed depending on the culture medium and strains. Intracellular pH was determined for the first time in *E. coli* and important results were achieved. In *E. coli* cultures grown with glucose as carbon source intracellular pH reached high values, but this increase was not observed for glycerol supplemented cultures. To study carbon and nitrogen influence on *E. coli* lysine acetylation, intracellular acetyl-CoA and acetyl-phosphate concentrations were determined and lysine acetylation was evaluated by western blot assays using an anti-acetyl Lys antibody. *E. coli* wt, *ackA* (encodes the acetate kinase enzyme (AckA)), *patZ* (encodes the PatZ enzyme), *cobB* (encodes the CobB enzyme) and *acs* (encodes the Acs enzyme) deletions strains showed a similar acetylation profile in minimal medium, with a higher level of lysine acetylation in glycerol than glucose as carbon source. However, Δ*pta* (deficient in the gene which encodes the

phosphotransacetylase (Pta) enzyme) strain showed a very low acetylation level and Δ*ackA* showed a high degree of acetylation in compex medium. No-relationship between intracellular pH and acetylation level was found in this study, which suggests that non-enzymatic acetylation is not directly related to intracellular pH in *E. coli*.

Finally, the main conclusions we can extract are: 1) A competitive lycopene production system using *E. coli* has been developed; 2) PatZ shows positive cooperativity in response to acetyl-CoA concentration; 3) PatZ oligomeric state is regulated by autoacetylation/deacetylation; 4) Acs is deacetylated by CobB in several lysines with monophasic kinetics; 5) CobB is inhibited by nicotinamide through a non-competitive mechanism. Moreover, a regulation mechanism for CobB depending on intracellular nicotinamide concentration has been suggested; 6) Acs lysine 609 mutation inhibits Acs catalytic ability and leads to a change in ATP-binding, increasing Acs ATP-affinity; 7) Acs T264 and D500 residues are essential for Acs catalytic mechanism and ATP-binding. Moreover, K270 residue has an essential role in Acs catalysis but its mutation does not affect to ATP-binding; 8) Carbon and nitrogen sources have a great influence on *E. coli* physiology and intracellular pH control and 9) No-relationship between intracellular pH and *E. coli* acetylation level was found in this study.

References

1. Kamionka M. Engineering of therapeutic proteins production in *Escherichia coli*. Curr Pharm Biotechnol. 2011;12: 268–74. doi:10.2174/138920111794295693

2. Huang C-J, Lin H, Yang X. Industrial production of recombinant therapeutics in *Escherichia coli* and its recent advancements. J Ind Microbiol Biotechnol. 2012;39: 383–399. doi:10.1007/s10295-011-1082-9

3. Ajikumar PK, Tyo K, Carlsen S, Mucha O, Phon TH, Stephanopoulos G. Terpenoids: opportunities for biosynthesis of natural product drugs using engineered microorganisms. Mol Pharm. 2008;5: 167–190. doi:10.1021/mp700151b

4. Sies H, Stahl W. Lycopene: antioxidant and biological effects and its bioavailability in the human. Proc Soc Exp Biol Med. 1998;218: 121–4.

5. Giovannucci E. A review of epidemiologic studies of tomatoes, lycopene, and prostate cancer. Exp Biol Med (Maywood). 2002;227: 852–9. doi:10.1177/153537020222701003

6. Bignotto L, Rocha J, Sepodes B, Eduardo-Figueira M, Pinto R, Chaud M, et al. Anti-inflammatory effect of lycopene on carrageenan-induced paw oedema and hepatic ischaemia–reperfusion in the rat. Br J Nutr. 2009;102: 126–134. doi:10.1017/S0007114508137886

7. Bernal V, Castaño-Cerezo S, Cánovas M. Acetate metabolism regulation in *Escherichia coli*: carbon overflow, pathogenicity, and beyond. Appl Microbiol Biotechnol. 2016;100: 8985–9001. doi:10.1007/s00253-016-7832-x

8. Valgepea K, Adamberg K, Vilu R. Decrease of energy spilling in *Escherichia coli* continuous cultures with rising specific growth rate and carbon wasting. BMC Syst Biol. 2011;5: 1–11. doi:10.1186/1752-0509-5-106

9. Zhao S, Xu W, Jiang W, Yu W, Lin Y, Zhang T, et al. Regulation of cellular metabolism by protein lysine acetylation. Science. 2010;327: 1000–1004. doi:10.1126/science.1179689

10. Castaño-Cerezo S, Bernal V, Post H, Fuhrer T, Cappadona S, Sánchez-Díaz NC, et al. Protein acetylation affects acetate metabolism, motility and acid stress response in *Escherichia coli*. Mol Syst Biol. 2014;10. doi:10.15252/msb.20145227

11. Weinert BT, Iesmantavicius V, Wagner SA, Schölz C, Gummesson B, Beli P, et al. Acetyl-phosphate is a critical determinant of lysine acetylation in *E. coli*. Mol Cell. 2013;51: 265–72. doi:10.1016/j.molcel.2013.06.003

12. Starai VJ, Celic I, Cole RN, Boeke JD, Escalante-Semerena JC. Sir2-dependent activation of acetyl-CoA synthetase by deacetylation of active lysine. Science. 2002;298: 2390–2392. doi:10.1126/science.1077650

13. Starai VJ, Escalante-Semerena JC. Identification of the protein acetyltransferase (Pat) enzyme that acetylates acetyl-CoA synthetase in *Salmonella enterica*. J Mol Biol. 2004;340: 1005–12. doi:10.1016/j.jmb.2004.05.010

Index

CHAPTER 1

Introduction

Escherichia coli: model organism

Escherichia coli (*E. coli*) is a Gram-negative bacterium discovered in 1884 by the German microbiologist Theodor Escherich [1]. *E. coli* has several characteristics that have made it a global model in biology and biotechnology including fast growth, easy availability and great ability to grow in different culture media. In nature, *E. coli* constitutes part of the microbiome of warm-blooded animals [2], and its impact on mammalian microflora is currently a subject of debate [3,4].

The establishment in 1958 of the Molecular Biology Central Dogma [5] and the development of molecular biology techniques, brought *E. coli* to the minds of the pharmaceutical and biotechnological industry [6,7]. Indeed, the production of recombinant proteins and other bio-products in *E. coli* is essential for the industry todays. Research into the central metabolism and regulation of this bacterium is essential to be able to continue optimizing all related biotechnological processes.

Escherichia coli and molecular biology tools

Modern molecular biology tools are essential for the genetic engineering of *E. coli*, and are responsible, to a great extent, for the success of this bacterium in the biotechnological field. The main molecular biology tools used in *E. coli* genetic engineering are resumed in Figure 1.

Plasmids are one of the most important tools for the genetic engineering of *E. coli*. Thus, cloning, the generation of mutants and overexpression and purification of recombinant proteins are all based on the use of plasmids. Plasmids are double-stranded circular, extrachromosomal self-replicative DNA molecules that were first described by Joshua Lederberg in 1952 [8]. Plasmids are present in eubacteria, archaea and some lower eukaryotic organisms. In the 1970s, synthetic plasmids for cloning were created, providing biological research with a powerful tool [9]. Plasmids usually contain several elements that make them useful in research, such as selection markers, a replication origin, regulatory elements to control expression, and transcription termination [10]. Since *E. coli* was sequenced in 1997, several molecular biology tools for genome modifications have been developed. The main technique used for genome modification is gene deletion and insertion [11]. *E. coli* genome modifications obtained by generating knockouts has provided important information for understanding the function of several genes and for constructing *E. coli* modified strains for use in biotechnology processes [12]. Important tools based on using plasmids or artificial chromosomes are *E. coli*-based

biosensors, which function by converting a biological response into a measurable proportional signal, usually based on fluorescence, luminescence or colorimetry [13]. Several studies have been carried out using *E. coli* biosensors to analyse oxidative stress, DNA damage, aromatic compounds or xenobiotics degradation [14–17].

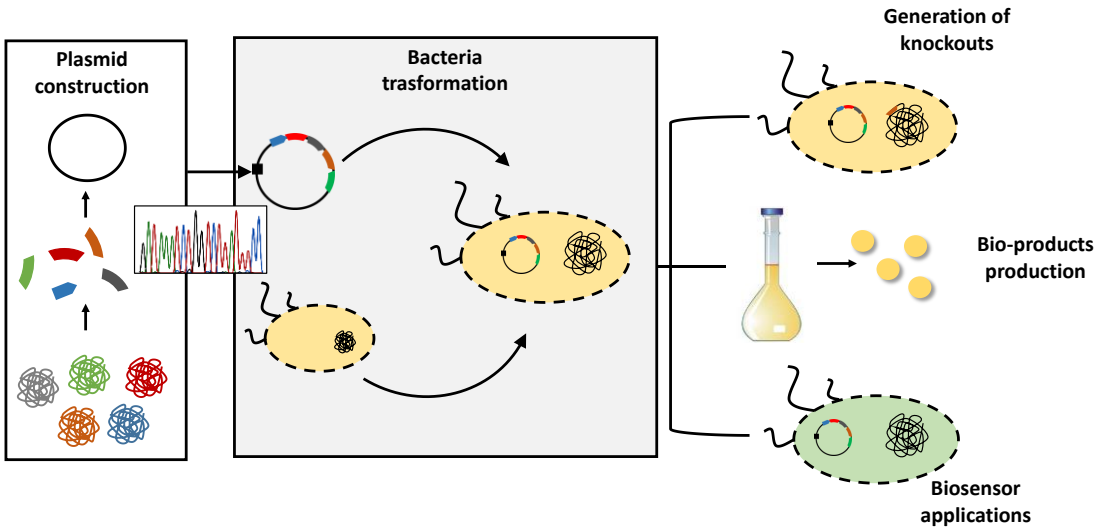

Figure 1. Molecular biology tools employed for *E. coli* genetic engineering.

An in-depth knowledge of *E. coli* metabolism, the molecular biology tools development and the demands of industry have led *E. coli* to becoming a key organism in synthetic biology. Synthetic biology is a multidisciplinary area involving biotechnology, genetic engineering, molecular biology, molecular engineering or systems biology to develop strains capable of synthesizing several novel compounds for the pharmaceutical industry, metabolites and molecules relevant for food additives, pigments, and, more recently, complex aliphatic molecules [18].

***Escherichia coli* in biotechnology: terpenoids**

Several decades ago, *E. coli* was used in L-threonine overproduction [19] and was the first expression host that was used for manufacturing a biopharmaceutical: human insulin [20]. Nowadays, *E. coli* is still the microorganism of choice by biotechnologists to produce high-value products, such as therapeutics, pre-biotics, nutraceuticals, pigments or biopolymers.

The main high-value compounds produced with engineered *E. coli* can be classified according to their chemical nature into aromatic compounds (pigments, vitamins and fragrances) terpenoids (monoterpenes, sesquiterpenes, diterpenes and carotenoids), sugar

oligomers (oligosaccharides and polysaccharides), polymers (Polyhydroxyalkanoates, polyamides or polyesters) and heterologous proteins [21,22].

Terpenoids, or isoprenoids, are a large family of organic compounds (over 55,000 different terpenoids have been isolated) derived from five-carbon isoprene units assembled, isopentenyl pyrophosphate (IPP) and dimethylallyl diphoshate (DMADP). Terpenoids can be classified according to their chain length into hemiterpenes (C5), monoterpenes (C10), sesquiterpenes (C15), diterpenes (C20), triterpenes (C30), tetraterpenes (C40), and polyterpenes (larger chain length) [23]. The natural chemical diversity of the terpenoid family has led them to being used in diverse industrial fields as flavoring agents, fragrances, disinfectants, agrochemicals, pharmaceuticals, and nutraceuticals [24].

Two pathways are known to synthetize IPP and DMADP in nature. The first pathway, known as the mevalonate (MEV) pathway, uses acetyl-CoA as a substrate to yield IPP, which can be interconverted to DMADP by an isomerase [25]. This pathway operates in eukaryotes, archaea and some bacteria. The second pathway, the non-mevalonate pathway or methyl D-erythritol 4-phosphate (MEP) pathway, uses pyruvate and glyceraldehyde-3-phosphate as substrates to form IPP and DMADP. The MEP pathway is present in eubacteria, plant plastids and in algae [26]. *E. coli* is capable of biosynthesizing IPP and DMADP through the non-mevalonate route. Thus, a wide variety of terpenoids can be produced using *E. coli* recombinant strains. The main high-value terpenoids produced with using engineered *E. coli* are resumed in Table 1.

Lycopene, a tetraterpenoid (C40) precursor of carotenoids, has traditionally been used as a food additive and a colorant, but new applications have been discovered as antioxidant [27], anticarcinogen [28] and anti-inflammatory [29]. In spite of the great number of lycopene applications, a biotechnological process to compete with its traditional extraction from tomato has not yet been developed, although in the last decade, several studies have reported on lycopene production by metabolic engineering, some based on *E. coli* [30–37]. Hence, the search for a competitive system for both lycopene production and extraction is of great interest in the biotechnology field.

Table 1. Main high-value terpenoids produced with engineered *E. coli.*

Product	Classification	Industrial application	Reference
Myrcene	Monoterpene	Starting material for high-value compounds	[38]
Amorphadiene	Sesquiterpene	Precursor of artemisinin (antimalarial agent)	[37]
Protoilludene	Sesquiterpene	Antitumoral and antimicrobial agent	[39]
Farnesene	Sesquiterpene	Precursor of jet fuel	[40]
Ent-Kaurene	Diterpene	Precursor of sweeteners such as steviol glycosides	[41]
β-Carotene	Carotenoid	Colorant, pharmacological applications	[42]
Astaxanthin	Carotenoid	Colorant, antioxidant and anti-inflammatory	[43]
Zeaxanthin	Carotenoid	Food additive and prevention of age-related macular degeneration	[44]

Escherichia coli acetate metabolism

E. coli can metabolize several carbon sources in order to grow, although its preferred carbon source, as for many other bacteria, is glucose, which enables a faster growth rate than other sugars. When different carbon sources are available, *E. coli* activates a regulation system known as the Phosphoenolpyruvate-Phosphotransferase System (PTS System) to choose between them. This system is the main system involved in the transport and phosphorylation of several sugars (PTS carbon sources) and controls the preferential consumption of glucose over other carbon sources when bacteria are exposed to more than one carbohydrate in a culture medium. It has a significant impact on carbon flux and distribution in the central carbon metabolism. Other PTS carbon sources, in addition to glucose, are fructose or mannose. When a PTS substrate is not available, *E. coli* is able to consume other substrates employing a different system to transport them into the cell. These carbon sources are known as non-PTS substrates (*e.g* acetate, glycerol) [45]. CRP (Catabolite Repression Protein or cAMP Receptor Protein) is a global transcription factor and the major carbon regulator in *E. coli*. When a PTS carbon source is not available, the intracellular levels of cAMP in cell increase. cAMP binds to CRP, and this

complex activates the transcription of non-PTS carbon source promoters, allowing the use of alternative carbon systems (Carbon Catabolite Repression, CCR) [46].

E. coli excretes several metabolites to the extracellular medium during cell growth to maintain cellular homeostasis. Acetate is the main excreted product when glucose acts as carbon source. However, when acetate is the only carbon source available, *E. coli* can also metabolize it as a non-PTS carbon source. Thus, excreted acetate can be consumed and reincorporated in the metabolism. This acetate excretion-consumption phenomenon is known as "acetate overflow". However, acetate overflow is an important drawback for industrial bioprocesses involving *E. coli*, because acetate inhibits cell growth in high density cultures, thus limiting the bioprocess yield [47]. For this reason, much effort has been made by the scientific community to deepen our knowledge of the acetate metabolism with the purpose of minimizing *E. coli* acetate overflow [48–54].

The pathways responsible for acetate overflow in *E. coli* are the Pta-AckA, Acs and PoxB pathways.

Pta-AckA pathway

The Pta-AckA pathway is composed of two enzymes, phosphotransacetylase (Pta) and acetate kinase (AckA), which catalyse the enzymatic interconversion of acetate to acetyl-CoA through an acetyl-phosphate intermediate in a reversible way (Figure 2). The Pta-AckA pathway is a low affinity (K_M 7-10 mM) high capacity pathway, which can efficiently take up acetate when it is present at high concentrations in the environment [55–57]. The *pta* and *ackA* genes are located in the same operon and transcription is regulated by the transcriptional regulator Fnr and by the aerobic respiration control protein ArcA [58].

Acs pathway

Acetyl-CoA synthetase protein (Acs) catalyses the irreversible conversion of acetate to acetyl-CoA through an acetyl-AMP intermediate. The Acs pathway is a high affinity route, which allows the uptake of acetate into the cell when it is present at low concentration in the extracellular medium [59,60] (Figure 2). Acs is finely regulated transcriptionally and post-translationally. The *acs* gene is directly regulated by the global transcription factor CRP and by the nucleoid proteins Fis and IHF, and indirectly by several other transcription factors [61,62]. Post-translationally, Acs is regulated by lysine acetylation, a regulation mechanism conserved in

all acyl-CoA synthetases AMP forming [60,63,64]. Acs acetylation will be further explained in the following sections.

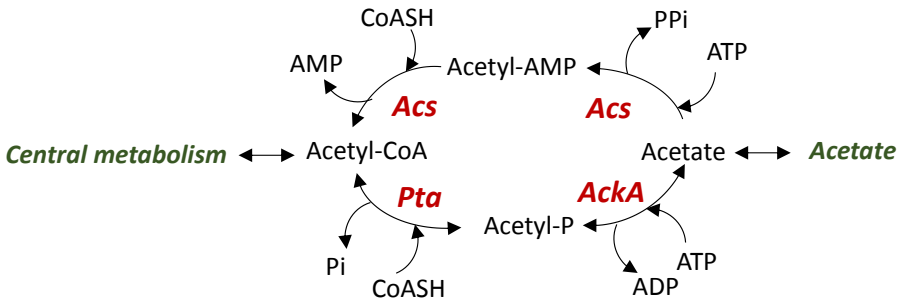

Figure 2. *E. coli* Pta-AckA and Acs pathways.

PoxB pathway

Pyruvate oxidase (PoxB) is a tetrameric peripheral membrane enzyme that catalyses pyruvate oxidation to release CO_2 and acetate. PoxB is the main enzyme responsible for acetate production in the *E. coli* stationary growth phase [65]. Its gene transcription is regulated by RpoS σ factor [66] and the expression is stimulated under stress conditions such as osmotic stress [67] or cultures with a limited glucose supply [68].

Post-translational modifications: lysine acetylation

Post-translational modifications (PTMs) conform an evolutionarily conserved regulatory mechanism consisting of the chemical modification of biosynthesized proteins. PTMs confer novel properties on the modified proteins, regulating protein localization, enzymatic activity, protein structure and stability and protein interactions with ligands or other proteins. Around thirty PTMs are known, including phosphorylation, glycosylation, ubiquitination, acylation, methylation and ADP-ribosylation [69], most of which are catalysed by enzymes and some of which can be reversed. Thus, these modifications help to increase the diversity and complexity of the limited genome at all levels of life [70]. Protein phosphorylation has been considered one of the most important and well-studied protein modifications for decades. However, the development of proteomic and bioinformatic techniques such as mass spectrometry (MS) and computational protein modeling has deepened our knowledge and/or has led to the discovery of other PTMs [71,72] (Figure 3).

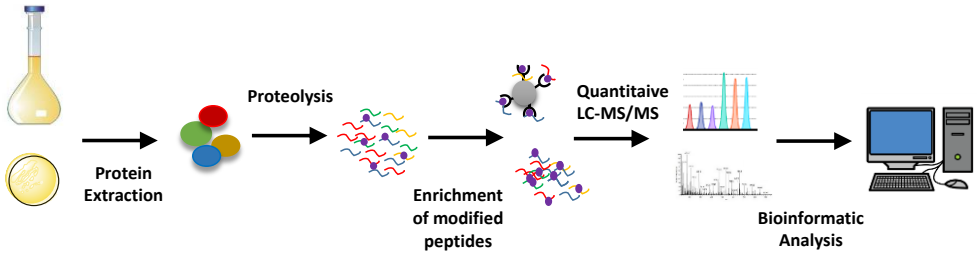

Figure 3. Poteomic experiment workflow.

Protein acetylation is a PTM consisting of the transfer of an acetyl group from a donor molecule (acetyl-CoA or acetyl-phosphate) to an amino residue of a protein. Although protein acetylation was discovered in 1963 [73] (shortly after protein phosphorylation [74]), acetylation was relatively ignored for the 30 years following its discovery. However, in the last 20 years, protein acetylation and the enzymes that regulate it have emerged as an essential regulatory mechanism involved in numerous cellular processes [75]. Figure 4 shows last ten years citations per year of papers containing "lysine acetylation" in the title (data obtained from Web of Science).

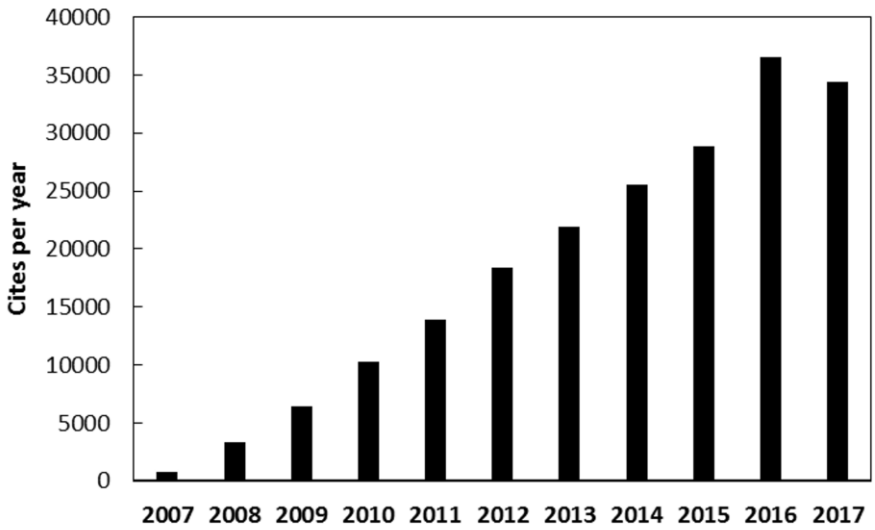

Figure 4. Last ten years citations per year of papers containing "lysine acetylation" in the title (data obtained from Web of Science).

Two types of protein acetylation can be defined depending on the nature of the modified amino group. The acetylation of the α-amino group of the N-terminal amino acid of a protein (known as N-α acetylation) and the acetylation of an ε-amino group of a lysine residue of a protein (known as N-ε acetylation). While N-α acetylation is frequent in archaea and eukaryotic organisms but not in bacteria [76,77], N-ε acetylation is a global PTM present in all domains of life [78–80]. Lysine acetylation has traditionally been associated with the regulation of histones. Histone acetylation is a well-studied acetylation system responsible for regulating gene expression in eukaryotic organisms [73,81,82]. To date, in addition to histones, many metabolic routes in many different organisms have been demonstrated to be regulated by lysine acetylation [83–89].

Lysine acetyltransferases: KATs

Lysine acetylation has been defined as a catalytic modification carried out by lysine acetyltransferases (KATs) (also known as acetyl-transferases (ATs), protein acetyltransferases (PATs) or histone acetyltransferases (HATs)).

KATs conform a great superfamily of enzymes that catalyse the transfer of an acetyl group from acetyl-CoA to a lysine residue of a protein. To date, many HATs have been identified from yeast to humans, resulting in, at least, five distinct subfamilies: HAT1, Gcn5/PCAF, MYST, p300/CBP, and Rtt109 [90]. KAT subfamilies do not have a sequence homology, although they contain a structurally conserved core region based on 3-stranded β-sheets with a long α-helix parallel. This conserved core interacts with acetyl-CoA ligand and is flanked on opposite sides by structurally non-conserved domains [91]. Biochemical, mutational and enzymatic analysis have revealed that KAT subfamilies use different catalytic strategies for acetyl transfer. Thus, while HAT1 and Rtt109 members need to associate with other protein regulatory subunits for full activity [92,93], Gcn5 and MYST proteins use two different catalytic mechanisms involving an essential glutamic acid [94,95], and the p300/CBP acetyltransferases transfer acetyl group through a mechanism in which two tyrosine residues are catalytically necessary [96].

Gcn5, Gcn5 like acetyltransferases, or GNATs (named for its founding member yeast Gcn5 (KAT2) [97]) are a family of acetyltransferases widely distributed from bacteria to humans. The catalytic mechanism involves a conserved glutamic acid, which acts as a general base to deprotonate the ε-amino group of the reactive lysine, facilitating the acetyl-CoA molecule attack

at the carbonyl carbon (Figure 5) [94,98,99]. Although direct deprotonation was proposed for Gcn5 enzymes several years ago, a recent Gcn5 crystal structure has revealed that the conserved glutamic residue is beyond the proton transfer distance [100]. A proton wire mechanism consisting of a continuous proton transfer pathway by hydrogen bonds with a water molecule has been proposed [101]. With respect to acetyl-transfer, two possible mechanisms have been proposed. The first is a ping-pong mechanism, in which the acetyl is attacked by the enzyme before being transferred to the amino residue [94], and the second mechanism, known as the sequential mechanism, involves direct acetyl transfer from acetyl-CoA to the amino residue [95].

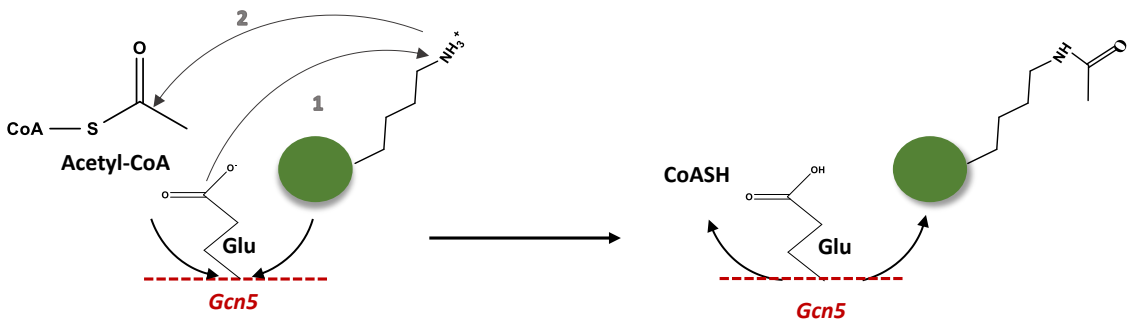

Figure 5. Gcn5 acetyltransferase mechanism. Conserved glutamic acid attack on ε-amino group (1) and unprotonated lysine attack on acetyl-CoA carbonyl (2) are represented.

Non-enzymatic lysine acetylation

Although lysine acetylation has traditionally been associated with lysine acetyltransferases, the *in vivo* importance of non-enzymatic acetylation has recently been discovered. MS studies carried out on the mitochondrial proteome revealed the existence of acetylated proteins, although the HATs mitochondrial function was not clear [102,103]. This fact led to the scientific community to consider the possibility of a non-enzymatic protein acetylation process [87], which was first described in 1970 [104]. Several studies have recently revealed the magnitude and importance of non-enzymatic lysine acetylation in eukaryotic organisms [87,102,105–107]. Non-enzymatic lysine acetylation has also been studied in prokaryote organisms, where the acetyl-phosphate metabolite was identified as the main acetyl donor [79,108–111].

Enzymatic reactions are characterized by their high specificity. Thus, lysine acetylation catalysed by acetyltransferases will depend on the specificity of enzymes and protein recognition. However, no specificity or consensus sequence exits in a non-enzymatic acetylation, so acetylation will depend on lysine reactivity, which is determined by lysine pKa and microenvironment, surface accessibility and acetyl donor concentrations. Acetylation catalysed by Gnc5 and Myst requires lysine deprotonation to transfer the acetyl group. This deprotonation is catalysed by an acetyltransferase, so N-ε lysine pKa is not an important factor. However, in non-enzymatic acetylation, lysine deprotonation will depend on N-ε pKa. The pka for a lysine N-ε residue is about 10.5. So, at pHs higher than 10.5 lysine will be deprotonated, but protonated at a lower pH. However, in a protein, the pKa of a residue is highly influenced by its chemical environment, leading some authors to focus on establishing a non-enzymatic lysine reactivity. Thus, the influence of pH, acetyl-CoA and acetyl-phosphate concentration, lysine surface accessibility and microenvironment are currently being evaluated in prokaryote and eukaryote organisms [87,108,111,112]. Recently a non-enzymatic acetylation mechanism involving an acetylated cysteine intermediate was identified as the majority in mitochondria. This mechanism would facilitate lysine acetylation because cysteine pKa is much lower than lysine pKa [113].

Sirtuins

Post-translational lysine acetylation can be reversed by a family of enzymes known as lysine deacetylases (KDACs) (also called protein deacetylases (PDACs), or histone deacetylases (HDACs)). KDACs can be divided into two groups. The first one depends on a Zn^{2+} dependent mechanism, while the second uses NAD^+ as a co-substrate. The first group of KDACs carries out lysine deacetylation through a hydrolysis reaction involving one of four sub-types of enzyme (class I, class IIa, class IIb and class IV) [114]. The second KDAC group are known as sirtuins and are conserved from bacteria to humans [115,116].

Sirtuins or Sir2-like enzymes conform a family of protein deacetylases that catalyse lysine deacetylation. They employ NAD^+ as a co-substrate and transfer the acetyl group from the lysine to the ribose of NAD^+, eliminating a nicotinamide molecule (NAM). The three resulting products are the deacetylated lysine, NAM and O-acetyl-ADP-ribose [117] (Figure 6).

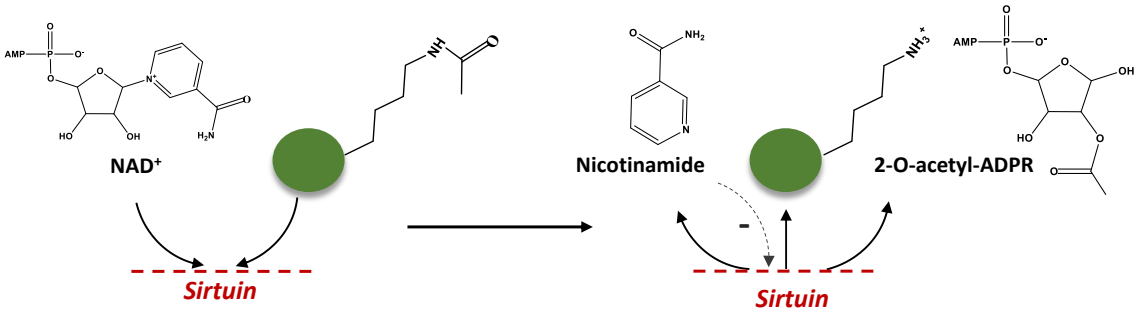

Figure 6. Sirtuins mechanism and nicotinamide inhibition.

In 2000, deacetylase activity of yeast Sir2 protein (silent information regulator 2 (SIR2)) and homologs (sirtuins) was identified [118], and a NAD^+ dependent mechanism was established [119–123]. Sirtuins are present from bacteria [63] (CobB sirtuins) to eukaryotes. In humans, seven sirtuins have been identified, that differing in structure and localization (Sirt 1-7) [115,124]. Recently it has been demonstrated that sirtuins can deacylate different acyl groups from lysine such as a hexanoyl, octanoyl, decanoyl, dodecanoyl, myristoyl, and palmitoyl groups [125,126], although the catalytic efficiency varies with the acyl group and the nature of the enzyme [127].

Sirtuins have a conserved structural core formed by a Rossman domain, a Zn^{2+}-finger domain and a connector loop. The N- and C-terminal regions differ in sequence and length, which might determine differences in substrate specificity [116]. Sirtuins substrates involve histone and non-histone proteins, and sirtuin-catalysed deacylations are responsible for regulating a variety of crucial cell processes such as transcription and metabolism [128,129]. Moreover, human sirtuins are involved in the regulation of cancer metabolism [130] and Sirt6 has been demonstrated to be a tumor repressor [131], so sirtuins have emerged as a promising target in cancer treatment investigation [132]. Due to the great interest in sirtuin regulation as the target for the treatment of metabolic diseases, sirtuins inhibition and activation has been widely studied.

NAM, a product of the sirtuin catalytic reaction, is a potent inhibitor of all of these enzymes. Although the mechanism of inhibition by NAM is not completely clear, most of the *in vitro* studies carried out with eukaryotic sirtuins point to a non-competitive inhibition *via* a base exchange mechanism that involves an intermediate to reform NAD^+ (transglycosidation

mechanism) [122,133–137]. With respect to sirtuin activators, large-scale screenings have yielded a great number of possible activators [138], resveratrol being the most studied [139].

Escherichia coli lysine acetylation

E. coli MS assays have allowed us to know that a high number of proteins are acetylated in this bacterium. Thus, since the first acetylome analysis in 2008, the number of known acetylated proteins has gradually increased (Table 2), and to date, over 2500 lysines in 800 proteins are known to be acetylated in *E. coli* [108,140–144]. Moreover, most of the acetylated proteins (64%), have a metabolic function, and almost 80% of these are involved in primary metabolism [89].

Table 2. Acetylated lysines and proteins identified by MS spectrometry in *E. coli*.

Acetylated lysines	Acetylated proteins	Year	References
125	85	2008	[143]
138	91	2009	[142]
1070	349	2013	[144]
2730	866	2014	[108]
2502	809	2014	[89]
2813	780	2015	[140]

In *E. coli* 25 putative acetyltransferases have been identified, although only one has been demonstrated to have lysine acetyltransferase activity, PatZ [64,145]. However, despite *in vitro* PatZ activity, *E. coli* acetylation largely depends on the concentration of acetyl-phosphate [108], a high-energy intermediate of the Pta-AckA pathway. High acetyl-phosphate concentrations have been found in *ackA* deletion strains, while very low concentrations are present in a *pta* deficient strain [146]. Thus, some recent studies have shown that *pta* and *ackA* deletions strongly alter protein acetylation in an acetyl-phosphate dependent way, which demonstrates the great importance of non-enzymatic acetylation in this microorganism [108,109]. Several *E. coli* proteins have been found that are acetylated in a non-enzymatic way (Table 3), such as the chemotaxis regulator protein CheY (first non-enzymatically acetylated protein identified in *E. coli*) [147], the RcsB transcription factor [148], the tyrosyl-tRNA synthetase protein [149] and

the DnaA regulatory protein [150]. The acetylation mechanism of N-hydroxyarylamine O-acetyltransferase protein (NhoA), α-subunit of RNA polymerase and S-adenosylmethionine synthase (SAM) remains unknown [151–153].

Recently, the importance of the carbon source on the degree of *E. coli* acetylation has been studied. Glucose consumption and acetate production induce protein acetylation [154], while *crp* deletion promotes a dramatic loss of acetylation [140]. Finally, *E. coli* growing on complex peptide-based medium showed a high acetylation level and a low growth rate due to the inefficient glucose consumption. However, when a magnesium supplemented medium is used, the glucose is completely consumed, with a concomitant increase in cell number and biomass, accompanied by a decrease in the acetylation level [155]. More generally, such conditions might open up new ways to understand the limitations of regulatory circuits *vs* acetylation.

***Escherichia coli* acetyltransferases: PatZ**

PatZ, which belongs to the Gcn5 acetyltransferases superfamily, is a large protein (886 residues) with two well-defined domains. The N-terminal domain is a predicted domain of unknown function with high similarity to the acyl-CoA synthetase (NDP-forming) superfamily of enzymes (residues 3 to 625), while the C-terminal domain (residues 725 to 884) consists of an acetyl-CoA binding fold, conserved in all GNAT proteins. Catalytic glutamic acid (E809) is predicted to be present in the C-terminal domain (Figure 4) [156].

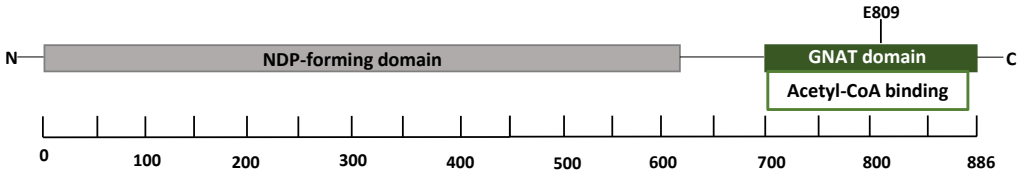

Figure 7. PatZ acetyltransferase domains distribution.

Salmonella enterica (*S. enterica*) Pat orthologue (*Se*Pat) was first identified in 2004 [145] and is the best-studied bacterial protein acetyltransferase. *Se*Pat has been described as the acetyltransferase responsible for Acs acetylation and inhibition. Several Pat enzymes have been identified in different organisms as well as protein substrates. Thus, in *S. enterica*, *Se*Pat

regulates the acetylation of Acs, propionyl-CoA synthetase (PrpE), glyceraldehyde 3-Phosphate dehydrogenase (GapA), isocitrate lyase (AceA) and HilD central regulator [145,157–159]. Several acyl-CoA synthetases are known to be substrates of Pat acetyltransferases in different microorganisms, such as Acs from *Bacillus subtilis* (*B. subtilis*) [160,161], 9 acyl-CoA synthetases from *Rhodopseudomonas palustris* (*R. palustris*) [162], acetoacetyl-CoA synthetase from *Streptomyces lividans* (*S. lividans*) [163], Acs and fatty acyl-CoA synthetase (FadD13) from *Mycobacterium tuberculosis* (*M. tuberculosis*) [164,165], and Acs and PrpE from *Mycobacterium smegtatis* (*M. smegtatis*) [36]. In *E. coli*, PatZ acetylation of RcsB transcription factor [148], RnaseR [166] , Rnase II [167] and DnaA [168] proteins have been characterized *in vitro*. Acetylation of Acs by PatZ has been demonstrated *in vivo* [64], although *in vitro* characterization has not been carried out (Table 3).

So far, PatZ has been poorly characterized. *patZ* gene transcription is positively regulated by CRP global transcription factor, so PatZ expression will be higher in the absent of PTS carbon sources such as glucose [64]. In *S. enterica, Se*Pat has been kinetically and thermodynamically characterized, revealing a positive cooperative behavior for acetyl-CoA substrate when Acs protein substrate was saturating. Moreover, *Se*Pat showed a tetrameric native structure with two different acetyl-CoA binding sites per monomer (one acetyl-CoA binding site in the N-terminal domain of unknown function) [169]. As regards Pat specificity and substrate recognition, *R. palustris* Pat orthologue, *Rp*Pat, showed relatively narrow substrate specificity and a recognition substrate sequence necessary motif *PX4GK* [162]. Recently, a structure of the GNAT domain of the *S. lividans* PatA in complex with a globular protein substrate revealed several substrate interactions through an extensive surface [170].

MS proteome analysis of *E. coli patZ* mutant strain showed increased protein acetylation in acetate-grown cells and in stationary phase glucose cultures, perhaps caused by the deregulation of non-enzymatic acetylation [89]. On the other hand, *patZ* mutant strain showed an increase in global propionylation compared with the wild type strain, suggesting that PatZ could also have regulatory activities for lysine propionylation in *E. coli* [171].

***Escherichia coli* desacetylases: CobB**

In *E. coli* the best-studied deacetylase enzyme is the sirtuin CobB, which was first described in *S. enterica* as being responsible for Acs activation through lysine deacetylation [63].

Other *E. coli* proteins such as Acs and Pta have been reported to functionally act as deacetylases of the chemotaxis signaling molecule CheY, although, to our knowledge, there is no proteomic study that shows deacetylase activity with other substrates [172,173]. Moreover, a new family of prokaryote deacetylases has been identified since identification of YcgC *E. coli* deacetylase [174]. In 2004 the CobB crystal structure revealed that it was a 34 KDa protein with a conserved structural core formed by a Rossman domain, a Zn^{2+}-finger domain and a connector loop [175]. In addition, *cobB* gene transcription seems to be constitutive in *E. coli* [64].

Several CobB substrates have been identified in *E. coli* and in other microorganisms. Thus, in *S. enterica*, CobB regulates the acetylation of Acs, PrpE, GapA, AceA and the HilD central regulator [145,157–159]. Acyl-CoA synthetases are known to be substrates of CobB in different microorganisms, such as Acs from *B. subtilis* [160,161] and *M. tuberculosis* [164,165] and 8 acyl-CoA synthetases from *R. palustris* [162]. In *E. coli*, CobB regulates the acetylation of Acs [64], the chemotaxis regulator CheY [176], the transcription factor RcsB [177], the RNase R protein [166], the tyrosyl-tRNA synthetase protein [149], the DnaA regulatory protein [152], the NhoA protein [167] and the SAM protein synthetase [151] (Table 3).

Recently, 69 acetyl-lysine residues in 51 proteins were identified as CobB substrates in *E. coli*. Moreover, the same study revealed that CobB deacetylates acetylated proteins both enzymatically and non-enzymatically [178]. *E. coli cobB* mutant strain MS/MS proteome analysis showed that protein deacetylation by CobB activates acetate metabolism and regulates flagella biosynthesis, motility and acid stress survival in *E. coli*, which highlights the major role of CobB in bacterial physiology [89]. A recent *E. coli* proteome analysis has identified 13 lysines that may be regulated by CobB through lysine depropionylation [171]. This finding could indicate the importance of CobB in a new PTM, lysine propionylation.

Several studies have tried to identify a consensus recognition sequence for CobB and other sirtuins [116,178–184]. Most of these studies are based on peptide microarrays to predict sirtuin substrates. Two of these studies concluded that Sirt1 and yeast Hst2 do not show a specificity against the peptides tested [180,184]. However, other works have observed peptide specificity [179,181–183], although there is no clear evidence of this sequence specificity when native proteins are used as substrates. In fact, the sirtuin specificity observed with peptide microarrays was not observed in *in vivo* proteome studies [89,108,185,186]. In recent years, two studies have focused on the complete and native protein specificity of sirtuins (human Sirt1-3

and *E. coli* CobB) [178,187]. The results suggest that structural protein components are the main determinants of sirtuin specificity, not the primary sequence surrounding acetylated lysine. Thus, the results obtained using acetylated peptides should be corroborated with additional studies using natively folded proteins.

Table 3. Proteins acetylated in *E. coli*.

Protein	Acetylated lysines	Acetylation mechanism	Deacetylation mechanism	References
Acs	K609	PatZ	CobB	[64]
CheY	K91, K109	Non-enzymatic	CobB, Acs, Pta	[172,176]
RcsB	K154	Non-enzymatic	CobB	[177]
	K180	PatZ		[148]
Tyrosyl-tRNA synthetase	K85, K235, K238	Non-enzymatic	CobB	[149]
NhoA	K214, K281	Unknown	CobB	[152]
Rnase R	K544	PatZ	Unknown	[166]
Rnase II	K501	PatZ	CobB	[167]
DnaA	K178	Non-enzymatic, PatZ	No deacetyltion	[168]
	K243	Non-enzymatic	CobB	[150]
α-RNA polymerase	K291, K298	Unknown	Unknown	[153]
S-adenosylmethionine synthetase	K37, K166	Unknown	CobB	[151]

ANL superfamily: acyl-CoA synthetases

The ANL superfamily of adenylating enzymes includes acyl- and aryl-CoA synthetases, firefly luciferase, and the adenylation domains of the modular non-ribosomal peptide synthetases (NRPSs). All ANL enzymes carry out a two-step catalysis involving an adenylate intermediate formation. The first step of the catalysis is very similar for the three subfamilies; the enzyme reacts with an ATP molecule and with a substrate (a carboxylate for the acyl- and aryl-CoA synthetases, firely luciferine for firely luciferase and an amino acid for the NRPSs) to

release a pyrophosphate and an adenylate intermediate bound to the enzyme. The adenylate intermediate reacts in a second partial reaction to release AMP (Figure 8) [188].

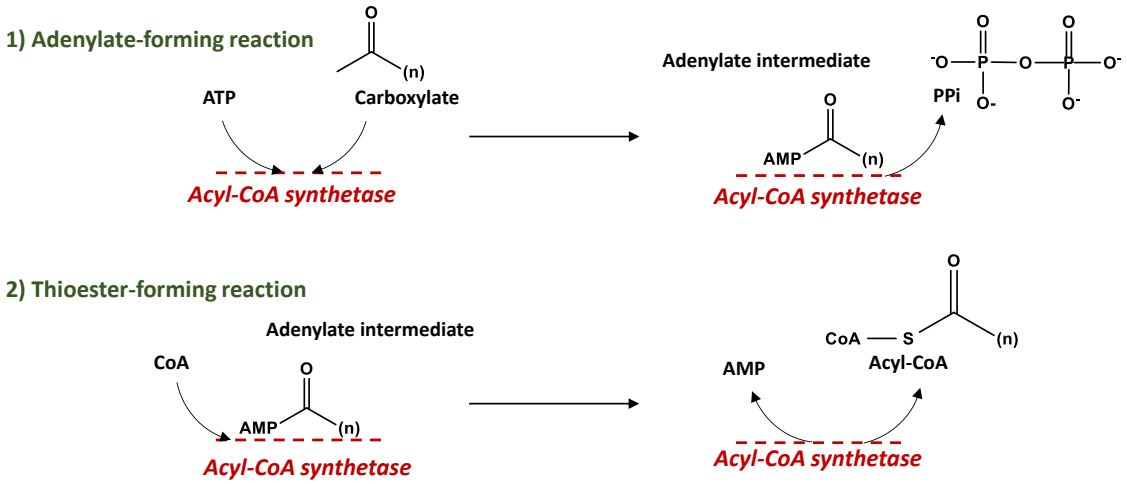

Figure 8. Acyl-CoA synthetases AMP-forming mechanism.

Acyl- and aryl-CoA synthetases are a family of enzymes responsible for the activation of carboxylates to form CoA ester derivatives. Acyl-CoA synthetases substrates are chemically very different in size (from acetate to long-fatty acids) and their metabolic role is essential to prokaryotes and eukaryotes organisms. Thus, in eukaryotes, fatty acids activation with CoA is an essential process to further the metabolism through anabolic (synthesis of lipids) or catabolic processes (mitochondrial β-oxidation). Eukaryotic organisms possess multiple acyl-CoA synthases with different fatty acid chain-length specificities (acetyl-CoA synthetase, short-chain acyl-CoA synthetases, medium-chain acyl-CoA synthetases, long-chain acyl-CoA synthetases and very long-chain acyl-CoA synthetases) [189]. In prokaryotes, the diversity of acyl-CoA synthetases is much lower. *E. coli* has several acyl-CoA synthetases for short-chain acids (acetyl-CoA synthetase, propionyl-CoA synthetase or malonyl-CoA synthetase) but a single medium and long-chain acyl-CoA synthetase, FadD [190] of broad substrate specificity. However, other prokaryotes such as mycobacteria have 36 FadD proteins known to date [191]. As regards aryl-CoA ligases, have been identified in a wide variety of enzymes for the degradation of aromatic compounds [192–194].

ANL structure and dynamic mechanism

ANL enzymes are formed by an overall two-domain architecture with a larger N-terminal domain and a smaller catalytic C-terminal domain, as was described since firefly luciferase crystal structure determination [195]. Detailed comparison of the conserved regions within the NRPS adenylation domains identified ten conserved regions, named A1-A10, some of which are conserved in all ANL members [196]. Subsequent to the structural determination of luciferase conformation, a number of additional enzyme structures in this family has been determined with different ligands. Thus, ANL enzymes adopt different conformations depending on the substrate to which they are bound. Two conformations have been observed for ANL enzymes: the adenylation conformation, responsible for the first step of the reaction [197–202], and the thioester-forming conformation, necessary to carry out the CoA binding [201–205]. These structures point to a dynamic mechanism involving a domain rearrangement that is strictly necessary for catalysis [188]. According to this mechanism, a flexible domain turns 140 ° to present opposing faces of the dynamic C-terminal domain to the active site. This turn implies that the catalytic amino acids in the two step are different [206].

Kinetic studies carried out with different ANL enzyme mutants have confirmed that the two partial reactions are catalytically independent and have also identified several important conserved amino acids for catalysis [197,199,207–211]. Thus, in the A3 motif there is a conserved sequence θθx(S/T)(S/T/G)G(S/T)TGxPK involved in ATP phosphates binding known as phosphate-binding-loop (P-loop), while in the A5 an aromatic residue interacts with the ATP adenine molecule and a glutamic acid interacts with a Mg^{2+} ion [201]. An aspartic acid in the A7 and an arginine from A8 motifs are involved in ATP ribose-binding [201] and a glycine, also from A8, participates in the thioester formation. Of special relevance is an invariant lysine from A10, which interacts with ATP phosphates. ANL A10 lysine mutants show a dramatic loss of activity for the beginning of the reaction, although the thioester formation catalytic capacity is not-altered [192,197,199,201,202,208–212].

Invariant A10 lysine has been demonstrated to be regulated by acetylation. This acetylation partially or totally blocks the adenylating capacity of the enzymes. Acyl-CoA synthetase acetylation was first discovered in *S. enterica* Acs (invariant K609 was acetylated) [63]. This acetylation blocked synthesis of the adenylate intermediate but did not affect the thioester-forming activity of the enzyme**.** Moreover, acetylation was reversed by the sirtuin

CobB. Two years later, the acetyltransferase Pat (*Se*Pat) was identified as being responsible for Acs acetylation in *S. enterica* [145]. To date, several acyl-CoA synthetases have been demonstrated to be regulated by acetylation-deacetylation catalysed by different acetyltransferases and sirtuins [164,165,213–217].

Acetyl-CoA synthetase

Acs is an ANL enzyme responsible for activating acetate to acetyl-CoA by consuming an ATP molecule. All cells, prokaryotic and eukaryotic, produce acetate. This acetate needs to be activated to acetyl-CoA before it can be incorporated in different metabolic pathways. Thus, Acs orthologues are found in bacteria, in some thermophilic archaea, and in eukaryotes, including fungi, plants and humans [218–222]. Moreover, Acs sequence is widely conserved in nature, which suggests a prokaryotic origin for eukaryotic Acs enzymes [223].

In *E. coli*, Acs activity is known to be regulated by acetylation and deacetylation catalysed by PatZ and CobB, respectively [64]. This regulation has been studied *in vivo*, although *in vitro* characterization has not been carried out. Recently, Acs acetylation by a non-enzymatic mechanism has been observed [108]. Thus, invariant A10 lysine K609 from Acs is acetylated, blocking the adenylating reaction, although this acetylation does not affect to the thioester forming step [175,224]. *E. coli* Acs is also capable of synthetizing propionyl-CoA from propionic acid and is propionylated in some lysines (K111, K221, and K609) [171,225]. Figure 9 shows the A1-A10 motifs present in *E. coli* Acs and the main catalytic residues identified by alignment.

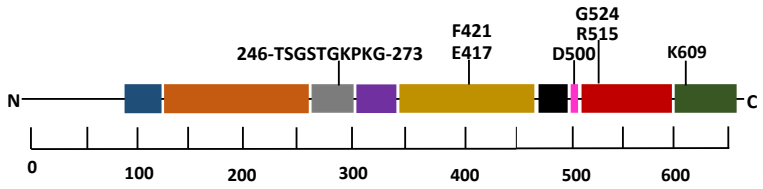

Figure 9. A1-A10 motifs present in *E. coli* Acs: A1 in blue, A2 in orange, A3 in grey (P-loop residues), A4 in purple, A5 in yellow (F421, E417 residues), A6 in black, and A7 in pink (D500 residue), A8 in red (G524 and R515 residues) and A10 in green (K609 residue). A9 motif is not conserved in *E. coli* Acs.

Due to the important role of *E. coli* Acs in extracellular acetate consumption, more research into this mechanism and its regulation is essential to continue optimizing the main biotechnological processes based on *E. coli* production.

References

1. Escherich T. The intestinal bacteria of the neonate and breast-fed infant. Rev Infect Dis. 1989;10: 1220–1225.

2. Finegold SM, Sutter VL, Mathisen GE. Normal indigenous intestinal flora. In: Press A, editor. Human Intestinal Microflora in Health and Disease. 1983. doi:10.1016/B978-0-12-341280-5.50007-0

3. Krogfelt KA, Cohen PS, Conway T. The life of commensal *Escherichia coli* in the mammalian intestine. EcoSal Plus. 2004;1. doi:10.1128/ecosalplus.8.3.1.2

4. Blount ZD. The unexhausted potential of *E. coli*. Elife. 2015;4: 1–12. doi:10.7554/eLife.05826

5. Crick F. Central Dogma of Molecular Biology. Nature. 1970;227: 561–563. doi:10.1038/227561a0

6. Kamionka M. Engineering of therapeutic proteins production in *Escherichia coli*. Curr Pharm Biotechnol. 2011;12: 268–274. doi:10.2174/138920111794295693

7. Huang C-J, Lin H, Yang X. Industrial production of recombinant therapeutics in *Escherichia coli* and its recent advancements. J Ind Microbiol Biotechnol. 2012;39: 383–399. doi:10.1007/s10295-011-1082-9

8. Lederberg J. Cell genetics and hereditary symbiosis. Physiol Rev. 1952;32: 403–430.

9. Novick R. The biology of plasmids. Trends Genet. 1997;13: 82–83. doi:10.1016/S0168-9525(97)84646-X

10. Preston A. Choosing a cloning vector. Methods Mol Biol. 2003;235: 19–26. doi:10.1385/1-59259-409-3:19

11. Vargas-Maya N, Franco B. *Escherichia coli* as a model organism and its application in biotechnology. In: INTECH, editor. Escherichia coli-Recent Aavances on pysiology, pathogenesis and biotechnological applications. 2017. doi:10.5772/67306

12. Baba T, Ara T, Hasegawa M, Takai Y, Okumura Y, Baba M, et al. Construction of *Escherichia coli* K-12 in-frame, single-gene knockout mutants: the Keio collection. Mol Syst Biol. 2006;2: 1–11. doi:10.1038/msb4100050

13. Karunakaran C, Rajkumar R, Bhargava K. Introduction to biosensors. Biosens Bioelectron. 2015;5: 1–68. doi:10.1016/B978-0-12-803100-1.00001-3

14. Truffer F, Buffi N, Merulla D, Beggah S, van Lintel H, Renaud P, et al. Compact portable biosensor for arsenic detection in aqueous samples with *Escherichia coli* bioreporter cells. Rev Sci Instrum. 2014;85: 1–4. doi:10.1063/1.4863333

15. Vollmer AC, Belkin S, Smulski DR, Van Dyk TK, Larossa R a. Detection of DNA damage by use of *Escherichia coli* carrying *recA*'::*lux*, *uvrA*'::*lux*, or *alkA*'::*lux* reporter plasmids. Appl Environ Microbiol. 1997;63: 2566–2571.

16. Vangnai AS, Kataoka N, Soonglerdsongpha S, Kalambaheti C, Tajima T, Kato J. Construction and application of an *Escherichia coli* bioreporter for aniline and chloroaniline detection. J Ind Microbiol Biotechnol. 2012;39: 1801–1810. doi:10.1007/s10295-012-1180-3

17. Lu C, Albano CR, Bentley WE, Rao G. Quantitative and kinetic study of oxidative stress

regulons using green fluorescent protein. Biotechnol Bioeng. 2005;89: 574–587. doi:10.1002/bit.20389

18. Padilla-Vaca F, Anaya-Velázquez F, Franco B. Synthetic biology: Novel approaches for microbiology. Int Microbiol. 2015;18: 71–84. doi:10.2436/20.1501.01.236

19. Huang HT. Production of L-threonine by auxotrophic mutants of *Escherichia coli*. Appl Microbiol. 1961;9: 419–424.

20. Riggs AD. Bacterial production of human insulin. Diabetes Care. 1981;4: 64–68.

21. Mohamed N. Baeshen. Production of biopharmaceuticals in *E. coli*: current scenario and future perspectives. J microbiolgy Biotechnol. 2014;25: 1–24. doi:10.4014/jmb.1405.05052

22. Becker J, Wittmann C. Systems metabolic engineering of *Escherichia coli* for the heterologous production of high value molecules — a veteran at new shores. Curr Opin Biotechnol. 2016;42: 178–188. doi:10.1016/j.copbio.2016.05.004

23. Breitmaier E. Terpenes : flavors, fragrances, pharmaca, pheromones. Weinheim, editor. WILEY-VCH; 2006. doi:10.1002/9783527609949

24. Ajikumar PK, Tyo K, Carlsen S, Mucha O, Phon TH, Stephanopoulos G. Terpenoids: opportunities for biosynthesis of natural product drugs using engineered microorganisms. Mol Pharm. 2008;5: 167–190. doi:10.1021/mp700151b

25. Chang W, Song H, Liu H, Pinghua L. Current development in isoprenoid biosynthesis and regulation. Curr Opin Chem Biol. 2014;17: 571–579. doi:10.1016/j.cbpa.2013.06.020

26. Rohmer M, Seemann M, Horbach S, Bringer-Meyer S, Sahm H. Glyceraldehyde 3-phosphate and pyruvate as precursors of isoprenic units in an alternative non-mevalonate pathway for terpenoid biosynthesis. J Am Chem Soc. 1996;118: 2564–2566. doi:10.1021/ja9538344

27. Sies H, Stahl W. Lycopene: antioxidant and biological effects and its bioavailability in the human. Proc Soc Exp Biol Med. 1998;218: 121–124.

28. Giovannucci E. A review of epidemiologic studies of tomatoes, lycopene, and prostate cancer. Exp Biol Med (Maywood). 2002;227: 852–859. doi:10.1177/153537020222701003

29. Bignotto L, Rocha J, Sepodes B, Eduardo-Figueira M, Pinto R, Chaud M, et al. Anti-inflammatory effect of lycopene on carrageenan-induced paw oedema and hepatic ischaemia–reperfusion in the rat. Br J Nutr. 2009;102: 126–134. doi:10.1017/S0007114508137886

30. Kim S, Keasling JD. Nonmevalonate isopentenyl diphosphate synthesis pathway in *Escherichia coli* enhances lycopene production. Biotechnol Bioeng. 2001;72: 408–415. doi:10.1002/1097-0290(20000220)72

31. Alper H, Miyaoku K, Stephanopoulos G. Characterization of lycopene-overproducing *E. coli* strains in high cell density fermentations. Appl Microbiol Biotechnol. 2006;72: 968–974. doi:10.1007/s00253-006-0357-y

32. Yuan LZ, Rouvière PE, Larossa R a, Suh W. Chromosomal promoter replacement of the isoprenoid pathway for enhancing carotenoid production in *E. coli*. Metab Eng. 2006;8: 79–90. doi:10.1016/j.ymben.2005.08.005

33. Rodríguez-Villalón A, Pérez-Gil J, Rodríguez-Concepción M. Carotenoid accumulation in bacteria with enhanced supply of isoprenoid precursors by upregulation of exogenous or endogenous pathways. J Biotechnol. 2008;135: 78–84. doi:10.1016/j.jbiotec.2008.02.023

34. Yoon K-W, Doo E-H, Kim S-W, Park J-B. *In situ recovery of lycopene during biosynthesis with recombinant Escherichia coli*. J Biotechnol. 2008;135: 291–294. doi:10.1016/j.jbiotec.2008.04.001

35. Zhou K, Zou R, Stephanopoulos G, Too H-P. Metabolite profiling identified methylerythritol cyclodiphosphate efflux as a limiting step in microbial isoprenoid production. PLoS One. 2012;7: e47513. doi:10.1371/journal.pone.0047513

36. Hayden JD, Brown LR, Gunawardena HP, Perkowski EF, Chen X, Braunstein M. Reversible acetylation regulates acetate and propionate metabolism in *Mycobacterium smegmatis*. Microbiology. 2013;159: 1986–1999. doi:10.1099/mic.0.068585-0

37. Martin VJJ, Pitera DJ, Withers ST, Newman JD, Keasling JD. Engineering a mevalonate pathway in *Escherichia coli* for production of terpenoids. Nat Biotechnol. 2003;21: 796–802. doi:10.1038/nbt833

38. Kim EM, Eom JH, Um Y, Kim Y, Woo HM. Microbial synthesis of myrcene by metabolically engineered *Escherichia coli*. J Agric Food Chem. 2015;63: 4606–4612. doi:10.1021/acs.jafc.5b01334

39. Yang L, Wang C, Zhou J, Kim SW. Combinatorial engineering of hybrid mevalonate pathways in *Escherichia coli* for protoilludene production. Microb Cell Fact. 2016;15: 1–8. doi:10.1186/s12934-016-0409-7

40. Zhu F, Zhong X, Hu M, Lu L, Deng Z, Liu T. *In vitro* reconstitution of mevalonate pathway and targeted engineering of farnesene overproduction in *Escherichia coli*. Biotechnol Bioeng. 2014;111: 1396–1405. doi:10.1002/bit.25198

41. Kong MK, Kang H-J, Kim JH, Oh SH, Lee PC. Metabolic engineering of the *Stevia rebaudiana* ent-kaurene biosynthetic pathway in recombinant *Escherichia coli*. J Biotechnol. 2015;214: 95–102. doi:10.1016/j.jbiotec.2015.09.016

42. Zhao J, Li Q, Sun T, Zhu X, Xu H, Tang J, et al. Engineering central metabolic modules of *Escherichia coli* for improving carotene production. Metab Eng. 2013;17: 42–50. doi:10.1016/j.ymben.2013.02.002

43. Lemuth K, Steuer K, Albermann C. Engineering of a plasmid-free *Escherichia coli* strain for improved *in vivo* biosynthesis of astaxanthin. Microb Cell Fact. 2011;10: 1–12. doi:10.1186/1475-2859-10-29

44. Li X-R, Tian G-Q, Shen H-J, Liu J-Z. Metabolic engineering of *Escherichia coli* to produce zeaxanthin. J Ind Microbiol Biotechnol. 2015;42: 627–636. doi:10.1007/s10295-014-1565-6

45. Kremling A, Geiselmann J, Ropers D, de Jong H. Understanding carbon catabolite repression in *Escherichia coli* using quantitative models. Trends Microbiol. 2015;23: 99–109. doi:10.1016/j.tim.2014.11.002

46. Görke B, Stülke J. Carbon catabolite repression in bacteria: many ways to make the most out of nutrients. Nat Rev Microbiol. 2008;6: 613–624. doi:10.1038/nrmicro1932

47. Bernal V, Castaño-Cerezo S, Cánovas M. Acetate metabolism regulation in *Escherichia*

coli: carbon overflow, pathogenicity, and beyond. Appl Microbiol Biotechnol. 2016;100: 8985–9001. doi:10.1007/s00253-016-7832-x

48. De Mey M, De Maeseneire S, Soetaert W, Vandamme E. Minimizing acetate formation in *E. coli* fermentations. J Ind Microbiol Biotechnol. 2007;34: 689–700. doi:10.1007/s10295-007-0244-2

49. Hädicke O, Bettenbrock K, Klamt S. Enforced ATP futile cycling increases specific productivity and yield of anaerobic lactate production in *Escherichia coli*. Biotechnol Bioeng. 2015;112: 2195–2199. doi:10.1002/bit.25623

50. Castaño-Cerezo S, Bernal V, Röhrig T, Termeer S, Cánovas M. Regulation of acetate metabolism in *Escherichia coli* BL21 by protein N-lysine acetylation. Appl Microbiol Biotechnol. 2015;99: 3533–3545. doi:10.1007/s00253-014-6280-8

51. Negrete A, Shiloach J. Constitutive expression of the sRNA GadY decreases acetate production and improves *E. coli* growth. Microb Cell Fact. 2015;14: 1–10. doi:10.1186/s12934-015-0334-1

52. Peebo K, Valgepea K, Maser A, Nahku R, Adamberg K, Vilu R. Proteome reallocation in *Escherichia coli* with increasing specific growth rate. Mol BioSyst. 2015;11: 1184–1193. doi:10.1039/C4MB00721B

53. Waegeman H, De Lausnay S, Beauprez J, Maertens J, De Mey M, Soetaert W. Increasing recombinant protein production in *Escherichia coli* K12 through metabolic engineering. N Biotechnol. 2013;30: 255–261. doi:10.1016/j.nbt.2011.11.008

54. Eiteman MA, Altman E. Overcoming acetate in *Escherichia coli* recombinant protein fermentations. Trends Biotechnol. 2006;24: 530–536. doi:10.1016/j.tibtech.2006.09.001

55. Brown TD. The enzymic interconversion of acetate and acetyl-coenzyme A in *Escherichia coli*. J Gen Microbiol. 1977;102: 327–336.

56. Castaño-Cerezo S, Pastor JM, Renilla S, Bernal V, Iborra JL, Cánovas M. An insight into the role of phosphotransacetylase (pta) and the acetate/acetyl-CoA node in *Escherichia coli*. Microb Cell Fact. 2009;8: 2109–2124. doi:10.1186/1475-2859-8-54

57. Kakuda H, Hosono K, Ichihara S. Identification and characterization of the *ackA* (acetate kinase a)-*pta* (phosphotransacetylase) operon and complementation analysis of acetate utilization by an *ackA*-*pta* deletion mutant of *Escherichia coli*. J Biochem. 1994;116: 916–922. doi:10.1093/oxfordjournals.jbchem.a124616

58. Shalel-Levanon S, San KY, Bennett GN. Effect of ArcA and FNR on the expression of genes related to the oxygen regulation and the glycolysis pathway in *Escherichia coli* under microaerobic growth conditions. Biotechnol Bioeng. 2005;92: 147–159. doi:10.1002/bit.20583

59. Kumari S, Tishel R, Eisenbach M, Wolfe AJ. Cloning, characterization, and functional expression of *acs*, the gene which encodes acetyl Coenzyme A synthetase in *Escherichia coli*. J Bacteriol. 1995;177: 2878–2886.

60. Starai VJ, Escalante-Semerena JC. Acetyl-coenzyme A synthetase (AMP forming). Cell Mol Life Sci. 2004;61: 2020–2030. doi:10.1007/s00018-004-3448-x

61. Valgepea K, Adamberg K, Nahku R, Lahtvee P-J, Arike L, Vilu R. Systems biology approach reveals that overflow metabolism of acetate in *Escherichia coli* is triggered by carbon catabolite repression of acetyl-CoA synthetase. BMC Syst Biol. 2010;4: 1–13.

doi:10.1186/1752-0509-4-166

62. Sclavi B, Beatty CM, Thach DS, Fredericks CE, Buckle M, Wolfe AJ. The multiple roles of CRP at the complex acs promoter depend on activation region 2 and IHF. Mol Microbiol. 2007;65: 425–440. doi:10.1111/j.1365-2958.2007.05797.x

63. Starai VJ, Celic I, Cole RN, Boeke JD, Escalante-Semerena JC. Sir2-dependent activation of acetyl-CoA synthetase by deacetylation of active lysine. Science. 2002;298: 2390–2392. doi:10.1126/science.1077650

64. Castaño-Cerezo S, Bernal V, Blanco-Catalá J, Iborra JL, Cánovas M. cAMP-CRP coordinates the expression of the protein acetylation pathway with central metabolism in *Escherichia coli*. Mol Microbiol. 2011;82: 1110–1128. doi:10.1111/j.1365-2958.2011.07873.x

65. Dittrich CR, Bennett GN, San K-Y. Characterization of the acetate-producing pathways in *Escherichia coli*. Biotechnol Prog. 2008;21: 1062–1067. doi:10.1021/bp050073s

66. Chang YY, Wang AY, Cronan JE. Expression of *Escherichia coli* pyruvate oxidase (PoxB) depends on the sigma factor encoded by the *rpoS*(*katF*) gene. Mol Microbiol. 1994;11: 1019–28.

67. Weber A, Kogl SA, Jung K. Time-dependent proteome alterations under osmotic stress during aerobic and anaerobic growth in *Escherichia coli*. J Bacteriol. 2006;188: 7165–7175. doi:10.1128/JB.00508-06

68. Martínez-Gómez K, Flores N, Castañeda HM, Martínez-Batallar G, Hernández-Chávez G, Ramírez OT, et al. New insights into *Escherichia coli* metabolism: Carbon scavenging, acetate metabolism and carbon recycling responses during growth on glycerol. Microb Cell Fact. 2012;11: 1–21. doi:10.1186/1475-2859-11-46

69. Yang X-J, Seto E. Lysine acetylation: codified crosstalk with other posttranslational modifications. Mol Cell. 2008;31: 449–461. doi:10.1016/j.molcel.2008.07.002

70. Prabakaran S, Lippens G, Steen H, Gunawardena J. Post-translational modification: Nature's escape from genetic imprisonment and the basis for dynamic information encoding. Wiley Interdiscip Rev Syst Biol Med. 2012;4: 565–583. doi:10.1002/wsbm.1185

71. Audagnotto M, Dal Peraro M. Protein post-translational modifications: *In silico* prediction tools and molecular modeling. Comput Struct Biotechnol J. 2017;15: 307–319. doi:10.1016/j.csbj.2017.03.004

72. Aebersold R, Mann M. Mass spectrometry-based proteomics. Nature. 2003;422: 198–207. doi:10.1038/nature01511

73. Phillips DMP. The presence of acetyl groups in histones. Biochem J. 1963;87: 258–263. doi:10.1042/bj0870258

74. Krebs G. Structure of the site phosphorylated phosphorylase B to a reaction. J Biol Chem. 1959;234: 1698–1705.

75. Verdin E, Ott M. 50 years of protein acetylation: from gene regulation to epigenetics, metabolism and beyond. Nat Rev Mol Cell Biol. 2014;16: 258–264. doi:10.1038/nrm3931

76. Polevoda B, Sherman F. N-terminal acetyltransferases and sequence requirements for N-terminal acetylation of eukaryotic proteins. J Mol Biol. 2003;325: 595–622.

77. Soppa J. Protein acetylation in archaea, bacteria, and eukaryotes. Archaea. 2010;20: 5399–5406. doi:10.1155/2010/820681

78. Choudhary C, Weinert BT, Nishida Y, Verdin E, Mann M. The growing landscape of lysine acetylation links metabolism and cell signalling. Nat Rev Mol Cell Biol. 2014;15: 536–550. doi:10.1038/nrm3841

79. Bernal V, Castaño-Cerezo S, Gallego-Jara J, Écija-Conesa A, de Diego T, Iborra JL, et al. Regulation of bacterial physiology by lysine acetylation of proteins. N Biotechnol. 2014;31: 586–595. doi:10.1016/j.nbt.2014.03.002

80. Baeza J, Smallegan MJ, Denu JM. Mechanisms and dynamics of protein acetylation in mitochondria. Trends Biochem Sci. 2016;41: 231–244. doi:10.1016/j.tibs.2015.12.006

81. Allfrey G, Faulkner R, Mirsky AE. Acetylation and methylation of histones and their possible role in the regulation of RNA synthesis. Biochemistry. 1964;315: 786–794.

82. Bannister AJ, Kouzarides T. Regulation of chromatin by histone modifications. Cell Res. 2011;21: 381–395. doi:10.1038/cr.2011.22

83. Okanishi H, Kim K, Masui R, Kuramitsu S. Acetylome with structural mapping reveals the significance of lysine acetylation in *Thermus thermophilus*. J Proteome Res. 2013;12: 3952–3968. doi:10.1021/pr400245k

84. Kim D, Yu BJ, Kim JA, Lee YJ, Choi SG, Kang S, et al. The acetylproteome of Gram-positive model bacterium *Bacillus subtilis*. Proteomics. 2013;13: 1726–1736. doi:10.1002/pmic.201200001

85. Xie L, Wang X, Zeng J, Zhou M, Duan X, Li Q, et al. Proteome-wide lysine acetylation profiling of the human pathogen *Mycobacterium tuberculosis*. Int J Biochem Cell Biol. 2015;59: 193–202. doi:10.1016/j.biocel.2014.11.010

86. Kim SC, Sprung R, Chen Y, Xu Y, Ball H, Pei J, et al. Substrate and functional diversity of lysine acetylation revealed by a proteomics survey. Mol Cell. 2006;23: 607–618. doi:10.1016/j.molcel.2006.06.026

87. Wagner GR, Payne RM. Widespread and enzyme-independent Nε-acetylation and Nε-succinylation of proteins in the chemical conditions of the mitochondrial matrix. J Biol Chem. 2013;288: 29036–29045. doi:10.1074/jbc.M113.486753

88. Zhao S, Xu W, Jiang W, Yu W, Lin Y, Zhang T, et al. Regulation of cellular metabolism by protein lysine acetylation. Science. 2010;327: 1000–1004. doi:10.1126/science.1179689

89. Castaño-Cerezo S, Bernal V, Post H, Fuhrer T, Cappadona S, Sanchez-Diaz N, et al. Protein acetylation affects acetate metabolism, motility and acid stress response in *Escherichia coli*. Mol Syst Biol. 2014;762: 1–16. doi:10.15252/msb.20145227

90. Friedmann DR, Marmorstein R. Structure and mechanism of non-histone protein acetyltransferase enzymes. FEBS J. 2013;280: 5570–5581. doi:10.1111/febs.12373

91. Yuan H, Marmorstein R. Histone acetyltransferases: rising ancient counterparts to protein kinases. Biopolymers. 2013;99: 98–111. doi:10.1002/bip.22128

92. Su D, Hu Q, Zhou H, Thompson JR, Xu RM, Zhang Z, et al. Structure and histone binding properties of the Vps75-Rtt109 chaperone-lysine acetyltransferase complex. J Biol Chem. 2011;286: 15625–15629. doi:10.1074/jbc.C111.220715

93. Kolonko EM, Albaugh BN, Lindner SE, Chen Y, Satyshur K a., Arnold KM, et al. Catalytic activation of histone acetyltransferase Rtt109 by a histone chaperone. Proc Natl Acad Sci. 2010;107: 20275–20280. doi:10.1073/pnas.1009860107

94. Tanner KG, Langer MR, Kim Y, Denu JM. Kinetic mechanism of the histone acetyltransferase GCN5 from yeast. J Biol Chem. 2000;275: 22048–22055. doi:10.1074/jbc.M002893200

95. Berndsen CE, Albaugh BN, Tan S, Denu JM. Catalytic mechanism of a MYST family histone acetyltransferase. Biochemistry. 2007;46: 623–629. doi:10.1021/bi602513x

96. Liu X, Wang L, Zhao K, Thompson PR, Hwang Y, Marmorstein R, et al. The structural basis of protein acetylation by the p300/CBP transcriptional coactivator. Nature. 2008;451: 846–850. doi:10.1038/nature06546

97. Hinnebusch AG, Fink GR. Positive regulation in the general amino acid control of *Saccharomyces cerevisiae*. Proc Natl Acad Sci U S A. 1983;80: 5374–5378.

98. Tanner KG. Catalytic mechanism and function of invariant glutamic acid 173 from the histone acetyltransferase GCN5 transcriptional coactivator. J Biol Chem. 1999;274: 18157–18160. doi:10.1074/jbc.274.26.18157

99. Dyda F, Klein DC, Hickman AB. GCN5-Related N-acetyltransferases: a structural overview. Annu Rev Biophys Biomol Struct. 2000;29: 81–103. doi:10.1146/annurev.biophys.29.1.81

100. Rezácová P, Borek D, Moy SF, Joachimiak A, Otwinowski Z. Crystal structure and putative function of small Toprim domain-containing protein from *Bacillus stearothermophilus*. Proteins. 2008;70: 311–319. doi:10.1002/prot

101. Jiang J, Lu J, Lu D, Liang Z, Li L, Ouyang S, et al. Investigation of the acetylation mechanism by GCN5 histone acetyltransferase. PLoS One. 2012;7: e36660. doi:10.1371/journal.pone.0036660

102. Rardin MJ, Newman JC, Held JM, Cusack MP, Sorensen DJ, Li B, et al. Label-free quantitative proteomics of the lysine acetylome in mitochondria identifies substrates of SIRT3 in metabolic pathways. Proc Natl Acad Sci. 2013;110: 6601–6606. doi:10.1073/pnas.1302961110

103. Sol EM, Wagner S a., Weinert BT, Kumar A, Kim HS, Deng CX, et al. Proteomic investigations of lysine acetylation identify diverse substrates of mitochondrial deacetylase Sirt3. PLoS One. 2012;7: e50545. doi:10.1371/journal.pone.0050545

104. Paik WK, Pearson D, Lee HW, Kim S. Nonenzymatic acetylation of histones with acetyl-CoA. BBA. 1970;213: 513–522. doi:10.1016/0005-2787(70)90058-4

105. Schwer B, Eckersdorff M, Li Y, Silva JC, Fermin D, Kurtev V, et al. Calorie restriction alters mitochondrial protein acetylation. Aging Cell. 2010;8: 604–606. doi:10.1111/j.1474-9726.2009.00503.x

106. Hebert AS, Dittenhafer-Reed KE, Yu W, Bailey DJ, Selen ES, Boersma MD, et al. Calorie restriction and SIRT3 trigger global reprogramming of the mitochondrial protein acetylome. Mol Cell. 2013;49: 186–199. doi:10.1016/j.molcel.2012.10.024

107. Kuo Y-M, Andrews AJ. Quantitating the specificity and selectivity of Gcn5-mediated acetylation of histone H3. PLoS One. 2013;8: e54896. doi:10.1371/journal.pone.0054896

108. Kuhn ML, Zemaitaitis B, Hu LI, Sahu A, Sorensen D, Minasov G, et al. Structural, kinetic and proteomic characterization of acetyl phosphate-dependent bacterial protein acetylation. PLoS One. 2014;9: e94816. doi:10.1371/journal.pone.0094816

109. Weinert BT, Iesmantavicius V, Wagner SA, Schölz C, Gummesson B, Beli P, et al. Acetyl-phosphate is a critical determinant of lysine acetylation in *E. coli*. Mol Cell. 2013;51: 265–

272. doi:10.1016/j.molcel.2013.06.003

110. Pisithkul T, Patel NM, Amador-Noguez D. Post-translational modifications as key regulators of bacterial metabolic fluxes. Curr Opin Microbiol. 2015;24: 29–37. doi:10.1016/j.mib.2014.12.006

111. Wang MM, You D, Ye BC. Site-specific and kinetic characterization of enzymatic and nonenzymatic protein acetylation in bacteria. Sci Rep. 2017;7: 1–12. doi:10.1038/s41598-017-13897-w

112. Baeza J, Smallegan MJ, Denu JM. Site-specific reactivity of nonenzymatic lysine acetylation. ACS Chem Biol. 2015;10: 122–128. doi:10.1021/cb500848p

113. James AM, Hoogewijs K, Logan A, Hall AR, Ding S, Fearnley IM, et al. Non-enzymatic N-acetylation of lysine residues by acetyl-CoA often occurs *via* a proximal S-acetylated thiol intermediate sensitive to glyoxalase II. Cell Rep. 2017;18: 2105–2112. doi:10.1016/j.celrep.2017.02.018

114. Gregoretti I V, Lee Y-M, Goodson H V. Molecular evolution of the histone deacetylase family: functional implications of phylogenetic analysis. J Mol Biol. 2004;338: 17–31. doi:10.1016/j.jmb.2004.02.006

115. Frye RA. Phylogenetic classification of prokaryotic and eukaryotic Sir2-like proteins. Biochem Biophys Res Commun. 2000;273: 793–798. doi:10.1006/bbrc.2000.3000

116. Cosgrove MS, Bever K, Avalos JL, Muhammad S, Zhang X, Wolberger C. The structural basis of sirtuin substrate affinity. Biochemistry. 2006;45: 7511–7521. doi:10.1021/bi0526332

117. Yuan H, Marmorstein R. Structural basis for Sirtuin activity and inhibition. J Biol Chem. 2012;287: 42428–42435. doi:10.1074/jbc.R112.372300

118. Landry J, Sutton A, Tafrov ST, Heller RC, Stebbins J, Pillus L, et al. The silencing protein SIR2 and its homologs are NAD-dependent protein deacetylases. Proc Natl Acad Sci U S A. 2000;97: 5807–5811. doi:10.1073/pnas.110148297

119. Sauve A a., Celic I, Avalos J, Deng H, Boeke JD, Schramm VL. Chemistry of gene silencing: the mechanism of NAD^+ -dependent deacetylation reactions. Biochemistry. 2001;40: 15456–15463. doi:10.1021/bi011858j

120. Chang JH, Kim HC, Hwang KY, Lee JW, Jackson SP, Bell SD, et al. Structural basis for the NAD-dependent deacetylase mechanism of Sir2. J Biol Chem. 2002;277: 34489–34498. doi:10.1074/jbc.M205460200

121. Borra MT, Langer MR, Slama JT, Denu JM. Substrate specificity and kinetic mechanism of the Sir2 family of deacetylases. Biochemistry. 2004;43: 9877–9887. doi:10.1021/bi049592e

122. Jackson MD, Schmidt MT, Oppenheimer NJ, Denu JM. Mechanism of nicotinamide inhibition and transglycosidation by Sir2 histone/protein deacetylases. J Biol Chem. 2003;278: 50985–50998. doi:10.1074/jbc.M306552200

123. Landry J, Slama JT, Sternglanz R. Role of NAD+in the deacetylase activity of the SIR2-like proteins. Biochem Biophys Res Commun. 2000;278: 685–690. doi:10.1006/bbrc.2000.3854

124. Frye RA. Characterization of five human cDNAs with homology to the yeast SIR2 gene: Sir2-like proteins (sirtuins) metabolize NAD and may have protein ADP-ribosyltransferase

activity. Biochem Biophys Res Commun. 1999;260: 273–279. doi:10.1006/bbrc.1999.0897

125. Jiang H, Khan S, Wang Y, Charron G, He B, Sebastian C, et al. Sirt6 regulates TNFα secretion *via* hydrolysis of long chain fatty acyl lysine. Nature. 2013;496: 110–113. doi:10.1038/nature12038

126. Feldman JL, Baeza J, Denu JM. Activation of the protein deacetylase SIRT6 by long-chain fatty acids and widespread deacylation by mammalian sirtuins. J Biol Chem. 2013;288: 31350–31356. doi:10.1074/jbc.C113.511261

127. Feldman JL, Dittenhafer-Reed KE, Kudo N, Thelen JN, Ito A, Yoshida M, et al. Kinetic and structural basis for acyl-group selectivity and NAD^+ dependence in sirtuin-catalyzed deacylation. Biochemistry. 2015;54: 3037–3050. doi:10.1021/acs.biochem.5b00150

128. Chen B, Zang W, Wang J, Huang Y, He Y, Yan L, et al. The chemical biology of sirtuins. Chem Soc Rev. 2015;5246: 5246–5264. doi:10.1039/c4cs00373j

129. Morris BJ. Seven sirtuins for seven deadly diseases of aging. Free Radic Biol Med. 2013;56: 133–171. doi:10.1016/j.freeradbiomed.2012.10.525

130. Guarente L. The many faces of sirtuins: Sirtuins and the warburg effect. Nat Med. 2014;20: 24–25. doi:10.1038/nm.3438

131. Sebastián C, Zwaans BMM, Silberman DM, Gymrek M, Goren A, Zhong L, et al. The histone deacetylase SIRT6 is a tumor suppressor that controls cancer metabolism. Cell. 2012;151: 1185–1199. doi:10.1016/j.cell.2012.10.047

132. Kleszcz R, Paluszczak J, Baer-Dubowska W. Targeting aberrant cancer metabolism - The role of sirtuins. Pharmacol Reports. 2015;67: 1068–1080. doi:10.1016/j.pharep.2015.03.021

133. Bitterman KJ, Anderson RM, Cohen HY, Latorre-Esteves M, Sinclair DA. Inhibition of silencing and accelerated aging by nicotinamide, a putative negative regulator of yeast Sir2 and human SIRT1. J Biol Chem. 2002;277: 45099–45107. doi:10.1074/jbc.M205670200

134. Guan X, Lin P, Knoll E, Chakrabarti R. Mechanism of inhibition of the human sirtuin enzyme SIRT3 by nicotinamide : computational and experimental studies. PLoS One. 2014;9: e0136127. doi:10.1371/journal.pone.0107729

135. Avalos JL, Bever KM, Wolberger C. Mechanism of sirtuin inhibition by nicotinamide: Altering the NAD^+ cosubstrate specificity of a Sir2 enzyme. Mol Cell. 2005;17: 855–868. doi:10.1016/j.molcel.2005.02.022

136. Wang T, Cui H, Ma N, Jiang Y. Nicotinamide-mediated inhibition of SIRT1 deacetylase is associated with the viability of cancer cells exposed to antitumor agents and apoptosis. Oncol Lett. 2013;6: 600–604. doi:10.3892/ol.2013.1400

137. Fischer F, Gertz M, Suenkel B, Lakshminarasimhan M, Schutkowski M, Steegborn C. Sirt5 deacylation activities show differential sensitivities to nicotinamide inhibition. PLoS One. 2012;7: e45098. doi:10.1371/journal.pone.0045098

138. David, A LG. Small molecule allosteric activator of sirtuins. Annu Rev Pharmacol Toxicol. 2014;54: 363–380. doi:10.1146/annurev-pharmtox-010611-134657.

139. Cao D, Wang M, Qiu X, Liu D, Jiang H, Yang N, et al. Structural basis for allosteric, substrate- dependent stimulation of SIRT1 activity by resveratrol. Genes Dev. 2015;29:

1316–1325. doi:10.1101/gad.265462.115.

140. Schilling B, Christensen D, Davis R, Sahu AK, Hu LI, Walker-Peddakotla A, et al. Protein acetylation dynamics in response to carbon overflow in *Escherichia coli*. Mol Microbiol. 2015;98: 847–863. doi:10.1111/mmi.13161

141. Castaño-Cerezo S, Bernal V, Post H, Fuhrer T, Cappadona S, Sánchez-Díaz NC, et al. Protein acetylation affects acetate metabolism, motility and acid stress response in *Escherichia coli*. Mol Syst Biol. 2014;10: 1–16. doi:10.15252/msb.20145227

142. Zhang J, Sprung R, Pei J, Tan X, Kim S, Zhu H, et al. Lysine acetylation is a highly abundant and evolutionarily conserved modification in *Escherichia coli*. Mol Cell Proteomics. 2009;8: 215–225. doi:10.1074/mcp.M800187-MCP200

143. Yu BJ, Kim JA, Moon JH, Ryu SE, Pan JG. The diversity of lysine-acetylated proteins in *Escherichia coli*. J Microbiol Biotechnol. 2008;18: 1529–1536.

144. Zhang K, Zheng S, Yang JS, Chen Y, Cheng Z. Comprehensive profiling of protein lysine acetylation in *Escherichia coli*. J Proteome Res. 2013;12: 844–851. doi:10.1021/pr300912q

145. Starai VJ, Escalante-Semerena JC. Identification of the protein acetyltransferase (Pat) enzyme that acetylates acetyl-CoA synthetase in *Salmonella enterica*. J Mol Biol. 2004;340: 1005–1012. doi:10.1016/j.jmb.2004.05.010

146. Wolfe AJ. The Acetate Switch. Microbiol Mol Biol Rev. 2005;69: 12–50. doi:10.1128/MMBR.69.1.12

147. Liarzi O, Barak R, Bronner V, Dines M, Sagi Y, Shainskaya A, et al. Acetylation represses the binding of CheY to its target proteins. Mol Microbiol. 2010;76: 932–943. doi:10.1111/j.1365-2958.2010.07148.x

148. Thao S, Chen C-S, Zhu H, Escalante-Semerena JC. Nε-lysine acetylation of a bacterial transcription factor inhibits Its DNA-binding activity. PLoS One. 2010;5: e15123. doi:10.1371/journal.pone.0015123

149. Venkat S, Gregory C, Gan Q, Fan C. Biochemical characterization of the lysine acetylation of tyrosyl-tRNA synthetase in *Escherichia coli*. ChemBioChem. 2017;18: 1928–1934. doi:10.1002/cbic.201700343

150. Li S, Zhang Q, Xu Z, Yao YF. Acetylation of lysine 243 inhibits the oriC binding ability of DnaA in *Escherichia coli*. Front Microbiol. 2017;8: 1–10. doi:10.3389/fmicb.2017.00699

151. Sun M, Guo H, Lu G, Gu J, Wang X, Zhang X, et al. Lysine acetylation regulates the activity of *Escherichia coli* S-adenosylmethionine synthase. Acta Biochim Biophys Sin (Shanghai). 2016;48: 723–731. doi:10.1093/abbs/gmw066

152. Zhang Q-F, Zhang Q, Gu J, Gong P, Wang X-D, Wang X, et al. Reversibly acetylated lysine residues play important roles in the enzymatic activity of *Escherichia coli* N-hydroxyarylamine O-acetyltransferase. FEBS J. 2013;280: 1966–1979. doi:10.1111/febs.12216

153. Lima BP, Thanh Huyen TT, Bäsell K, Becher D, Antelmann H, Wolfe AJ. Inhibition of acetyl phosphate-dependent transcription by an acetylatable lysine on RNA polymerase. J Biol Chem. 2012;287: 32147–32160. doi:10.1074/jbc.M112.365502

154. Lima BP, Antelmann H, Katrin G, Khanh Chi B, Becher D, Brinsmade SR, et al. Involvement of protein acetylation in glucose-induced transcription of a stress-responsive promoter.

Mol Microbiol. 2011;81: 1190–1204. doi:10.1111/j.1365-2958.2011.07742.x

155. Christensen DG, Orr JS, Rao C V, Wolfe J. Increasing growth yield and decreasing acetylation in *Escherichia coli* by optimizing the carbon-to-magnesium ratio in peptide-based media. Appl Environ Microbiol. 2017;83: 1–13. doi:10.1128/AEM.03034-16

156. Dyda F, Klein DC, Hickman AB. GCN5-related N-acetyltransferases: a structural overview. Annu Rev Biophys Biomol Struct. 2000;29: 81–103. doi:10.1146/annurev.biophys.29.1.81

157. Garrity J, Gardner JG, Hawse W, Wolberger C, Escalante-Semerena JC. N-lysine propionylation controls the activity of propionyl-CoA synthetase. J Biol Chem. 2007;282: 30239–30245. doi:10.1074/jbc.M704409200

158. Wang Q, Zhang Y, Yang C, Xiong H, Lin Y, Yao J, et al. Acetylation of metabolic enzymes coordinates carbon source utilization and metabolic flux. Science. 2010;327: 1004–1007. doi:10.1126/science.1179687

159. Hung CC, Eade CR, Altier C. The protein acyltransferase Pat post-transcriptionally controls HilD to repress *Salmonella* invasion. Mol Microbiol. 2016;102: 121–136. doi:10.1111/mmi.13451

160. Gardner JG, Grundy FJ, Henkin TM, Escalante-Semerena JC. Control of acetyl-Coenzyme A synthetase (AcsA) activity by acetylation/deacetylation without NAD $^{+}$involvement in *Bacillus subtilis*. J Bacteriol. 2006;188: 5460–5468. doi:10.1128/JB.00215-06

161. Gardner JG, Escalante-Semerena JC. In *Bacillus subtilis*, the sirtuin protein deacetylase, encoded by the srtN gene (formerly *yhdZ*), and functions encoded by the acuABC genes control the activity of acetyl coenzyme a synthetase. J Bacteriol. 2009;191: 1749–1755. doi:10.1128/JB.01674-08

162. Crosby HA, Rank KC, Rayment I, Escalante-Semerena JC. Structural insights into the substrate specificity of the *Rhodopseudomonas palustris* protein acetyltransferase RpPat: identification of a loop critical for recognition by RpPat. J Biol Chem. 2012;287: 41392–41404. doi:10.1074/jbc.M112.417360

163. Tucker AC, Escalante-Semerena JC. Acetoacetyl-CoA synthetase activity is controlled by a protein acetyltransferase with unique domain organization in *Streptomyces lividans*. Mol Microbiol. 2013;49: 1841–1850. doi:10.1016/j.jacc.2007.01.076

164. Hua Xu, Subray S. Hegde and JSB. The reversible acetylation and inactivation of *Mycobacterium tuberculosis* acetyl-CoA synthetase is dependent on cAMP. Biochemistry. 2011;50: 5883–5892. doi:10.1021/bi200156

165. Nambi S, Gupta K, Bhattacharya M, Ramakrishnan P, Ravikumar V, Siddiqui N, et al. Cyclic AMP-dependent protein lysine acylation in *Mycobacteria* regulates fatty acid and propionate metabolism. J Biol Chem. 2013;288: 14114–14124. doi:10.1074/jbc.M113.463992

166. Liang W, Deutscher MP. Post-translational modification of RNase R is regulated by stress-dependent reduction in the acetylating enzyme Pka (YfiQ). RNA. 2012;18: 37–41. doi:10.1261/rna.030213.111

167. Song L, Wang G, Malhotra A, Deutscher MP, Liang W. Reversible acetylation on Lys501 regulates the activity of RNase II. Nucleic Acids Res. 2016;44: 1979–1988. doi:10.1093/nar/gkw053

168. Zhang Q, Zhou A, Li S, Ni J, Tao J, Lu J, et al. Reversible lysine acetylation is involved in

DNA replication initiation by regulating activities of initiator DnaA in *Escherichia coli*. Sci Rep. 2016;6: 1–13. doi:10.1038/srep30837

169. Thao S, Escalante-semerena JC. Biochemical and thermodynamic analyses of *Salmonella enterica* Pat , a multidomain , multimeric N -Lysine acetyltransferase involved in carbon and energy metabolism. MBio. 2011;2: 1–8. doi:10.1128/mBio.00216-11

170. Tucker AC, Taylor KC, Rank KC, Rayment I, Escalante-Semerena JC. Insights into the specificity of lysine acetyltransferases. J Biol Chem. 2014;289: 36249–36262. doi:10.1074/jbc.M114.613901

171. Sun M, Xu J, Wu Z, Zhai L, Liu C, Cheng Z, et al. Characterization of protein lysine propionylation in *Escherichia coli*: global profiling, dynamic change, and enzymatic regulation. J Proteome Res. 2016;15: 4696–4708. doi:10.1021/acs.jproteome.6b00798

172. Baron S, Eisenbach M. CheY acetylation is required for ordinary adaptation time in *Escherichia coli* chemotaxis. FEBS Lett. 2017;591: 1958–1965. doi:10.1002/1873-3468.12699

173. Barak R, Prasad K, Shainskaya A, Wolfe AJ, Eisenbach M. Acetylation of the chemotaxis response regulator CheY by acetyl-CoA synthetase purified from *Escherichia coli*. J Mol Biol. 2004;342: 383–401. doi:10.1016/j.jmb.2004.07.020

174. Tu S, Guo SJ, Chen CS, Liu CX, Jiang HW, Ge F, et al. YcgC represents a new protein deacetylase family in prokaryotes. Elife. 2015;4: 1–17. doi:10.7554/eLife.05322

175. Zhao K, Chai X, Marmorstein R. Structure and substrate binding properties of CobB, a Sir2 homolog protein deacetylase from *Escherichia coli*. J Mol Biol. 2004;337: 731–741. doi:10.1016/j.jmb.2004.01.060

176. Li R, Gu J, Chen YY, Xiao C Le, Wang LW, Zhang ZP, et al. CobB regulates *Escherichia coli* chemotaxis by deacetylating the response regulator CheY. Mol Microbiol. 2010;76: 1162–1174. doi:10.1111/j.1365-2958.2010.07125.x

177. Hu LI, Chi BK, Kuhn ML, Filippova E V, Walker-Peddakotla AJ, Bäsell K, et al. Acetylation of the response regulator RcsB controls transcription from a small RNA promoter. J Bacteriol. 2013;195: 4174–4186. doi:10.1128/JB.00383-13

178. Abouelfetouh A, Kuhn ML, Hu LI, Scholle MD, Sorensen DJ, Sahu AK, et al. The *E. coli* sirtuin CobB shows no preference for enzymatic and nonenzymatic lysine acetylation substrate sites. Microbiol Open. 2015;4: 66–83. doi:10.1002/mbo3.223

179. Garske AL, Denu JM. SIRT1 top hits: Use of one-bead, one-compound acetyl-peptide libraries and quantum dots to probe deacetylase specificity. Biochemistry. 2006;10: 94–101. doi:10.1038/nature13314.A

180. Blander G, Olejnik J, Krzymanska-Olejnik E, McDonagh T, Haigis M, Yaffe MB, et al. SIRT1 shows no substrate specificity *in vitro*. J Biol Chem. 2005;280: 9780–9785. doi:10.1074/jbc.M414080200

181. Gurard-Levis ZA, Kilian KA, Kim J, Bähr K, Mrksich M. Peptide arrays identify isoform-selective substrates for profiling endogenous lysine deacetylase activity. ACS Chem Biol. 2010;5: 863–873. doi:10.1021/cb100088g

182. Rauh D, Fischer F, Gertz M, Lakshminarasimhan M, Bergbrede T, Aladini F, et al. An acetylome peptide microarray reveals specificities and deacetylation substrates for all human sirtuin isoforms. Nat Commun. 2013;4: 2327–2342. doi:10.1038/ncomms3327

183. Smith BC, Settles B, Hallows WC, Craven MW, Denu JM. SIRT3 substrate specificity determined by peptide arrays and machine learning. ACS Chem Biol. 2011;6: 146–157. doi:10.1021/cb100218d

184. Khan AN, Lewis PN. Unstructured conformations are a substrate requirement for the Sir2 family of NAD-dependent protein deacetylases. J Biol Chem. 2005;280: 36073–36078. doi:10.1074/jbc.M508247200

185. Baeza J, Dowell JA, Smallegan MJ, Fan J, Amador-Noguez D, Khan Z, et al. Stoichiometry of site-specific lysine acetylation in an entire proteome. J Biol Chem. 2014;289: 21326–21338. doi:10.1074/jbc.M114.581843

186. Bheda P, Jing H, Wolberger C, Lin H. The substrate specificity of sirtuins. Annu Rev Biochem. 2016;85: 405–429. doi:10.1146/annurev-biochem-060815-014537

187. Knyphausen P, De Boor S, Kuhlmann N, Scislowski L, Extra A, Baldus L, et al. Insights into lysine deacetylation of natively folded substrate proteins by sirtuins. J Biol Chem. 2016;291: 14677–14694. doi:10.1074/jbc.M116.726307

188. Gulick AM. Conformational dynamics in the acyl-CoA synthetases, adenylation domains of non-ribosomal peptide synthetases, and firefly luciferase. ACS Chem Biol. 2009;4: 811–827. doi:10.1021/cb900156h

189. Watkins PA. Fatty acid activation. Prog Lipid Res. 1997;36: 55–83. doi:10.1016/S0163-7827(97)00004-0

190. Fujita Y, Matsuoka H, Hirooka K. Regulation of fatty acid metabolism in bacteria. Mol Microbiol. 2007;66: 829–839. doi:10.1111/j.1365-2958.2007.05947.x

191. Trivedi OA, Arora P, Sridharan V, Tickoo R, Mohanty D, Gokhale RS. Enzymic activation and transfer of fatty acids as acyl-adenylates in *Mycobacteria*. Lett to Nat. 2004;428: 4–6. doi:10.1038/nature02406.1.

192. Law A, Boulanger MJ. Defining a structural and kinetic rationale for paralogous copies of phenylacetate-CoA ligases from the cystic fibrosis pathogen *Burkholderia cenocepacia* J2315. J Biol Chem. 2011;286: 15577–15585. doi:10.1074/jbc.M111.219683

193. Tian Y, Suk D-H, Cai F, Crich D, Mesecar AD. *Bacillus anthracis* O-succinylbenzoyl-CoA synthetase: reaction kinetics and a novel inhibitor mimicking its reaction intermediate. Biochemistry. 2008;47: 12434–12447. doi:10.1016/j.neuron.2009.10.017.A

194. Abe-Yoshizumi R, Kamei U, Yamada A, Kimura M, Ichihara S, Di E, et al. Biodegradation of aromatic compounds by *Escherichia coli*. BMC Bioinformatics. 2014;5: 109–125. doi:10.1128/MMBR.65.4.523

195. Conti E, Franks NP, Brick P. Crystal structure of firefly luciferase throws light on a super-family of adenylate-forming enzymes. Structure. 1996;4: 287–298. doi:10.1016/S0969-2126(96)00033-0

196. Marahiel MA, Stachelhaus T, Mootz HD. Modular peptide synthetases involved in nonribosomal peptide synthesis. Chem Rev. 1997;97: 2651–2674. doi:10.1021/cr960029e

197. Crosby HA, Rank KC, Rayment I, Escalante-Semerena JC. Structure-guided expansion of the substrate range of methylmalonyl Coenzyme A synthetase (MatB) of *Rhodopseudomonas palustris*. Appl Environ Microbiol. 2012;78: 6619–6629. doi:10.1128/AEM.01733-12

198. Chen Y, Jiang Y, Guo Z. Mechanistic insights from the crystal structure of *Bacillus subtilis* O-succinylbenzoyl-CoA synthetase complexed with the adenylate intermediate. Biochemistry. 2016;55: 6685–6695. doi:10.1021/acs.biochem.6b00889

199. Osman KT, Du L, He Y, Luo Y. Crystal structure of *Bacillus cereus* D-alanyl carrier protein ligase (DltA) in complex with ATP. J Mol Biol. 2009;388: 345–355. doi:10.1016/j.jmb.2009.03.040

200. Hisanaga Y, Ago H, Nakagawa N, Hamada K, Ida K, Yamamoto M, et al. Structural basis of the substrate-specific two-step catalysis of long chain fatty acyl-CoA synthetase dimer. J Biol Chem. 2004;279: 31717–31726. doi:10.1074/jbc.M400100200

201. Kochan G, Pilka ES, von Delft F, Oppermann U, Yue WW. Structural snapshots for the conformation-dependent catalysis by human medium-chain acyl-Coenzyme A synthetase ACSM2A. J Mol Biol. 2009;388: 997–1008. doi:10.1016/j.jmb.2009.03.064

202. Scaglione A, Fullone MR, Montemiglio LC, Parisi G, Zamparelli C, Vallone B, et al. Structure of the adenylation domain Thr1 involved in the biosynthesis of 4-chlorothreonine in *Streptomyces sp.* OH-5093—protein flexibility and molecular bases of substrate specificity. FEBS J. 2017;284: 2981–2999. doi:10.1111/febs.14163

203. Gulick AM, Starai VJ, Horswill AR, Homick KM, Escalante-semerena JC. The 1 . 75 Å crystal structure of acetyl-CoA synthetase bound to adenosine-5 ′ -propylphosphate and Coenzyme A. Biochemistry. 2003;42: 2866–2873. doi:10.1021/bi0271603

204. Sundlov J a., Fontaine DM, Southworth TL, Branchini BR, Gulick AM. Crystal structure of firefly luciferase in a second catalytic conformation supports a domain alternation mechanism. Biochemistry. 2012;51: 6493–6495. doi:10.1021/bi300934s

205. Shah MB, Ingram-smith C, Cooper LL, Qu J, Meng Y, Kerry S, et al. The 2.1Å crystal structure of an acyl-CoA Synthetase from *Methanosarcina acetivorans* reveals an alternate acyl binding pocket for small branched acyl substrates. Proteins. 2009;77: 685–698. doi:10.1002/prot.22482.

206. Reger AS, Wu R, Dunaway-mariano D, Gulick AM. Structural characterization of a 1400 domain movement in the two-step reaction catalyzed by 4-chlorobenzoate:CoA ligase. Biochemistry. 2008;47: 8016–8025. doi:10.1021/bi800696y.

207. Fan M, Xiao Y, Li M, Chang W. Crystal structures of *Arabidopsis thaliana* oxalyl-CoA synthetase essential for oxalate degradation. Mol Plant. 2016;9: 1349–1352. doi:10.1016/j.molp.2016.06.002

208. Chen Y, Sun Y, Song H, Guo Z. Structural basis for the ATP-dependent configuration of adenylation active site in *Bacillus subtilis* O-succinylbenzoyl-Coa synthetase. J Biol Chem. 2015;290: 23971–23983. doi:10.1074/jbc.M115.676304

209. Wu R, Cao J, Lu X, Reger AS, Gulick AM, Dunway-Mariano D. Mechanism of 4-chlorobenzoate: Coenzyme A ligase catalysis. Biochemistry. 2008;47: 8026–8039. doi:10.1021/bi800698m

210. Horswill AR, Escalante-Semerena JC. Characterization of the propionyl-CoA synthetase (PrpE) enzyme of *Salmonella enterica*: Residue lys 592 is required for propionyl-AMP synthesis. Biochemistry. 2002;41: 2379–2387. doi:10.1021/bi015647q

211. Ingram-smith C, Woods BI, Smith KS. Characterization of the acyl substrate binding pocket of acetyl-CoA synthetase. Biochemistry. 2006;45: 11482–11490. doi:10.1021/bi061023e

212. Branchini BR, Murtiashaw MH, Magyar R a., Anderson SM. The role of lysine 529, a conserved residue of the acyl-adenylate- forming enzyme superfamily, in firefly luciferase. Biochemistry. 2000;39: 5433–5440. doi:10.1021/bi9928804

213. Starai VJ, Takahashi H, Boeke JD, Escalante-Semerena JC. Short-chain fatty acid activation by acyl-coenzyme A synthetases requires SIR2 protein function in *Salmonella enterica* and *Saccharomyces cerevisiae*. Genetics. 2003;163: 545–555.

214. Crosby HA, Heiniger EK, Harwood CS, Escalante- JC. Reversible N-Lysine acetylation regulates the activity of acyl-CoA synthetases involved in anaerobic benzoate catabolism in *Rhodopseudomonas palustris*. Mol Microbiol. 2010;76: 874–888. doi:10.1111/j.1365-2958.2010.07127

215. Gardner JG, Escalante-Semerena JC. Biochemical and mutational analyses of AcuA, the acetyltransferase enzyme that controls the activity of the acetyl-coenzyme A synthetase (AcsA) in *Bacillus subtilis*. J Bacteriol. 2008;190: 5132–5136. doi:10.1128/JB.00340-08

216. You D, Yao LL, Huang D, Escalante-Semerena JC, Ye BC. Acetyl coenzyme A synthetase is acetylated on multiple lysine residues by a protein acetyltransferase with a single Gcn5-type N-acetyltransferase (GNAT) domain in *Saccharopolyspora erythraea*. J Bacteriol. 2014;196: 3169–3178. doi:10.1128/JB.01961-14

217. Schwer B, Bunkenborg J, Verdin RO, Andersen JS, Verdin E. Reversible lysine acetylation controls the activity of the mitochondrial enzyme acetyl-CoA synthetase 2. Proc Natl Acad Sci U S A. 2006;103: 10224–10229. doi:10.1073/pnas.0603968103

218. Kornberg HL. The role and control of the glyoxylate cycle in *Escherichia coli*. Biochem J. 1966;991: 1–11.

219. Loikkanen I, Haghighi S, Vainio S, Pajunen A. Expression of cytosolic acetyl-CoA synthetase gene is developmentally regulated. Mech Dev. 2002;115: 139–141.

220. Van den Berg MA, Steensma HY. *acs2*, a *Saccharomyces cerevisiae* gene encoding acetyl-coenzyme A synthetase, essential for growth on glucose. Eur J Biochem. 1995;231: 704–713.

221. Fujino T, Kondo J, Ishikawa M, Morikawa K, Yamamoto TT. Acetyl-CoA synthetase 2, a mitochondrial matrix enzyme involved in the oxidation of acetate. J Biol Chem. 2001;276: 11420–11426. doi:10.1074/jbc.M008782200

222. Yamashita H, Fukuura A, Nakamura T, Kaneyuki T, Kimoto M, Hiemori M, et al. Purification and partial characterization of acetyl-CoA synthetase in rat liver mitochondria. J Nutr Sci Vitaminol (Tokyo). 2002;48: 359–64.

223. Karan D, David JR, Capy P. Molecular evolution of the AMP-forming acetyl-CoA synthetase. Gene. 2001;265: 95–101. doi:10.1016/S0378-1119(01)00358-4

224. Reger AS, Carney JM, Gulick AM. Biochemical and crystallographic analysis of substrate binding and conformational changes in acetyl-CoA synthetase. Biochemistry. 2007;46: 6536–6546. doi:10.1021/bi6026506

225. Liu F, Gu J, Wang X, Zhang XE, Deng J. Acs is essential for propionate utilization in *Escherichia coli*. Biochem Biophys Res Commun. 2014;449: 272–277. doi:10.1016/j.bbrc.2014.05.015

CHAPTER 2

Objectives

Objectives

Escherichia coli (*E. coli*) is a model organism in the biology and biotechnology fields. Indeed, several biotechnological processes use *E. coli* to get high-value products, such as therapeutics, pre-biotics, nutraceuticals, pigments or biopolymers. To optimize all these bioprocesses is essential to understand *E. coli* metabolism and regulation. *E. coli* excretes several metabolites to extracellular medium during cell growth to maintain cellular homeostasis. Acetate is the main excreted product when glucose is used as carbon source. Moreover, excreted acetate can be consumed and reincorporated in the metabolism. This acetate excretion-consumption phenomenon is known as "acetate overflow". However, acetate overflow is an important drawback for industrial bioprocesses involving *E. coli*, because acetate inhibits cell growth in high density cultures and it generates an energetic and carbon loss, limiting yield. Lysine protein acetylation is a post-translational modification widely abundant in *E. coli* and responsible for regulation of several proteins. Acetate metabolism is closely related to lysine acetylation through acetyl-phosphate and acetyl-CoA pools and acetyl-CoA synthetase protein (Acs) regulation. In this way, the study of acetate metabolism and lysine acetylation is essential to deepen our knowledge of the *E. coli* metabolism and regulation. For all these reasons, the main objectives of this PhD thesis are:

1. To design a competitive semi-continuous system for lycopene overproduction and extraction as an example of a biotechnological process based on *E. coli* metabolism **(Chapter 3)**.
2. To characterize the *E. coli* PatZ acetyltransferase enzyme. Acs acetylation kinetics will be determined and PatZ biochemical and biophysical characterization will be carried out **(Chapter 4)**.
3. To characterize the *E. coli* CobB sirtuin enzyme. Acs deacetylation kinetics will be characterized and CobB inhibition by nicotinamide will be studied *in vitro* and *in vivo* **(Chapter 5)**.
4. To decipher the *E. coli* Acs catalytic mechanism and to identify the essential residues responsible for ATP-binding. The effect of lysine 609 acetylation on Acs catalytic activity will be also evaluated **(Chapter 6)**.
5. To study the influence of carbon and nitrogen sources on main factors that affect lysine acetylation in *E. coli*: acetate overflow, intracellular pH, and acetyl-CoA and acetyl-phosphate concentrations. These factors will be evaluated in *E. coli* wt strain and in five

deficient strains involved in acetate metabolism. Intracellular *E. coli* pH will be measured for the first time in a continuously culture. Finally, the effect of carbon and nitrogen source on acetyl-CoA**,** acetyl-phosphate and succinyl-CoA intracellular concentrations and on lysine protein acetylation will be also evaluated **(Chapter 7)**.

CHAPTER 3

Lycopene overproduction and in situ extraction in organic-aqueous culture systems using a metabolically engineered Escherichia coli

The results presented in this chapter are based on the publication:

Julia Gallego-Jara, Teresa de Diego, Álvaro del Real, Ana Écija-Conesa, Arturo Manjón, and Manuel Cánovas

Lycopene overproduction and *in situ* extraction in organic-aqueous culture systems using a metabolically engineered *Escherichia coli*

AMB Express. 2015; 5. doi: 10.1186/s13568-015-0150-3

Abstract

Lycopene is an important compound with an increasing industrial value. However, there is still no biotechnological process to obtain it. In this study, a semi-continuous system for lycopene extraction from recombinant *Escherichia coli* (*E. coli*) BL21 cells is proposed. A two-phase culture mode using organic solvents was found to maximize lycopene production through *in situ* extraction from cells. Within the reactor, three phases were formed during the process: an aqueous phase containing the recombinant *E. coli*, an interphase, and an organic phase. Lycopene was extracted from the cells to both the interphase and the organic phase and, consequently, thus enhancing its production. Maximum lycopene production (74.71 ± 3.74 mg L^{-1}) was obtained for an octane-aqueous culture system using the *E. coli* BL21LF strain, a process that doubled the level obtained in the control aqueous culture. Study of the interphase by transmission electron microscopy (TEM) showed the proteo-lipidic nature and the high storage capacity of lycopene. Moreover, a cell viability test by flow cytometry (FC) after 24 h of culture indicated that 24 % of the population could be re-used. Therefore, a batch series reactor was designed for semi-continuous lycopene extraction. After five cycles of operation (120 h), lycopene production was similar to that obtained in the control aqueous medium. A final specific lycopene yield of up to 49.70 ± 2.48 mg g^{-1} was reached at 24 h, which represents to the highest titer to date. In conclusion, the aqueous-organic semi-continuous culture system proposed is the first designed for lycopene extraction, representing an important breakthrough in the development of a competitive biotechnological process for lycopene production and extraction.

Introduction

Lycopene is a tetraterpenoid (C40) precursor of carotenoids. Traditionally, it was considered a colorant and a food additive, but new applications have been proposed for use as an antioxidant [1], and anticarcinogen [2,3] and for preventing against cardiovascular diseases [4], hepatic fibro-genesis [5] or human papillomavirus persistence [6]. In spite of its great importance, most of lycopene is obtained from tomato, and no competitive biotechnological process exists for its production.

In industry, methods based on metabolic engineering are the most profitable due to their high productivity and, consequently, the search for a biotechnological method for lycopene production is an important challenge for many researchers. In the last decade, many studies have been reported concerning lycopene production by metabolic engineering, some of which are based on *E. coli*, the most important cell factory microorganism in biotechnology [7–14]. Recombinant *E. coli* are capable of biosynthesizing lycopene through either the mevalonate (MEV pathway) or the non-mevalonate route (2-C-methyl-D-erythritol 4-phosphate or MEP

pathway). Although *E. coli* possesses the genes of the MEP pathway for isopentenyl pyrophosphate (IPP) synthesis, it still requires the following three enzymes, geranylgeranyl pyrophosphate (GGPP) synthase (*crt*E), phytoene synthase (*crt*B) and phytoene desaturase (*crt*I) to be able to synthesize lycopene. Therefore, a recombinant bacterium which contains these enzymes is necessary (Appendix Figure S1). Previous works demonstrated that carotenoid production can be improved by increasing the amount of IPP and its isomer dimethylallyl pyrophosphate (DMAPP) amount available in the recombinant *E. coli* engineered [13,15,16]. Besides to *E. coli*, carotenogenic microorganisms, such as *Blakeslea trispona* [17] and the non-carotenogenic yeasts, *Pichia pastoris* [18] and *Saccharomyces cerevesiae* [19], have been used to produce lycopene.

Despite the achievements made to date, there is still no competitive biotechnological method to compete with lycopene extraction from tomatoes. The main problems of these metabolic engineering processes are plasmid instability and the low capability to accumulate lycopene in the cytoplasmic membrane from non-carotenogenic organisms [20]. Hence, the *in situ* recovery of lycopene from a recombinant *E. coli* strain is the goal for achieving a competitive biotechnological process. To our knowledge there are few studies concerning lycopene extraction from *E. coli*. It has been reported an *in situ* process based on lycopene overproduction and recovery using octane and decane as extraction solvents [12]. However, the lycopene percentage extracted was quite low. The partial digestion of bacterial walls with lysozyme improved the system extractive capacity, although this digestion was quickly reverted as bacteria duplicated. In 2011, an *in situ* extraction process of retinoids from *E. coli* was reported [21], in which dodecane was used as extraction solvent, attaining a 68-fold higher productivity than attained with the aqueous system.

Hence, the search for a competitive system concerning both lycopene production and extraction is of great interest in the biotechnology field. In this chapter, we propose the first semi-continuous system to produce and extract high amounts of lycopene employing a recombinant *E. coli* strain.

Methods

Cell mass and specific growth rate

Cell mass was determined using a linear calibration curve relating optical density at 600 nm (OD_{600}) and dry cell weight (R^2= 0.99). Cells were filtered and washed thoroughly with distilled water, and then dried at 130 °C for 24 h to a constant weight using a thermobalance (Electronic Moisture Analyzer model MA35, Sartorius). The exponential growth phase was identified and the specific growth rate was determined for all culture strains cultures [22].

Transformation and culture conditions

Chemically competent *E. coli* K12 [23] and BL21-Gold (DE3) (Agilent Technologies) cells were transformed with the pAC-Lyc plasmid, which contained three genes of the lycopene pathway, *crtE*, *crtB* and *crtI*, and a chloramphenicol resistance gene, by heat shock at 42 °C. The resulting strains were called *E.coli* K12L and *E. coli* BL21L, respectively. Then, *E. coli* BL21L was made competent again and co-transformed with the pET-SIDF and pET-SIDFG plasmids, obtaining the strains *E. coli* BL21LF and *E. coli* BL21LG, respectively (Table 1). These plasmids contained the genes *dxs, idi, ispD, ispF* (pET-SIDF) and *dxs, idi, ispD, ispF* and *ispG* (pET-SIDFG) and an expression system controlled by the inducible promoter T7. Besides, they showed ampicillin resistance. The plasmids pAC-Lyc, pET-SIDF and pET-SIDFG were kindly supplied by Prof. G. Stephanopoulos (Department of Chemical Engineering, Institute of Technology, Cambridge, Massachusetts, EEUU) [13]. Lycopene biosynthesis was carried out in triplicate in 500 ml flasks containing 50 ml of M9 minimal medum (MM9) with 20 mM glucose or 40 mM glycerol using an orbital shaking at 200 rpm and 28 °C. MM9 medium contained: 10 mM $(NH_4)_2SO_4$, 8.5 mM NaCl, 40 mM Na_2HPO_4, 20 mM KH_2PO_4, 185 µM $FeCl_3$, 175 µM EDTA, 7 µM $ZnSO_4$, 7 µM $CuSO_4$, 7 µM $MnSO_4$, 7 µM $CoCl_2$, 7 µM $MgSO_4$, 0.1 mM $CaCl_2$, and 1 µM thiamine·HCl. The culture medium was supplemented with appropriate antibiotics (30 µg mL^{-1} chloramphenicol and/or 100 µg mL^{-1}ampicillin).

Table 1. Recombinant *E. coli* cells used in this study.

Strain	Plasmids			Named in this study
	pAC-Lyc	pET-SIDF	pET-SIDFG	
***E. coli* K12**	X			*E.coli* K12L
***E. coli* BL21**	X			*E. coli* BL21L
	X	X		*E. coli* BL21LF
	X		X	*E. coli* BL21LG

Lycopene extraction

Metabolically engineered *E. coli* cells were harvested by centrifugation at 10,000 × g for 5 min at 4 °C. The cell pellet was resuspended in 1 mL of acetone and vigorously stirred for 10 min at 4 °C. The mixture was then centrifuged at 10,000 × g for 10 min, and the acetone supernatant was filtered through a 0.2 µm nylon sterile filter. Then, samples were lyophilized (Thermo Scientific Heto PowerDry) and the final extract was resuspended in 0.1 mL of a 50:50 (v:v) mixture of A:B mobile phases for HPLC analysis. The lycopene extracted from the interphase was

treated using the same procedure. The organic solvent phase was filtered through a 0.2 µm nylon sterile filter and lyophilized.

Lycopene quantification by HPLC

The HPLC separation was performed on a Shimadzu HPLC equipped with a multi-channel pump (mod LC-20AD) and a DAD detector (mod SPD-M20A) with a Develosil® C30-UG-5 column (250 mm x 4.6 mm x 5 µm) from Phenomenex. Elution conditions were based on the chromatographic method developed by Sander et al. [24] with modifications. Two mobile phases were used: phase A, composed of methanol and water (96:4, v:v) and phase B, tert-butyl methyl ether. The flow rate was 1.2 mL min^{-1} and the injection volume 40 µL. The column was thermostated at 30 °C. The separation of carotenoid standards and extracts was carried out using a linear mobile phase gradient from 50:50 (volume ratio, A:B) to 37:63 (volume ratio, A:B) in 12 min; then the system was restored to its initial condition for 5 min. The concentrations of lycopene, 13-cis-lycopene and phytoene were calculated using response factors relative to the internal standard, β-apo-8-carotenal. Carotenoid identification was carried out by comparing the retention times and absorption spectra characteristics (Appendix Figure S2) by reference to standards purchased from Sigma Aldrich. Detection was performed at 472 nm for lycopene and 13-cis-lycopene and at 285 nm for phytoene (Appendix Table S1). Measurements obtained from cell extracts were compared to curves generated from standards (R^2 = 0.99).

Transmission electron microscopy

E. coli BL21LF cells and interphase samples were fixed with 3 % glutaraldehyde for 30 min and prepared as previously described by Huxley et al. [25]. The ultrathin sections were cut in a Reichert–Young ultramicrotom. Staining was carried out with 2 % uranyl acetate. Sections were then examined by using a Carl Zeiss EM 10 C electron microscope.

Flow cytometry

Samples were run by FC in a Becton Dickinson FASort model equipped with an argon laser for excitation at 488 nm and 15 mW and filters at 525 and 630 nm. Samples were adjusted to an event rate of 800–2000 cells s^{-1} and a total of 10,000 events were registered per sample. To determine cell viability by FC, double staining was performed accordingly to Hewitt et al. [26]. Fluoresceinpropidium iodide (PI) and trimethine oxonol (Bis-oxonol, BOX) were used for viability studies on living cells. The FC probe PI was purchased from Sigma Aldrich, while BOX was purchased from Molecular Probes Inc. Stained cells were diluted in phosphate buffered saline solution (PBS) (137 mM NaCl, 2.7 mM KCl, 10 mM Na_2HPO_4 and 1.8 mM KH_2PO_4) pH 7.2 FALS and RALS values allowed cell debris discrimination and a total of 10,000 events were used for statistical data analysis.

Heat stressed cells treated at 60 °C for 30 min and exponentially growing cells were used as positive and negative controls, respectively. The green fluorescence channel for BOX-stained cells (X-axis) was plotted *versus* the red fluorescence channel for PI stained cells (Y-axis). Flow cytometry data were analysed with WinList 5.0 (Verity Software House) software.

Results

Optimization of IPTG concentration

Recombinant *E. coli* BL21LF and *E. coli* BL21LG (Table 1) were cultivated in MM9 medium containing 20 mM glucose as carbon source with 200 rpm orbital shaking and 28 °C. When the cultures reached 0.5 OD_{600}, the IPTG (isopropyl β-D-1-thiogalactopyranoside) inductor was added at concentrations ranging from 0 to 1 mM. Samples were taken from each culture for lycopene extraction at 24 h, when the lycopene production was maximum. As shown in Figure 1, a positive correlation between lycopene production and inductor concentration was noted for the two recombinant *E. coli* BL21 strains. Based on these results, the IPTG concentration selected was 0.1 and 0.4 mM for *E. coli* BL21LF and *E. coli* BL21LG, respectively.

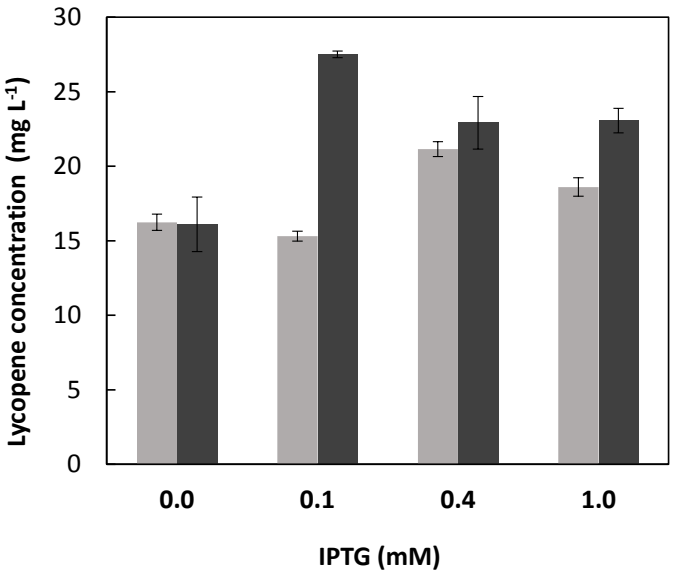

Figure 1. Lycopene production at different IPTG concentrations after 24h in glucose culture. Grey bars and solid bars represent the results obtained using *E. coli* BL21F and the *E. coli* BL21G, respectively. Data represent the means and standard deviations from three separate experiments.

Optimization of culture conditions

In order to determine the optimal culture conditions, besides lycopene, the 13-cis-lycopene and phytoene content were quantified, the first since it is a lycopene isomer and is often produced by lycopene oxidative degradation [1] and the second, as the precursor of lycopene. To select a carbon source for lycopene production, 50 ml batch cultures for the whole

recombinant *E. coli* strains (K12L, BL21L, BL21LF and BL21LG) were carried out using either 40 mM glycerol or 20 mM glucose (Appendix Figure S3). All cultures were made by orbital shaking at 200 rpm and 28 °C, which is the optimal temperature for lycopene biosynthesis [27]. The biomass, lycopene, 13-cis-lycopene and phytoene content were determined at 24 h. The specific growth rate was also calculated for each culture (Table 2).

Glycerol cultures exhibited the highest lycopene production, whereas glucose cultures showed the highest cell mass and specific growth rate. In all cultures, the phytoene concentration was very low compared with lycopene (lower than 5 %), demonstrating an optimal expression of pAC-Lyc plasmid [11]. The maximum lycopene content was obtained from the *E. coli* BL21LF strain when glycerol was used as carbon source (Figure 2). Therefore, glycerol was selected as carbon source for lycopene production with *E. coli* BL21LF in all subsequent studies.

Table 2. Effect of carbon source on cell growth (OD_{600}), lycopene production and specific growth rate (μ_{max}) in the *E. coli* aqueous cultures. Data represent the means and standard deviations from three separate experiments.

Carbon source	OD_{600}	Lycopene (mg/L)	μ_{max} (h^{-1})
Glucose			
***E. coli* K12L**	3.56±0.07	16.18±0.81	0.33±0.03
***E. coli* BL21L**	3.86±0.04	11.51±0.52	0.43±0.01
***E. coli* BL21LF**	4.27±0.04	27.51±1.35	0.43±0.02
***E. coli* BL21LG**	3.29±0.17	21.15±1.01	0.35±0.04
Glycerol			
***E. coli* K12L**	3.61±0.15	20.88±1.04	0.27±0.01
***E. coli* BL21L**	3.95±0.24	14.84±0.74	0.30±0.04
***E. coli* BL21LF**	2.79±0.04	37.56±1.41	0.31±0.01
***E. coli* BL21LG**	1.55±0.06	27.28±0.81	0.28±0.06

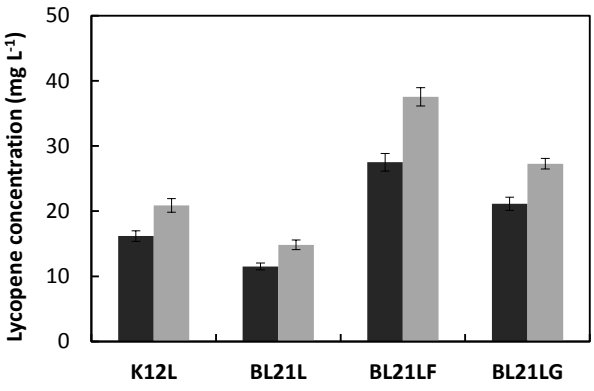

Figure 2. Comparison between glucose (solid bars) and glycerol (grey bars) as main carbon sources for lycopene production after 24 h using the recombinant *E. coli* strains. Data represent the means and standard deviations from three separate experiments.

The effect of key fermentation control parameters, such as shaking speed and light, on the production of lycopene were also tested. In the whole set of cultures exposed to light, the concentration of 13-cis-lycopene was very low compared with lycopene (lower than 8 %). When these same cultures were grown in darkness, no differences were detected for the isomer concentration, thus this additional precaution was discarded (data not shown). Orbital shaking speed was investigated as a putative bioreactor parameter responsible for controlling dissolved oxygen content and maximum cell density. Batch cultures in 500 mL flasks with 50 mL MM9 medium were carried out at three orbital shaking speeds: 100, 200 and 400 rpm. However, there were no differences in lycopene production.

Lycopene production was evaluated in detail using glycerol as carbon source and the selected *E. coli* BL21LF in 50 mL batch culture and with 200 rpm orbital shaking at 28 °C. For this purpose, three samples were taken at different times up to 24 h (Figure 3). Lycopene production started during the exponential growth phase, and the maximum lycopene concentration was reached in the stationary phase, since it is a secondary metabolite biomass dependent.

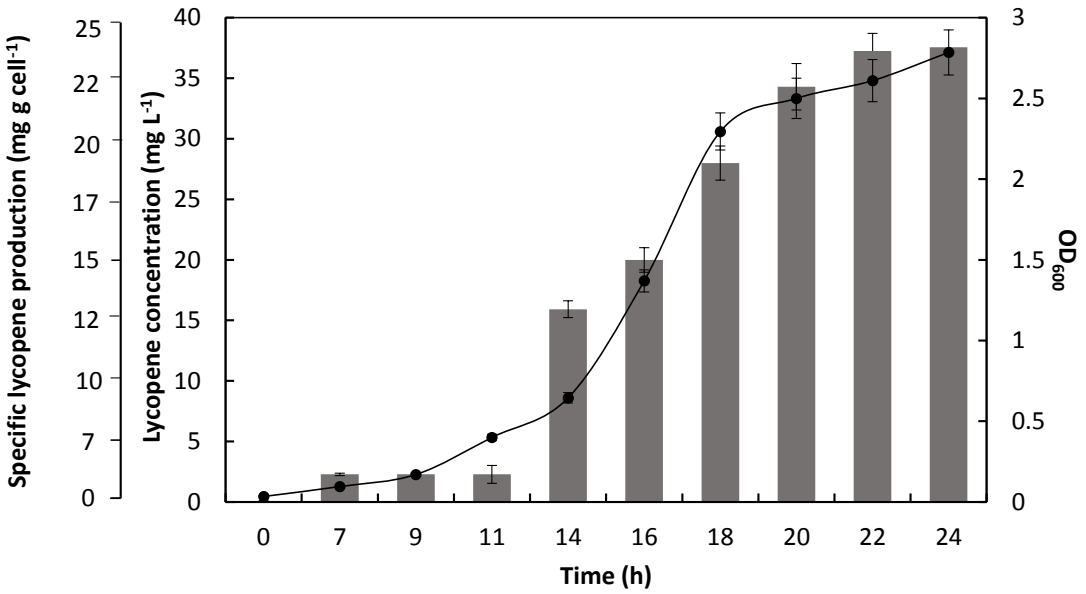

Figure 3. Specific lycopene content (grey bars) and biomass (●) of recombinant *E. coli* BL21LF in 50 ml batch culture with 40 mM glycerol, 200 rpm and 28 °C. Data represent the means and standard deviations from three separate experiments.

Increase of lycopene production *via in situ* extraction in organic-aqueous culture systems

The effect of organic solvents on cell growth and lycopene production in metabolically engineered *E. coli* BL21LF was investigated in batch cultures. Organic solvents for lycopene extraction were selected as a function of the solvent logarithm of its partition coefficient in n-

octanol and water (log P), which ranged from 3.76, 4.27, 4.78, 5.8 to 6.31 for heptane, hexane, octane, decane, undecane and dodecane, respectively.

Batch cultures were performed using an organic:culture broth volume ratio of 1:5 (v/v) for the whole set of the 50 mL cultures. Organic solvent was added when the biomass reached 0.5 OD_{600}, in order to not affect cell growth. Hexane and heptane were rejected; hexane due to its high volatility and heptane as a consequence of its toxicity to cells. An aqueous culture without organic solvent was used as control system and the resulting lycopene production (37.56 ± 1.41 mg L^{-1}) was used to normalize lycopene biosynthesis.

In all the aqueous-organic systems, three phases were visible after 24 h in the presence of organic solvent: an aqueous phase containing the *E. coli* BL21LF cells, an interphase and the organic phase. This tri-phasic culture system and normalized lycopene production at 24 h for all the organic-aqueous culture systems can be seen in Figure 4A and B. Interestingly, lycopene production greatly increased with the addition of organic solvent except for undecane, although the lycopene production profile presented a negative correlation with the solvent log P. Final lycopene production after 24 h was 198.9 %, 148.6 % and 115.97 % for octane, decane and dodecane, respectively, with respect to the control aqueous culture. In these organic-aqueous culture systems, lycopene was extracted from the cells to the interphase and the organic phase, which greatly enhanced production. Maximum lycopene production was obtained for the octane-aqueous system reaching 74.71 ± 3.74 mg L^{-1} (198.9 %). This lycopene production was distributed among the three phases formed: 12.24 ± 0.61 mg L^{-1} into *E. coli* BL21LF cells of the aqueous phase, 57.14 ± 2.85 mg L^{-1} in the interphase and 5.32 ± 0.24 mg L^{-1} in the octane phase. As regards to the cell density, the OD_{600} of the aqueous media was similar to the aqueous-organic systems at 24 h, around 4.00 ± 0.35. The *E. coli* BL21LF growth culture is shown in Appendix Figure S3.

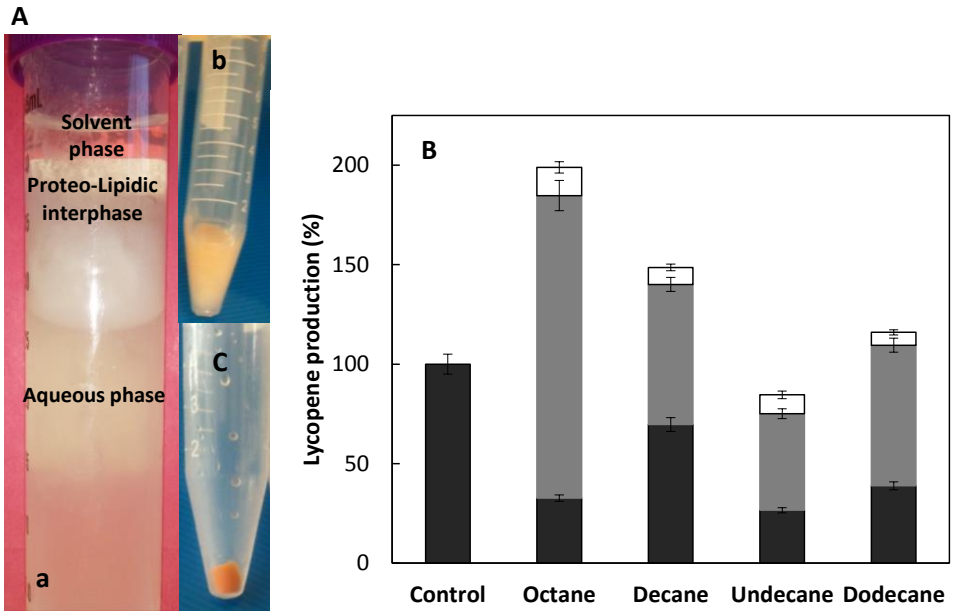

Figure 4. (A) (a) Tri-phasic culture system for aqueous-organic systems. (b) Interphase. (c) *E. coli* BL21LF cells. Both phases were orange by the presence of lycopene. **(B)** Lycopene production normalized at 24 h for the organic-aqueous culture systems with *E. coli* BL21LF, distributed among three phases: aqueous phase containing *E. coli* BL21LF cells (solid bars), interphase (grey bars) and organic phase (open bars).

In order to study the physicochemical properties of the interphase formed in the aqueous-organic systems, TEM was used (Figure 5A). Spherical particles of homogeneous size ranging from 15 to 20 nm were observed, demonstrating its proteo-lipidic nature and with high lycopene storage capacity of these particles, representing 76.5 % (57.14 ± 2.85 mg L^{-1}) of the total culture content. TEM was also used to visualize *E. coli* BL21LF cells after 24 h (Figure 5B-F). Pictures B and C show *E. coli* BL21LF cells in the aqueous medium, whereas D and E show *E. coli* BL21F cells within the octane-aqueous culture system, and F shows *E. coli* BL21LF in the heptane-aqueous culture system. As depicted, *E. coli* BL21LF cell growth in aqueous media entirely maintained the outer membrane structure, and even the lipid double layer could be observed. But when the octane-aqueous culture system was employed, the cells partially lost the structural integrity of their outer membrane. This explains the high extractive capacity of octane for lycopene and the proteo-lipidic interphase formation. Cells completely lost their structural integrity when heptane was used.

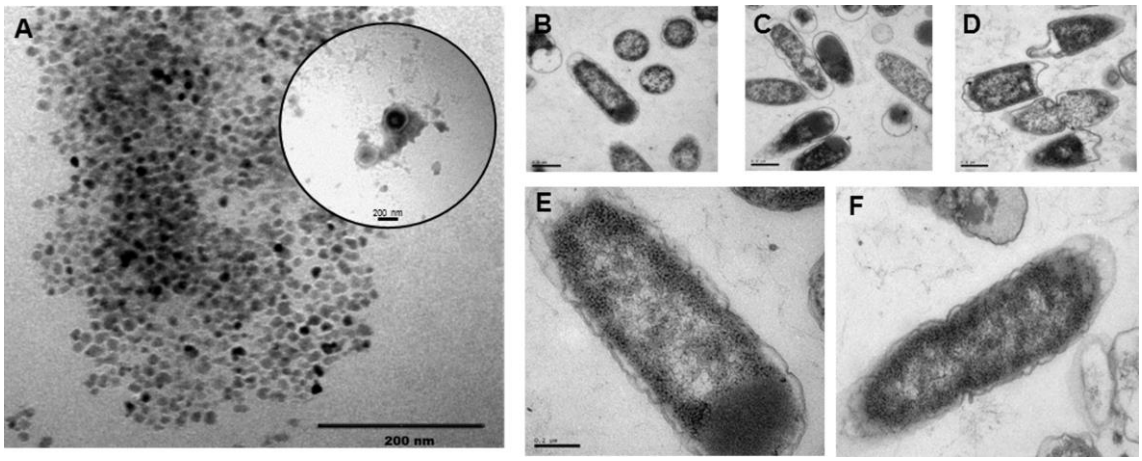

Figure 5. (A) Transmission electron microscopy of the interphase of the octane-aqueous culture prepared with negative staining. Transmission electron microscopy of *E. coli* BL21LF: **(B)** and **(C)** in aqueous media, **(D)** and **(E)** in aqueous-octane culture system and **(F)** in aqueous-heptane culture system. Amplifications were 40,000 x for B, C and D and 100,000 x for E and F.

To determine cell viability, FC using scattered light was chosen. Two fluorochromes were employed simultaneously: BOX and PI. BOX is a lipophilic anionic compound, which accumulates intracellularly when the cytoplasmic membrane is depolarised, while PI binds to DNA, but cannot cross an intact cytoplasmic membrane [26]. Cell analysis by FC demonstrated that, during a fed-batch culture in an aqueous-octane system, there was a gradual change in the physiological state of *E. coli* BL21LF. From samples taken at 24 h, three main sub-populations of cells were observed (Figure 6). These populations corresponded to healthy unstained cells (A3); cells with a depolarised cytoplasmic membrane (A4), stained with BOX; and dead cells with permeabilised membranes, namely cells stained with both PI and BOX (A2). From Figure 6, the cell number and the percentage within each quadrant was determined using the FC software. The results are shown in Table 3. Cells from a microbial culture can be grouped according to their different metabolic states and/or extent of cell integrity: a) intact and metabolically active cells, showing growth capacity, b) depolarized cells, unable to maintain their intact membrane potential, but that can be recovered temporarily [28], c) and dead cells with permeabilised and depolarised membrane [26]. The aqueous-octane culture system *E. coli* BL21LF after 24 h, resulted in an 11.5 % of healthy unstained cells and a 13.24 % of depolarised but recoverable BOX stained cells. Therefore, both of them (24.74 %) can be considered viable for the continuous production of lycopene.

Table 3. Cells number and percentage in each one of the FC windows. Cell debris was identified on the basis of the FALS and RALS values.

Window	Cells number	Percentage (%)
A1	179	1.79
A2	7347	73.47
A3	1150	11.50
A4	1324	13.24

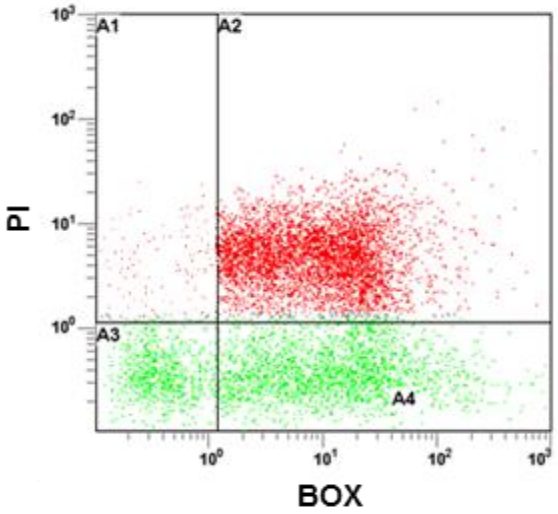

Figure 6. FC of the *E. coli* BL21LF strains in an aqueous-octane culture system. Green fluorescence of cells (axis X) due to BOX is plotted *vs* red fluorescence (axis Y) due to PI. Samples were taken from the batch reactor at 24 h.

Aqueous-octane culture system for *in situ* extraction and semi-continuous lycopene production

Maximum lycopene production was obtained from the octane-aqueous system (1:5 volume ratio) after 24 h of culture, when cell growth had ceased and the lycopene content was distributed among the three phases. From these results, a series batch reactor was designed for lycopene extraction, as depicted in Figure 7A. The aqueous-octane culture system was maintained in operation for 24 h, then the volume of the aqueous phase corresponding to a final 0.05 OD_{600} was used as the inoculum for a second batch reactor (taking into account the viable cells fraction). This process was repeated 5 times.

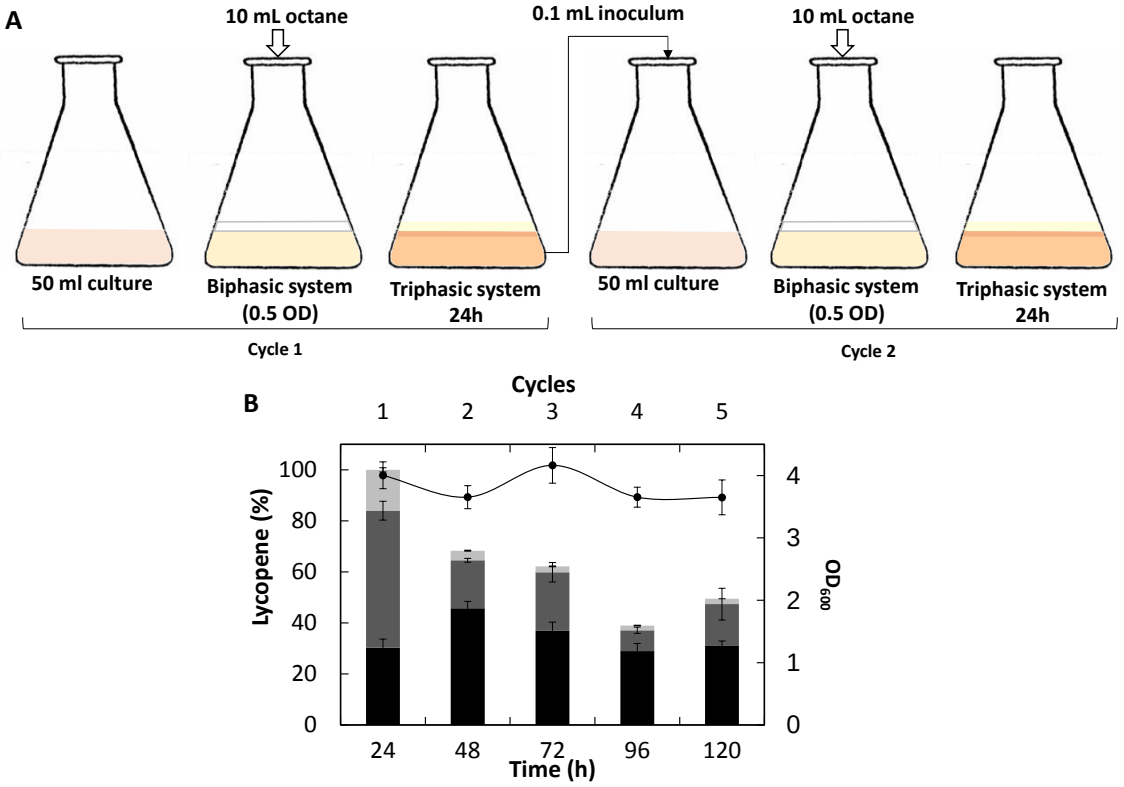

Figure 7. (A) Series batch reactor for lycopene over-production using *E. coli* BL21LF in an aqueous-octane culture system. **(B)** Normalized lycopene production distributed within each phase for each cycle: aqueous phase containing *E. coli* BL21LF cells (solid bars), interphase (grey bars) and organic phase (light grey bars), and biomass (●). Data represent the means and standard deviations from three separate experiments.

Figure 7B displays the lycopene production distributed in each phase and cycle. The lycopene produced in the first cycle was used to normalize the lycopene content of the remaining cycles. In the first three, the lycopene production was 74.71 ± 3.74 mg L^{-1}, 51.03 ± 2.51 mg L^{-1} and 46.45 ± 2.13 mg L^{-1}, respectively, all of them higher than that obtained in the aqueous medium (37.56 ± 1.41 mg L^{-1}). Lycopene production was 29.01 ± 1.52 mg L^{-1} and 36.96 ± 1.82 mg L^{-1} for the fourth and fifth cycle, respectively, similar to that obtained in the aqueous medium. The biomass reached in each batch reactor was similar, about 3.82 ± 0.35 OD, although production deceased with each cycle.

Discussion

Metabolic engineering to increase lycopene production in *E. coli* has previously focused on overexpression of the several key isoprenoid genes [29]. Hence, the first part of this study was focused on the optimization of both the recombinant *E coli* strain and culture conditions. When the recombinant *E. coli* BL21LF and *E. coli* BL21G strains were used in combination with the IPTG-induced, lycopene production increased, although excessive IPTG concentration reduced lycopene biosynthesis (Figure 1). This finding is consistent with previous observations

of the induction inhibitory effects of lycopene production [7,11,12] since, a high induction could cause a shortage of the available precursors for the essential metabolic roles. The IPTG concentrations selected were 0.1 and 0.4 mM for *E. coli* BL21LF and *E coli* BL21LG, respectively. The lower lycopene production obtained with *E. coli* BL21LG was probably due to the high energy cost of the extra *ispG* gene overexpression, which encodes the HDS protein. It has been revealed that *ispG* gene basal expression is higher than the expression of other of isoprenoid genes under normal growth conditions [10]. Accordingly, a high multi-copy expression vector may cause a metabolic imbalance. In addition, the HDS enzyme (4-hydroxy-2-methyl-2-butenyl 4-diphosphate synthase) flavodoxin reductase and NADPH dependent metalloprotein, [30,31] involves an extra expense of reducing power to carry out their catalytic functions [32]. These assumptions could explain the *E. coli* BL21LG strain delay metabolic.

In previous studies, glycerol and glucose were compared as carbon sources for secondary metabolite production, glycerol being seen as a better carbon source than glucose [33–35]. Glycerol reduces cell growth, but stimulates metabolite production [36].

On the other hand, the recombinant *E. coli* BL21 and K12 strains showed differences in lycopene production, the latter producing 1.4-fold more than the *E. coli* BL21L strain (Figure 2). Significant differences have been demonstrated at gene transcription and metabolomic profile levels between both *E. coli* strains [9]. In addition, the outer membranes of *E. coli* K12 and *E. coli* BL21 also show differences in lipoprotein and lipid composition, which may influence cell envelope permeability and integrity. These differences could affect potential lycopene accumulation [37,38].

The maximum lycopene production and specific lycopene production were 37.56 ± 1.41 mg L^{-1} and 25.34 ± 1.2 mg g $cell^{-1}$, respectively, which was obtained during stationary growth phase using *E. coli* BL21LF in 40 mM glycerol and 0.1 mM IPTG (Figure 2). This production is excellent compared with the lycopene levels previously reported. Stephanopoulos group's (2006) created a triple knockout strain, Δ*gdhA* Δ*aceE* Δ*fdhF*, which exhibited a lycopene production of 8.15 mg g $cell^{-1}$ [9]. Kin et al. (2011) used a metabolically engineered *E. coli* strain, reporting a lycopene production of 32 mg g $cell^{-1}$ in fed-batch cultures with glycerol supplemented with glucose as auxiliary carbon source [27]. Recently, a higher level of lycopene production (33.43 mg g $cell^{-1}$) was attained by native appY promoter replacement of a T5 promoter, and the deletion of the *iclR* gene in *E. coli* CBW 12241 [14]. High lycopene production was also achieved (18.49 mg g $cell^{-1}$) using a CRP (Catabolite Repression Protein or cAMP Receptor Protein) engineering strategy [39].

One of the main limitations of biotechnological lycopene production is the fact that it is stored as an intracellular product in the membrane [40]. Therefore, special care must be taken

into account to identify the optimal parameters for continuous lycopene production. It has been assumed that the upper limit for the carotenoid production in a non-carotenogenic *E. coli* is around 2 mg g cell^{-1} due to the limited lipophilic carotenoid storage capacity of the membrane [41,42]. Hence, a new strategy is needed to overcome the lycopene accumulation barrier. Optimal parameters must be determined in order to promote lycopene production during both the exponential and stationary phase, while stimulating *in situ* extraction to prevent accumulation in the cell membrane. Moreover, when the whole cells are employed as biocatalyst, productivity may decrease due to end-product inhibition or accumulation: however, if the product is continuously removed by a solvent phase, an increase in activity/productivity can be attained. To achieve this aim, a two-phase culture system using an organic solvent was proposed to maximize the lycopene production through *in situ* extraction from the cells. Few studies using organic solvents for terpenes extraction have been published. It has been reported a two-phase culture system with dodecane for retinoids extraction using a metabolically engineered *E. coli* [21]. In a previous report, a two-phase culture system with decane and 0.1 % (w/v) Span 20 was successfully applied for lycopene production (9.6 ± 1.0 mg g^{-1}) [12]. However, lycopene was inefficiently extracted from the recombinant *E. coli* strain without partial digestion of the cell wall with lysozyme. The authors used *E coli* spheroplasts in order to increase the extraction, but their instability reduced the possibility of designing a continuous system.

Another aspect to consider in a biphasic system is the organic solvent toxicity toward microorganisms. This toxicity depends on its inherent toxicity and the intrinsic tolerance of the bacterial species and strains [43]. The toxicity of a solvent correlates with the log P, meaning that, organic solvents with a log P of between 1.5 and 4.0 are toxic for microorganisms. Six organic solvents were selected for lycopene extraction as a function of the log P, ranging from 3.76 to 6.31. In all aqueous-organic systems tested in this study three phases were formed after 2 h of culture: an aqueous phase containing cells, an interphase and an organic phase (Figure 4A). Lycopene was removed from the cells to the interphase and the organic phase, thus enhancing production. Maximum lycopene production was obtained from octane-aqueous systems (5:1, v/v) (74.71 ± 3.74 mg L^{-1} or 49.70 ± 2.48 mg g cell^{-1}), a 2-fold improvement over that attained in aqueous culture. This production was also much higher than that obtained from tomato, 0.42 mg g^{-1}, which suggest it is a promising strategy for its industrial production [44]. This lycopene production rate is, to our knowledge, the highest reported in the literature to date. Moreover, the proteo-lipidic nature of the interphase demonstrated by TEM (Figure 5A), showed a high lycopene storage capacity of 76.5 % (57.15 ± 2.86 mg L^{-1}) with respect to the total production of lycopene in aqueous-octane systems (Figure 4B). This interface was formed from partial outer membrane disintegration, while cells with structural integrity were found in the

aqueous-octane systems after 24 h (Figure 5D, E). Additionally, FC analysis of *E. coli* BL21LF cells showed a significant percentage (24.74 %) of viable and cultivatable cells for continuous lycopene production (Figure 6, Table 3). From these results, a series batch reactor for semi-continuous lycopene extraction was designed (Figure 7A). The biomass reached was similar for the all cycles, although lycopene production decreased with each of cycle. The results further support the idea that cell depolarisation indicates a decline in cell functionality due to energy depletion, but does not involve cell death. Besides, lycopene accumulation in the cell membrane seems to affect lycopene biosynthesis, since the amount of lycopene extracted from cells to the interphase and the organic phase decreased in each cycle. Nevertheless, the lycopene production obtained from the fifth cycle (120 h) was 36.96 ± 1.82 mg L^{-1}, similar to that obtained in the aqueous medium (Figure 7B).

In this study, semi-continuous lycopene overproduction and *in situ* extraction using a metabolically engineered *E. coli* strain is attained for the first time with an octane-aqueous culture system (1:5 volume ratio). In the future, we hope these findings will be useful for industry and constitute an important step forward in the development of a competitive biotechnological lycopene production system.

References

1. Chasse G, Mak ML, Deretey E, Farkas I, Torday LL, Papp JG, et al. An *ab initio* computational study on selected lycopene isomers. J Mol Struct THEOCHEM. 2001;571: 27–37. doi:10.1016/S0166-1280(01)00424-9
2. Giovannucci E, Rimm EB, Liu Y, Stampfer MJ, Willett WC. A prospective study of tomato products, lycopene, and prostate cancer risk. J Natl Cancer Inst. 2002;94: 391–398. doi:10.1093/jnci/94.5.391
3. Rabi T, Gupta S. Dietary terpenoids and prostate cancer chemoprevention. Front Biosci. 2008;13: 3457–3469. doi:10.2741/2940
4. Rao A. Lycopene, tomatoes, and the prevention of coronary heart disease. Exp Biol Med. 2002;227: 908–913. doi:10.1177/153537020222701011
5. Kitade Y, Watanabe S, Masaki T, Nishioka M, Nishino H. Inhibition of liver fibrosis in LEC rats by a carotenoid, lycopene, or a herbal medicine, Sho-saiko-to. Hepatol Res. 2002;22: 196–205. doi:10.1016/S1386-6346(01)00132-2
6. Sedjo RL, Roe DJ, Abrahamsen M, Harris RB, Craft N, Baldwin S, et al. Vitamin A, carotenoids and risk of persistent oncogenic human Papillomavirus Infection. Cancer Epidem Biomarkers Prev. 2002. pp. 876–884.
7. Kim S, Keasling JD. Nonmevalonate isopentenyl diphosphate synthesis pathway in *Escherichia coli* enhances lycopene production. Biotechnol Bioeng. 2001;72: 408–415. doi:10.1002/1097-0290(20000220)72
8. Martin VJJ, Pitera DJ, Withers ST, Newman JD, Keasling JD. Engineering a mevalonate pathway in *Escherichia coli* for production of terpenoids. Nat Biotechnol. 2003;21: 796–802. doi:10.1038/nbt833
9. Alper H, Miyaoku K, Stephanopoulos G. Characterization of lycopene-overproducing *E. coli* strains in high cell density fermentations. Appl Microbiol Biotechnol. 2006;72: 968–974. doi:10.1007/s00253-006-0357-y
10. Yuan LZ, Rouvière PE, LaRossa R a., Suh W. Chromosomal promoter replacement of the isoprenoid pathway for enhancing carotenoid production in *E. coli*. Metab Eng. 2006;8: 79–90. doi:10.1016/j.ymben.2005.08.005
11. Rodríguez-Villalón A, Pérez-Gil J, Rodríguez-Concepción M. Carotenoid accumulation in bacteria with enhanced supply of isoprenoid precursors by upregulation of exogenous or endogenous pathways. J Biotechnol. 2008;135: 78–84. doi:10.1016/j.jbiotec.2008.02.023
12. Yoon K-W, Doo E-H, Kim S-W, Park J-B. *In situ* recovery of lycopene during biosynthesis with recombinant *Escherichia coli*. J Biotechnol. 2008;135: 291–294. doi:10.1016/j.jbiotec.2008.04.001
13. Zhou K, Zou R, Stephanopoulos G, Too H-P. Metabolite profiling identified methylerythritol cyclodiphosphate efflux as a limiting step in microbial isoprenoid production. PLoS One. 2012;7: e47513. doi:10.1371/journal.pone.0047513
14. Chen Y-Y, Shen H-J, Cui Y-Y, Chen S-G, Weng Z-M, Zhao M, et al. Chromosomal evolution of *Escherichia coli* for the efficient production of lycopene. BMC Biotechnol. 2013;13: 6–10. doi:10.1186/1472-6750-13-6
15. Jin YS, Stephanopoulos G. Multi-dimensional gene target search for improving lycopene biosynthesis in *Escherichia coli*. Metab Eng. 2007;9: 337–347. doi:10.1016/j.ymben.2007.03.003

16. Zhang C, Chen X, Zou R, Zhou K, Stephanopoulos G, Too HP. Combining genotype improvement and statistical media optimization for isoprenoid production in *E. coli*. PLoS One. 2013;8: e75164. doi:10.1371/journal.pone.0075164

17. Xu F, Yuan QP, Zhu Y. Improved production of lycopene and b-carotene by *Blakeslea trispora* with oxygen-vectors. Process Biochem. 2007;42: 289–293. doi:10.1016/j.procbio.2006.08.007

18. Araya-Garay JM, Feijoo-Siota L, Rosa-Dos-Santos F, Veiga-Crespo P, Villa TG. Construction of new *Pichia pastoris* X-33 strains for production of lycopene and beta-carotene. Appl Microbiol Biotechnol. 2012;93: 2483–2492. doi:10.1007/s00253-011-3764-7

19. Bahieldin A, Gadalla NO, Al-Garni SM, Almehdar H, Noor S, Hassan SM, et al. Efficient production of lycopene in *Saccharomyces cerevisiae* by expression of synthetic crt genes from a plasmid harboring the ADH2 promoter. Plasmid. 2014;72: 18–28. doi:10.1016/j.plasmid.2014.03.001

20. Wang G-S, Grammel H, Abou-Aisha K, Sägesser R, Ghosh R. High-level production of the industrial product lycopene by the photosynthetic bacterium *Rhodospirillum rubrum*. Appl Environ Microbiol. 2012;78: 7205–715. doi:10.1128/AEM.00545-12

21. Jang H-J, Yoon S-H, Ryu H-K, Kim J-H, Wang C-L, Kim J-Y, et al. Retinoid production using metabolically engineered *Escherichia coli* with a two-phase culture system. Microb Cell Fact. 2011;10: 1–12. doi:10.1186/1475-2859-10-59

22. Sauer U, Lasko DR, Fiaux J, Hochuli M, Glaser R, Szyperski T, et al. Metabolic flux ratio analysis of genetic and environmental modulations of *Escherichia coli* central carbon metabolism. J Bacteriol. 1999;181: 6679–6688.

23. Baba T, Ara T, Hasegawa M, Takai Y, Okumura Y, Baba M, et al. Construction of *Escherichia coli* K-12 in-frame, single-gene knockout mutants: the Keio collection. Mol Syst Biol. 2006;2:1-11. doi:10.1038/msb4100050

24. Sander LC, Sharpless KE, Craft NE, Wise S a. Development of engineered stationary phases for the separation of carotenoid isomers. Anal Chem. 1994;66: 1667–1674. doi:10.1021/ac00082a012

25. Huxley H, Zubay G. Electron microscope observations on the structure of microsomal particles from *E. coli*. J Mol Biol. 1960;2: 10–18.

26. Hewitt CJ, Nebe-Von Caron G, Nienow AW, McFarlane CM. Use of multi-staining flow cytometry to characterise the physiological state of *Escherichia coli* W3110 in high cell density fed-batch cultures. Biotechnol Bioeng. 1999;63: 705–711. doi:10.1002/(SICI)1097-0290(19990620)63:6<705::AID-BIT8>3.0.CO;2-M

27. Kim YS, Lee JH, Kim NH, Yeom SJ, Kim SW, Oh DK. Increase of lycopene production by supplementing auxiliary carbon sources in metabolically engineered *Escherichia coli*. Appl Microbiol Biotechnol. 2011;90: 489–497. doi:10.1007/s00253-011-3091-z

28. Cánovas M, García V, Bernal V, Torroglosa T, Iborra JL. Analysis of *Escherichia coli* cell state by flow cytometry during whole cell catalyzed biotransformation for L-carnitine production. Process Biochem. 2007;42: 25–33. doi:10.1016/j.procbio.2006.07.027

29. Alper H, Miyaoku K, Stephanopoulos G. Construction of lycopene-overproducing *E. coli* strains by combining systematic and combinatorial gene knockout targets. Nat Biotechnol. 2005;23: 612–616. doi:10.1038/nbt1083

30. Seemann M, Tse Sum Bui B, Wolff M, Miginiac-Maslow M, Rohmer M. Isoprenoid biosynthesis in plant chloroplasts via the MEP pathway: direct thylakoid/ferredoxin-dependent photoreduction of GcpE/IspG. FEBS Lett. 2006;580: 1547–5152.

doi:10.1016/j.febslet.2006.01.082

31. Rohdich F, Zepeck F, Adam P, Hecht S, Kaiser J, Laupitz R, et al. The deoxyxylulose phosphate pathway of isoprenoid biosynthesis: studies on the mechanisms of the reactions catalyzed by IspG and IspH protein. Proc Natl Acad Sci U S A. 2003;100: 1586–1591. doi:10.1073/pnas.0337742100

32. Hunter WN. The non-mevalonate pathway of isoprenoid precursor biosynthesis. J Biol Chem. 2007;282: 21573–21577. doi:10.1074/jbc.R700005200

33. Martin VJJ, Yoshikuni Y, Keasling JD. The *in vivo* synthesis of plant sesquiterpenes by *Escherichia coli*. Biotechnol Bioeng. 2001;75: 497–503. doi:10.1002/bit.10037

34. Lee SY. High cell-density culture of *Escherichia coli*. Trends Biotechnol. 1996;14: 98–105. doi:10.1016/0167-7799(96)80930-9

35. Yoon SH, Lee SH, Das A, Ryu HK, Jang HJ, Kim JY, et al. Combinatorial expression of bacterial whole mevalonate pathway for the production of β-carotene in *E. coli*. J Biotechnol. 2009;140: 218–226. doi:10.1016/j.jbiotec.2009.01.008

36. Fang A, Demain A. Influence of aeration and carbon source on production of microcin B17 by *Escherichia coli* ZK650. Appl Microbiol Biotechnol. 1997;47: 547–553.

37. Marisch K, Bayer K, Scharl T, Mairhofer J, Krempl PM, Hummel K, et al. A comparative analysis of industrial *Escherichia coli* K-12 and B strains in high-glucose batch cultivations on process-, transcriptome- and proteome level. PLoS One. 2013;8: e70516. doi:10.1371/journal.pone.0070516

38. Yoon SH, Han M-J, Jeong H, Lee CH, Xia X-X, Lee D-H, et al. Comparative multi-omics systems analysis of *Escherichia coli* strains B and K-12. Genome Biol. 2012;13: 1–13. doi:10.1186/gb-2012-13-5-r37

39. Huang L, Pu Y, Yang X, Zhu X, Cai J, Xu Z. Engineering of global regulator cAMP receptor protein (CRP) in *Escherichia coli* for improved lycopene production. J Biotechnol. 2015;199: 55–61. doi:10.1016/j.jbiotec.2015.02.006

40. Fraser PD, Sandmann G. *In vitro* assays of three carotenogenic membrane-bound enzymes from *Escherichia coli* transformed with different crt genes. Biochem Biophys Res Commun. 1992;185: 9–15.

41. Albrecht M, Misawa N, Sandmann G. Metabolic engineering of the terpenoid biosynthetic pathway of *Escherichia coli* for production of the carotenoids beta-carotene and zeaxanthin. Biotechnol Lett. 1999;21: 791–795. doi:10.1023/A:1005547827380

42. Sandmann G. Carotenoid biosynthesis and biotechnological application. Arch Biochem Biophys. 2001;385: 4–12. doi:10.1006/abbi.2000.2170

43. Ramos JL, Duque E, Gallegos M-T, Godoy P, Ramos-Gonzalez MI, Rojas A, et al. Mechanisms of solvent tolerance in gram-negative bacteria. Annu Rev Microbiol. 2002;56: 743–768. doi:10.1146/annurev.micro.56.012302.161038

44. Sharma SK, Le Maguer M. Kinetics of lycopene degradation in tomato pulp solids under different processing and storage conditions. Food Res Int. 1996;29: 309–315. doi:10.1016/0963-9969(96)00029-4

45. Schierle J, Bretzel W, Bühler I, Faccin N, Hess D, Steiner K, et al. Content and isomeric ratio of lycopene in food and human blood plasma. Food Chem. 1997;59: 459–465. doi:10.1016/S0308-8146(96)00177-X

Appendix

Table S1. Retention times and absorption spectra characteristics of carotenoids.

Peak HPLC	Carotenoid	Tr (min)	λ (nm) experimental	λ (nm) theoretical	References
1	phytoene	7.79	(276) 285 (296)	(276) 286 (296.2)	[24]
2	(*13 cis*)-Lycopene	8.93	297 360 439 466 495	297 360.4 439 465 495.5	[45]
3	(*all trans*)-Lycopene	10.12	294 360 445 471 502	295 360.0 445 472 502.0	[45]

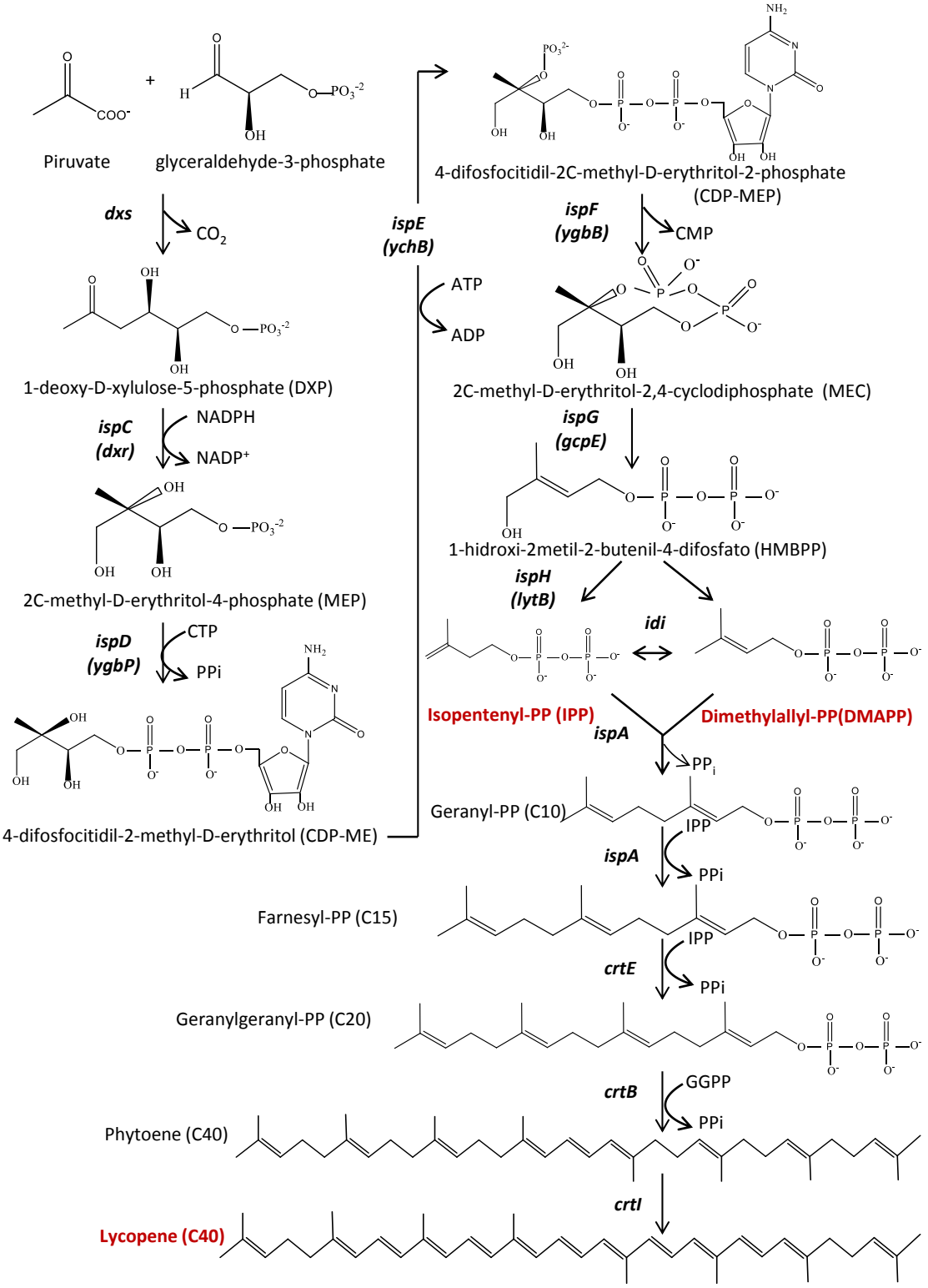

Figure S1. Biosynthetic pathway of lycopene in *E. coli* from a native 2-C-methyl-D-erythritol 4-phosphate pathway (non-mevalonate pathway). Gene names and its encoded enzymes follow: *dxr* DXP reductoisomerase, *dxs* DXP synthase, *idi* IPP isomerase, *ispA* FPP synthase, *crtE* GGPP synthase, *crtB* phytoene synthase, *crtI* phytoene desaturase.

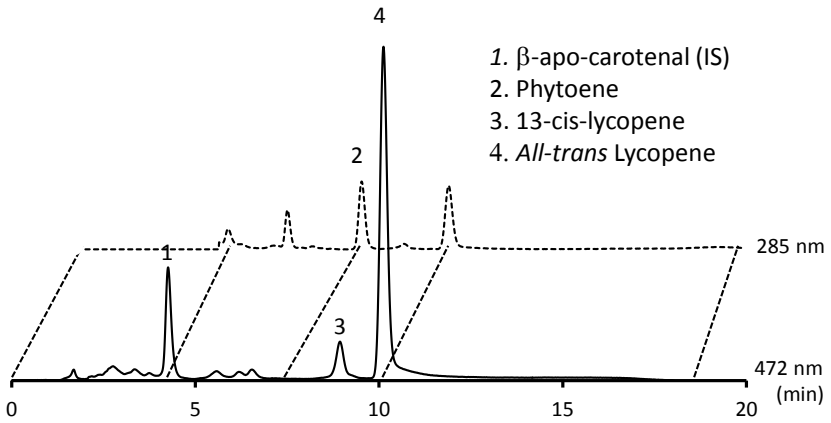

Figure S2. Chromatogram of reference standards for 20 min measured at 472and 285 nm, respectively.

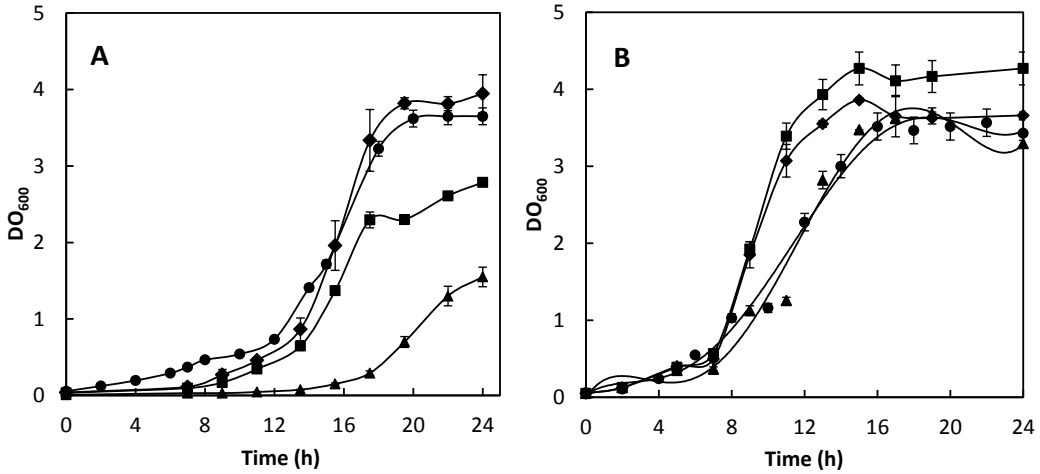

Figure S3. Effect of the carbon source (**(A)** 40 mM glycerol and **(B)** 20 mM glucose) on cell growth by metabolically engineered *E. col* strains: BL21 LF (▲), BL21LG. (♦), BL21L and (●) K12L, in 50 ml batch culture.

CHAPTER 4

The protein acetyltransferase Patz from Escherichia coli is regulated by autoacetylation-induced oligomerization

The results presented in this chapter are based on the publication:

Teresa de Diego Puente, Julia Gallego-Jara, Sara Castaño-Cerezo, Vicente Bernal Sánchez, Vanesa Fernández Espín, José García de la Torre, Arturo Manjón Rubio and Manuel Cánovas Díaz

The protein acetyltransferase PatZ from *Escherichia coli* is regulated by autoacetylation-induced oligomerization

Journal of Biological Chemistry. 2015; 38: 23077–23093. doi: 10.1074/jbc.M115.649806

jbc.M115.649806.

Abstract

Lysine acetylation is an important post-translational modification in the metabolic regulation of both prokaryotes and eukaryotes. In *Escherichia coli* (*E. coli*), PatZ is the only known acetyltransferase protein and is responsible for acetyl-CoA synthetase (Acs) acetylation. In this study, we demonstrated PatZ positive cooperativity in response to acetyl-CoA and the regulation of Acs activity by the acetylation level. Furthermore, functional analysis of an E809A mutant demonstrated that the conserved glutamate residue is not relevant for the PatZ catalytic mechanism. Biophysical studies demonstrated that PatZ is a stable tetramer in solution and is transformed to its octameric form by autoacetylation. Moreover, this modification is reversed by the sirtuin CobB. Finally, an *in silico* PatZ tetramerization model based on hydrophobic and electrostatic interactions is proposed and validated by 3D hydrodynamic analysis. These data reveal, for the first time, the structural regulation of an acetyltransferase by autoacetylation in a prokaryotic organism.

Introduction

Post-translational modification (PTM) of proteins by lysine acetylation has been traditionally associated with eukaryotic organisms. However, in recent years, interest in PTM in prokaryotic organisms has increased greatly [1]. Many metabolic enzymes are known to be acetylated in *E. coli* [2], although the physiological importance of acetylation has not been studied in detail. Acetylation has traditionally been described as a reversible PTM catalysed by an acetyltransferase with acetyl-CoA as acetyl donor. However, recently the importance of non-enzymatic acetylation has been discovered, using acetyl-CoA or acetyl-phosphate as acetyl donors in prokaryotic and eukaryotic organisms [2–4].

In *E. coli*, the Nε-acetyltransferase PatZ is the only enzyme known to be involved in the post-translational acetylation of proteins. PatZ is an acetyltransferase belonging to the Gcn5-related N-acetyltransferases superfamily, which catalyses the transfer of an acetyl group from acetyl-CoA to a primary amine [5]. PatZ is a large multidomain protein with 886 residues (~ 98 kDa) that has a C-terminal acetyl-CoA binding fold whose predicted structure belongs to the large GNAT superfamily of acetyltransferases (residues 725 to 884). The N-terminal domain is a predicted domain with high similarity to the acyl-CoA synthetase (NDP-forming) superfamily of enzymes (residues 3 to 625) [6]. Many members of this family are oligomeric proteins [7]. In fact, *Se*Pat, *Salmonella enterica* (*S. enterica*) PatZ ortholog, oligomerizes to a tetramer due to its binding to acetyl-CoA [8].

It has recently been described that in *E. coli*, PatZ is acetylated *in vivo* [2,9], although the consequences of PatZ acetylation are not known. Regarding the acetyltransferase catalytic mechanism, it has not been studied in bacteria, although studies carried out in other GNAT suggest the existence of two possible mechanisms, a Bi-Bi sequential and a ping-pong catalytic mechanism [10–14].

One of the best known PatZ substrates is Acs, an enzyme regulated by acetylation in bacteria such as *S. enterica*, *E. coli*, *Bacillus subtilis*, *Rhodopseudomonas palustris,* and *Mycobacterium tuberculosis* (*M. tuberculosis*) [15–19]. In *E. coli*, Acs reversible lysine acetylation is mainly regulated by two enzymes, the Gcn5-like acetyltransferase Pat [15–19] and a deacetylase, the NAD^+-dependent sirtuin-like deacetylase CobB [16–20]. Acs is a key enzyme in prokaryotic and eukaryotic metabolism since it synthesizes acetyl-CoA from acetate, ATP and CoA *via* an acetyl-AMP intermediate and is involved in metabolism homeostasis due to its direct link with acetyl-CoA. Besides, acetyl-CoA is involved in the energy metabolism, acting as substrate and playing a critical role in overall metabolism modulation, which makes it a key operator in the regulation of metabolic fluxes. It is important to note that in exponentially growing aerobic cultures of *E. coli*, cytosolic acetyl-CoA concentrations vary from 0.5 to 0.6 mM with glucose and from 0.2 to 1.7 mM with acetate as the sole carbon sources [21]. In this sense, the Acs enzyme is essential in limited carbon source conditions accompanied by a low extracellular concentration of acetate [22,23].

Hence, the main objective of this study was to ascertain the kinetic and biochemical characteristics of PatZ and the effect on the regulation of Acs by lysine acetylation. This characterization will provide a deeper understanding of protein acetylation in *E. coli*.

Methods

Construction of PatZ overexpression plasmids

The 2658-bp *patZ* gene of *E. coli* BW25113 was PCR-amplified and cloned into the pRSETA plasmid. The resulting plasmid was named pRSET*patZ*. Single amino acid mutant E809A was obtained by site-directed mutagenesis from pRSET*patZ* using PCR. The resulting plasmid was named pRSET$patZ^{E809A}$. The quintuple-mutant (substitution of lysines at 146, 149, 391, 447, 635 for arginines), was obtained by sequential site directed mutagenesis since pRSET*patZ.* The resulting plasmid was named pRSER$patZ^{5(K\rightarrow R)}$. The 2100 bp fragment corresponding to a truncated acetyltransferase defective *patZ* gene (1-2100 bp) was PCR-amplified and cloned into the pRSETA plasmid. The resulting plasmid was named pRSET$patZ^{Acs\text{-}like}$. The 558 bp fragment

encoding the GNAT domain of PatZ (2100-2658 bp) was cloned in the same way, resulting in plasmid pRSET*patZ*^{GNAT}. The Acs and CobB proteins were overexpressed using the ASKA collection plasmids [24]. All molecular biology enzymes used were from Thermo Fisher Scientific. The strains, plasmids and primers used are listed in Appendix Table S1.

Overproduction and purification of proteins

Chemically competent *E. coli* BL21 (DE3) wt or Δ*patZ* strains were transformed by heat shock at 42 °C. Cultures were grown overnight at 30 °C with orbital shaking (200 rpm). The culture medium used was Terrific broth (TB) (12 g L^{-1} tryptone, 24 g L^{-1} yeast extract, 4 % v/v glycerol, 0.17 M KH_2PO_4 and 0.72 M K_2HPO_4) containing ampicillin (100 µg mL^{-1}) (for pRSETA) or chloramphenicol (30 µg/mL) (for ASKA plasmids).The expression was induced with isopropyl β-D-1-thiogalactopyranoside (IPTG), 1 mM (for pRSETA) or 0.1 mM (for ASKA plasmids). Cells were harvested by centrifugation, thoroughly washed with 0.9 % NaCl and resuspended in 10 mL of binding buffer (50 mM potassium phosphate pH 7.5 containing 500 mM NaCl and 20 mM imidazole), supplemented with EDTA-free protease inhibitor (SigmaFast Protease Inhibitor Cocktail Tablet, from Sigma Aldrich). Cells were lysed by sonication for 2 min (20 s each pulse) on ice using a Vibra Cell sonicator (Sonicator Sonics & Materials,). The lysates were clarified by centrifugation at 10000 x g for 15 min at 4 °C.

Recombinant proteins were purified by immobilized metal affinity chromatography (IMAC). The cell free extract was loaded onto a 5 mL HisGraviTrap column (GE Healthcare), and washed with washing buffer (50 mM potassium phosphate buffer pH 7.5 containing 500 mM NaCl and 50 mM imidazole). The His6-tagged proteins were eluted with an elution buffer (50 mM potassium phosphate buffer pH 7.5 containing 500 mM NaCl and 500 mM imidazole). The salts and imidazole from protein-containing fractions were removed with a PD-10 Sephadex G-25 column (GE Healthcare). Purified proteins were kept in storage buffer (50 mM potassium phosphate buffer pH 7.5 containing 100 mM NaCl and 10 % v/v glycerol) at - 80 °C until used. Finally, Amicon Ultra centrifugal-15 filters (Millipore) were used to concentrate the proteins.

SDS-PAGE and native electrophoresis

Proteins were analysed by SDS/PAGE electrophoresis on 10 % acrylamide gels using a Mini-Protean cell (Biorad). For native electrophoresis, NativePAGE 4-16 % Bis-Tris gels and Native unstained Protein Standard (Life Technologies) were used. The proteins were detected by Coomassie Blue staining (Thermo Fisher Scientific).

Detection of lysine acetylated proteins by western blot analysis

Lysine acetylated proteins were separated by SDS-PAGE or native-PAGE. The proteins were transferred to polyvinylidene fluoride (PVDF) membranes using a semidry transfer unit (Trans-Blot® SD Semi-Dry Transfer Cell, Bio-Rad). The membranes were blocked with 1 % (w/v) bovine serum albumin (BSA) in TBST (10 mM Tris-HCl, 0.15 M NaCl, 0.05% Tween-20, pH 7.5) for 1 hour. The membranes were incubated with a primary rabbit monoclonal anti-acetyl Lys antibody (InmuneChem) and a goat anti-rabbit secondary antibody (Santa Cruz Biotechnology). Finally, the membrane was incubated for 10 min with Amersham ECL Western blotting detection reagent (Thermo Scientific).

Acetylation and deacetylation assays

All acetyltransferase/deacetylase enzymatic experiments were performed at 37 °C in 50 mM potassium phosphate buffer at pH 7.5 with a reaction volume of 200 µL. A blank assay without enzyme under the same conditions was carried out to subtract the chemical hydrolysis of acetyl-CoA. The concentration of the 2-nitro-5-thiobenzoate anion $(TNB^2)^-$ anion was determined using a molar extinction coefficient of 15.53 mM^{-1} cm^{-1}, which was experimentally determined from the slopes of three independent experiments using 62.5 to 500 µM cysteine and 0.3 mM DTNB (5,5'-dithiobis-2-nitrobenzoic acid) as standard. The amount of purified PatZ enzyme was optimized. Experiments were carried out at a PatZ concentration of 60 nM. The initial rates of colour development, obtained as milliunits of absorbance per minute at 412 nm (Synergy HT spectrophotometer, Bio-Tek), were converted to units of absorbance per minute by means of the PathCheck Sensor feature. Pseudo-first-order kinetic parameters were determined using Prism v6 (GraphPad) analytical software. A non-enzyme control was used to correct the background.

Data for Acs and PatZ autoacetylation were fitted to the equation $V_0 = (V_{max} \times [S]) / (K_M + [S])$, where V_0 is the initial velocity, V_{max} is the maximum velocity, [S] is the substrate concentration, and K_M is the substrate concentration for half-maximal velocity.

Data for acetyl-CoA were fitted to the equation $V_0 = (V_{max} \times [S]h) / (K_{0.5}^h + [S]h)$, where h represents the Hill coefficient and $K_{0.5}^h$ denotes the substrate concentration for half-maximal velocity. The parameters were determined from curves with an R^2 value of 0.98.

Deacetylation assays were carried out with a 3:1 CobB:PatZ molar ratio and a 1 mM NAD^+ concentration.

Acetyl-CoA synthetase activity

The acetyl-CoA synthetase assay used was based on the coupled assay reported by Williamson and Corkey [25]. AMP production was detected *via* a coupled-enzyme assay in which myokinase (MK), pyruvate kinase (PK) and lactate dehydrogenase (LDH) couple AMP production to NADH oxidation. Acs was purified from *E.coli* BL21 (DE3) Δ*patZ* and preincubated with different PatZ concentrations at 0.1 mM acetyl-CoA for 1 h prior to measuring its synthetic activity. Then, standard acetyl-CoA synthetase assays (0.2 mL) were performed at 37 °C in 50 mM potassium phosphate buffer at pH 7.5 containing 3.0 mM PEP (phosphoenolpyruvate), 5 units MK, 1 unit PK, 1.5 units LDH, 5 mM $MgCl_2$, 2.5 mM ATP, 1.5 mM CoA, 0.1 mM NADH, 5 mM acetate and 1 mM dithiothreitol (DTT). This reaction was started with the addition of 40 µL of 0.1 µM Acs. All reactions were performed in triplicate. Specific activity was calculated from the extinction coefficient of 6.22 mM^{-1} cm^{-1} for the oxidation of two molecules of NADH for each AMP released. One unit of Acs activity is defined as 1 µmole acetyl-CoA formed per minute at pH 7.5 and 37 °C. The specific activity of Acs is expressed as a percentage.

Differential Scanning Calorimetry

A differential scanning calorimeter (DSC) 2920 (TA Instruments) was used for the calorimetric analysis of PatZ in different media. Samples were analysed using a programmed heating scan rate of 1 °C min^{-1} from 30 °C to 120 °C. All experiments were carried out at 0.1 mg mL^{-1} in 50 mM phosphate buffer, pH 7.5, and 0 to 1.5 mM acetyl-CoA. Phosphate buffer without protein was used as reference. No peaks were visible on the rescan in any case, which means that all transitions were irreversible. For data analysis and conversion Universal Analysis Software (TA Instrument v 0.4) was used and collected DSC data were normalized for protein concentration. Heat capacity (Cp) was expressed in kcal mol^{-1} K^{-1} (1 cal = 4.184 J).

Gel permeation chromatography

Gel permeation chromatography (GPC) was performed with an HPLC (Agilent technologies) using a Supelco Discovery Bio GFC 300 column (4.6 × 50 mm and 5 µm particle, Sigma Aldrich). The eluent was 50 mM phosphate buffer pH 7.5, containing 100 mM NaCl, with a flow rate of 0.05 mL min^{-1}. The injection volume was 50 µl. The elution of proteins was monitored by absorbance at 280 nm. A set of protein standards (Sigma Aldrich) was used to generate standard curves from elution times of molecules with known molecular masses: thyroglobulin (670 kDa), catalase (250 kDa), ɣ-globulin (150 kDa), bovine serum albumin (67 kDa), ovalbumin (44.3 kDa) and ribonuclease type A I (13.7 kDa). Blue dextran and p-aminobenzoic acid were used to determine column exclusion limits. The void volume (V_0) and

the total volume (V_T) of the column were 0.35 mL and 0.8 mL, respectively. A standard curve using linear regression analysis was obtained: K_{av} = -0.02 (Mw) + 1.44 having an R^2 = 0.97. Data represent mean values with standard deviations for three separate experiments.

Liquid Chromatography–Tandem Mass Spectrometry Assay

Samples were alkylated with 100 mM iodoacetamide (IAA) for 30 min at room temperature in the dark. Proteins were digested with 0.5-1 µg of Trypsin Gold Proteomics Grade (Promega) for 3 h at 37 °C. The reaction was stopped with 0.1 % formic acid and samples were dried using a vacuum evaporator. Tryptic peptides generated from the samples were separated and analysed by Liquid Chromatography–Tandem Mass Spectrometry Assay (LC/MS). An Agilent 1100 (Agilent Technologies) was equipped with a Zorbax SB-C18 HPLC column (Agilent Technologies) and connected to an Agilent Ion Trap XCT Plus mass spectrometer (Agilent Technologies) using an electrospray (ESI) interface. Two mobile phases were used, phase A, composed of water/acetonitrile/formic acid (94.9:5:0.1, v/v) and phase B, consisting of water/acetonitrile/formic acid (10:89.9:0.1, v/v).

The digested peptides were resuspended in 20 µL of phase A and eluted using a linear gradient from 0-80 % phase B for 180 min and at a flow rate of 10 µL min^{-1}. The mass spectrometer was operated in the positive mode with a capillary spray voltage of 3500 V, and a scan speed of 8100 (m/z)/sec from 50 to 2200 m/z, with a target mass of 1000 m/z, and 3 spectra averaging. The nebulizer gas pressure was set at 15 psi, and the drying gas a flow rate at 5 L min^{-1} at a temperature of 350 °C. MS/MS data were collected in an automated data-dependent mode (AutoMS mode). Data processing was performed with Data Analysis program for LC/MSD Trap Version 3.3 (Bruker Daltonik) and Spectrum Mill MS Proteomics Workbench (Agilent Technologies) [26,27]. After automatic validation of the results, the identified proteins with the sequence of the digested peptides were compiled. Peptides were considered valid with a score threshold of eight, and a percentage-scored peak intensity higher than 70%.

Dynamic light scattering

Dynamic light scattering (DLS) measurements were carried out in a NanoSizer ZS (Malvern Instruments), operating a laser of 632.8 nm at an angle of 173 °. The autocorrelation function was processed by using the ZetaSizer v7.03 software associated with the instrument in the CONTIN mode. This procedure determines a diffusion coefficient that is presented as a distribution of the hydrodynamic radius, R_h. The hydrodynamic measurements were carried out at 20 °C (T=293K) in 100 mM NaCl, 50 mM potassium phosphate buffer at pH 7.5 with a PatZ protein concentration of 10 µM. The experiment consisted of 12 measurements of 11 runs each,

with 30 seconds per run, which amounted to 11 minutes of data acquisition time. The CONTIN analysis allows for two modalities in the distribution, expressing the amount of solute of a given R_h in terms of either contribution to scattering intensity of as mass fraction. The former is particularly sensitive to the presence of large particles even if their population is very small, while the latter detects the sample's major species. A limitation of DLS-derived distributions is that R_h is handled in a logarithmic scale, and peaks have, even for monodisperse samples, a merely instrumental width, so that components of a paucidisperse sample cannot be differentiated if their R_h do not differ widely. Nonetheless, the Protein Workshop mode, specific for protein samples, of the ZetaSizer software was useful for our purposes.

Analytical ultracentrifugation

Analytical ultracentrifugation (AUC) experiments were performed in a Beckman Coulter Optima XL-I analytical ultracentrifuge (Beckman-Coulter) using an An50Ti eight-hole rotor, 12-mm path-length charcoal-filled Epon double-sector centrepieces, employing the UV–visible detection system. The experiments were carried out in the same buffer and temperature mentioned above with a PatZ protein concentration of 10 μM. A wavelength of 280 nm was used in the absorbance optics. Sedimentation velocity (SV) runs were carried out for 8 hours at a rotor speed of 40000 rpm using 400 μl samples in the above mentioned solvent. A series of 400 scans, without time intervals between them, were acquired for each sample. Least squares boundary modelling of the sedimentation velocity data was used to calculate sedimentation coefficient, s, distributions with the size-distribution c(s) method [28] implemented in the SEDFIT v13.0b software [29]. As the measurements are made at 20 ˚C, the *s* determined are practically identical to the standard coefficient, $s_{20,w}$. Unlike DLS, AUC-SV has excellent resolution, enabling the differentiation of components (peaks in the c(s) distribution) with close $s_{20,w}$ values. In addition to rather reliable sedimentation coefficients, AUC-SV also provides approximate estimations of the molecular weights.

Results

PatZ shows positive cooperativity in response to acetyl-CoA substrate

Acs Nε-lysine acetylation by PatZ was kinetically characterized. PatZ kinetic analysis showed a typical hyperbolic response *versus* Acs substrate (0 to 40 μM) at a fixed saturating concentration of acetyl-CoA (1.0 mM) (Figures 1A, B).

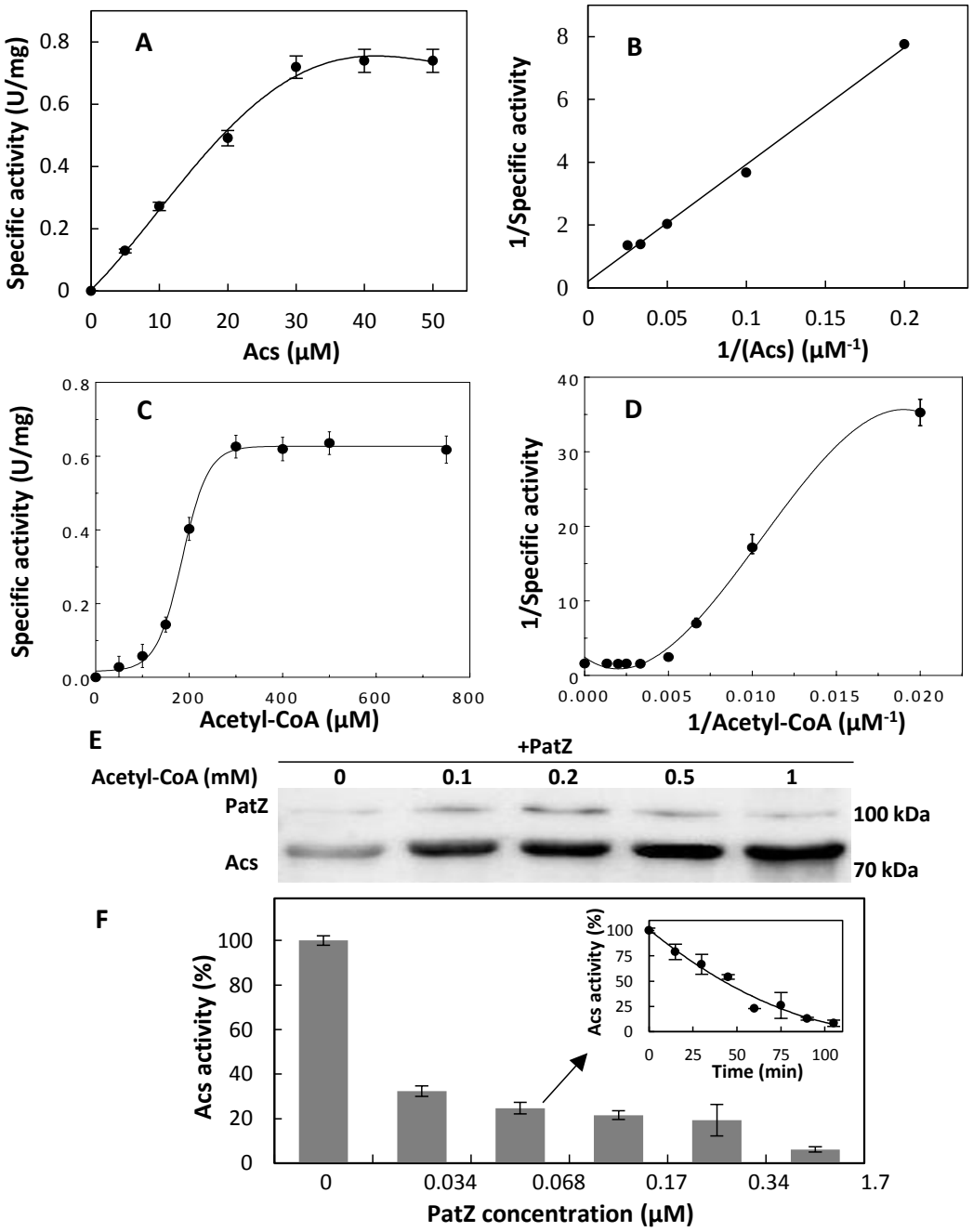

Figure 1. PatZ activity on Acs. **(A)** Substrate saturation curve of the PatZ-dependent acetylation reaction rate at different concentrations of Acs. **(B)** Double-reciprocal plot of the kinetic data. PatZ was used at 60 nM, and acetyl-CoA at 1.0 mM. **(C)** Substrate saturation curve of the PatZ-dependent acetylation reaction velocity at different concentrations of acetyl-CoA. **(D)** Double-reciprocal plot of the kinetic data indicating a concave curve. PatZ enzyme was present at 60 nM, and Acs was present at a saturating concentration of 40 µM. **(E)** Western blot of the Acs protein. Acs untreated (lane 1) and lysine acetylated by PatZ at 0.1mM (lane 2), 0.2 mM (lane 3), 0.5 mM (lane 4) and 1.0 mM (lane 3) of acetyl-CoA. **(F)** Acs activity *versus* acetylation degree. Percentage of acetyl-CoA synthetase activity (Acs) incubated at different concentrations of PatZ for 30 min and 0.1 mM of acetyl-CoA at 37 °C. The insert shows the loss of Acs activity *versus* acetylation time as a result of the incubation with 68 nM PatZ and 0.1 mM acetyl-CoA.

In contrast, when Acs was held at a fixed saturating concentration (40 μM) and the acetyl-CoA concentration was varied (50 to 800 μM) (Figure 1C), PatZ activity showed a sigmoidal dependence. The kinetic cooperativity observed in PatZ was revealed by the double-reciprocal plot of the rate data, which was upwardly concave (Figure 1D) and could be described by the Hill equation [30]. The calculated Hill coefficient (h) was 7.91 ± 0.22 (R^2 = 0.99), which describes the PatZ positive cooperativity on acetyl-CoA. The kinetic parameters determined are displayed in Table 1. These data showed that enzymatic rate was slightly higher for the substrate Acs than for acetyl-CoA, while the $K_{0.5}$ was much higher for acetyl-CoA.

Table 1. Kinetic parameters of PatZ with acetyl-CoA and Acs as substrates.

Substrate	V_{max}(U/mg)	K_M (μM)	$K_{0.5}$ (μM)	k_{cat} (s^{-1})	k_{cat}/K_M($s^{-1}M^{-1}$)
Acetyl-CoA	0.63 ± 0.006	-	185.20 ± 2.5	1.02 ± 0.05	5.49 x 10^3
Acs	0.73 ± 0.024	14.78 ± 0.8	-	1.19 ± 0.04	8.1 x 10^2

Acs activity is regulated by the acetylation level

Western blot was performed to confirm PatZ Nε-acetyl-transferase activity on Acs using anti-acetyl Lys antibody. Acs was incubated with PatZ and 0-1 mM acetyl-CoA concentration for 30 minutes (Figure 1E). As can be seen, there was an increase in Acs acetylation in response to increasing acetyl-CoA concentrations.

In order to identify the acetylated lysines of Acs by PatZ, a MS assay was conducted after Acs incubation at different acetyl-CoA concentrations with PatZ. The Acs purified from a Δ*patZ* strain was acetylated at K199 and K226. These acetylations were independent of PatZ, probably due to non-enzymatic acetylation. Moreover, these acetylated lysines explain the low signal shown by Acs in the first line of the western blot (Figure 1E). Acs showed sixteen acetylated lysines at 1.0 mM acetyl-CoA in the presence of PatZ. The identified lysine acetylation sites were 50, 54, 68, 111, 130, 131, 199, 200, 207, 221, 226, 400, 401, 604, 609 and 617. To determine whether the Acs acetylation was mediated chemically or enzymatically, an acetylation assay of Acs incubated at 1 mM acetyl-CoA concentration in the absence of PatZ was carried out. The lysine acetylation sites identified by chemical acetylation were 130, 131, 199, 200, 207, 226 and 221. Therefore, nine site-specific of lysine acetylation in Acs were due to enzymatic acetylation by PatZ. The results are given in Table 2. An example of the assignment of acetylation to Lys 54 and 68 of Acs by LC-MS/MS analysis is shown in Figure 2A.

Table 2. MS assay of Acs and PatZ proteins.

Protein	Acetyl-CoA (mM)	Acetylated Lysine residues
Acs	0	2 (199, 226)
	0.1	7 (50, 68, 130, 131, 199, 226, 609)
	0.5	13 (50, 54, 68, 111, 130, 131, 199, 207, 221, 226, 400, 401, 609)
	1	16 (50, 54, 68, 111, 130, 131, 199, 200, 207, 221, 226, 400, 401, 604, 609, 617)
PatZ	1	6 (146, 149, 391, 447, 635, 819)

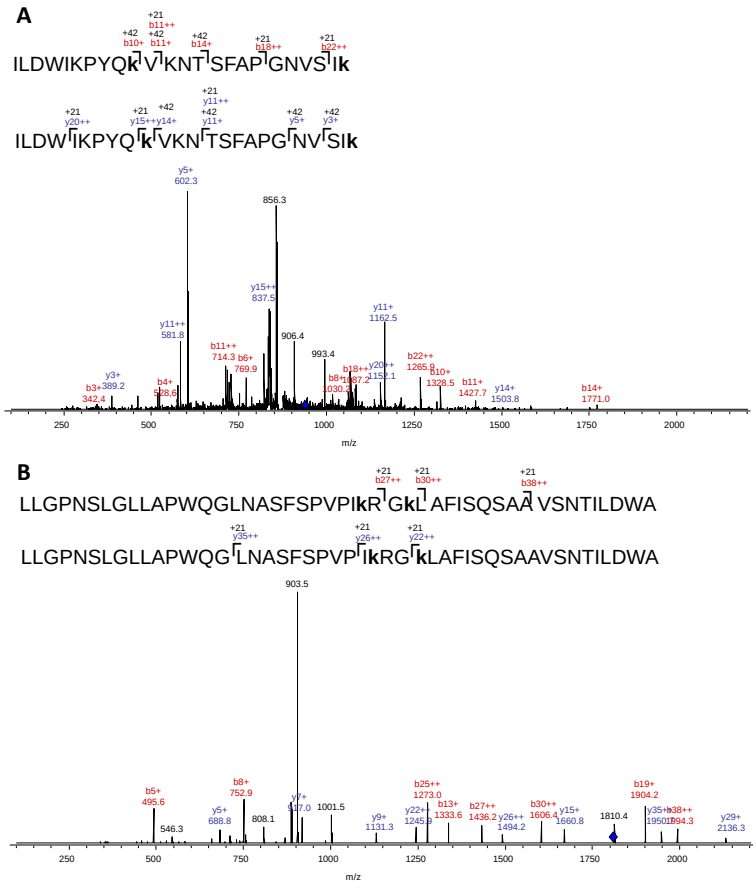

Figure 2. Identification of lysine acetylation by LC-MS/MS analysis. **(A)** Assignment of acetylation to Lys 54 and 68 of Acs. MS/MS spectrum of precursor ion m/z 944.67^{3+} of modified peptide (ILDWIKPYQkVKNTSFAPGNVSIk) from Acs. **(B)** Assignment of acetylation to Lys 146 and 149 of PatZ. MS/MS spectrum of precursor ion m/z 1806.73^{3+} of modified peptide (LLGPNSLGLLAPWQGLNASFSPVPIkRGkLAFISQSAAVSNTILDWAQQR) from PatZ. The labelled peaks correspond to masses of b and y ions series shown in red and blue colours, respectively. Manual inspection of b and y ions series of these spectra indicates mass increments of 42 Da for ion^{+} and 21 Da for ion^{2+} in some cases when compared with the corresponding ion series of the unmodified peptides, revealing possibly acetylated lysine. Acetylation at the location was indicated in bold lowercase letter, “k”.

Purified Acs from *E. coli* BL21 (DE3) Δ*patZ* was incubated with different PatZ concentrations and 0.1 mM acetyl-CoA at 37 °C for 30 min before measuring Acs activity. The acetyl-CoA synthetase activity decreased in response to the acetylation level by PatZ (Figure 1F). The Acs synthetic activity was also measured at 0 and 0.1 mM acetyl-CoA in the absence of PatZ and was found to be the same in both cases, 620.86 ± 12.6 U/mg.

Potential role for the E809 residue of PatZ in the catalytic mechanism

Although the GNAT family acyltransferases mechanism is not completely understood, most evidence suggests a sequential mechanism operates to transfer the acetyl group from acetyl-CoA to the targeted protein *via* a ternary complex. The reaction mechanism is initiated by the nucleophilic attack of the deprotonated amine on the carbonyl functional group of acetyl-CoA [10–12,31]. This proposed mechanism of catalysis involves a conserved glutamic acid (E809 in PatZ) acting as a general base, deprotonating the amine. To determine the role of E809, a PatZ mutant protein harbouring an E809 to alanine mutation was generated. The pH dependence of the acetyltransferase activity with Acs and acetyl-CoA as substrates was determined and compared with the wt enzyme (Figure 3A). As can be seen, PatZ^{E809A} showed lower activity than PatZ at low pH (5-7). However, this activity increased with the pH, reaching similar activity levels to those of the wt enzyme. At high pH values (9-10) lysine residues were spontaneously deprotonated (pK_a = 9.6).

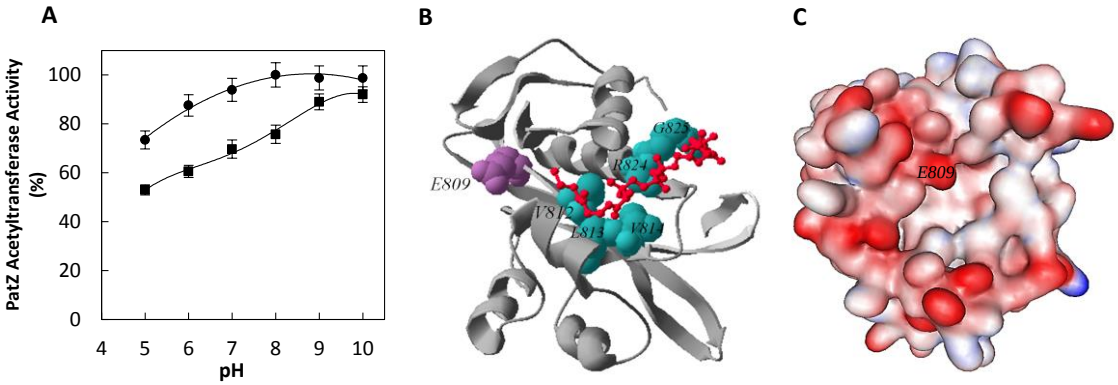

Figure 3. PatZ activity *versus* pH. **(A)** pH dependent activity of PatZ (●) and PatZ^{E809A} mutant (■) on Acs. The PatZ wt and mutant concentration was 60 nM. The Acs concentration was 40 µM at 1 mM of acetyl-CoA. **(B)** PatZ catalytic domain model generated by Phyre2 server. Coenzyme A binding pocket and conserved glutamic acid are shown in wireframe mode coloured green and purple, respectively. Acetyl-CoA substrate is shown in red. The figure was made with Swiss Model PDB viewer [32]. **(C)** Electrostatic surface PatZ catalytic domain (red represents negative electrostatic potential; blue represents positive electrostatic potential, and white is neutral).

Phyre2 [33] and 3D ligand site [34] web servers were used to predict acetyl-CoA ligand-binding sites of the PatZ catalytic domain (sequence from 725 to 884) in multi-template/*ab initio* mode (Figure 3B). Five templates were selected to model PatZ GNAT domain (sequence from 725 to 884), which were from *Kribbella flavida* (*K. flavida*) (4MY3, Pdb id code), *Salmonella typhimurium* (*S. typhimurium*) (3DR8, Pdb id code), *Mycobacterium smegmatis* (*M. smegmatis*) (4ORF, Pdb id code), *M. tuberculosis* (4AVC, Pdb id code), *S. enterica* (4U5Y, Pdb id code) and *Saccharomyces cerevisiae* (*S. cerevisiae*), based on heuristics to maximize confidence (99 % in all cases), percentage identity (21 %, 26 %, 29 %, 19 % and 19%, respectively) and alignment coverage by each template (Figure 4). The Coenzyme A binding pocket includes V812, L813, V814, G824 and R825 residues, as detected by the fpocket2 program (Figure 3B) [35,36]. WebLab Viewer Lite software was used to display the electrostatic surface of the PatZ catalytic domain (Figure 3C).

```
PatZ              ------------------------RCLFRPIL------------PEDEPQLQQFISRVTKEDL 751
4MY3              ------------------------EALQVRDAE------------DADWPAILPFFREIVSAGE 30
3DR8              ------------------------AXTIRFAD------------KADCAAITEIYNHAVLHTA 28
4ORF              LVRIARQRLAAFITPIPVQVRTGEWFYLRPVL------------PGDVER---------TSETL 169
4AVC              LLRTARQRLAAFVSPIPVRLADGTQLXLRPVL------------PGDRERTVHGHIQFSGETL 182
4U5Y              --------------EADVVLRDGGTARVRPIT------------VDDAERLVSFYEQVSDESK 62
1YGH              ------------------------I-EFRVVNNDNTKENMMVLTG--------------LKNI 123
                                          .*

PatZ              YYRYFSEINEFTHEDLANMTQIDYDR-EMAF------------VAVRRIDQTEEILGVTRAI- 800
4MY3              TYAYDPELTDEQARSLW-XTPSGPQS-RTTV------------AV--DA--DGTVLGSANXYP 75
3DR8              --------------AIWNDRTVDTDN-RLAWYEARQLLGYPVLVS--EE--NGVVTGYASFGD 72
4ORF              YRRFQSV-RKPTRALLEYLFEVDYAD-HFVW------------VM--TEGALGPVIADARFV- 215
4AVC              YRRFXSA-RVPSPALXHYLSEVDYVD-HFVW------------VV--TD--GSDPVADARFV- 226
4U5Y              YYRFFAPYPRLCAKDVHRFTHHDFVD-RVGL------------AA--TI--GGEFIATVRYD- 107
1YGH              ---FQKQLPKMPKEY---IARLVYDRSHLSM------------AVI--RKPLTVVGGITYR- 161
                                          .                          .

PatZ              -S--DPDNIDAEFAV-LVRSDLKGLGLGRRLMEKLITYTRDHGLQRLNG-ITMPNNRGMVALA 858
4MY3              NRP-GPGAHVASASF-XVAAAARGRGVGRALCQDXIDWAGREGFRAIQFNAVVETNTVAVKLW 136
3DR8              WRSFDGFRYTVEHSV-YVHPAHQGKGLGRKLLSRLIDEARRCGKHVXVA-GIESQNAASIRLH 133
4ORF              -RE-GHNATMAEVAF-TVGDDYQGRGIGSFLMGALIVSANYVGVQRFNA-RVLTDNMAMRKIM 274
4AVC              -RD-ETDPTVAEIAF-TVADAYQGRGIGSFLIGALSVAARVDGVERFAA-RXLSDNVPXRTIX 285
4U5Y              -R----IADEAEVAF-LVQDAHQGRGVASALLEHIAAVARERGIRRFAA-EVLPANNKMIKVF 163
1YGH              -P--FDKREFAEIVFCAISSTEQVRGYGAHLMNHLKDYVRNTSNI-KYF-LTYADNYA-IGYF 221
                            ..    :    :  * :  *       .   .           *

PatZ              RKLGFNVDIQLEEGI------------VGLTLNLAQR---E---------------------- 884
4MY3              QSLGFRVIGTVPEAF------------HHPTHG-----YVGLHVX--------HRPL------ 168
3DR8              HSLGFTVTAQXPQVG------------VKFGR------WLDLTFXQ-LQL--DEHAAPDAC-- 173
4ORF              DRLGAVWV------V------------VMTEVDVPPVDTVPFEPELIDQIRDATRKVIRAVSQ 319
4AVC              DRYGAVWQRE-DVGV------------ITTXIDVPGPGELSLGREXVDQINRVARQVIEAVG- 333
4U5Y              MDAGYTQKRSFEDGV------------VRLEFD----------------------------L 185
1YGH              KKQGFTKEITLDKSIWMGYIKDYEGGTLMQCSMLPRIRYLD---------------------- 261
                     *
```

Figure 4. Multiple alignment of GNAT domain from *E. coli* (PatZ), *K. flavida* (4MY3, PDB ID code), *S. typhimurium* (3DR8, PDB ID code), *M. smegmatis* (4ORF, PDB ID code), *M. tuberculosis* (4AVC, PDB ID code), *S. enterica* (4U5Y, PDB ID code) and *S. cerevisiae* (1YGH, PDB ID code). *, fully conserved residue; :, residues with high similarity; ., residues with low similarity. Sequence alignment generated in T-Coffee web server (v11).

Autoacetylation/Deacetylation of PatZ

It has been recently reported that PatZ is acetylated *in vivo* in *E. coli* [2,9]. However this acetylation has not been studied in detail and the consequences of this regulation are unknown. The kinetic of PatZ autoacetylation was determined at a fixed PatZ concentration (60 nM) and different acetyl-CoA concentrations (0-1 mM) using the DTNB assay. The activity plot was fitted to a nonlinear of Michaelis-Menten enzyme kinetics (R^2= 0.98) with a K_M of 0.11 ± 0.01 mM (Figure 5A). To test the kinetic mechanism of self-catalysed PatZ, its concentration dependence was examined, and a linear concentration dependence of log PatZ autoacetylation velocity on the log PatZ concentration was observed; y = 1.16 x – 2.39, with R^2=0.97 (Figure 5C). Western blotting confirmed that PatZ showed deacetylation by CobB (Figure 5D) with a 1:3 (PatZ:CobB) molar concentration ratio and a reaction time of 5 hours. Therefore, PatZ acetylation is reversible.

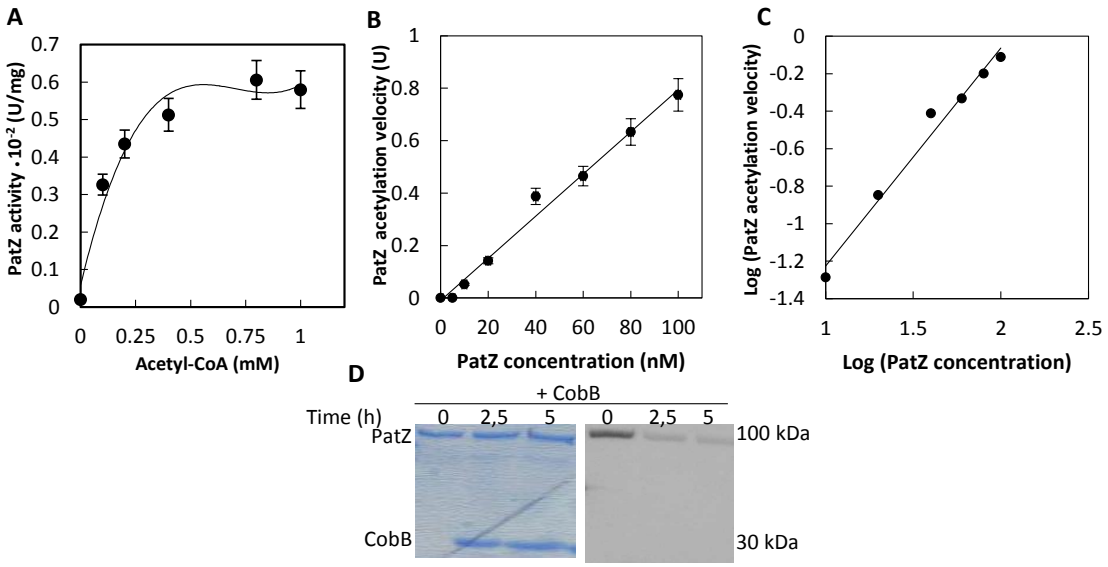

Figure 5. PatZ acetylation/deacetylation. **(A)** Substrate saturation curve of the PatZ-dependent acetylation reaction rate at different concentrations of acetyl-CoA. The PatZ concentration was 60 nM. **(B)** Nonlinear concentration dependence of PatZ autoacetylation rate at 1 mM acetyl-CoA. **(C)** log-log of data in B was fitted to a linear regression, y = 1.16 x-2.38, R^2=0,98. **(D)** PatZ deacetylation by CobB western blot. The concentration ratio was 1:3 (PatZ:CobB).

To characterize the self-catalysed reaction of PatZ, the acetyltransferase activity of $PatZ^{GNAT}$ (GNAT C-terminal catalytic domain of PatZ) on Acs and $PatZ^{Acs\text{-}like}$ (truncated N-terminal PatZ fragment lacking the GNAT domain) was analysed by western blot (Figures 6A, B), using wt PatZ ($PatZ^{wt}$) and $PatZ^{GNAT}$ at 60 nM. $PatZ^{GNAT}$ was seen to be catalytically inactive on both substrates, Acs and $PatZ^{Acs\text{-}like}$, which suggest that the N-terminal domain of PatZ is essential for

acetyltrasferase activity. Besides, Acs was acetylated by PatZ^{wt}, while PatZ^{wt} could not acetylate PatZ$^{Acs\text{-}like}$.

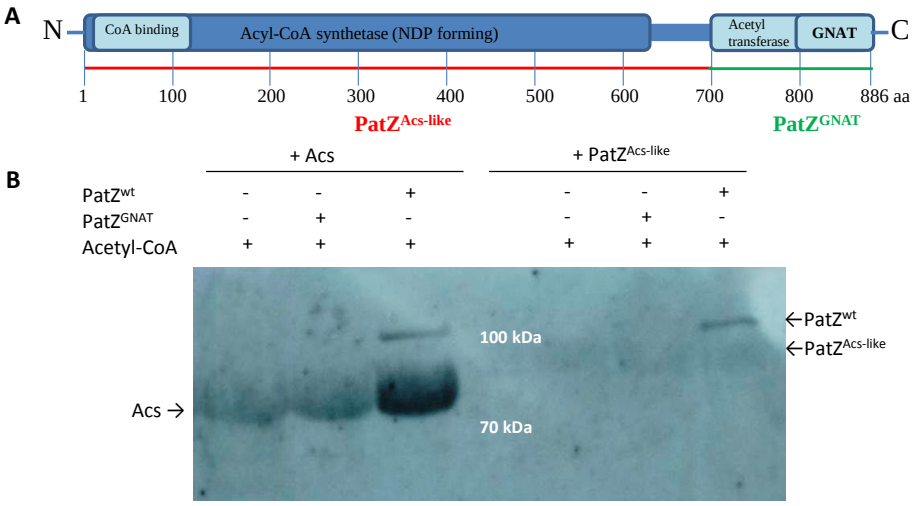

Figure 6. Western blot of Acs and PatZ$^{Acs\text{-}like}$ incubated with PatZ^{GNAT} and PatZ^{wt}**. (A)** Multidomain PatZ protein that belongs to the GNAT superfamily, indicating the PatZ^{GNAT} (truncated GNAT C-terminal catalytic domain) and PatZ$^{Acs\text{-}like}$ (truncated N-terminal domain of PatZ within GNAT domain). **(B)** Acs and PatZ$^{Acs\text{-}like}$ western blot incubated in presence of 1 mM acetyl-CoA with 60 nM PatZ^{wt} or PatZ^{GNAT}.

A MS assay of PatZ incubated with a saturating acetyl-CoA concentration (1 mM) was conducted. The results are shown in Table 2. Six acetylated lysine residues were identified, five on the surface of the protein core (146, 149, 391, 446, and 635) and one in the catalytic (GNAT) domain (819). An example of the assignment of acetylation to 146 and 149 of PatZ by LC-MS/MS analysis is shown in Figure 2B.

Tetrameric PatZ oligomerizes to an octameric form by acetylation

In order to understand the changes induced in PatZ by acetylation, biophysical studies were conducted, determining the molecular weight of the native protein by gel filtration chromatography (Figure 7A). In the absence of acetyl-CoA, purified PatZ eluted mainly at 8.2 min, with a left shoulder peak appearing at 7.3 min, and with an apparent molecular weight of 410 ± 21 kDa and 798 ± 40 kDa, respectively, which correspond to tetrameric and an octameric forms. In contrast, at a saturating acetyl-CoA concentration (1.5 mM) the main peak eluted at 7.3 with a right shoulder at 8.2 min, corresponding to a protein population in which the octamer species is predominant.

Purified PatZ was also analysed by DLS and AUC. Structural information can be extracted from both the diffusion coefficient, D, and s. These are related to the friction coefficient, f, by

the expressions $D = RT/(N_A f)$ and $s = M(1-v\rho)/(NA f)$, which are combined in the well-known Svedberg equation $s/D = M(1-v\rho)/RT$. R is the ideal gas constant, T the absolute temperature, N_A the Avogadro number, v the specific volume of the protein solute and ρ the density of the buffer solvent, while f is proportional to the solvent viscosity, η_0, and depends on the conformation (size and shape) of the solute molecules. The friction coefficient is customarily expressed as an equivalent hydrodynamic radius, R_h, defined as $R_h = f/(6\pi\eta_0)$, which can be obtained as either, $R_h = RT/(N_A 6\pi\eta_0 D)$ or $R_h = M(1-v\rho)/(N_A 6\pi\eta_0 s)$. The hydrodynamic measurements were carried out at 20 ˚C (T = 293K), in the same buffer as used for gel permeation. The SEDNTERP software [29] can be used to estimate the values η_0 = 1.00 cP and ρ = 1.01 g/cm^3 from the solvent composition. The same program is used to estimate the required protein solute properties from the amino acid sequence. Using the sequence of the monomer, the following properties were obtained for PatZ: M = 98.0 kDa, and v = 0.742 cm^3/g.

Figure 7B (a,b) shows the results of the DLS measurements. Disregarding the appearance of a small amount of aggregated material, the single peak in the mass distribution corresponds to the protein in its oligomeric forms. The analysis of this peak by the ZetaSizer software showed that it corresponds to a polydisperse material (the Protein Workshop mode of the instrument software indicating the coexistence of different oligomers) with M = 420 ± 150 kDa and R_h = 7.7 ± 2.4 nm.

Figure 7C (a, b and c) shows the AUC results. The main feature is the peak in c(s) with $s_{20,w}$ = 12.4 S and M~446 kDa. The results also showed two other minor but significant peaks, one with $s_{20,w}$ = 18.0 S and M~800 kDa, and another with $s_{20,w}$ = 4.6 S and M~97 kDa (Figure 6C, c). As indicated in the Methods section, M values in AUC-SV are approximate.

The mass and intensity distribution of the R_h obtained by DLS reveals the existence of some aggregated protein but, as reported by the ZetaSizer software, the weight fraction of aggregates is smaller than 2 % (Figure 6B). Indeed, that material does not show up in the mass distribution. Results of the AUC measurements (Figure 7C) show that they are quite small and non-biased, indicating the good quality of the fit.

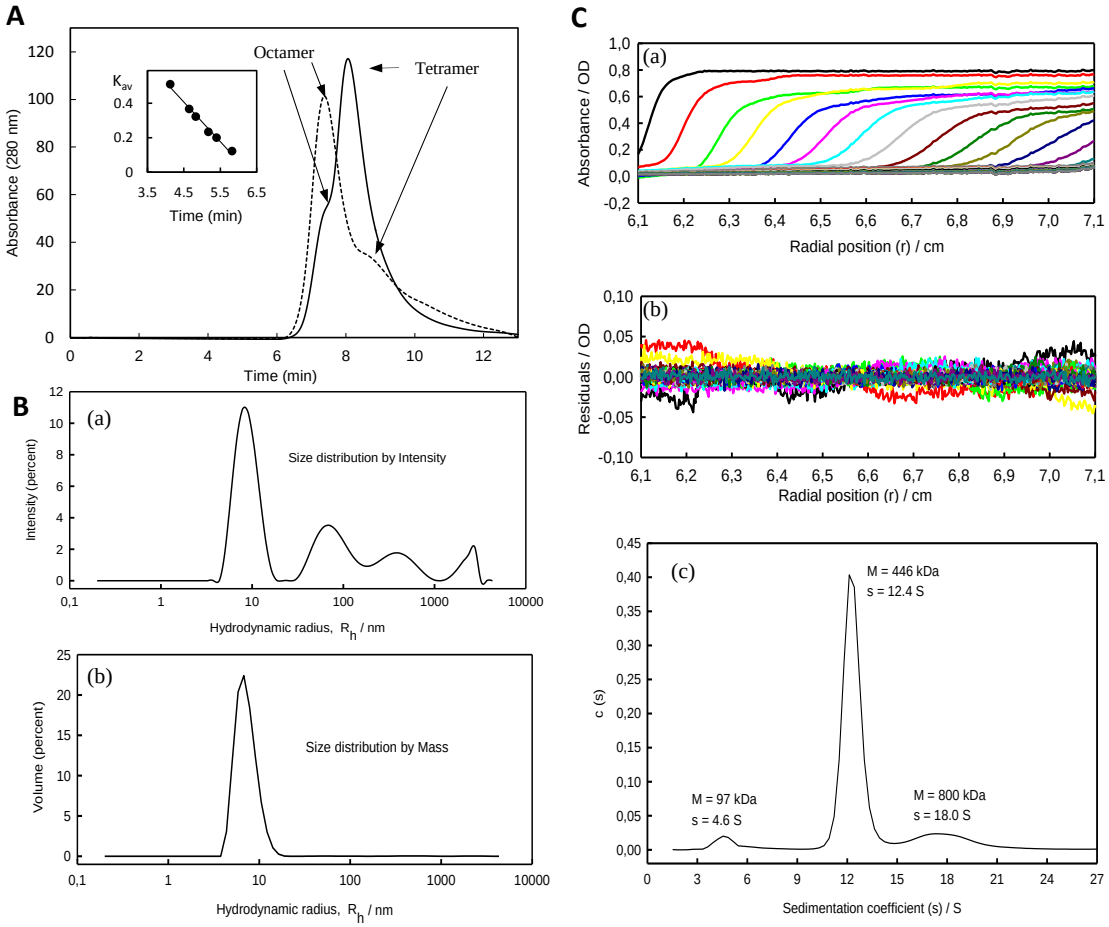

Figure 7. PatZ structural studies**. (A)** Oligomeric state of PatZ in the absence of acetyl-CoA (—) and 1 mM acetyl-CoA (---) by gel filtration chromatography, at a flow rate of 0.05 mL/min. The insert shows a typical linear regression of standard curve with a set of proteins standards of known molecular masses**. (B)** Size distributions from DLS: (a) by scattering intensity (b) by mass **(C)** AUC results (a) scans in absorbance optics (b) residuals of fitted scans (c) fitted distribution coefficients with s and M values as provided by SEDFIT.

With the same purpose of understanding the PatZ oligomeric states, interconversion between the two oligomeric forms of PatZ was monitored by native PAGE at different acetyl-CoA concentrations (Figure 8A). In the absence of acetyl-CoA the tetramer was the main form observed but, when the acetyl-CoA concentration was increased, an octameric structure was formed and the tetramer band was less abundant. Western blot with an anti-acetyl Lys antibody revealed that only the octameric form was acetylated (Figure 8B). To confirm that PatZ autoacetylation induces a change in its oligomerization status, lysine acetylated residues of PatZ were mutated to arginine (non-acetylable mutation). These lysine residues were 146, 149, 391, 447 and 635 ($PatZ^{5(K\rightarrow R)}$). The oligomerization of $PatZ^{5(K\rightarrow R)}$ and $PatZ^{E809A}$ were studied by native PAGE. In both cases, the tetrameric form was observed in the absence of acetyl-CoA (Figure 8C).

However, an octameric structure was formed at 1 mM acetyl-CoA for PatZ^{E809A} mutant but it was not observed for PatZ$^{5(K\rightarrow R)}$.

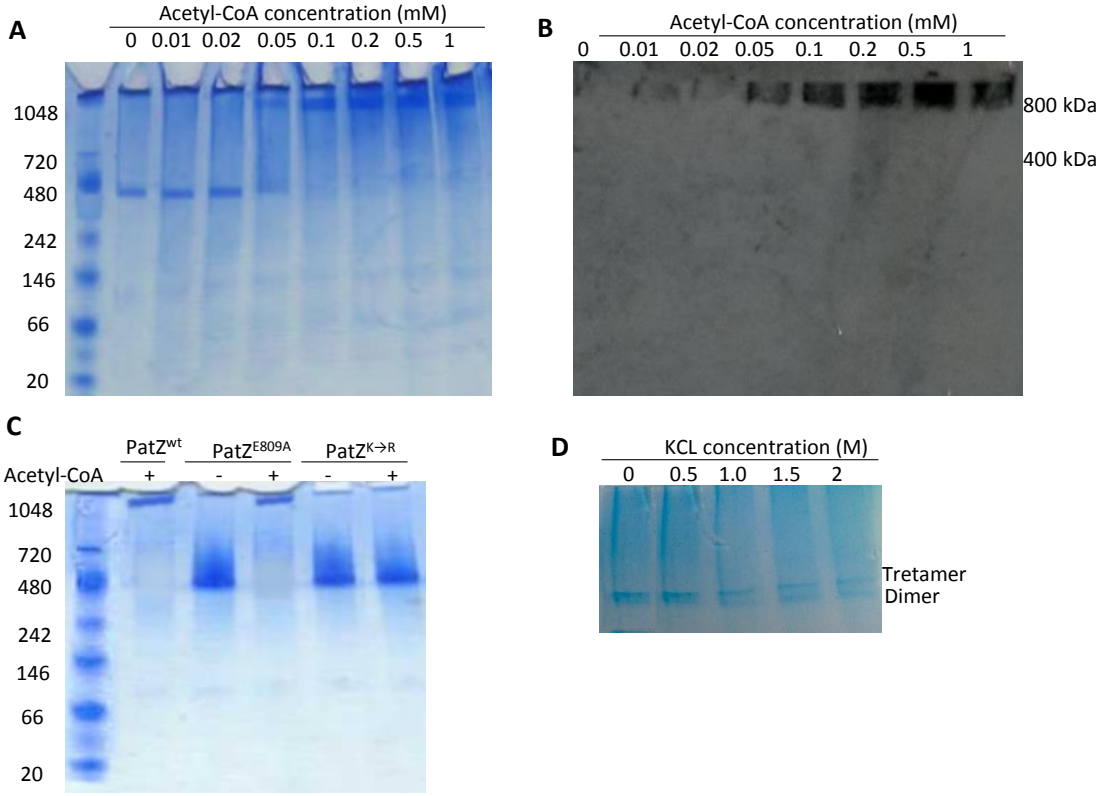

Figure 8. Deacetylated PatZ native western blot. **(A)** Deacetylated PatZ native PAGE at different acetyl-CoA concentration: lane 1 (0 mM), lane 2 (0.01 mM), lane 3 (0.02 mM), lane 4 (0.05 mM), lane 5 (0.1 mM), lane 6 (0.2 mM), lane 7 (0.5 mM) and lane 8 (1 mM) **(B)** Western-blot analysis using anti-acetyl Lys antibody. **(C)** Native PAGE analysis of PAtZ^{E809A} and PatZ$^{5(K\rightarrow R)}$ in the absence and in the presence of 1 mM acetyl-CoA. **(D)** PatZ native PAGE incubated with KCL. Homotetrameric PatZ dissociation in the presence of KCl. The incubations were carried out at 25 °C for 2 days in solutions containing final concentrations of KCl from 0 to 2.0 M.

To study intersubunits electrostatic interactions in the PatZ tetramer purified and mainly tetrameric PatZ was incubated at 25 °C for 2 days in solutions containing different KCl concentrations (0 to 2.0 M) and analysed by native PAGE (Figure 8D) [37]. The native PAGE analysis showed that the homotetramer molecule dissociated to homodimers at a KCl concentration of 0.5 M or higher. The maximal dissociation occurred at 2.0 M KCl, but homotetramers were observed at all KCl concentrations while monomers were not observed in any of the conditions assayed. The addition of KCl probably disrupted interdimer electrostatic interactions in the PatZ tetramer, while intermonomers interactions were not affected.

To further clarify PatZ oligomerization by acetylation and its physiological function, DSC was used. DSC measures the heat capacity of states and the excess heat associated with transitions induced by temperature changes. Purified PatZ DSC assays were performed at 0, 0.5 and 1.5 mM acetyl-CoA (Figure 9A). Table 3 shows the PatZ thermodynamic parameters estimated from the DSC data. Tetrameric PatZ showed a single peak upon thermal denaturation in the absence of acetyl-CoA, reflecting a first-order protein denaturation pattern, N →D (N is the native state and D the denatured state) characterized by a T^0_m of 80.19 ± 2 °C. In contrast, the protein showed a double-peaked denaturation curve in the presence of 0.5 mM acetyl-CoA (non-saturating concentration considering the concentration of PatZ in the assay), characterized by a T^0_m of 81.15 ± 2 °C and a T^1_m of 104.81 ± 4 °C (Table 3). Finally, the protein showed a single peak at a saturating acetyl-CoA concentration (1.5 mM), with a T^1_m of 102.23 ± 3 °C, similar to the T^1_m value for 0.5 mM acetyl-CoA. Subsequently, denaturation of PatZ was studied at different concentrations of acetyl-CoA, from 0.25 to 1.5 mM (thermograms not shown) and in all non-saturating acetyl-CoA concentrations, two peaks were observed in the thermograms. The data were analysed according to the van't Hoff equation [38] and the model (Figure 9B), based on a relationship between the total protein concentration and the concentration of ligand or substrate, and the melting temperature, as expressed by the following equation (Equation 1) [39];

$$\ln\frac{[L]}{[enzyme]} = \frac{A}{n} - \frac{(\Delta H^o - \Delta Cp^o T_m^o)}{nR}\frac{1}{T_m} + \frac{\Delta Cp^o \ln(T_m / T_m^o)}{nR}$$

where R is the gas constant (8.31 x 10^{-3} kJ mol^{-1} K^{-1}), n is the number of binding sites for substrate and A is a constant (-1284.1 ± 0.2). Using the above equation for PatZ thermodynamic analysis with several acetyl-CoA concentrations, a value of 7.2 ± 0.02 was obtained for n. This indicates that between seven and eight binding sites for this ligand exist on the active oligomer, which agrees with the formation of an active PatZ octamer.

Table 3. Thermodynamic parameters of PatZ obtained from DSC thermograms.

PatZ	Acetyl-CoA (mM)	T^0_m (°C)	ΔH^0 (J/mol)	ΔCp^0 (W/g)	T^1_m (°C)	ΔH^1 (J/mol)	ΔCp^1 (W/g)
Tetramer	0	80.19 ± 2	1560 ± 8	-0.1	-	-	-
	0.5	81.15 ± 2	1614 ± 10	-0.15	104.81 ± 4	1453 ± 7	-0.002
Octamer	1.5	-	-	-	102.23 ± 3	1668 ± 11	-0.005

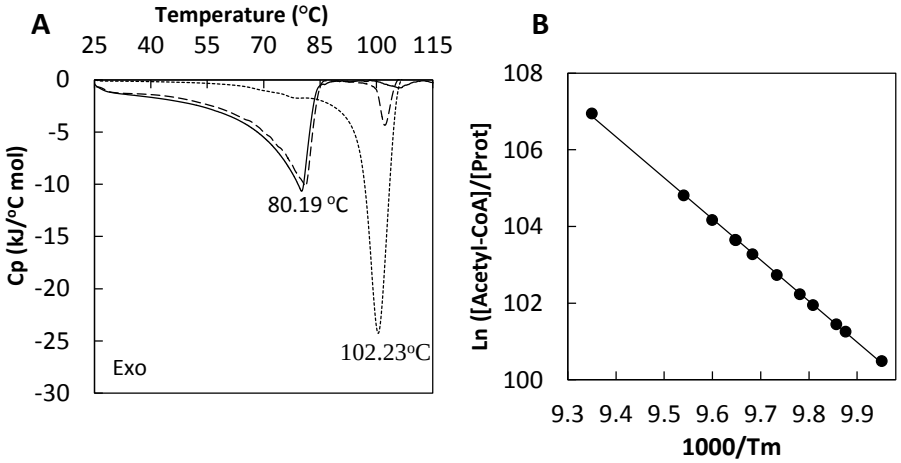

Figure 9. PatZ differential scanning calorimetry. **(A)** DSC thermograms of PatZ. Experiments were run at different acetyl-CoA concentrations: 0 (—), 0.5 (---) and 1.5 mM (···). **(B)** van't Hoff plot according to Equation 1 for PatZ DSC experiments in the presence of different concentrations of acetyl-CoA. The logarithm of the ligand concentration is plotted as a function of T_m^{-1}, the reciprocal of the temperature of maximal excess specific heat. The standard deviation of the points from the least squares curve corresponds to ± 0.20 °C in T_m (R^2 = 0.99).

***In silico* protein–protein docking**

In order to propose a PatZ model for the tetrameric state based on the above results, *in silico* protein–protein docking was performed by ClusPro 2.0 server [40–43]. Phyre 2 server [33] was used to predict the PatZ monomer structure. This model was generated with 95 % of the residues modelled at > 90 % confidence level and only 44 residues were modelled by *ab initio*. The PDB file generated by Phyre2 was uploaded on ClusPro2 for monomer–monomer interaction analysis. The output in the form of the structure of a predicted complex was obtained. Five structures based on the best scores were retrieved. Taking into account the scores obtained and favouring hydrophobic interaction between monomers we chose the best model. In the proposed dimer, the link between the C-terminal PatZ monomers occurs *via* a large hydrophobic surface which matches with the CoA binding domain (Figure 10A). Finally, ClusPro2 was also used to generate a dimeric structure of this dimer based on electrostatic interactions corresponding to the tetramer form. The output of the predicted complex was obtained. Five structures based on best scores were downloaded. The best candidate structure was selected taking into account the scores and the electrostatic surface interaction. In this model, the electrostatic interaction demonstrated experimentally by the dissociation of the homotetrameric PatZ in the presence of KCl (Figure 8D), occurs in most of the interface between dimers (Figure 10B).

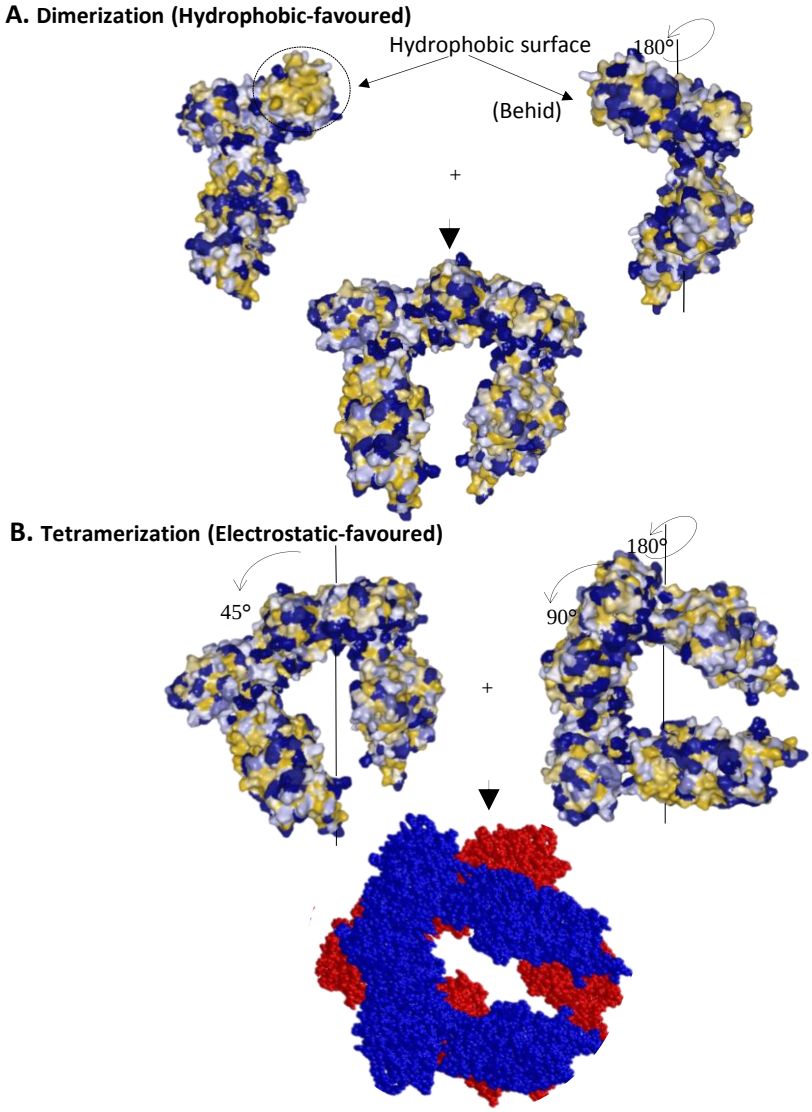

Figure 10. *In silico* PatZ oligomerization by monomer and dimer docking simulations performed by the ClusPro 2.0 server. **(A)** PatZ monomers dimerization by favoured hydrophobic interactions. The triangulated macromolecular surface [44] is shown in hydrophobic colour scale (32 colours) from yellow-brown (most hydrophobic) to blue (most hydrophilic). **(B)** PatZ dimers tetramerization by favoured electrostatic interactions. Dimers of the tetramer are coloured in red and blue. All figures were created using Protein Workshop [45].

In order to deepen our knowledge on PatZ tetramer acetylation, Phyre2 server [33] was also used to model the PatZ sequence with the acetylated lysine residues in the core protein (146, 149, 391, 447, 635) changed to glutamine residues to simulate the effect of acetylation on the PatZ structure. Glutamine was selected because of its similar side-chain conformational entropy to acetyl lysine [46,47]. This model was generated with 94 % of the residues modelled at > 90% confidence level and only 45 residues were modelled by *ab initio*. Then, this model was compared with the native PatZ model (Figure 11). The mutant PatZ model presented a more

compact structure (model dimensions (nm); X= 77.21; Y= 82.39; Z=94.65) than the native model (model dimensions (Å); X= 74.86; Y= 116.23; Z=93.76). This structural change resulting from the acetylation of PatZ could promote the formation of the octamer. It seems likely that the predominant effect of the acetylation is to alter the shape and charge characteristics of a surface patch allowing contact between monomers that was not permitted in the tetramer wt protein.

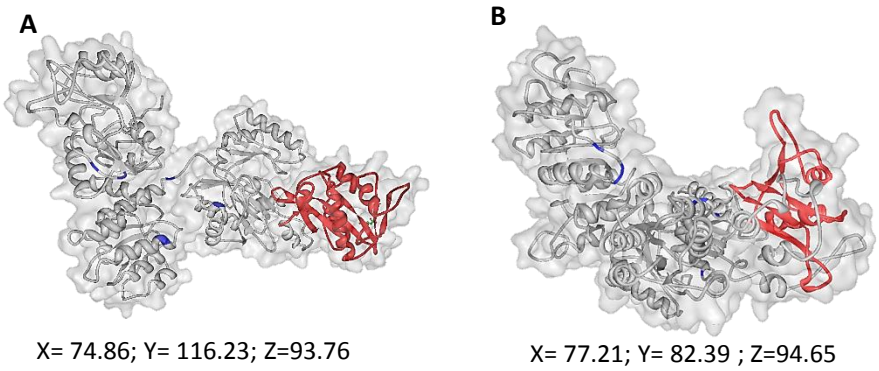

Figure 11. Deacetylated and acetylated PatZ models generated by Phyre2 server. PatZ models of native **(A)** and mutant **(B)**. Catalytic domain is indicated in red and lysine residues changed to glutamine are indicated in purple. Coordinates indicate the model dimension in Å. The figure was made using Protein Workshop [45].

Validation of *in silico* PatZ tetramerization model using three-dimensional hydrodynamic analysis

The essential value of hydrodynamic studies is the information that they provide on the structure of proteins. For many years, hydrodynamic coefficients have been used to probe the overall conformation (e.g. globular, fibrous, denaturated, etc) of proteins in solution. In recent years, methodologies and computational tools have been developed to calculate the solution properties from detailed, residue- and even atomic-level structures [48–50]. Apart from data for the solute and solvent properties, the input necessary for the calculation of solution properties is simply a PDB formatted file of atomic coordinates. For this reason such tools are now widely used to validate structures obtained from crystallography, NMR or *in silico* methods, by comparing the results experimentally determined with those obtained computationally. For the simple hydrodynamic coefficient, as in the present case, the most widely used tool is HYDROPRO [48,50]. Calculation of the *s* requires the values for ρ, T, η_0. v, and M to be known. These are available in our case, but, note that the result for R_h is independent of these quantities and is directly calculated from the set of atomic coordinates.

Based on our PatZ modelled structures for the tetramer and the monomer by ClusPro2 and Phyre2 servers respectively, using HYDROPRO version 10 [50] we obtained the results listed in Table 4. The agreement between the experimental and calculated *s* and R_h is excellent: differences of less than 5 %. Considering the diversity of aspects involved in (i) the *in silico* structure prediction of PatZ oligomeric forms, (ii) the DLS and, especially, the AUC experiments and (iii) data processing, it can be affirmed that the hydrodynamic experiments and calculations fully validate the *in silico* molecular modelling and docking studies of the PatZ monomeric subunit for the tetrameric assembly.

Table 4. Experimental and calculated properties from hydrodynamic studies.

Property	Technique	Tetramer	Monomer	Octamer
Mass (kDa)	DLS	< 420[(a)]	-	-
	AUC	~ 446[(b)]	~ 97[(b)]	~ 800[(b)]
	Sequence	392	98	784
s (S)	AUC	12.4	4.6	18.0
	HYDROPRO	12.9	5.2	-
R_h (nm)	DLS	< 7.7[(a)]	-	-
	AUC	7.3	4.1	9.9
	HYDROPRO	6.9	4.3	-

(a) Average over oligomers. The actual value should be slightly smaller
(b) Approximate values from AUC-SV

With an even simpler approximate methodology, the hydrodynamic radius of the tetramer model was calculated using the Protein workshop viewer [45] and taking into account the macromolecular surface [44]. The calculated average radius was 7.03 ± 0.5 nm, which is in accordance with the DLS and AUC results and the more precise HYDROPRO calculation.

Discussion

PatZ activity is controlled by positive cooperativity and Acs activity is regulated by the degree of acetylation

PatZ kinetic data for acetyl-CoA (Figure 1C; Table 1) pointed to atypical sigmoidal activity reflecting positive cooperativity (Hill coefficient =7.91 ± 0.22). Positive cooperativity is unusual in enzymes belonging to the GNAT family, although this behaviour has been described in PatZ

homologous enzyme, *Se*Pat, with a Hill coefficient of 2.2 ± 0.2 [8] suggesting that the structural basis for this behaviour is protein tetramerization in the presence of acetyl-CoA.

The kinetic parameters of PatZ were within the range of those reported for other lysine acetyltransferases (KATs) proteins [51]. The acetylation of Acs by PatZ was confirmed by western blot and MS analysis (Figure 1E and Table 2). Moreover, the acetyl-CoA synthetase activity assay (Figure 1F) confirmed that *E. coli* Acs activity was dependent on the acetylation degree caused by PatZ. Besides, the Acs synthetic activity measured at 0 and 0.1 mM acetylCoA in the absence of PatZ, was the same in both cases.

It is well known that in *S. enterica*, Pat-catalysed acetylation of Acs results in the modification of its K609 residue, which inhibits AMP-acetyl forming activity [15]. In contrast, we observed that the number of site-specific lysine residues of Acs acetylated by PatZ increased with acetyl-CoA concentration (Table 2) and a correlation between Acs activity and its acetylation degree was established. In fact, our group has recently reported quantitative changes in the acetylation ratios of some of these residues after deacetylation with CobB *in vitro* [9].

PatZ kinetics for Acs acetylation (Table 1) indicated that the limiting factor was the acetyl-CoA concentration, since the $K_{0.5}$ for this substrate was 12.5 times higher than for the Acs protein. These results suggest a mechanism for linking the physiological state of the cell with the acetylation state of Acs, so the concentration of acetyl-CoA in the cell will determine the acetylation of Acs by PatZ. One could speculate that the post-translational regulation of Acs prevents the accumulation of acetyl-CoA while avoiding the depletion of free coenzyme A and metabolic energy, as previously proposed [23,52]. In addition, it has recently been demonstrated that depletion of *patZ* gene leads to high *E. coli* proteome acetylation in acetate cultures. This increase in chemical acetylation could be the consequence of non-regulated Acs activity by PatZ [9].

Conserved glutamic acid 809 from PatZ is not important for catalysis

To date, studies on the acetyltransferases kinetic mechanism suggest, for most MYST and GNAT families, a direct-attack mechanism within a ternary complex. In this mechanism a conserved glutamic acid residue functions as a general base by assisting in the deprotonation of the ε-amino group of the acetylable lysine residue [10, 31, 52, 53]. This was demonstrated in the MYST family member Esa1, where the conserved active-site E338 deprotonates the N-ε-lysine of histone, facilitating the nucleophilic attack on the bound acetyl-CoA [14]. In the GNAT family member Gcn5, the E173 deprotonates the ε-amino group of the targeted lysine of the protein

[12]. Based on this premise, local sequence alignment of histone acetyltransferase Gcn5 (1YGH, pdb id code) and GNAT domain of PatZ showed that this residue is conserved in position 809 (Figure 4) [54].

To determine the role of the E809 in PatZ catalytic activity, we generated a PatZ mutant protein harbouring an E809 to A and checked that it acted as a potential catalytic base in the reaction (Figure 3A). The activity of the mutant enzyme was 20 % lower at pH 7 than for the native enzyme, although activity gradually recovered at pH values above 9 as a result of the spontaneous deprotonation of the ε-amino group of the targeted lysine residue on Acs. This result suggested that the E809 residue was not relevant for PatZ activity.

It is important to note that there are examples where an invariant glutamic is not necessary for catalysis [55]. For example, the yeast Hpa2 GNAT has no obvious catalytic residue that might function as a general base, and has been proposed that a net positive electrostatic potential of the active site would favour an uncharged state of lysine residue [56]. This positive potential is not found in the GNAT catalytic domain PatZ (Figure 3C). Other acetyltransferases, such as Hat1, AAT and AAC6, also have a net negative charge of the active site [57–59]. Thus an alternative mechanism must be necessary for proton transfer. This has been proposed for the GNAT family member serotonin N-Acetyltransferase, in which two histidines residues are involved in the deprotonation [60].

On the other hand, the mutant structure without acetyl-CoA determined by native PAGE, presented an apparent molecular mass of ~ 410 kDa (Figure 8C), suggesting that the E809 does not alter the ability of protein to correctly fold and oligomerize. In the same way, circular dichroism spectra of the yGCN5-E173Q protein were identical to those of the native protein, suggesting that the protein did not undergo significant structural changes that could be attributed to the glutamate-to glutamine substitution native [10].

The GNAT catalytic domain model of PatZ was generated with 99 % of the residues modelled and no residue was modelled by *ab initio* (Figure 3B). The coenzyme A binding pocket includes V812, L813, V814, G824 and R825 residues, which are also conserved in the GNAT family (Figure 4) [53]. These residues create a hydrophobic core for acetyl-CoA attachment, and it is also possible that acidic side-chains in the vicinity of the PatZ active site could play a role in deprotonation of lysine residue (Figures 3B, C).

PatZ is a homotetramer that forms a thermostable octamer by autoacetylation

In contrast to the eukaryotic enzymes, prokaryotic acetyl-transferases adopt various quaternary structures. A number of structurally characterized GNAT superfamily members have

been found to be multimeric [53]. A similar oligomeric behaviour has been described for *S. enterica*. *Se*Pat oligomerizes from a monomer to a tetramer form in the presence of acetyl-CoA [8]. However, the fact that PatZ was mainly in stable tetrameric form in the absence of acetyl-CoA demonstrated that the tetramerization process was independent of acetyl-CoA ligand binding. In contrast, the presence of acetyl-CoA was required for the formation of the octamer state (Figure 7). Hydrodynamic experiments using the two techniques, DLS and AUC, confirm the oligomeric nature and composition of the protein, which is predominately tetrameric, with some octamers, and an even smaller but still detectable amount of monomers observed by AUC. As seen in Table 4, the approximate molecular weights observed from the AUC are in a 1:4:8 proportion. The DLS value, which must correspond to an average, is slightly above that of the tetramer because, compared with the other two species, there is more octamer than monomer. Regarding the R_h, the values for each species were determined from the s, using the exact values of M and those of v, ρ, T, and η_0 (Table 4). Again, the DLS hydrodynamic radius was slightly higher than that of the tetramer. Therefore, the results of the two hydrodynamic techniques are consistent. In addition, it is important to highlight that hydrodynamic results agree with those of gel filtration chromatography analysis. This technique showed that, in the absence of acetyl-CoA, purified PatZ eluted mainly as a tetramer with a certain presence of octamers and an apparent molecular weight of 410 ± 21 kDa and 798 ± 40 kDa, respectively.

Native PAGE showed that the formation of the octamer occurred above a 0.05 mM acetyl-CoA concentration (Figure 8A), which agrees with the Michaelis-Menten kinetic constant for PatZ autoacetylation of 0.11 ± 0.01 mM (Figure 5A). Moreover, western blot of native PAGE showed that only the PatZ octamer form has acetylated lysine residues. These results suggest that the formation of the octamer occurred *via* tetramer acetylation and not from the monomer, since the tetramer band disappeared gradually with a concomitant increase of the octamer band (Fig 8B). Besides, Native PAGE of $PatZ^{5(K\rightarrow R)}$ showed that an octamer form was not observed at 1 mM acetyl-CoA (Figure 8C). This result confirms that the autoacetylation of these lysine residues (146, 149, 391, 447 and 635) is responsible for inducing PatZ octamerization.

The acetylation kinetics of Acs by PatZ (Figure 1A) showed that the octamer form was a functionally active form since the acetyltransferase activity was measured at a fixed saturating acetyl-CoA concentration. A linear concentration dependence of log PatZ autoacetylation rate *versus* log Pat concentration at saturating concentration of acetyl-CoA (1 mM) was detected (Figures 5B, C). This suggests that the reaction mechanism is first order, indicating an intramolecular process [54]. The autoacetylation of histone acetyltransferases, such as p300,

Tip-60 or the MYST acetyltransferases Esa1 and hMOF [46–49], has been described. Furthermore, the acetylation of these acetyltransferases is reversed by deacetylases as described for PatZ in this study (Figure 5D).

In order to obtain a deeper understanding of the oligomeric nature of PatZ, the Predict protein server [58] was used to predict PatZ monomer solvent accessibility. The result showed that 31.38 % of the residues are exposed, 9.37 % are intermediate and 59.26 % are buried within the protein. This largely hydrophobic interface could be involved in monomer contact to form the stable dimer in solution. This would explain the limited presence of PatZ monomers in equilibrium sedimentation studies, DSC analysis, and their absence in native PAGE and the elution profile of PatZ from a gel filtration column. Moreover, the results of the dissociation studies of homotetrameric PatZ in the presence of KCl (Figure 8D) suggest that the PatZ homotetramer is stabilized, mainly by favourable electrostatic contacts between the two homodimers [37]. In contrast, most of the interactions between monomers are hydrophobic. A similar behaviour has been demonstrated for histone acetyltransferase Hpa2, which forms dimers *via* an extensive, interdigitated, and largely hydrophobic interface and which forms a tetramer in the presence of acetyl-CoA [59].

With respect to PatZ domains, $PatZ^{Acs\text{-}like}$ showed a tetrameric form suggesting that dimers and tetramers are formed from the N-t domain (Figure 8C). However, the N-t domain was also necessary for catalytic PatZ activity (Figure 6B). In fact, it has been demonstrated that full-length *Se*Pat is necessary for efficient binding to acetyl-CoA [8] and that the specificity of the GNAT-protein interaction is dictated by an extensive interaction surface [60]. Moreover, the tetramer $PatZ^{Acs\text{-}like}$ could not be acetylated by $PatZ^{wt}$ (Figure 6B). From this result, we hypothesize that a $PatZ^{wt}$ tetramer cannot recognize another tetramer, suggesting that the autoacetylation mechanism consists of an intramolecular self-catalysis based on an acetylation between monomers, although more studies are needed to confirm this.

DSC experiments were carried out to understand the physiological consequences of this octamerization induced by tetramer autoacetylation. The results showed that PatZ has 8 acetyl-CoA binding sites in the octameric form at a saturating concentration of acetyl-CoA, and is characterized by a T_m of 104.81 ± 4 ^oC, while the PatZ tetramer was a T_m of 80.19 ± 2 ^oC in the absence of acetyl-CoA. These date (Figure 9) and PatZ acetyltransferase activity analyses (Figure 1A) revealed that the octamer is functionally active and more thermostable than the tetramer. In fact, in other protein acetyltransferases, it has been described that multiple acetylated lysines play critical role in protein stability [61]. In the same way, K709 of component HIF-1

transcriptional complex is acetylated by p300, which increases protein stability [62]. This specific environmental function of protein acetylation might explain the association of tetramers to form an active PatZ octamer by acetylation and to increase its stability in response to cell stress situations [63].

The kinetic, structural and functional characteristics of the PatZ activity have physiologically relevant consequences. Kinetic data revealed that acetyl-CoA concentration limits the acetylation of Acs. This is possible due to the positive cooperativity of PatZ towards its substrate acetyl-CoA, which, in turn, is related to changes in protein structure and its oligomeric state. When cellular concentrations of acetyl-CoA increase (*e.g.* as a consequence of high Acs activity during growth on acetate), PatZ tetramers self-acetylate, which promotes the formation of PatZ octamers, which are more stable and active. This fact would prevent the accumulation of acetyl-CoA while avoiding the depletion of free coenzyme A [23, 38]. This work supports a major role for PatZ as a molecular sensor of acetyl-CoA concentration.

In conclusion, this study demonstrates for the first time the structural regulation of an acetyltransferase by autoacetylation in a prokaryotic organism, a common post-translational event in eukaryotic organisms. Surprisingly PatZ autoacetylation is correlated with its oligomerization and structural stability, as well as with its activity. This study represents a breakthrough in prokaryotic protein modification studies.

References

1. Pisithkul T, Patel NM, Amador-Noguez D. Post-translational modifications as key regulators of bacterial metabolic fluxes. Curr Opin Microbiol. 2015;24: 29–37. doi:10.1016/j.mib.2014.12.006

2. Weinert BT, Iesmantavicius V, Wagner SA, Schölz C, Gummesson B, Beli P, et al. Acetyl-phosphate is a critical determinant of lysine acetylation in *E. coli*. Mol Cell. 2013;51: 265–272. doi:10.1016/j.molcel.2013.06.003

3. Wagner GR, Payne RM. Widespread and enzyme-independent Nε-acetylation and Nε-succinylation of proteins in the chemical conditions of the mitochondrial matrix. J Biol Chem. 2013;288: 29036–29045. doi:10.1074/jbc.M113.486753

4. Kuhn ML, Zemaitaitis B, Hu LI, Sahu A, Sorensen D, Minasov G, et al. Structural, kinetic and proteomic characterization of acetyl phosphate-dependent bacterial protein acetylation. PLoS One. 2014;9: e94816. doi:10.1371/journal.pone.0094816

5. Dyda F, Klein DC, Hickman AB. GCN5-related N-acetyltransferases: a structural overview. Annu Rev Biophys Biomol Struct. 2000;29: 81–103. doi:10.1146/annurev.biophys.29.1.81

6. Marchler-Bauer A, Derbyshire MK, Gonzales NR, Lu S, Chitsaz F, Geer LY, et al. CDD: NCBI's conserved domain database. Nucleic Acids Res. 2014;43: 222–226. doi:10.1093/nar/gku1221

7. Burk DL, Ghuman N, Wybenga-Groot LE, Berghuis AM. X-ray structure of the AAC(6')-Ii antibiotic resistance enzyme at 1.8 A resolution; examination of oligomeric arrangements in GNAT superfamily members. Protein Sci. 2003;12: 426–437. doi:10.1110/ps.0233503

8. Thao S, Escalante-semerena JC. Biochemical and thermodynamic analyses of *Salmonella enterica* Pat , a multidomain , multimeric N -Lysine acetyltransferase involved in carbon and energy metabolism. MBio. 2011;2: 1–8. doi:10.1128/mBio.00216-11

9. Castaño-Cerezo S, Bernal V, Post H, Fuhrer T, Cappadona S, Sanchez-Diaz N, et al. Protein acetylation affects acetate metabolism, motility and acid stress response in *Escherichia coli*. Mol Syst Biol. 2014;762: 1–16. doi:10.15252/msb.20145227

10. Trievel RC, Rojas JR, Sterner DE, Venkataramani RN, Wang L, Zhou J, et al. Crystal structure and mechanism of histone acetylation of the yeast GCN5 transcriptional coactivator. Proc Natl Acad Sci U S A. 1999;96: 8931–6.

11. Rojas JR, Trievel RC, Zhou J. Structure of *Tetrahymena* GCN5 bound to Coenzyme A and a histone H3 peptide. Nature. 1999;401: 93–98.

12. Tanner KG, Langer MR, Kim Y, Denu JM. Kinetic mechanism of the histone acetyltransferase GCN5 from yeast. J Biol Chem. 2000;275: 22048–55. doi:10.1074/jbc.M002893200

13. Yan Y, Harper S, Speicher DW, Marmorstein R. The catalytic mechanism of the ESA1 histone acetyltransferase involves a self-acetylated intermediate. Nat Struct Biol. 2002;9: 862–869. doi:10.1038/nsb849

14. Berndsen CE, Albaugh BN, Tan S, Denu JM. Catalytic mechanism of a MYST family histone acetyltransferase. Biochemistry. 2007;46: 623–629. doi:10.1021/bi602513x

15. Starai VJ, Escalante-Semerena JC. Identification of the protein acetyltransferase (Pat) enzyme that acetylates acetyl-CoA synthetase in *Salmonella enterica*. J Mol Biol. 2004;340: 1005–1012. doi:10.1016/j.jmb.2004.05.010

16. Gardner JG, Grundy FJ, Henkin TM, Escalante-Semerena JC. Control of acetyl-Coenzyme A synthetase (AcsA) activity by acetylation/deacetylation without NAD $^{+}$involvement in *Bacillus subtilis*. J Bacteriol. 2006;188: 5460–8. doi:10.1128/JB.00215-06

17. Crosby HA, Heiniger EK, Harwood CS, Escalante- JC. Reversible N-Lysine acetylation regulates the activity of acyl-CoA synthetases involved in anaerobic benzoate catabolism in *Rhodopseudomonas palustris*. Mol Microbiol. 2010;76: 874–888. doi:10.1111/j.1365-2958.2010.07127

18. Hua Xu, Subray S. Hegde and JSB. The reversible acetylation and inactivation of *Mycobacterium tuberculosis* acetyl-CoA synthetase is dependent on cAMP. Biochemistry. 2011;50: 5883–5892. doi:10.1021/bi200156

19. Castaño-Cerezo S, Bernal V, Blanco-Catalá J, Iborra JL, Cánovas M. cAMP-CRP coordinates the expression of the protein acetylation pathway with central metabolism in *Escherichia coli*. Mol Microbiol. 2011;82: 1110–1128. doi:10.1111/j.1365-2958.2011.07873.x

20. Starai VJ, Celic I, Cole RN, Boeke JD, Escalante-Semerena JC. Sir2-dependent activation of acetyl-CoA synthetase by deacetylation of active lysine. Science. 2002;298: 2390–2392. doi:10.1126/science.1077650

21. Bennett BD, Kimball EH, Gao M, Osterhout R, Van SJ, Rabinowitz JD. Absolute metabolite concentrations and implied enzyme active site occupancy in *Escherichia coli*. Nat Chem Biol. 2010;5: 593–599. doi:10.1038/nchembio.186

22. Renilla S, Bernal V, Fuhrer T, Castaño-Cerezo S, Pastor JM, Iborra JL, et al. An insight into the role of phosphotransacetylase (pta) and the acetate/acetyl-CoA node in *Escherichia coli*. Microb Cell Fact. 2009;8: 2109–2124. doi:10.1007/s00253-011-3536-4

23. Chan CH, Garrity J, Crosby HA, Escalante-Semerena JC. In *Salmonella enterica*, the sirtuin-dependent protein acylation/deacylation system (SDPADS) maintains energy homeostasis during growth on low concentrations of acetate. Mol Microbiol. 2011;80: 168–183. doi:10.1111/j.1365-2958.2011.07566.x

24. Kitagawa M, Ara T, Arifuzzaman M, Ioka-Nakamichi T, Inamoto E, Toyonaga H, et al. Complete set of ORF clones of *Escherichia coli* ASKA library (a complete set of *E. coli* K-12 ORF archive): unique resources for biological research. DNA Res. 2005;12: 291–299. doi:10.1093/dnares/dsi012

25. Williamson J, Corkey B. Assays of intermediates of the citric acid. In: Lowenstein J, Kaplan N, Colowick N, editors. Methods of Enzymology. Academic P. 1969. pp. 494–497.

26. Moulder R, Filén J-J, Salmi J, Katajamaa M, Nevalainen OS, Oresic M, et al. A comparative evaluation of software for the analysis of liquid chromatography-tandem mass spectrometry data from isotope coded affinity tag experiments. Proteomics. 2005;5: 2748–2760. doi:10.1002/pmic.200401187

27. Kapp EA, Schütz F, Connolly LM, Chakel JA, Meza JE, Miller CA, et al. An evaluation, comparison, and accurate benchmarking of several publicly available MS/MS search algorithms: sensitivity and specificity analysis. Proteomics. 2005;5: 3475–3490.

doi:10.1002/pmic.200500126

28. Laue TM, Shah B, Ridgeway TM, Pelletier SL. Computer-aided interpretation of analytical sedimentation data for proteins. In: Rowe A, Horton J, editors. Ultracentrifugation in Biochemistry and Polymer. Royal Soc Chem; 1992. pp. 90–124.

29. Schuck P. Size-distribution analysis of macromolecules by sedimentation velocity ultracentrifugation and lamm equation modeling. Biophys J. 2000;78: 1606–1619. doi:10.1016/S0006-3495(00)76713-0

30. Hill A. The possible effects of the aggregation of the molecules of hemoglobin on its dissociation curves. J Physiol. 1910;40: 4–7.

31. Tanner KG. Catalytic mechanism and function of invariant glutamic acid 173 from the histone acetyltransferase GCN5 transcriptional coactivator. J Biol Chem. 1999;274: 18157–18160. doi:10.1074/jbc.274.26.18157

32. Guex N, Peitsch MC. SWISS-MODEL and the Swiss-PdbViewer: an environment for comparative protein modeling. Electrophoresis. 1997;18: 2714–2723. doi:10.1002/elps.1150181505

33. Kelley LA, Sternberg MJE. Protein structure prediction on the Web: a case study using the Phyre server. Nat Protoc. 2009;4: 363–371. doi:10.1038/nprot.2009.2

34. Wass MN, Kelley LA, Sternberg MJE. 3DLigandSite: predicting ligand-binding sites using similar structures. Nucleic Acids Res. 2010;38: 469–473. doi:10.1093/nar/gkq406

35. Le Guilloux V, Schmidtke P, Tuffery P. Fpocket: An open source platform for ligand pocket detection. BMC Bioinformatics. 2009;10: 1–11. doi:10.1186/1471-2105-10-168

36. Schmidtke P, Le Guilloux V, Maupetit J, Tufféry P. Fpocket: online tools for protein ensemble pocket detection and tracking. Nucleic Acids Res. 2010;38: 582–589. doi:10.1093/nar/gkq383

37. Rochet JC, Brownie ER, Oikawa K, Hicks LD, Fraser ME, James MN, et al. Pig heart CoA transferase exists as two oligomeric forms separated by a large kinetic barrier. Biochemistry. 2000;39: 11291–11302.

38. Privalov PL. Stability of proteins: small globular proteins. Adv Protein Chem. 1979;33: 167–241.

39. Fukada H, Sturtevant JM, Quiocho FA. Thermodynamics of the binding of L-arabinose and of D-galactose to the L-arabinose-binding protein of *Escherichia coli*. J Biol Chem. 1983;258: 13193–13198.

40. Kozakov D, Beglov D, Bohnuud T, Mottarella SE, Xia B, Hall DR, et al. How good is automated protein docking? Proteins. 2013;81: 2159–2166. doi:10.1002/prot.24403

41. Kozakov D, Brenke R, Comeau SR, Vajda S. PIPER: an FFT-based protein docking program with pairwise potentials. Proteins. 2006;65: 392–406. doi:10.1002/prot.21117

42. Comeau SR, Gatchell DW, Vajda S, Camacho CJ. ClusPro: a fully automated algorithm for protein-protein docking. Nucleic Acids Res. 2004;32: 96–99. doi:10.1093/nar/gkh354

43. Comeau SR, Gatchell DW, Vajda S, Camacho CJ. ClusPro: an automated docking and discrimination method for the prediction of protein complexes. Bioinformatics. 2004;20:

45–50. doi:10.1093/bioinformatics/btg371

44. Xu D, Zhang Y. Generating triangulated macromolecular surfaces by Euclidean distance transform. PLoS One. 2009;4: e8140. doi:10.1371/journal.pone.0008140

45. Moreland JL, Gramada A, Buzko O V, Zhang Q, Bourne PE. The Molecular Biology Toolkit (MBT): a modular platform for developing molecular visualization applications. BMC Bioinformatics. 2005;6: 1–7. doi:10.1186/1471-2105-6-21

46. Avbelj F, Fele L. Role of main-chain electrostatics, hydrophobic effect and side-chain conformational entropy in determining the secondary structure of proteins. J Mol Biol. 1998;279: 665–684. doi:10.1006/jmbi.1998.1792

47. Creamer TP. Side-chain conformational entropy in protein unfolded states. Proteins. 2000;40: 443–450. doi:10.1002/1097-0134(20000815)40:3<443::AID-PROT100>3.0.CO;2-L

48. García De La Torre J, Huertas ML, Carrasco B. Calculation of hydrodynamic properties of globular proteins from their atomic-level structure. Biophys J. 2000;78: 719–730. doi:10.1016/S0006-3495(00)76630-6

49. García de la Torre J, Huertas ML, Carrasco B. HYDRONMR: prediction of NMR relaxation of globular proteins from atomic-level structures and hydrodynamic calculations. J Magn Reson. 2000;147: 138–146. doi:10.1006/jmre.2000.2170

50. Ortega A, Amorós D, García de la Torre J. Prediction of hydrodynamic and other solution properties of rigid proteins from atomic- and residue-level models. Biophys J. 2011;101: 892–898. doi:10.1016/j.bpj.2011.06.046

51. Albaugh BN, Arnold KM, Denu JM. KAT(ching) Metabolism by the Tail: Insight into the links between lysine acetyltransferases and metabolism. Chembiochem. 2012;12: 290–298. doi:10.1002/cbic.201000438.)

52. Starai VJ, Escalante-Semerena JC. Acetyl-coenzyme A synthetase (AMP forming). Cell Mol Life Sci. 2004;61: 2020–2030. doi:10.1007/s00018-004-3448-x

53. Vetting MW, S de Carvalho LP, Yu M, Hegde SS, Magnet S, Roderick SL, et al. Structure and functions of the GNAT superfamily of acetyltransferases. Arch Biochem Biophys. 2005;433: 212–226. doi:10.1016/j.abb.2004.09.003

54. Karanam B, Jiang L, Wang L, Kelleher NL, Cole PA. Kinetic and mass spectrometric analysis of p300 histone acetyltransferase domain autoacetylation. J Biol Chem. 2006;281: 40292–40301. doi:10.1074/jbc.M608813200

55. Yuan H, Rossetto D, Mellert H, Dang W, Srinivasan M, Johnson J, et al. MYST protein acetyltransferase activity requires active site lysine autoacetylation. EMBO J. 2012;31: 58–70. doi:10.1038/emboj.2011.382

56. Creaven M, Hans F, Mutskov V, Col E, Caron C, Dimitrov S, et al. Control of the histone-acetyltransferase activity of Tip60 by the HIV-1 transactivator protein, Tat. Biochemistry. 1999;38: 8826–8830. doi:10.1021/bi9907274

57. Thompson PR, Wang D, Wang L, Fulco M, Pediconi N, Zhang D, et al. Regulation of the p300 HAT domain via a novel activation loop. Nat Struct Mol Biol. 2004;11: 308–315. doi:10.1038/nsmb740

58. Yachdav G, Kloppmann E, Kajan L, Hecht M, Goldberg T, Hamp T, et al. PredictProtein--an open resource for online prediction of protein structural and functional features. Nucleic Acids Res. 2014;42: 337–343. doi:10.1093/nar/gku366

59. Angus-Hill ML, Dutnall RN, Trafrov ST, Sternglanz R, Ramakrishnan V. Crystal structure of the histone acetyltransferase Hpa2 : a tetrameric member of the Gcn5-related N-acetyltransferase superfamily. J Mol Biol. 1999;294: 1311–1325.

60. Tucker AC, Taylor KC, Rank KC, Rayment I, Escalante-Semerena JC. Insights into the specificity of lysine acetyltransferases. J Biol Chem. 2014;289: 36249–36262. doi:10.1074/jbc.M114.613901

61. Itahana Y, Ke H, Zhang Y. p53 Oligomerization is essential for its C-terminal lysine acetylation. J Biol Chem. 2009;284: 5158–5164. doi:10.1074/jbc.M805696200

62. Geng H, Liu Q, Xue C, David LL, Beer TM, Thomas G V, et al. HIF1α protein stability is increased by acetylation at lysine 709. J Biol Chem. 2012;287: 35496–35505. doi:10.1074/jbc.M112.400697

63. Wood QM and TK. Protein acetylation in procaryotes increases stress resistance. Biochem Biophys Res Commun. 2011;410: 846–851. doi:10.1016/j.bbrc.2011.06.076.Protein

64. Datsenko K a, Wanner BL. One-step inactivation of chromosomal genes in *Escherichia coli* K-12 using PCR products. Proc Natl Acad Sci U S A. 2000;97: 6640–6645. doi:10.1073/pnas.120163297

Appendix

Table S1. Strains, plasmids and primers used in this study. Restriction nuclease sites are in grey. Bold typeface indicates the modified codon during site-directed mutagenesis.

***E. coli* Strain**	**Genotype**	**Source**
BL21 (DE3)	F– ompT gal dcm lon hsdSB(rB- mB-) λ(DE3)	Agilent Technologies
BL21 (DE3) Δ*patZ*	F– ompT gal dcm lon hsdSB(rB- mB-) λ(DE3) *patZ*:kan	This study [64]
DH10B	F- mcrA Δ(mrr-hsdRMS-mcrBC) Φ80dlacZΔM15 ΔlacX74 endA1 recA1 deoR Δ(ara,leu)7697 araD139 galU galK nupG rpsL λ-	Invitrogen
Plasmid	**Genotype**	**Source**
pRSETA	N-terminal, rTEV-cleavable His6-tag overexpression vector, Amp^R	Invitrogen
ASKA*acs*	N-terminal, His6-tag overexpression vector, Cam^R. Encodes Acs wt	ASKA collection [24]
ASKA*cobB*	N-terminal, His6-tag overexpression vector, Cam^R. Encodes CobB wt	ASKA collection [24]
pRSETA*patZ*	Encodes PatZ wt	This study
pRSETA*patZ*^{E809A}	Encodes PatZ ^{E809A} mutant	This study
PRSET*patZ*$^{5(K\rightarrow R)}$	Encodes PatZ$^{K146,\ 149,\ 391,\ 447,\ 635R}$ mutant	This study
pRSETA*patZ*^{GNAT}	Encodes PatZ^{GNAT}variant	This study
pRSETA*patZ*$^{Acs\text{-}like}$	Encodes PatZ^{-GNAT}variant	This study
Primer	**Sequence**	
pRSETA*patZ* Rev	GGTGGTAAGCTTTATGATTCCTCGCGCTGGGC	
pRSETA*patZ* Fwd	GGTGGTCTCGAGACCATGAGTCAGCGAGGACTGGA	
pRSETA*patZ*^{E809A} Rev	GAACCAGTA**CAG**CAAATGCGGCATCGATGTTATC	
pRSETA*patZ*^{E809A} Fwd	GATAACATCGATGCC**GCA**TTTGCTGTACTGGTTC	
pRSET*patZ*$^{K146,\ 149R}$ Rev	CAG**CCT**GCCGCGTCTAATCGGCACAG	
pRSET*patZ*$^{K146,\ 149R}$ Fwd	CTGTGCCGATTAGACGCGGC**AGG**CTG	
pRSET*patZ*^{K391R} Rev	CATATTTGCTGCGGGGATGATG**TCT**TACCGCTTCAATTAATACTTG	
pRSET*patZ*^{K391R} Fwd	AAGTATTAATTGAAGCGGTA**AGA**CATCATCCCCGCAGCAAATATG	
pRSET*patZ*^{K447R} Rev	GTTTCGCGTAGTTG**CCT**CTGATTACGCCGG	
pRSET*patZ*^{K447R} Fwd	CCGGCGTAATCAG**AGG**CAACTACGCGAAAC	
pRSET*patZ*^{K635R} Rev	CACGAATCTTTTTACT**TCT**GATCCCCTGAATAACC	
pRSET*patZ*^{K635R} Fwd	GGTTATTCAGGGGATC**AGA**AGTAAAAAGATTCGTG	
pRSETA*patZ*^{GNAT} Rev	GGTGGTAAGCTTTATGATTCCTCGCGCTGGGC	
pRSETA*patZ*^{GNAT} Fwd	GGTGGTCTCGAGAACGAGAGTCGGCTGGCAG	
pRSETA*patZ*$^{Acs\text{-}like}$ Rev	GGTGGTAAGCTTGCAGCGTTCACCGTTTTTCAAT	
pRSETA*patZ*$^{Acs\text{-}like}$ Fwd	GGTGGTCTCGAGACCATGAGTCAGCGAGGACTGGA	

CHAPTER 5

Characterization of CobB kinetics and inhibition by nicotinamide

The results presented in this chapter are based on the publication

Julia Gallego-Jara, Ana Écija Conesa, Teresa de Diego Puente, Gema Lozano Terol and Manuel Cánovas Díaz

Characterization of CobB kinetics and inhibition by nicotinamide

PLoS ONE. 2017; 12: e0189689. doi: 10.1371/journal.pone.0189689

Abstract

Lysine acetylation has emerged as a global protein regulation system in all domains of life. Sirtuins, or Sir2-like enzymes, are a family of histone deacetylases characterized by their employing NAD^+ as a co-substrate. Sirtuins can deacetylate several acetylated proteins, but a consensus substrate recognition sequence has not yet been established. Product inhibition of many eukaryotic sirtuins by nicotinamide (NAM) and its analogues has been studied *in vitro* due to their potential role as anticancer agents. In this work, the kinetics of CobB, the main *Escherichia coli* (*E. coli*) deacetylase, have been characterized. To our knowledge, this is the first kinetic characterization of a sirtuin employing a fully acetylated and natively folded protein as a substrate. CobB deacetylated several acetyl-CoA synthetase acetylated lysines with a single kinetic rate. In addition, *in vitro* NAM inhibition of CobB has been characterized, and the intracellular NAM concentrations have been determined under different growth conditions. The results suggest that NAM can act as a CobB regulator *in vivo*. A nicotinamidase deletion strain was thus phenotypically characterized, and it behaved similarly to the Δ*cobB* strain. The results of this work demonstrate the potential regulatory role of the NAM metabolite *in vivo*.

Introduction

Protein lysine acetylation is a post-translational modification (PTM) in which the scientific community is increasingly interested [1–3]. Lysine acetylation consists of the transfer of an acetyl group from a donor molecule such as acetyl-CoA or acetyl-phosphate to a lysine amino acid of a protein. This transfer can be catalysed by a lysine acetyltransferase enzyme (KAT) [4,5] or occur in a non-enzymatic or chemical manner [6,7]. The number of proteins that are modified post-translationally by acetylation is continuously discovered in all types of organisms. This PTM has traditionally been associated with transcriptional regulation (histone modifications) [8], although in the past 10 years, many metabolic routes have been demonstrated to be regulated by lysine acetylation [9–15].

Protein acetylation can be reversed by a family of enzymes known as the lysine deacetylases (KDACs). KDACs can be classified into two main groups. The first group acts in a Zn^{2+}-dependent manner, while the members of the second group, also known as sirtuins or Sir2-like enzymes, deacetylate lysines in a reaction that employs NAD^+ [16,17] as a co-substrate. Sirtuins remove an acetyl group from the ε-amino group of a lysine in a reaction that consumes NAD^+ and releases NAM, *O*-acetyl-ADP-ribose, and the deacetylated protein [18]. Many eukaryotic species possess multiple sirtuin paralogs (human sirt1-7) that differ in structure and

cell localization. Archaea and bacteria also produce sirtuins, *e.g*., the bacterial CobB [19–21]. In *E. coli*, the most studied deacetylase is CobB, a bacterial sirtuin that was first characterized in *Salmonella enterica* (*S. enterica*) [21]. Other *E. coli* proteins such as Acs and Pta have been reported to functionally act as deacetylases of the chemotaxis signalling molecule CheY, although, to our knowledge, there is not a proteomic study that shows a deacetylase activity with other substrates [22,23]. In addition, it has recently been demonstrated that YcgC protin deacetylates several acetylated lysines from different proteins without needing NAD^+ or Zn^{2+} as co-substrates [24]. Sirtuins share a common structural core formed by a Rossman domain, a Zn^{2+}-finger domain and a connector loop. The N- and C-terminal regions differ in sequence and length, which might determine differences in substrate specificity [25].

With respect to sirtuin substrates, eukaryotic sirtuins have been linked to cell survival, apoptosis, and stress resistance [26,27]. The typical substrates of archaea and bacteria sirtuins are DNA regulatory proteins (such as the chromatin protein Alba) and metabolic enzymes (such as acyl-CoA synthetases) [2,21,28–33]. In *E. coli*, acetyl-CoA synthetase (Acs) regulation by acetylation-deacetylation has been studied *in vitro* [15,34,35]. Thus, Acs is acetylated at K609 by the acetyltransferase PatZ, also known Pka or YfiQ, inhibiting its catalytic activity, while enzymatic activity is recovered by CobB deacetylation [34–36]. The CheY chemotaxis response regulator [37,38], the N-hydroxyarylamine O-acetyltransferase (Nhoa) protein [39] and the RcsB transcription factor [15,40] have also been identified as CobB substrates. Recent proteomic studies have identified as many as 69 acetyl-lysine residues among 51 proteins to be CobB substrates [7] and have also found 183 proteins that interact with this sirtuin [41]. Several studies have tried to identify a consensus recognition sequence for CobB and other sirtuins [18,42–48], but the results are not clear and do not always correspond to proteomic studies performed *in vivo* [7,15,49,50]. Due to the interest in sirtuins as targets for the treatment of metabolic diseases [51,52], several studies have addressed the regulation and inhibition of these enzymes. NAM, a product of the sirtuin catalytic reaction, is a potent inhibitor for all of these enzymes. Although the mechanism of inhibition by NAM is not completely clear, most of the *in vitro* studies carried out with eukaryotic sirtuins point to non-competitive inhibition *via* a base-exchange mechanism that involves reacting with an intermediate to reform NAD^+ (transglycosidation mechanism) [53–56].

Herein we carry out a CobB sirtuin study by kinetically characterizing acetylated Acs deacetylation. To our knowledge, this report is the first kinetic characterization of a sirtuin deacetylation reaction with a complete natively folded substrate. In addition, we studied CobB inhibition by NAM *in vitro* and *in vivo*. The results of this work represent an advance in the study

of sirtuin specificity and substrate recognition; in addition, our data suggest a new level of CobB regulation *in vivo via* inhibition by NAM, a poorly studied metabolite with a central metabolic role.

Methods

Molecular biology

To generate overexpression plasmids, the *cobB* and nicotinamidase (*pncA*) genes of *E. coli* BW25113 were PCR-amplified and cloned into pBAD24-MBP (Maltose Binding Protein) (kindly transferred by Dr. Antonio Sánchez-Amat, University of Murcia) and pRSETA (Invitrogen) plasmids, respectively. To overexpress Acs protein, the correspondent ASKA plasmid was employed [57]. Single amino acid mutant Acs K609A was obtained by site-directed mutagenesis from *acs*ASKA plasmid. To carry out the complementation assays, the *pncA* and *cobB* genes were PCR-amplified from *E. coli* BW25113 genomic DNA and cloned into the pBAD24 plasmid [58]. All molecular biology enzymes that were used were purchased from Thermo Fisher Scientific. The strains, plasmids and primers used are listed in Appendix Table S1.

Escherichia coli strains and culture conditions

E. coli BW25113 and its deletion strains (Appendix Table S1) were grown in batch mode in minimal M9 medium (10 mM $(NH_4)_2SO_4$, 8.5 mM NaCl, 40 mM Na_2HPO_4, 20 mM KH_2PO_4, 185 µM $FeCl_3$, 175 µM EDTA, 7 µM $ZnSO_4$, 7 µM $CuSO_4$, 7 µM $MnSO_4$, 7 µM $CoCl_2$, 7 µM $MgSO_4$, 0.1 mM $CaCl_2$, and 1 µM thiamine·HCl) or in complex TB7 medium [59] (10 g L^{-1} tryptone buffered at pH 7.0 with 100 mM potassium phosphate) supplemented with glucose 20 mM (TB7-glucose) or glycerol 40 mM (TB7-glycerol) as the carbon source. Cell growth was monitored spectrophotometrically by determining the optical density at 600 nm (OD_{600}). Kanamycin (50 mg mL^{-1}), ampicillin (100 mg mL^{-1}), and chloramphenicol (30 mg mL^{-1}) were added when needed.

Overexpression and purification of proteins

Chemically competent *E. coli* BL21 (DE3) (CobB and PncA overexpression) or *E. coli* BL21 (DE3) Δ*cobB* (Acs and Acs K609A overexpression) strains were transformed by heat shock at 42 °C with overexpression plasmids. Cultures were grown overnight at 30 °C with orbital shaking (200 rpm). The culture medium that was used was Luria-Bertani broth (LB) (10 g L^{-1} tryptone, 5 g L^{-1} yeast extract and 5 g L^{-1} NaCl). Expression was induced with 1 mM isopropyl β-D-1-thiogalactopyranoside (IPTG) (*cobB*pBAD24-MBP and *pncA*pRSETA) or 0.1 mM IPTG (*acs*ASKA) when OD_{600} reached 0.5-0.6. Cells were harvested by centrifugation, thoroughly washed with

0.9 % NaCl and resuspended in binding buffer (50 mM potassium phosphate, pH 7.5, containing 500 mM NaCl and 20 mM imidazole for immobilized metal affinity chromatography (IMAC) purification and 20 mM Tris-HCl, pH 7.5, containing 200 mM NaCl for amylose purification) that was supplemented with an EDTA-free protease inhibitor (SigmaFast Protease Inhibitor Cocktail Tablet, from Sigma Aldrich). Cells were lysed on ice by sonication for 2 min (20 s each pulse) using a Vibra Cell sonicator (Sonicator Sonics & Materials). The lysates were clarified by centrifugation at 10000 x g for 15 min at 4 °C. Recombinant Acs, Acs K609A and PncA proteins were purified by using IMAC. The cell-free extract was loaded onto a 5 mL His GraviTrap column (GE Healthcare), and the column was washed with washing buffer (50 mM potassium phosphate buffer, pH 7.5, containing 500 mM NaCl and 50 mM imidazole). The His_6-tagged proteins were eluted with an elution buffer (50 mM potassium phosphate buffer, pH 7.5, containing 500 mM NaCl and 500 mM imidazole). CobB sirtuin was purified using an amylose resin (New England Biolabs). The resin was washed with a binding buffer, and CobB was eluted using an amylose elution buffer (20 mM Tris-HCl, pH 7.5, containing 200 mM NaCl and 10 mM maltose). Maltose binding protein (MBP) CobB tag was cleaved by incubating the protein with H3V 3C protease (Pierce) over night at 4 °C. MBP-tag and protease were removed with a His GraviTrap column. Purified proteins were dialyzed (Pur-a-lyzer dialysis kits) into 50 mM potassium phosphate buffer, pH 7.5, containing 100 mM NaCl and 10 % v/v glycerol. Proteins were stored at -80 °C until used. Finally, Spin-X UF concentrators (Corning) were employed to concentrate the proteins. Proteins were analysed by using SDS-PAGE electrophoresis with 10 % acrylamide gels in a Mini-Protean cell (Bio-Rad).

Western blot analysis

Proteins with acetylated lysines were separated by using SDS-PAGE and transferred to polyvinylidene fluoride (PVDF) membranes using a semi-dry transfer unit (Trans-Blot® SD Semi-Dry Transfer Cell, Bio-Rad). The membranes were blocked with 1 % (w/v) bovine serum albumin (BSA) in TBST (10 mM Tris-HCl, 0.15 M NaCl, 0.05% Tween-20, pH 7.5) for 1 hour.The membranes were incubated with a rabbit monoclonal primary anti-acetyl Lys antibody (ImmuneChem) and a goat anti-rabbit secondary antibody (Santa Cruz Biotechnology). Finally, the membrane was incubated for 10 min with Amersham ECL western blotting detection reagent (Thermo Scientific). ImageJ Gel Analyzer software was used for densitometric quantification.

Liquid Chromatography–Tandem Mass Spectrometry Assay

Samples were alkylated by incubation with 100 mM iodoacetamide (IAA) for 30 min at room temperature in the dark. Proteins were digested with 0.5-1 µg of proteomics grade Trypsin

Gold (Promega) for 3 h at 37 °C. The reaction was stopped by the addition of 0.1 % formic acid, and the samples were dried using a vacuum evaporator. Tryptic peptides generated from the samples were separated and analysed by liquid chromatography–tandem mass spectrometry assay (LC-MS). An Agilent 1100 (Agilent Technologies) was equipped with a Zorbax SB-C18 HPLC column (Agilent Technologies) and connected to an Agilent Ion Trap XCT Plus mass spectrometer (Agilent Technologies) that had an electrospray (ESI) interface. Two mobile phases were used: phase A was composed of water/acetonitrile/formic acid (94.9:5:0.1, v/v), and phase B consisted of water/acetonitrile/formic acid (10:89.9:0.1, v/v). The digested peptides were resuspended in 20 µL of phase A and eluted using a linear gradient of 0-80 % phase B for 180 min at a flow rate of 10 µL min^{-1}. The mass spectrometer was operated in positive mode with a capillary spray voltage of 3500 V, at a scan speed of 8100 (m/z)/sec from 50 to 2200 m/z, with a target mass of 1000 m/z, and three scans were averaged. The nebulizer gas pressure was set at 15 psi, and the drying gas flowed at 5 L min^{-1} at a temperature of 350 °C. MS/MS data were collected in an automated data-dependent mode (AutoMS mode). Data processing was performed with the Data Analysis program for LC/MSD Trap Version 3.3 (Bruker Daltonik) and the Spectrum Mill MS Proteomics Workbench (Agilent Technologies) [60,61]. After automated validation of the results, the identified proteins and the sequences of the digested peptides were compiled. Peptides with a score threshold of eight and a percentage-scored peak intensity higher than 70 % were considered valid.

Acs enzyme assay

The acetyl-CoA synthetase assay was based on the coupled assay reported by Williamson and Corkey [62]. AMP production was detected *via* a coupled enzyme assay in which myokinase (MK), pyruvate kinase (PK) and lactate dehydrogenase (LDH) couple AMP production to NADH oxidation. Standard acetyl-CoA synthetase assays (0.2 mL) were performed at 37 °C in 50 mM potassium phosphate buffer at pH 7.5 containing 3.0 mM PEP (phosphoenolpyruvate), 5 units MK, 1 unit PK, 1.5 units LDH, 5 mM MgCl2, 2.5 mM ATP, 1.5 mM CoA, 0.1 mM NADH, 5 mM acetate and 1 mM dithiothreitol (DTT). The reaction was started by the addition of Acs. All reactions were performed in triplicate. Specific activity was calculated using the extinction coefficient of NADH (6.22 mM^{-1} cm^{-1}) and was based on the oxidation of two molecules of NADH for each AMP molecule released. One unit of Acs activity is defined as 1 µmole of acetyl-CoA formed per minute at pH 7.5 and 37 °C.

CobB and nicotinamidase enzymatic assay

The continuous CobB assay that was employed was based on the coupled assay published by Denu et al. [63]. In this assay, NAM released by CobB is converted into nicotinamidic acid by nicotinamidase catalysis. A coupled reaction based on glutamate dehydrogenase (GDH) uses the ammonia and α-ketoglutarate (αKG) to oxidize NADH. Standard CobB assays (0.1 mL) were performed at 37 °C in 50 mM potassium phosphate buffer at pH 7.5 and contained 3 mM αKG, 1 mM DTT, 3 units of GDH, 0.4 mM NADH, 1 µM nicotinamidase and 5 mM NAD^+. The reaction was started by the addition of CobB. All reactions were performed in triplicate. Specific activity was calculated using the extinction coefficient of NADH (6.22 mM^{-1} cm^{-1}) and was based on one molecule of NADH being oxidized for each NAM molecule released. One unit of CobB activity is defined as 1 µmole of NAM formed per minute at pH 7.5 and 37 °C.

Intracellular NAM measurement

Cultures (50 mL) were harvested during the exponential (OD_{600}=1) or stationary growth phases, and the collected pellets were washed with 0.9 % NaCl and stored at -80 °C. NAM extraction was carried out by using a freeze-thaw method with methanol [64]. Cell pellets were resuspended in 1 mL of pure methanol at -20 °C with 15 µM d_4-NAM (deuterated nicotinamide), which was employed as an internal standard. The suspensions were put in liquid nitrogen for 5 min to ensure a completely frozen sample and then on ice for 10 min to thaw them. This freeze-thaw cycle was repeated three times. Then, samples were centrifuged at 16000 rpm and 0 °C, and the supernatants were evaporated to dryness. To quantify intracellular metabolites, samples were resuspended in 0.3 mL of HPLC water. The analyses were carried out on an HPLC-MS/MS system consisting of an Agilent 1100 Series HPLC (Agilent Technologies) that was connected to an Agilent Ion Trap XCT Plus mass spectrometer (Agilent Technologies) and used an ESI interface. Samples were injected onto an Agilent Zorbax SB-Aq HPLC column (5 µm, 150 x 4.6 mm) that was thermostatted at 40 °C and eluted at a flow rate of 200 µL min^{-1}. Mobile phase A, consisting of water with 0.1 % formic acid, and mobile phase B, consisting of acetonitrile with 0.1 % formic acid, were used for the chromatographic separation. The elution program consisted of 10 % phase B for 10 minutes and then a gradient from 10 to 100 % of mobile phase B in 15 minutes. Finally, 100 % solvent B was maintained for 5 additional minutes. The mass spectrometer was operated in positive polarity mode with a capillary spray voltage of 3500 V and a scan speed of 22000 (m/z)/sec from 50-250 m/z, with the target mass located at 125 m/z. The Smart ICC target was set to 200.000 counts, whereas the maximum accumulation time was 20 msec. The nebulizer gas pressure was set to 30 psi, whereas the drying gas was set to a flow

rate of 8 L min^{-1} and the temperature was set to 350 °C. The ion chromatograms were extracted, and the peak areas were quantified using the Data Analysis program in LC/MSD Trap Version 3.2 (Bruker Daltonik). The peak area data of the compound in the standards were used to calculate the calibration curve, which was then used to determine the concentrations of NAM and d_4-NAM in the samples. To determine intracellular NAM concentrations a cell volume of 0.7 μm^3 was employed and viable cell mass was determined using a linear calibration curve relating optical density at 600 nm and dry cell weight.

Electron microscopy

E. coli strains were grown in TB7-glycerol complex medium. The cells were harvested in mid-exponential phase (OD_{600}=1) and fixed with 3 % glutaraldehyde for 30 minutes. After two washes with 0.9 % NaCl, each cell suspension was placed on electron microscopy (TEM) grids and stained for 15 s with 2 % uranyl acetate before their flagella were examined in a Philips Tecnai 12 electron microscope operating at 120 kV.

Migration assays

Strains were grown TB7-glycerol complex medium until mid-exponential phase (OD_{600}=1). One microliter of these cultures was inoculated into semisolid agar (10 g L^{-1} tryptone, 5 g L^{-1} NaCl and 0.25 % agar). The migration diameter was measured after 16 h at 30 °C.

Extracellular metabolite quantification

Extracellular acetate, glucose and glycerol were analysed by using an HPLC (Shimadzu Scientific Instruments) equipped with differential refractive and UV detectors and a cation-exchange column (HPX- 87H, Bio-Rad). The mobile phase was 5 mM H_2SO_4 at 0.5 mL min^{-1} flow rate, and the temperature was 65 °C.

Results

Kinetics of Acs deacetylation by CobB are monophasic

Acetyl-CoA synthetase protein was purified from an *E. coli* BL21 (DE3) Δ*cobB* strain to achieve a high Acs acetylation level. To ensure that Acs was acetylated, an LC-MS/MS assay was carried out to determine the Acs acetylation state. In total, 15 acetylated lysines were found in the Acs sequence, namely, K68, K111, K130, K200, K207, K221, K226, K348, K370, K400, K555, K585, K604, K609 and K617. These 15 acetylated lysines had been previously detected by other authors [7,15,35,49,65,66]. Acetylated Acs (10 µM) was incubated for 4 h with CobB (800 nM)

(12:1 ratio) and NAD^+ (5 mM). Aliquots were taken and processed for western blot and Acs activity measurements. Acs activity increased about twenty five-fold after 2 hours of incubation with CobB. This increase coincided with a decrease in chemiluminescent signal from the western blot. However, the reaction was not completed to 2 h of incubation. We therefore knew that Acs deacetylation was being partially inhibited, likely by NAM reaction product. The results are shown in Figure 1.

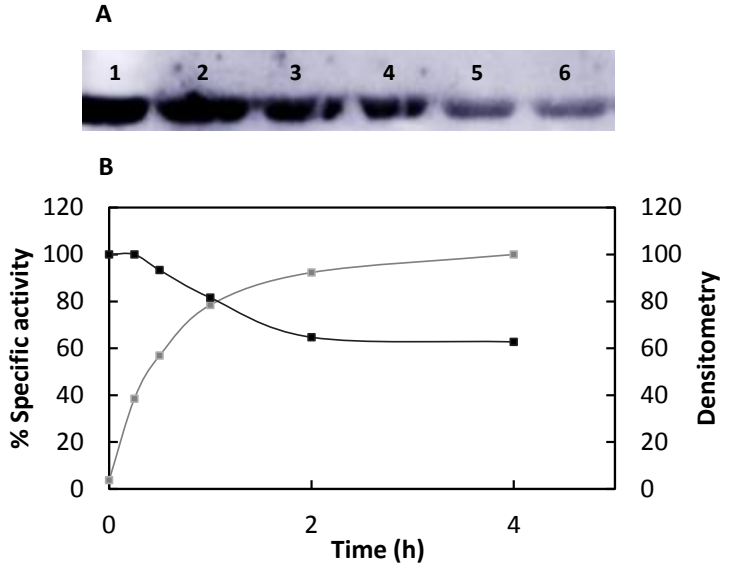

Figure 1. Acs is deacetylated and activated by CobB**. (A)** Western blot with anti-acetyl Lys of Acs incubated with CobB and NAD^+ at 0 (lane 1), 0.25 (lane 2), 0.5 (lane 3), 1 (lane 4), 2 (lane 5) and 4 (lane 6) hours of agitation at 37 °C. **(B)** Acs specific activity (%) at 0, 0.25, 0.5, 1, 2 and 4 hours (grey curve) and densitometry of Acs western blot (black curve).

NAM inhibition of sirtuins is well known and has been studied in many sirtuins [53–56,67,68]. To study the effect of NAM inhibition, *E. coli* nicotinamidase or PncA (an enzyme that consumes NAM to generate ammonium and nicotinate) was coupled to the reaction. Acetylated Acs (10 µM) was incubated with CobB (800 nM) with and without *E. coli* PncA (1 µM), and Acs activity was measured for 4 hours. Acs activation rate was 8.5 times higher when nicotinamidase was present (8.95 U/mg in the absence of nicotinamidase and 76.62 U/mg in the presence of nicotinamidase). Thus, Acs total activation time was reduced from 2 hours to 15 minutes when NAM was continuously degraded by PncA.

To study the kinetics of Acs deacetylation by CobB using a continuous assay, the sirtuin reaction was coupled to PncA and GDH activities. It is important to highlight that NAM product inhibition was eliminated with this assay, since NAM is continuously degraded. NADH oxidation was studied at different acetylated Acs concentrations with a constant concentration of NAD^+ (5 mM, saturated). The CobB concentration was 0.7 µM in the reactions. CobB exhibited hyperbolic

Michaelis-Menten kinetics when the acetylated Acs concentration was varied from 0 to 60 µM (Figure 2A). The calculated kinetic parameters are shown in Table 1.

Table 1. Kinetic parameters of CobB activity with acetylated Acs as a substrate.

K_M (µM)	V_{max} (U/mg)	K_{cat} (s^{-1})	K_{cat}/K_M (s^{-1} μM^{-1})
16.19 ± 3.23	101 ± 7.66	2404.76	148.53

To know if the results observed corresponded only with K609 deacetylation or with several acetylated lysines, the recombinant protein Acs K609A (lysine K609 was substituted by an alanine residue) was overexpressed and purified from an *E. coli* BL21 (DE3) Δ*cobB* strain to achieve a high acetylation level. Acs K609A deacetylation was studied kinetically at a protein concentration of 20 µM with a CobB and NAD^+ concentrations of 0.7 µM and 5 mM, respectively. The resultant deacetylation activity was compared with the obtained for Acs wt protein. Data are expressed in deacetylation percentage in Figure 2B (100 % deacetylation was fixed for Acs wt deacetylation). A western blot assay of the deacetylation reactions was carried out using an anti-acetyl Lys antibody (Figure 2C). The Acs K609A kinetics and western blot assays demonstrated that the kinetics of Acs wt deacetylation by CobB studied are the result of the deacetylation of several Acs acetylated lysines, not only of K609. However, Acs activity was not recovered if K609 was acetylated or mutated, as has been reported for *S. enterica* Acs and other acyl-CoA synthetases [21,31,69,70].

Since enzymatic CobB activity (µmol NAM produced min^{-1}), the number of deacetylated lysines per Acs molecule was calculated at each Acs concentration that was assayed (1 NAM produced per an acetylated lysine deacetylated by CobB). The results are shown in Figure 2D. Approximately 20 lysines were deacetylated by CobB when deacetylation showed a linear dependence on Acs concentration (0-12 µM).

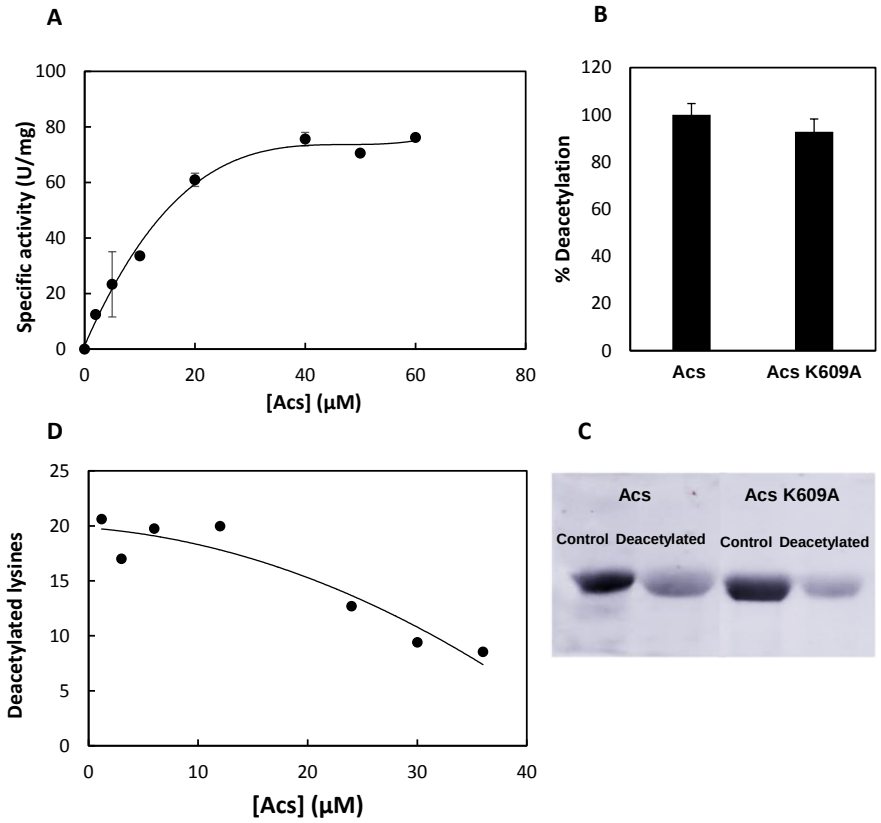

Figure 2. CobB activity on acetylated Acs. **(A)** Substrate saturation curve of CobB at different Acs concentrations. **(B)** Acs and Acs K609A mutant deacetylation (%). **(C)** Western blot with anti-Acetyl Lys of Acs (lanes 1 and 2) and Acs K609A mutant (lanes 3 and 4) before (control) and after CobB deacetylation (deacetylated). **(D)** Number of lysines deacetylated by CobB per Acs molecule at different Acs concentrations.

CobB is non-competitively inhibited by nicotinamide

NAM is a sirtuin reaction product and a well-known inhibitor of sirtuins [53–56,67,68]. NAM inhibition of yeast and mammalian sirtuins has been biochemically and kinetically studied [54,55,67,71,72], but to our knowledge, it has not been studied in depth in a bacterial sirtuin. To study CobB NAM inhibition, acetylated Acs was incubated in a 12:1 ratio with CobB. Acs activity was measured after 4 hours of reaction. NAM concentrations were quantified in a parallel assay employing coupled PncA and GDH reactions. The highest CobB activity (0 % inhibition) was assured by coupling the nicotinamidase enzyme. The value was determined by studying CobB activity at 0.5 mM NAD^+ and different NAM concentrations (Figure 3A). The IC_{50} value was approximately 52 µM. To determine the inhibition constant (K_i), NAD^+ concentration was varied from 0 to 1 mM (10, 50, 500 and 1000 µM) at different NAM concentrations and a Dixon plot (1/v vs NAM concentrations at different [NAD^+]) was made (Figure 3B). The calculated value of K_i was approximately 108 µM NAD^+. To complete the inhibition study, a double-reciprocal plot (1/v *versus* 1/ [NAD^+]) at different NAM concentrations was carried out (Figure

3C). These plots suggest that the activity of the CobB sirtuin has a non-competitive inhibition mechanism. This result is in concordance with the transglycosidation mechanism proposed for most examples of sirtuin NAM inhibition [53,56,73].

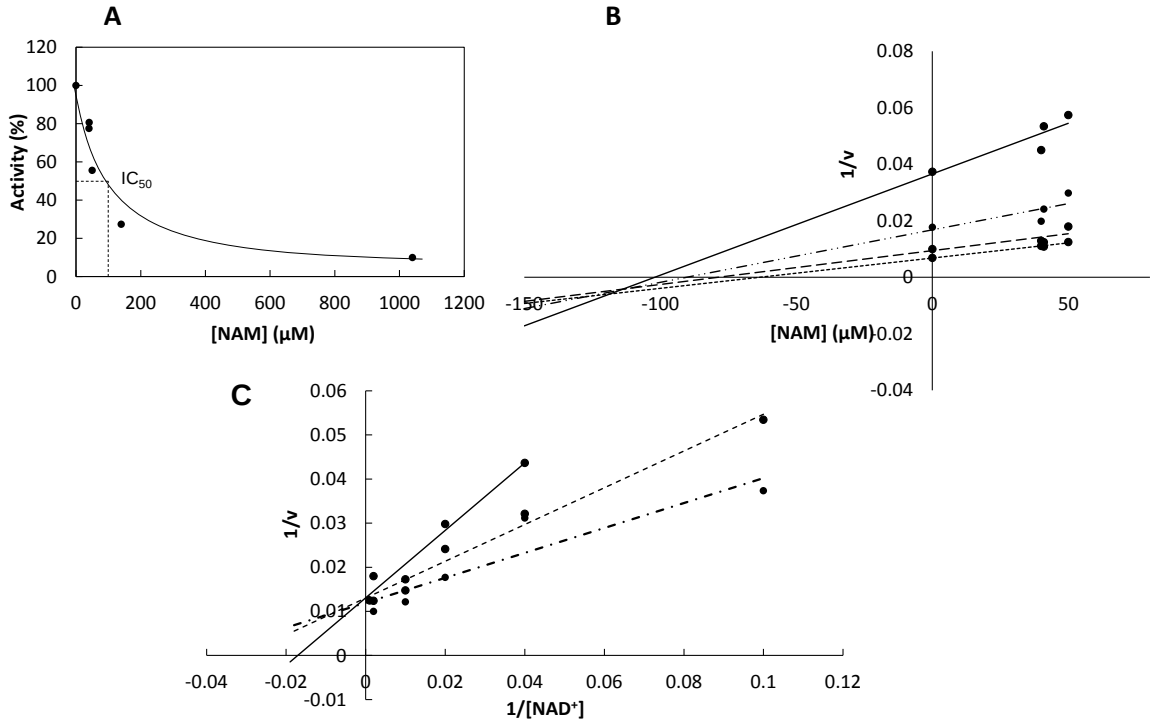

Figure 3. Analysis of CobB inhibition by nicotinamide. **(A)** CobB activity on acetylated Acs at different NAM concentrations. **(B)** Dixon plot ((1/v) vs [NAM]) of CobB deacetylation at different NAD^+ concentrations: 10 (——), 50 (– ·), 500 (– –) and 100 µM (---). **(C)** Double-reciprocal plot (1/v *versus* 1/ [NAD^+]) of CobB deacetylation at different NAM concentrations: 0 (– ·), 40 (·····) and 50 (—) µM. Presented data are average of triplicates. Standard deviations were always less than 10 %.

Nicotinamide concentrations are high enough to regulate CobB *in vivo*

NAM is an *E. coli* metabolite in the NAD^+ salvage pathway, an important route that allows NAD^+ recycling. NAM is synthetized from NAD^+ by the protein NMN nucleosidase and is released by PncA to form nicotinamidic acid. In this study, *E. coli* PncA has been biochemically characterized. To kinetically characterize PncA, kinetics assays were performed in which the NAM concentration was varied from 0 to 5 mM and the PncA concentration was 0.76 µM. The enzyme showed Michaelis-Menten kinetics with values of 0.175 ± 0.027 mM and 2.05 ± 0.07 U/mg for K_M and V_{max}, respectively (Figure 4). This K_M value is higher than the value reported for nicotinamidase enzymes from other organisms (2-110 µM) [74,75]. PncA inhibition by 3-pyridinecarbonitrile and 3-pyridinecarboxaldehide, a potent irreversible and a reversible competitive inhibitors of *Mycobacterium tuberculosis* nicotinamidase [74], respectively, was

evaluated. PncA activity was measured at different NAM concentrations after incubating the enzyme with 1 mM inhibitor for 10 minutes at 37 °C. PncA activity was undetectable in both assays. This result confirms PncA inhibition by 3-pyridinecarbonitrile and 3-pyridinecarboxaldehide *in vitro.* The relatively high nicotinamidase K_M determined in this work could suggest, based on this inhibition study (Figure 3), that *E. coli* intracellular NAM concentrations are high enough to regulate CobB activity *in vivo*.

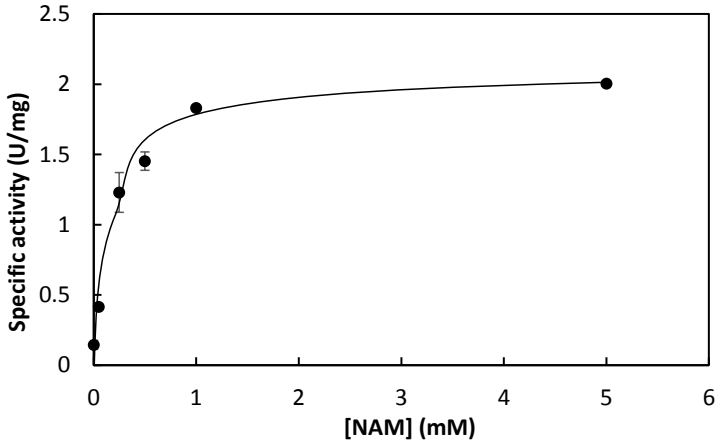

Figure 4. Nicotinamidase kinetics characterization. Substrate saturation curve of nicotinamidase at different NAM concentrations.

To study *in vivo* CobB regulation by NAM, intracellular NAM concentrations were measured during the exponential and stationary growth phases for both the *E. coli* wt strain and a Δ*pncA* mutant growing in minimal and complex media with glucose or glycerol as their carbon sources. The resultant concentrations are summarized in Table 2.

NAM concentrations in cells were higher in complex than in minimal medium and higher concentrations were generally found during exponential growth. The Δ*pncA* mutant showed higher NAM concentrations than the wt strain (approximately 2.5 times higher in complex TB7 medium). The maximum concentration was quantified for the *pncA* mutant during the exponential growth phase growing in TB7 complex medium supplemented with glycerol.

Table 2. Intracellular NAM concentrations. NAM concentrations measured during exponential (X) and stationary (S) growth phases of *E. coli* wt and Δ*pncA* mutant strains growing in minimal and complex media with glucose or glycerol as the carbon source.

	wt X	**wt S**	**Δ*pncA* X**	**Δ*pncA* S**
TB7 + Glucose	36.51 ± 7,.52	38.15 ± 1.66	91.95 ± 4	31.96 ± 0.93
TB7 + Glycerol	67.89 ± 20.02	28.31 ± 5.03	198.45 ± 24.65	77.65 ± 12.87
MM9 + Glucose	21.20 ± 2.81		63.82 ± 8.33	33.55 ± 2.3
MM9 + Glycerol	33.98 ± 4.26	14.35 ± 2.60	47.03 ± 0.1	46.86 ± 3.06

CobB could be regulated *in vivo* by nicotinamide

To study *in vivo* CobB regulation by NAM, physiological characterization of *E. coli* wt, Δ*cobB* and Δ*pncA* strains was carried out. Specific growth rates, glucose and glycerol consumption and acetate overflow were analysed for the strains growing in minimal and complex media with glucose or glycerol as carbon source. Specific growth rates in MM9 medium with glucose were lower in the *cobB* mutant than in the wt strain, while significant differences were not observed in the rest of media. The *pncA* mutant also grew slower than *E. coli* wt, with a value similar to that observed for Δ*cobB*. The results are shown in Table 3.

Table 3. Specific growth rate. Specific growth rate (h^{-1}) of *E. coli* wt, Δ*cobB* and Δ*pncA* strains growing in minimal and complex media with glucose or glycerol as the carbon source.

Medium	**wt**	**Δ*cobB***	**Δ*pncA***
MM9 + Glucose	0.72 ± 0.02	0.58 ± 0.02	0.56 ± 0.02
MM9 + Glycerol	0.49 ± 0.01	0.48 ± 0.01	0.53 ± 0.02
TB7 + Glucose	1.01 ± 0.14	1.07 ± 0.05	0.85 ± 0.03
TB7 + Glycerol	0.95 ± 0.13	0.84 ± 0.06	0.77 ± 0.04

Glucose and glycerol consumption were not affected by *cobB* or *pncA* depletion (data not shown); however, extracellular acetate levels, as a consequence of *E. coli* acetate overflow from bacteria growing in MM9 with glucose, were higher in the mutant strains (Figure 5). Observing similar behaviour in the deletion strains suggests total or partial CobB inhibition in the Δ*pncA* strain due to a higher intracellular NAM concentration.

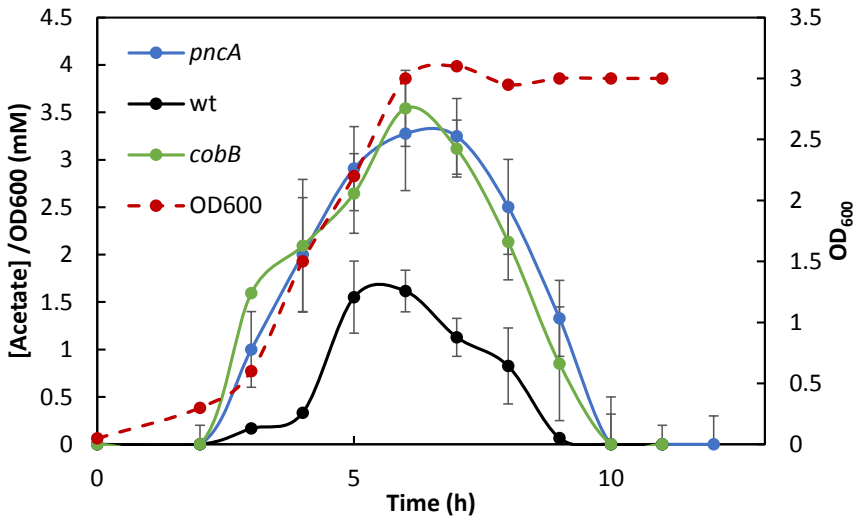

Figure 5. Acetate overflow. Extracellular acetate concentrations (mM) per OD (600 nm) of *E. coli* wt (black line), Δ*cobB* (green line) and Δ*pncA* (blue line) strains grown in minimal medium with 20 mM glucose. *E. coli* wt growth curve is shown as a discontinuous red line.

To analyse the acetylation levels in the strains, a western blot of total protein extract, employing an anti-acetyl Lys antibody, was carried out. The strains were grown in TB7 supplemented and non-supplemented with glucose, and cells were harvested during the mid-exponential (OD_{600}=1) and stationary phases. The western blot did not show differences in the acetylation of the protein extracts. The similar acetylation patterns in wt and Δ*cobB* strains have been previously detected by other authors [7,15].

To complete the physiological characterization of the *E. coli* wt, Δ*cobB* and Δ*pncA* strains, the presence of their flagella was analysed using TEM. CobB regulates the RcsB transcription factor by deacetylating its K154 and the absence of CobB causes an increase in the number of flagella [7,15,40]. We hypothesized that a CobB-inhibited strain would also show an increase in the number of flagella, so TEM imaging of the three strains during the exponential growth phase in TB7 with glucose as carbon source was carried out. The results are shown in Figure 6 (A1-C1). The *cobB*-deficient strain had significantly more and longer flagella than the wt strain. *E. coli* lacking the nicotinamidase protein also showed a phenotype that was similar to but less pronounced than that of Δ*cobB*. The Δ*pncA* strain had more flagella than the *E. coli* wt, but fewer than the Δ*cobB* strain. A migration assay using semi-solid agar plates was employed to quantify cells migration diameter. The assay was carried out on triplicate and the results are shown in Figure 6 (A2-C2). A migration diameter of 0.43 ± 0.05 cm was observed on *E. coli* wt plates, while a 5.30 ± 0.14 cm and 4.40 ± 0.26 cm was measured for Δ*cobB* and Δ*pcnA* strains. To verify the effect of *cobB* and *pncA* deletions, the mutant strains Δ*cobB* and Δ*pncA* were transformed with *cobB*pBad24 and *pncA*pBad24, respectively. Cells phenotype was evaluated through TEM and

migration assays. The results are shown in Figure 6 (D1, D2, E1, E2). Both of mutant strains (Δ*cobB* and Δ*pncA*) recovered the wt phenotype when were complemented with the expression plasmids. These assays prove that the migration and flagella expression observed in Δ*cobB* and Δ*pncA* are consequence of genes deletion. Finally, an epistasis experiment was carried out to determine if the effect of PncA depends upon CobB. Thus, PncA was overexpressed in the *cob* mutant and phenotype was evaluated with semi-solid agar plates and TEM. Results are shown in Figure 6 (F1 and F2). Cells showed a Δ*cobB* phenotype and no effect was observed with PncA overexpression. This result points out that PncA has not a CobB-independent effect on *Escherichia coli* migration.

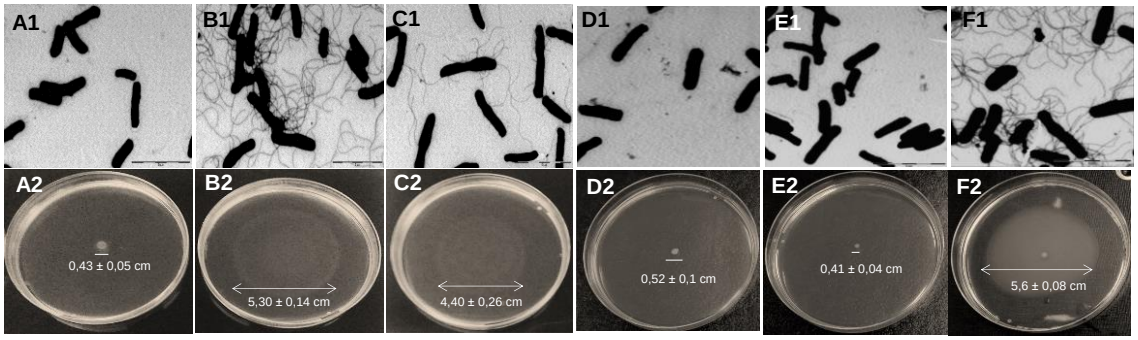

Figure 6. TEM and migration assays**.** TEM images of **(A1)** *E. coli* wt, **(B1)** Δ*cobB*, **(C1)** Δ*pncA*, **(D1)** Δ*cobB* + *cobB*pBAD24, **(E1)** Δ*pncA*+ *pncA*pBAD24 and **(F1)** Δ*cobB* + *pncA*pBAD24 strains during the exponential growth phase in TB7 medium supplemented with glycerol. Semi-solid agar plates of **(A2)** *E. coli* wt, **(B2)** Δ*cobB*, **(C2)** Δ*pncA* strains, **(D2)** Δ*cobB* + *cobB*pBAD24, **(E2)** Δ*pncA*+ *pncA*pBAD24 and **(F2)** Δ*cobB* + *pncA*pBAD24 strains. Migration distances (diameter) and standard deviation from the mean migration of three biological replicates are shown.

Discussion

Sirtuins are an important family of enzymes that are widely distributed in all domains of life. They are involved in many metabolic processes such as glucose or lipid metabolism, DNA repair, transcription regulation and tumour proliferation [76]. The kinetics of sirtuin activity against acetylated peptides have been studied and most of these studies have found a sirtuin selectivity for acetylated peptides substrates [43–48]; however there is no clear evidence of this sequence specificity when native proteins are used as substrates. Thus, one of the biggest challenges in sirtuin research is to determine how specificity is determined in natively folded substrate proteins. In recent years, a few studies have focused on complete and native protein specificity of sirtuins [42,77]. The results suggest that structural protein components are the main determinants of sirtuin specificity. The kinetics study carried out in this work, examining natively folded Acs deacetylation by CobB, is in concordance with this hypothesis. The results

have shown a single kinetic phase for several acetylated lysines of Acs, indicating the same binding affinity or specificity for acetylated lysines at different positions (Figure 2). The results of this study and the lack of understanding of the reasons for the discrepancy between the *in vitro* and *in vivo* results suggest that the results of assays carried out using peptides as substrates should be contrasted with new results, which use whole native proteins.

NAM inhibition of several eukaryotic sirtuins has been studied, and the mechanism of inhibition has been characterized. The mechanism of NAM inhibition is based on NAM intercepting the ADP-ribosyl-enzyme-acetyl-peptide intermediate, resulting in regeneration of the NAD^+ substrate (transglycosidation) [53]. Several crystal structures of sirtuins with NAM have been determined. In these structures, NAM binds to the peptide-sirtuin reaction intermediate, but the binding location is not clear. In some structures, NAM appears to be bound to the pocket where the NAD^+ substrate binds (C pocket) despite this binding not being consistent with non-competitive inhibition [67]. In other structures, NAM binds in a pocket other than the NAD^+-binding pocket [56,72]. The characterization of CobB inhibition suggests that non-competitive NAM inhibition occurs, which would agree with the transglycosidation mechanism. The kinetic parameters (K_i and IC_{50}) that describe CobB inhibition by NAM have also been determined. The obtained values (IC_{50}=52 µM and K_i=108 µM) are very similar to those found when NAM inhibits other sirtuins. The K_i parameters of hSIRT2 and HST2 are 33.9 and 298 µM [53], respectively, while the IC_{50} values for Sirt1, Sirt2 and Sirt3 have been recently established at 175, 80 and 72 µM [71]. The K_i value determined for CobB is also in agreement with the only inhibition study of a bacterial sirtuin (Sir2Af2 from the sulfate-reducing Archaea *Archeaoglobus fulgidus*), which reported a K_i value of 26 µM [78]. These inhibition parameters, including the CobB K_i calculated in this study, are in the range from 20-300 µM.

Nicotinamidase is a relatively unstudied enzyme in *E. coli*. PncA participates in the NAD^+ salvage pathway in *E. coli*, which is a route to NAD^+ recycling. In this study, nicotinamidase has been kinetically characterized for the first time, and the physiology of the deletion strain Δ*pncA* has been studied. The results showed that a deficiency in PncA causes several differences between the mutant strain and wt *E. coli* and point to a clear similarity between the Δ*pncA* and Δ*cobB* strains. Physiological characterization of wt, Δ*cobB* and Δ*pncA* strains showed that when the mutant strains grew in minimal M9 medium supplemented with glucose, their specific growth rate (Table 3) was much lower than that of the wt strain in the same conditions. The levels of extracellular acetate, a result of *E. coli* acetate overflow, were also different in the Δ*cobB* and Δ*pncA* strains than in the wt (Figure 5), being higher in the mutant stains. This fact could be due to low activity by acetylated Acs in these mutants. Acs activity constitutes one of

the two routes to assimilate acetate from the extracellular *E. coli* medium, where it was excreted to as a consequence of overflow metabolism [79,80]. The absence or inhibition of CobB would cause an increase in the acetylation of Acs that would totally or partially block this acetate pathway [21]. In addition, the flagella and motility in the three studied strains were analysed by TEM and semi-solid agar assays (Figure 6). It has been reported that the transcription factor RcsB is acetylated by acetyl-phosphate and deacetylated by CobB at K154 [7,15,40]. Besides, RcsB K154 acetylation increases the expression of the flagella regulon, provoking an increase in motility and number of flagella. The Δ*cobB* mutant also shows this phenotype when RcsB is acetylated [15]. In this study, the *pncA* deletion strain showed more flagella and motility than the wt strain (a ten-fold increase), but flagella expression and motility were less pronounced than those of Δ*cobB*. This result suggests that in the Δ*pncA* mutant, the transcription factor RcsB could be partially inhibited by lysine acetylation as a consequence of low or no CobB deacetylase activity.

Intracellular NAM concentrations in wt and Δ*pncA* strains have been determined under different conditions. In the wt *E. coli* strain, NAM concentrations ranged between 30 and 70 µM during exponential growth phase. Stationary NAM concentrations were always lower (wt MM9 stationary NAM concentrations were not detected). Based on the *in vitro* inhibition of CobB (Figure 3), these concentrations could regulate CobB activity *in vivo*. To our knowledge, this example is the first time that an intracellular bacterial NAM concentration has been determined to date. Previous studies have quantified NAM concentrations in yeast (10-150 µM) [81] and in mammalian tissues (11-400 µM) [82–84]. These concentrations are very similar to those determined in this study in *E. coli*. Intracellular NAM concentrations were higher in the Δ*pncA* strain than in wt *E. coli* (approximately two times higher). These higher concentrations could justify the physiological behaviour of the *pncA* deletion strain, *e.g*., conditions in which the CobB protein is totally or partially inhibited. This result suggests that CobB is regulated *in vivo* by NAM concentration. Previous studies have demonstrated that yeast processes regulated by Sir2 are altered by additional copies of the NAD^+-salvage route genes such as *npt1* (nicotinate phosphoribosyltransferase), *pnc1* (nicotinamidase), *nma1*, and *nma2* (nicotinate mononucleotide adenylyltransfereases 1 and 2) [85], and exogenous NAM [68]. In addition, pnc1 overexpression activate Sir2 *in vivo*, altering *Saccharomyces* longevity [86]. In addition, human breast cancer cell treatment with NAM induces cellular apoptosis *in vivo* through Sirt1 inhibition [87], although a recent study points to the fact that NAM addition to cells can stimulate sirtuins due to rapid in vivo conversion of NAM to NAD^+ [88].

The role of NAM as an *in vivo* inhibitor of CobB activity, as suggested in this study, identifies this metabolite and the nicotinamidase PncA as potential regulators of central *E. coli* metabolism due to the global role of CobB (Figure 7). Thus, we have suggested that NAM concentrations could regulate very different aspects of *E. coli*, specifically, acetate consumption and flagellum expression. The results of this work open the way for future studies on the regulatory roles of the NAD^+ salvage route and NAM, and how they affect post-translational acetylation in *E. coli*.

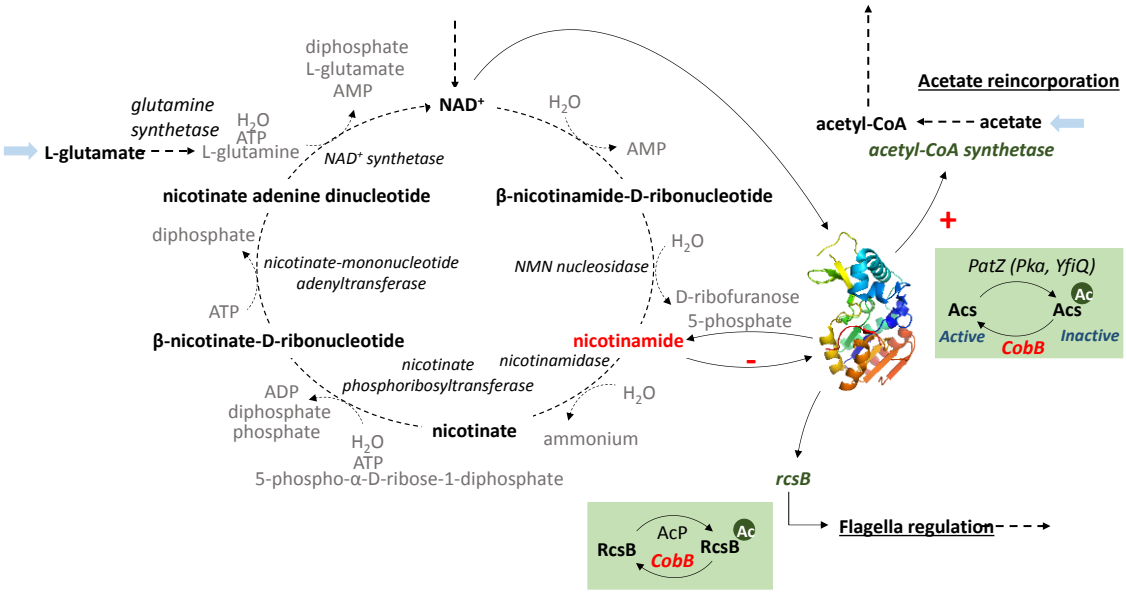

Figure 7. Central role of the NAM metabolite in *E. coli* metabolism.

References

1. Verdin E, Ott M. 50 years of protein acetylation: from gene regulation to epigenetics, metabolism and beyond. Nat Rev Mol Cell Biol. 2014;16: 258–264. doi:10.1038/nrm3931

2. Bernal V, Castaño-Cerezo S, Gallego-Jara J, Écija-Conesa A, de Diego T, Iborra JL, et al. Regulation of bacterial physiology by lysine acetylation of proteins. N Biotechnol. 2014;31: 586–595. doi:10.1016/j.nbt.2014.03.002

3. Hentchel KL, Escalante-Semerena JC. Acylation of biomolecules in prokaryotes: a widespread strategy for the control of biological function and metabolic stress. Microbiol Mol Biol Rev. 2015;79: 321–346. doi:10.1128/MMBR.00020-15

4. Friedmann DR, Marmorstein R. Structure and mechanism of non-histone protein acetyltransferase enzymes. FEBS J. 2013;280: 5570–5581. doi:10.1111/febs.12373

5. Vetting MW, S de Carvalho LP, Yu M, Hegde SS, Magnet S, Roderick SL, et al. Structure and functions of the GNAT superfamily of acetyltransferases. Arch Biochem Biophys. 2005;433: 212–226. doi:10.1016/j.abb.2004.09.003

6. Weinert BT, Iesmantavicius V, Wagner SA, Schölz C, Gummesson B, Beli P, et al. Acetyl-phosphate is a critical determinant of lysine acetylation in *E. coli*. Mol Cell. 2013;51: 265–272. doi:10.1016/j.molcel.2013.06.003

7. Kuhn ML, Zemaitaitis B, Hu LI, Sahu A, Sorensen D, Minasov G, et al. Structural, kinetic and proteomic characterization of acetyl phosphate-dependent bacterial protein acetylation. PLoS One. 2014;9: e94816. doi:10.1371/journal.pone.0094816

8. Sterner DE, Berger SL. Acetylation of histones and transcription-related factors. Microbiol Mol Biol Rev. 2000;64: 435–459. doi:10.1128/MMBR.64.2.435-459.2000

9. Okanishi H, Kim K, Masui R, Kuramitsu S. Acetylome with structural mapping reveals the significance of lysine acetylation in *Thermus thermophilus*. J Proteome Res. 2013;12: 3952–3968. doi:10.1021/pr400245k

10. Kim D, Yu BJ, Kim JA, Lee YJ, Choi SG, Kang S, et al. The acetylproteome of Gram-positive model bacterium *Bacillus subtilis*. Proteomics. 2013;13: 1726–1736. doi:10.1002/pmic.201200001

11. Xie L, Wang X, Zeng J, Zhou M, Duan X, Li Q, et al. Proteome-wide lysine acetylation profiling of the human pathogen *Mycobacterium tuberculosis*. Int J Biochem Cell Biol. 2015;59: 193–202. doi:10.1016/j.biocel.2014.11.010

12. Kim SC, Sprung R, Chen Y, Xu Y, Ball H, Pei J, et al. Substrate and functional diversity of lysine acetylation revealed by a proteomics survey. Mol Cell. 2006;23: 607–618. doi:10.1016/j.molcel.2006.06.026

13. Wagner GR, Payne RM. Widespread and enzyme-independent Nε-acetylation and Nε-succinylation of proteins in the chemical conditions of the mitochondrial matrix. J Biol Chem. 2013;288: 29036–29045. doi:10.1074/jbc.M113.486753

14. Zhao S, Xu W, Jiang W, Yu W, Lin Y, Zhang T, et al. Regulation of cellular metabolism by protein lysine acetylation. Science. 2010;327: 1000–1004. doi:10.1126/science.1179689

15. Castaño-Cerezo S, Bernal V, Post H, Fuhrer T, Cappadona S, Sánchez-Díaz NC, et al. Protein acetylation affects acetate metabolism, motility and acid stress response in *Escherichia coli*. Mol Syst Biol. 2014;10: 1–16. doi:10.15252/msb.20145227

16. Gregoretti I V, Lee Y-M, Goodson H V. Molecular evolution of the histone deacetylase family: functional implications of phylogenetic analysis. J Mol Biol. 2004;338: 17–31. doi:10.1016/j.jmb.2004.02.006

17. Frye RA. Phylogenetic classification of prokaryotic and eukaryotic Sir2-like proteins. Biochem Biophys Res Commun. 2000;273: 793–798. doi:10.1006/bbrc.2000.3000

18. Cosgrove MS, Bever K, Avalos JL, Muhammad S, Zhang X, Wolberger C. The structural basis of sirtuin substrate affinity. Biochemistry. 2006;45: 7511–7521. doi:10.1021/bi0526332

19. Frye RA. Characterization of five human cDNAs with homology to the yeast SIR2 gene: Sir2-like proteins (sirtuins) metabolize NAD and may have protein ADP-ribosyltransferase activity. Biochem Biophys Res Commun. 1999;260: 273–279. doi:10.1006/bbrc.1999.0897

20. Landry J, Sutton A, Tafrov ST, Heller RC, Stebbins J, Pillus L, et al. The silencing protein SIR2 and its homologs are NAD-dependent protein deacetylases. Proc Natl Acad Sci U S A. 2000;97: 5807–5811. doi:10.1073/pnas.110148297

21. Starai VJ, Celic I, Cole RN, Boeke JD, Escalante-Semerena JC. Sir2-dependent activation of acetyl-CoA synthetase by deacetylation of active lysine. Science. 2002;298: 2390–2392. doi:10.1126/science.1077650

22. Baron S, Eisenbach M. CheY acetylation is required for ordinary adaptation time in *Escherichia coli* chemotaxis. FEBS Lett. 2017;591: 1958–1965. doi:10.1002/1873-3468.12699

23. Barak R, Prasad K, Shainskaya A, Wolfe AJ, Eisenbach M. Acetylation of the chemotaxis response regulator CheY by acetyl-CoA synthetase purified from *Escherichia coli*. J Mol Biol. 2004;342: 383–401. doi:10.1016/j.jmb.2004.07.020

24. Tu S, Guo SJ, Chen CS, Liu CX, Jiang HW, Ge F, et al. YcgC represents a new protein deacetylase family in prokaryotes. Elife. 2015;4: 1–17. doi:10.7554/eLife.05322

25. Yuan H, Marmorstein R. Structural basis for Sirtuin activity and inhibition. J Biol Chem. 2012;287: 42428–42435. doi:10.1074/jbc.R112.372300

26. Kleszcz R, Paluszczak J, Baer-Dubowska W. Targeting aberrant cancer metabolism - The role of sirtuins. Pharmacol Reports. 2015;67: 1068–1080. doi:10.1016/j.pharep.2015.03.021

27. Kim E-J, Um S-J. SIRT1 : roles in aging and cancer. BMB Rep. 2008;41: 751–756. doi:10.5483/BMBRep.2008.41.11.751

28. Bell SD. The interaction of Alba, a conserved archaeal chromatin protein, with Sir2 and its regulation by acetylation. Science. 2002;296: 148–151. doi:10.1126/science.1070506

29. Starai VJ, Escalante-Semerena JC. Acetyl-coenzyme A synthetase (AMP forming). Cell Mol Life Sci. 2004;61: 2020–2030. doi:10.1007/s00018-004-3448-x

30. Gardner JG, Escalante-Semerena JC. In *Bacillus subtilis*, the sirtuin protein deacetylase, encoded by the srtN gene (formerly *yhdZ*), and functions encoded by the acuABC genes control the activity of acetyl coenzyme a synthetase. J Bacteriol. 2009;191: 1749–1755. doi:10.1128/JB.01674-08

31. Crosby HA, Heiniger EK, Harwood CS, Escalante- JC. Reversible N-Lysine acetylation regulates the activity of acyl-CoA synthetases involved in anaerobic benzoate catabolism

in *Rhodopseudomonas palustris*. Mol Microbiol. 2010;76: 874–888. doi:10.1111/j.1365-2958.2010.07127

32. Hayden JD, Brown LR, Gunawardena HP, Perkowski EF, Chen X, Braunstein M. Reversible acetylation regulates acetate and propionate metabolism in *Mycobacterium smegmatis*. Microbiology. 2013;159: 1986–1999. doi:10.1099/mic.0.068585-0

33. Schwer B, Bunkenborg J, Verdin RO, Andersen JS, Verdin E. Reversible lysine acetylation controls the activity of the mitochondrial enzyme acetyl-CoA synthetase 2. Proc Natl Acad Sci U S A. 2006;103: 10224–10229. doi:10.1073/pnas.0603968103

34. Zhao K, Chai X, Marmorstein R. Structure and substrate binding properties of CobB, a Sir2 homolog protein deacetylase from *Escherichia coli*. J Mol Biol. 2004;337: 731–741. doi:10.1016/j.jmb.2004.01.060

35. De Diego Puente T, Gallego-Jara J, Castaño-Cerezo S, Sánchez VB, Espín VF, De La Torre JG, et al. The protein acetyltransferase PatZ from *Escherichia coli* is regulated by autoacetylation-induced oligomerization. J Biol Chem. 2015;290: 23077–23093. doi:10.1074/jbc.M115.649806

36. Starai VJ, Escalante-Semerena JC. Identification of the protein acetyltransferase (Pat) enzyme that acetylates acetyl-CoA synthetase in *Salmonella enterica*. J Mol Biol. 2004;340: 1005–1012. doi:10.1016/j.jmb.2004.05.010

37. Yan J, Barak R, Liarzi O, Shainskaya A, Eisenbach M. *In vivo* acetylation of CheY, a response regulator in chemotaxis of *Escherichia coli*. J Mol Biol. 2008;376: 1260–1271. doi:10.1016/j.jmb.2007.12.070

38. Liarzi O, Barak R, Bronner V, Dines M, Sagi Y, Shainskaya A, et al. Acetylation represses the binding of CheY to its target proteins. Mol Microbiol. 2010;76: 932–943. doi:10.1111/j.1365-2958.2010.07148.x

39. Zhang Q-F, Zhang Q, Gu J, Gong P, Wang X-D, Wang X, et al. Reversibly acetylated lysine residues play important roles in the enzymatic activity of *Escherichia coli* N-hydroxyarylamine O-acetyltransferase. FEBS J. 2013;280: 1966–1979. doi:10.1111/febs.12216

40. Hu LI, Chi BK, Kuhn ML, Filippova E V, Walker-Peddakotla AJ, Bäsell K, et al. Acetylation of the response regulator RcsB controls transcription from a small RNA promoter. J Bacteriol. 2013;195: 4174–4186. doi:10.1128/JB.00383-13

41. Liu CX, Wu FL, Jiang HW, He X, Guo SJ, Tao SC. Global identification of CobB interactors by an *Escherichia coli* proteome microarray. Acta Biochim Biophys Sin (Shanghai). 2014;46: 548–555. doi:10.1093/abbs/gmu038

42. Abouelfetouh A, Kuhn ML, Hu LI, Scholle MD, Sorensen DJ, Sahu AK, et al. The *E. coli* sirtuin CobB shows no preference for enzymatic and nonenzymatic lysine acetylation substrate sites. Microbiol Open. 2015;4: 66–83. doi:10.1002/mbo3.223

43. Garske AL, Denu JM. SIRT1 top hits: Use of one-bead, one-compound acetyl-peptide libraries and quantum dots to probe deacetylase specificity. Biochemistry. 2006;10: 94–101. doi:10.1038/nature13314.A

44. Blander G, Olejnik J, Krzymanska-Olejnik E, McDonagh T, Haigis M, Yaffe MB, et al. SIRT1 shows no substrate specificity *in vitro*. J Biol Chem. 2005;280: 9780–9785. doi:10.1074/jbc.M414080200

45. Gurard-Levis ZA, Kilian KA, Kim J, Bähr K, Mrksich M. Peptide arrays identify isoform-selective substrates for profiling endogenous lysine deacetylase activity. ACS Chem Biol. 2010;5: 863–873. doi:10.1021/cb100088g

46. Rauh D, Fischer F, Gertz M, Lakshminarasimhan M, Bergbrede T, Aladini F, et al. An acetylome peptide microarray reveals specificities and deacetylation substrates for all human sirtuin isoforms. Nat Commun. 2013;4: 2327–2342. doi:10.1038/ncomms3327

47. Smith BC, Settles B, Hallows WC, Craven MW, Denu JM. SIRT3 substrate specificity determined by peptide arrays and machine learning. ACS Chem Biol. 2011;6: 146–157. doi:10.1021/cb100218d

48. Khan AN, Lewis PN. Unstructured conformations are a substrate requirement for the Sir2 family of NAD-dependent protein deacetylases. J Biol Chem. 2005;280: 36073–36078. doi:10.1074/jbc.M508247200

49. Baeza J, Dowell JA, Smallegan MJ, Fan J, Amador-Noguez D, Khan Z, et al. Stoichiometry of site-specific lysine acetylation in an entire proteome. J Biol Chem. 2014;289: 21326–21338. doi:10.1074/jbc.M114.581843

50. Bheda P, Jing H, Wolberger C, Lin H. The substrate specificity of sirtuins. Annu Rev Biochem. 2016;85: 405–429. doi:10.1146/annurev-biochem-060815-014537

51. Guarente L. Sirtuins in aging and diseases. In: Walker JM, editor. Methods in Molecular Biology. Humana Press; 2013. pp. 3–10. doi:10.1007/978-1-62703-637-5_1

52. Sebastián C, Satterstrom FK, Haigis MC, Mostoslavsky R. From sirtuin biology to human diseases: an update. J Biol Chem. 2012;287: 42444–42452. doi:10.1074/jbc.R112.402768

53. Jackson MD, Schmidt MT, Oppenheimer NJ, Denu JM. Mechanism of nicotinamide inhibition and transglycosidation by Sir2 histone/protein deacetylases. J Biol Chem. 2003;278: 50985–50998. doi:10.1074/jbc.M306552200

54. Guan X, Lin P, Knoll E, Chakrabarti R. Mechanism of inhibition of the human sirtuin enzyme SIRT3 by nicotinamide : computational and experimental studies. PLoS One. 2014;9: e0136127. doi:10.1371/journal.pone.0107729

55. Fischer F, Gertz M, Suenkel B, Lakshminarasimhan M, Schutkowski M, Steegborn C. Sirt5 deacylation activities show differential sensitivities to nicotinamide inhibition. PLoS One. 2012;7: e45098. doi:10.1371/journal.pone.0045098

56. Zhao K, Harshaw R, Chai X, Marmorstein R. Structural basis for nicotinamide cleavage and ADP-ribose transfer by NAD^+-dependent Sir2 histone/protein deacetylases. Proc Natl Acad Sci U S A. 2004;101: 8563–8568. doi:10.1073/pnas.0401057101

57. Kitagawa M, Ara T, Arifuzzaman M, Ioka-Nakamichi T, Inamoto E, Toyonaga H, et al. Complete set of ORF clones of *Escherichia coli* ASKA library (a complete set of *E. coli* K-12 ORF archive): unique resources for biological research. DNA Res. 2005;12: 291–299. doi:10.1093/dnares/dsi012

58. Guzman LM, Belin D, Carson MJ, Beckwith J. Tight regulation, modulation, and high-level expression by vectors containing the arabinose PBAD promoter. J Bacteriol. 1995;177: 4121–4130. doi:10.1128/JB.177.14.4121-4130.1995

59. Christensen DG, Orr JS, Rao C V, Wolfe J. Increasing growth yield and decreasing acetylation in *Escherichia coli* by optimizing the carbon-to-magnesium ratio in peptide-based media. Appl Environ Microbiol. 2017;83: 1–13. doi:10.1128/AEM.03034-16

60. Moulder R, Filén J-J, Salmi J, Katajamaa M, Nevalainen OS, Oresic M, et al. A comparative evaluation of software for the analysis of liquid chromatography-tandem mass spectrometry data from isotope coded affinity tag experiments. Proteomics. 2005;5: 2748–2760. doi:10.1002/pmic.200401187

61. Kapp EA, Schütz F, Connolly LM, Chakel JA, Meza JE, Miller CA, et al. An evaluation, comparison, and accurate benchmarking of several publicly available MS/MS search algorithms: sensitivity and specificity analysis. Proteomics. 2005;5: 3475–3490. doi:10.1002/pmic.200500126

62. Williamson J, Corkey B. Assays of intermediates of the citric acid. In: Lowenstein J, Kaplan N, Colowick N, editors. Methods of Enzymology. Academic P. 1969. pp. 494–497.

63. Smith BC, Hallows WC, Denu JM. A continuous microplate assay for sirtuins and nicotinamide producing enzymes. Anal Biochem. 2009;394: 101–109. doi:10.1016/j.ab.2009.07.019

64. Duportet X, Bastos R, Aggio M, Granato S. The biological interpretation of metabolomic data can be misled by the extraction method used. Metabolomics. 2012;8: 410–421. doi:10.1007/s11306-011-0324-1

65. Zhang J, Sprung R, Pei J, Tan X, Kim S, Zhu H, et al. Lysine acetylation is a highly abundant and evolutionarily conserved modification in *Escherichia coli*. Mol Cell Proteomics. 2009;8: 215–225. doi:10.1074/mcp.M800187-MCP200

66. Schilling B, Christensen D, Davis R, Sahu AK, Hu LI, Walker-Peddakotla A, et al. Protein acetylation dynamics in response to carbon overflow in *Escherichia coli*. Mol Microbiol. 2015;98: 847–863. doi:10.1111/mmi.13161

67. Avalos JL, Bever KM, Wolberger C. Mechanism of sirtuin inhibition by nicotinamide: Altering the NAD^+ cosubstrate specificity of a Sir2 enzyme. Mol Cell. 2005;17: 855–868. doi:10.1016/j.molcel.2005.02.022

68. Bitterman KJ, Anderson RM, Cohen HY, Latorre-Esteves M, Sinclair DA. Inhibition of silencing and accelerated aging by nicotinamide, a putative negative regulator of yeast Sir2 and human SIRT1. J Biol Chem. 2002;277: 45099–45107. doi:10.1074/jbc.M205670200

69. Horswill AR, Escalante-Semerena JC. Characterization of the propionyl-CoA synthetase (PrpE) enzyme of *Salmonella enterica*: Residue lys 592 is required for propionyl-AMP synthesis. Biochemistry. 2002;41: 2379–2387. doi:10.1021/bi015647q

70. Nambi S, Gupta K, Bhattacharya M, Ramakrishnan P, Ravikumar V, Siddiqui N, et al. Cyclic AMP-dependent protein lysine acylation in *Mycobacteria* regulates fatty acid and propionate metabolism. J Biol Chem. 2013;288: 14114–14124. doi:10.1074/jbc.M113.463992

71. Feldman JL, Dittenhafer-Reed KE, Kudo N, Thelen JN, Ito A, Yoshida M, et al. Kinetic and structural basis for acyl-group selectivity and NAD^+ dependence in sirtuin-catalyzed deacylation. Biochemistry. 2015;54: 3037–3050. doi:10.1021/acs.biochem.5b00150

72. Sanders BD, Zhao K, Slama JT, Marmorstein R. Structural basis for nicotinamide inhibition and base exchange in Sir2 enzymes. Mol Cell. 2007;25: 463–472. doi:10.1016/j.molcel.2006.12.022

73. Feldman JL, Dittenhafer-Reed KE, Denu JM. Sirtuin catalysis and regulation. J Biol Chem. 2012;287: 42419–42427. doi:10.1074/jbc.R112.378877

74. Seiner DR, Hegde SS, Blanchard JS. Kinetics and inhibition of nicotinamidase from *Mycobacterium tuberculosis*. Biochemistry. 2010;49: 9613–9619. doi:10.1021/bi1011157

75. French JB, Cen Y, Vrablik TL, Xu P, Allen E, Hana-Rose W, et al. Characterization of nicotinamidases: steady-state kinetic parameters, class-wide inhibition by nicotinaldehydes and catalytic mechanism. Biochemistry. 2011;49: 10421–10439. doi:10.1021/bi1012518

76. Mei Z, Zhang X, Yi J, Huang J, He J, Tao Y. Sirtuins in metabolism, DNA repair and cancer. J Exp Clin Cancer Res. 2016;35: 1–14. doi:10.1186/s13046-016-0461-5

77. Knyphausen P, De Boor S, Kuhlmann N, Scislowski L, Extra A, Baldus L, et al. Insights into lysine deacetylation of natively folded substrate proteins by sirtuins. J Biol Chem. 2016;291: 14677–14694. doi:10.1074/jbc.M116.726307

78. Sauve AA, Schramm VL. Sir2 regulation by nicotinamide results from switching between base exchange and deacetylation chemistry. Biochemistry. 2003;42: 9249–9256. doi:10.1021/bi034959l

79. Renilla S, Bernal V, Fuhrer T, Castaño-Cerezo S, Pastor JM, Iborra JL, et al. Acetate scavenging activity in *Escherichia coli*: interplay of acetyl–CoA synthetase and the PEP–glyoxylate cycle in chemostat cultures. Appl Microbiol Biotechnol. 2012;93: 2109–2124. doi:10.1007/s00253-011-3536-4

80. Wolfe AJ. The Acetate Switch. Microbiol Mol Biol Rev. 2005;69: 12–50. doi:10.1128/MMBR.69.1.12

81. Yang T, Sauve A. NAD metabolism and sirtuins: metabolic regulation of protein deacetylation in stress and toxicity. AAPS J. 2006;8: 632–643. doi:10.1208/aapsj080472

82. Hagino Y, Lan SJ, Ng CY. Metabolism of pyridinium precursors of pyridine nucleotides in perfused rat Liver. J Biol Chem. 1968;10: 4980–4989.

83. Hoshino J, Schlüter U, Kröger H. Nicotinamide methylation and its relation to NAD synthesis in rat liver tissue culture. Biochemical basis for the physiological activities of 1-methylnicotinamide. BBA - Gen Subj. 1984;801: 250–258. doi:10.1016/0304-4165(84)90074-6

84. Smythe G a., Braga O, Brew BJ, Grant RS, Guillemin GJ, Kerr SJ, et al. Concurrent quantification of quinolinic, picolinic, and nicotinic acids using electron-capture negative-ion gas chromatography–mass spectrometry. Anal Biochem. 2002;301: 21–26. doi:10.1006/abio.2001.5490

85. Anderson RM, Bitterman KJ, Wood JG, Medvedik O, Cohen H, Lin SS, et al. Manipulation of a nuclear NAD^+ salvage pathway delays aging without altering steady-state NAD^+ levels. J Biol Chem. 2002;277: 18881–18890. doi:10.1074/jbc.M111773200

86. Anderson RM, Bitterman KJ, Wood JG, Medvedik O, Sinclair DA. Nicotinamide and PNC1 govern lifespan extension by calorie restriction in *Saccharomyces cerevisiae*. Nature. 2003;423: 181–185. doi:10.1038/nature01578

87. Wang T, Cui H, Ma N, Jiang Y. Nicotinamide-mediated inhibition of SIRT1 deacetylase is associated with the viability of cancer cells exposed to antitumor agents and apoptosis. Oncol Lett. 2013;6: 600–604. doi:10.3892/ol.2013.1400

88. Hwang ES, Song SB. Nicotinamide is an inhibitor of SIRT1 *in vitro*, but can be a stimulator

in cells. Cell Mol Life Sci. 2017; 1–16. doi:10.1007/s00018-017-2527-8

89. Baba T, Ara T, Hasegawa M, Takai Y, Okumura Y, Baba M, et al. Construction of *Escherichia coli* K-12 in-frame, single-gene knockout mutants: the Keio collection. Mol Syst Biol. 2006;2: 1–11. doi:10.1038/msb4100050

Appendix

Table S1. Strains, plasmids and primers used in this study. Restriction nuclease sites are in grey. Bold typeface indicates the modified codon during site-directed mutagenesis.

***E. coli* strain**	**Genotype**	**Source**
BW25113	*lacI* q *rrnB*T14 D*lacZ*WJ16 *hsdR*514 D(*araBAD*)AH33 D(*rhaBAD*)LD78	Keio collection [89]
BW25113 Δ*cobB*	[BW25113] *cobB:kan*	Keio collection [89]
BW25113 Δ*pncA*	[BW25113] *pncA:kan*	Keio collection [89]
BL21 (DE3)	F- ompT gal dcm lon hsdSB(rB- mB-) λ(DE3)	Agilent Technologies
BL21 (DE3) Δ*cobB*	[BL21 (DE3)] *cobB:kan*	[15]
DH10B	F- mcrA Δ(mrr-hsdRMS-mcrBC) Φ80dlacZΔM15 ΔlacX74 endA1 recA1 deoR Δ(ara,leu)7697 araD139galU galK nupG rpsL λ-	Invitrogen
Plasmid		
***acs*ASKA**	N-terminal, His_6-tag overexpression vector, Cam^R. Encodes *acs* wt.	ASKA collection [57]
***cobB*pBAD24-MBP**	C-terminal, His_6-tag-MBP overexpression vector, Kan^R. Encodes *cobB* wt.	This study
***pncA*pRSETA**	N-terminal, His6-tag overexpression vector, Amp^R. Encodes *pncA* wt.	This study
pBAD24cobB	Expression vector Amp^R. Encodes *pncA* wt.	This study
pBAD24pncA	Expression vector Amp^R. Encodes *pncA* wt.	This study
Primers	**Sequence**	
***cobB*pBAD24-MBP cloning Fwd**	GGTGGTGAATTCATGCTGTCGCGTCGGGGT	
***cobB*pBAD24-MBP cloning Rev**	GGTGGTCTCGAGTCAGGCAATGCTTCCCGCT	
***pncA*pRSETA cloning Fwd**	GGTGGTCTCGAGATGCCCCCTCGCGCGCCCTG	
***pncA*pRSETA cloning Rev**	GGTGGTAAGCTTTTACCCCTGTGTCTCTTCCC	
***acs*K609AASKA mutagenesis Fwd**	CTAAAACCCGCTCCGGC**GCA**ATTATGCGCCGTATTC	
***acs*K609AASKA mutagenesis Rev**	GAATACGGCGCATAATT**GCG**CCGGAGCGGGTTTTAG	
cobBpBAD24 cloning Fwd	GGTGGTGAATTCATGCTGTCGCGTCGGGGT	
cobBpBAD24 cloning Rev	GGTGGTAAGCTTTCAGGCAATGCTTCCCGCT	
pncApBAD24 cloning Fwd	GGTGGTGAATTCATGCCCCCTCGCGCCCT	
pncApBAD24 cloning Rev	GGTGGTAAGCTTTTACCCCTGTGTCTCTTCCC	

CHAPTER 6

Characterization of acetyl-CoA synthetase kinetics and ATP-binding

Abstract

The superfamily of adenylating enzymes is a large family of enzymes broadly distributed from bacteria to humans. They catalyse carboxylate activation in two steps involving a large change in protein conformation. Acetyl-CoA synthetase (Acs), member of this family, is a metabolic enzyme with an essential role in *Escherichia coli* (*E. coli*) acetate metabolism, whose catalytic activity is regulated by acetylation/deacetylation *in vivo*. In this chapter, the kinetics and thermodynamic parameters of deacetylated and acetylated Acs are studied for the adenylating step. Moreover, the role of the T264, K270, D500 and K609 residues in catalysis and ATP-binding is also determined, the results showing that Acs wt *E. coli* enzyme binds ATP in an endothermic way. The dissociation constant has been determined and ATP-binding showed no significant differences between acetylated and deacetylated enzyme, although K_{cat} was much higher for the deacetylated enzyme. However, K609 lysine mutation resulted in an increase in ATP-Acs-affinity and in a total loss of enzymatic activity, while T264 and D500 mutant proteins showed a total loss of ATP-binding ability and a decrease in catalytic activity. The results presented in this chapter demonstrate the importance of the studied residues in Acs ATP-binding and represent an advance in our understanding of the adenylation step of the superfamily of adenylating enzymes.

Introduction

The ANL superfamily of adenylating enzymes contains acyl- and aryl-CoA synthetases, firefly luciferase, and the adenylation domains of the modular non-ribosomal peptide synthetases (NRPSs). ANL enzymes are broadly distributed in prokaryotes and eukaryotes and share a sequence identity of ~ 20 %. Although ANL enzymes show differences in their respective catalytic mechanisms, all of them are structurally homologous and share a global mechanism of two-step catalysis: a first adenylation reaction and a diverse set of second partial reactions [1]. Acyl- and aryl-CoA synthetases catalyse the activation of a wide variety of carboxylates into the acyl- aryl-CoA derivatives in two independent reactions, as was described in 1956 by Paul Berg [2]. In the first one the carboxylate is activated into a carboxyl-AMP intermediate. In the second reaction a CoA molecule reacts with the adenylate intermediate to lead to the acyl- aryl-CoA and AMP. Carboxylic substrates can vary from acetate (2C) to long fatty acids such as myristic acid (14C). Acyl-CoA formation has been widely studied for 60 years [2] and a ping-pong kinetic mechanism has been established for many of these synthetases [3–7] (Figure 1).

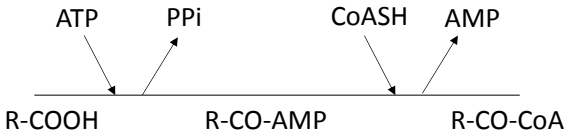

Figure 1. Acyl- and aryl-CoA synthetases ping-pong mechanism.

The structure of the ANL superfamily of adenylating enzymes is formed by a long non-catalytic N-terminal domain and a short C-terminal domain containing the main catalytic residues. The substrates are positioned at the interface of the two domains. A structural characteristic of ANL enzymes shows that they adopt different conformations due to their flexibility. Two main conformations have been well established for several ANL enzymes: an adenylating or closed conformation to carry out the first catalytic reaction and a second open conformation (called thioester-forming conformation for acyl-CoA synthases) to carry out the final catalytic step. To achieve the second conformation a ~ 140 ° rotation of the C-terminal domain is necessary [1]. Moreover, members of ANL superfamily contain ten highly sequence-conserved motifs (A1-A10). Several conserved residues have been shown to be involved in ATP-binding in the structures crystalized in the presence of ATP [8–16]. The ATP-binding residues include some invariant amino acids such as an aspartic (A7 domain), an arginine (A8 domain), a lysine (A10 domain) and a conserved phosphate-binding sequence known as phosphate binding loop (P-loop) (S/T)(S/T/G)G(S/T)TGxPK (A3 domain). Thus, the invariant aspartic acid has been found to interact through hydrogen bonds with the ATP ribose molecule [9,11,14,16], and the arginine with the β-phosphate of the PPi [8–11,14]. Some ATP pyrophosphate atoms have been observed interacting with the catalytic essential lysine of the A10 domain and with several residues of the P-loop sequence. However, although it is clear that the P-loop residues surround the beta and gamma phosphates of pyrophosphate, the A10 conserved lysine interactions have been not completely established [8–13,15,16].

Acs is an important metabolic enzyme in prokaryote and eukaryote organisms, whose physiological role is to activate acetate to acetyl-CoA to be used in several metabolic routes. Moreover, prokaryotic organisms, such as *E. coli* bacterium, can consume acetate from the environment as carbon source. *E. coli* is able to take up extracellular acetate to acetyl-CoA by two independent routes, one of these routes being catalysed by the enzyme Acs [17,18]. Acyl-CoA synthetase post-translational regulation by reversible lysine acetylation has been studied for Acs and other AMP-forming synthetases [19–24]. Acetylation of the A10 domain invariant

lysine (K609 in *E. coli* Acs) total or partially inhibits the catalytic activity of these enzymes, which can be recovered when a sirtuin deacetylase deacetyles this lysine. Moreover, the acetylation of this lysine only affects the first partial reaction (adenylation) but not the second step [25,26].

In this study, Acs kinetics and thermodynamic parameters for ATP-binding are described. Due to the lack of an Acs crystal structure in the adenylating conformation, one model was predicted using ANL enzyme structures determined in this conformation as templates. From the Acs model, four single amino acids were selected to study their role in catalysis and ATP-binding: T264, K270, D500 and K609. The results point to the important role of these residues in catalytic ability and ATP-binding of *E. coli* Acs enzyme.

Methods

Plasmids construction

To overexpress Acs protein, the corresponding ASKA plasmid was used (ASKA*acs*) [27]. Overexpression plasmids of the single amino acid mutant proteins Acs T264A, K270A, D500A and K609A (selected residues were changed to alanine) were obtained by site-directed mutagenesis from ASKA*acs* plasmid. To purify CobB deacetylase protein, *cobB* gen of *E. coli* BW25113 was PCR-amplified and cloned into pBAD24-MBP [28]. All molecular biology enzymes used were purchased from Thermo Fisher Scientific. The strains, plasmids and primers used are listed in Appendix Table S1.

Protein overexpression and purification

Chemically competent *E. coli* BL21 (DE3) strains were transformed by heat shock at 42 °C with overexpression plasmids. Cultures were grown overnight at 30 °C with orbital shaking (200 rpm). The culture medium was Luria-Bertani broth (LB) (10 g L^{-1} tryptone, 5 g L^{-1} yeast extract and 5 g L^{-1} NaCl). Expression was induced with 0.1 mM Isopropyl β-D-1-thiogalactopyranoside (IPTG) when the culture optical density at 600 nm (OD_{600}) reached 0.5-0.6. Cell pellets were harvested by centrifugation (20 min; 6000 x g) and resuspended in binding buffer (50 mM potassium phosphate, 500 mM NaCl, 25 mM imidazole, pH 8). Cells were disrupted by three passages of the crude extract through a French pressure cell system at 20,000 psi. Following the removal of cell debris by centrifugation at 18000 x g for 30 min at 4 °C, the supernatant was applied onto a Ni (II)-loaded 5 mL His-Trap HP column (GE Heathcare) previously equilibrated in binding buffer. Protein was eluted using a linear gradient of imidazole from 0 to 500 mM at a

flow rate of 5 mL min^{-1}. The protein buffer was then changed to buffer A (Tris-HCl 50 mM, dithiothreitol (DTT) 2 mM, pH 7.4) using a HiPrep™ 26/10 desalting column (GE Heathcare) at a flow rate of 5 mL min^{-1}. CobB sirtuin was purified using an amylose resin (New England Biolabs) following a previously reported protocol [28].

Protein deacetylation

Selected proteins were deacetylated with CobB sirtuin. The reactions were carried out with a 1:50 ratio (Acs:CobB) in the presence of 2 mM NAD^+ at 30 °C for 8 hours [28]. To separate Acs and CobB proteins, reactions were loaded onto a 5 ml Hi-trap Q HP (GE Heathcare) column anionic exchange column, at a flow rate of 5 mL min^{-1} previously equilibrated with the same buffer A. A step gradient procedure was used to separate the proteins with increasing ionic strength from 0 to 1 M of NaCl. The final Acs fractions (acetylated and deacetylated) were then concentrated and further purified using a Superdex 75 10/300 GL gel filtration column (GE Heathcare) equilibrated with buffer B (Tris-HCl 100 mM, NaCl 150 mM, TCEP 1 mM, $MgCl_2$ 3 mM, pH 7.4) at a flow rate of 0.5 mL min^{-1}. Proteins were stored at -80 °C until use. Finally, Spin-X UF concentrators (Corning) were used to concentrate the proteins.

Circular dichroism

Circular dichroism spectroscopy (CD) was performed on a PiStar-180 spectrophotometer (Applied Photophysics, U.K.) equipped with a N_2 purge and a Peltier system for temperature control. Far-UV CD spectra (190-240 nm) were obtained at 20 °C from protein samples (0.15 mg mL^{-1}) in 50 mM potassium phosphate buffer pH 7.4 containing NaCl (20 mM). The spectra were obtained in a 0.1 cm path length cuvette every 1 nm. Data were converted to molar ellipticity units by using the mean residue mass of 110.40 kDa.

Kinetics characterization

The acetyl-CoA synthetase assay was based on the coupled assay reported by Williamson and Corkey [29]. AMP production was detected *via* a coupled enzyme assay in which myokinase (MK), pyruvate kinase (PK) and lactate dehydrogenase (LDH) couple AMP production to NADH oxidation. Standard acetyl-CoA synthetase assays (0.2 mL) were performed at 37 °C in 50 mM potassium phosphate buffer at pH 7.5 containing 3.0 mM PEP (phosphoenolpyruvate), 5 units MK, 1 unit PK, 1.5 units LDH, 5 mM MgCl2, 2.5 mM ATP, 1.5 mM CoA, 0.1 mM NADH, 5 mM acetate and 1 mM DTT.The reaction was started by the addition of Acs. All reactions were performed in triplicate. Specific activity was calculated using the extinction coefficient of NADH

(6.22 mM^{-1} cm^{-1}) and was based on the oxidation of two molecules of NADH for each AMP molecule released. One unit of Acs activity is defined as 1 µmole of acetyl-CoA formed per minute at pH 7.5 and 37 °C. Acs inhibition asays were carried out employing a pyrophosphate detection kit (Sigma Aldrich) following the commercial protocol.

Isothemal titration calorimetry assays

To study binding affinities between Acs proteins and ATP, isothemal titration calorimetry (ITC) assays were carried out using an ITC200 micro-calorimeter (MicroCal). The protein concentration was fixed at 70 µM, while the ligand concentration in the titration procedure was adjusted to 800 µM. Titrations were performed at 25 °C and consisted of 30 10-µL injections, separated by 3 min, into a 2 ml sample cell containing the protein. Data were fitted to a one-binding-site model using Origin 7.0 (MicroCal). Each binding isotherm was measured in duplicate, and values for thermodynamic parameters were averaged. The Gibbs free energy change (ΔG) was calculated using the equation $\Delta G = -RT \ln(Ka)$ where T = 298 K.

Results

Acs structural model prediction

To ascertain the 3D disposition of the residues involved in the adenylating step of the *E. coli* Acs reaction a structural model was predicted using SWISS-MODEL software [30]. Nine ANL enzymes, which had been previously crystalized in the adenylating conformation, were used as templates to generate the models. The resultant quality parameters of the nine predicted models are summarized in Appendix Table S2. From the QMEAN values [31], two models were selected, which were based on medium chain acyl-CoA synthetase from human mitochondria (PDB code: 3c5e) [8] and 4-coumarate:CoA ligase from *Nicotiana tabacum* (PDB code: 5bsm) templates [13]. The models were named model 1 and 2, respectively (Figure 2). Models showed a z-score QMEAN of -2.45 and -2.71, respectively. Interestingly, the models corresponded to a monomeric and a dimeric Acs protein state. Models were compared with templates through structures alignment. The structures were essentially identical (Figure 2A2 and 2B2) and conserved lysines from A10 motif were located at the same positions (Figure 2A3 and 2B3).

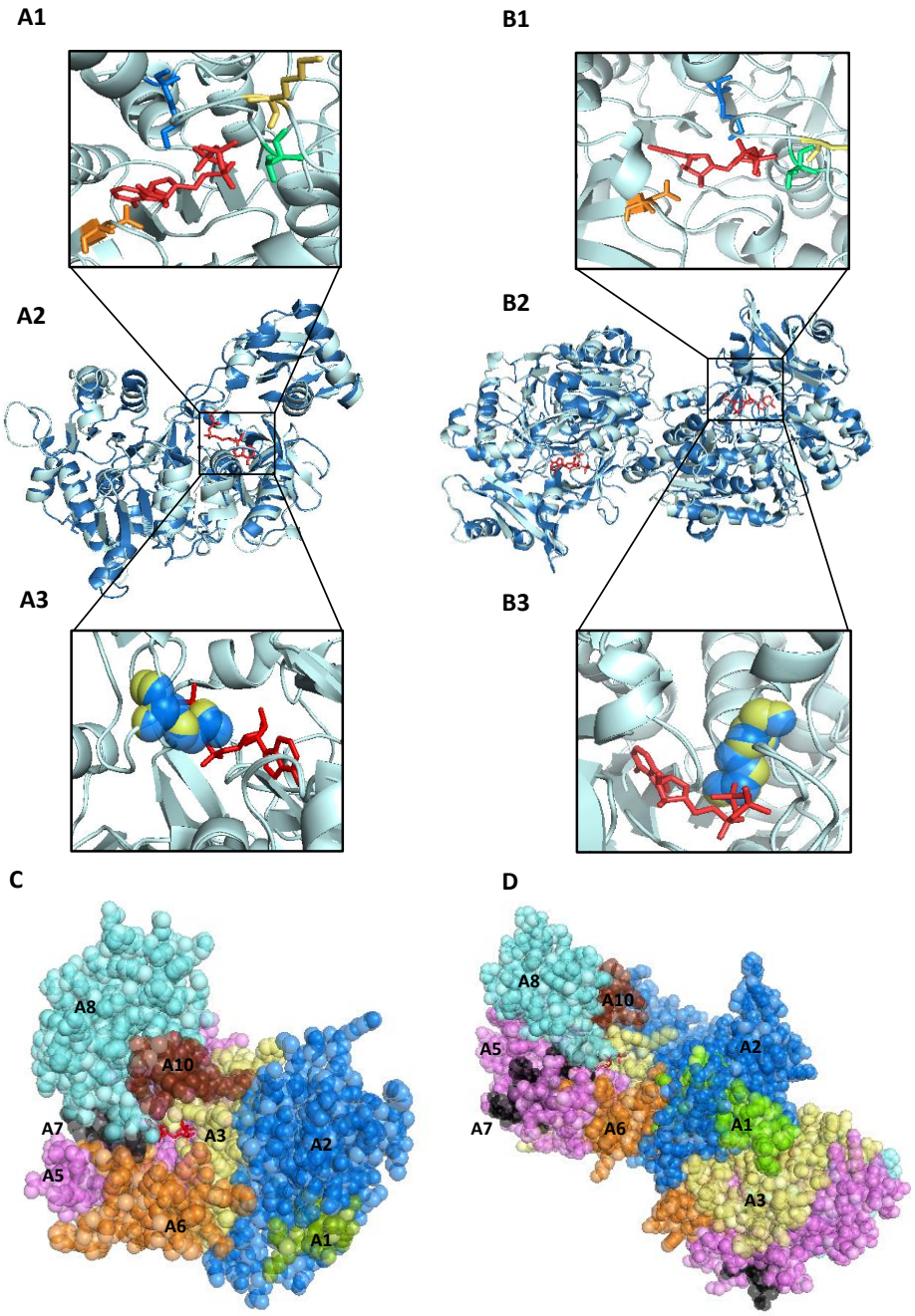

Figure 2. *E. coli* Acs models. **(A)** Model 1 (generated using medium chain acyl-CoA synthetase from human mitochondria): (A1) Selected residues (K609 in blue, T264 in green, K270 in yellow, and D500 in orange) surrounding ATP (red) ligand; (A2) Model 1 (light blue) aligned with target structure (dark blue): (A3) Conserved A10 lysines K609 from model (blue) and K557 from target (yellow) and ATP ligand (red). **(B)** Model 2 (generated using 4-coumarate:CoA ligase from *Nicotiana tabacum* as target template): (B1) Selected residues (K609 in blue, T264 in green, K270 in yellow and D500 in orange) surrounding ATP (red) ligand; (B2) Model 2 (light blue) aligned with target structure (dark blue); (B3) Conserved A10 lysines K609 from model (blue) and K526 from template (yellow) and ATP ligand (red). **(C)** Conserved motifs A1-A10 from model 1 (ATP ligand is in red). **(D)** Conserved motifs A1-A10 from model 2 (ATP ligand is in red). Figure was made using PyMOL Molecular Graphics System, Version 2.0 Schrödinger, LLC.

In order to compare the *E. coli* Acs protein sequence with other ANL enzymes sequences, a protein alignment was carried out. The *E. coli* Acs sequence was aligned with Acs from *Salmonella entrica* (*S. enterica*), medium chain acyl-CoA synthetase from human mitochondria, 2-succinylbenzoate-CoA ligase (MenE) from *Bacillus subtilis* (*B. subtilis*), D-alanyl carrier protein ligase (DltA) from and *Bacillus cereus* (*B. cereus*) 4-chloro benzoyl-CoA ligase (4CBCL) from *Alcaligenes faecalis* (*A. faecalis*) sequences (Figure 3). Identity percentages were 95 %, 25 %, 23 %, 37 % and 21 %, respectively. From protein alignment and 3D models, four residues were selected from the Acs *E. coli* sequence to study their role in Acs catalytic mechanism: threonine 264 (T264) and lysine 270 (K270) from A3 motif P-loop, aspartic acid 500 (D500) from A7 motif and lysine 609 (K609) from A10 motif. Figure 3 shows the protein alignment carried out with the selected residues in yellow. All residues were surrounding ATP ligand in the predicted Acs models as is shown in Figure 2A and 2B.

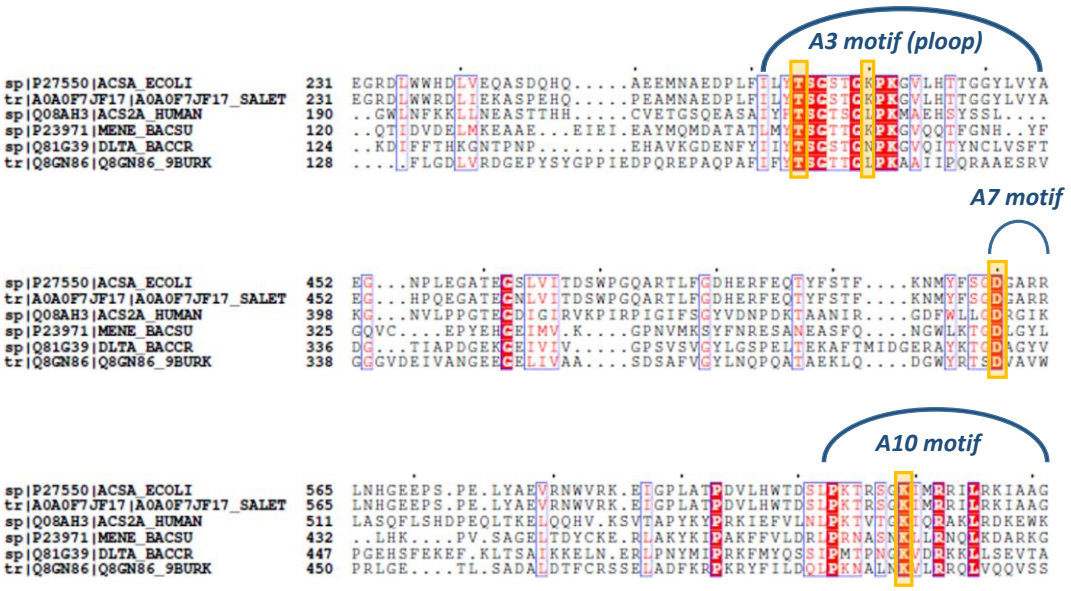

Figure 3. Protein alignment. Conserved residues (red) and selected residues to single substitutions (yellow box) are shown.

The single amino acid substitutions do not affect the Acs conformational structure

To study Acs wt and mutant proteins, all of them were deacetylated *in vitro* by CobB after purification, excepting acetylated Acs wt protein (ac. wt). Purified and deacetylated proteins were analysed by CD in order to investigate the effect of the substitutions and acetylation on the conformation of Acs. As shown in Figure 4, the observed spectra were very similar to the Acs wt spectrum, which indicated the absence of major structural changes. The α-helical content

was also determined through 222 nm values and the results are shown in Table 1 [32]. The percentage of α-helical varied from 12.2 to 15.2 %, again suggesting that the Acs structure was not affected by the analysed mutations.

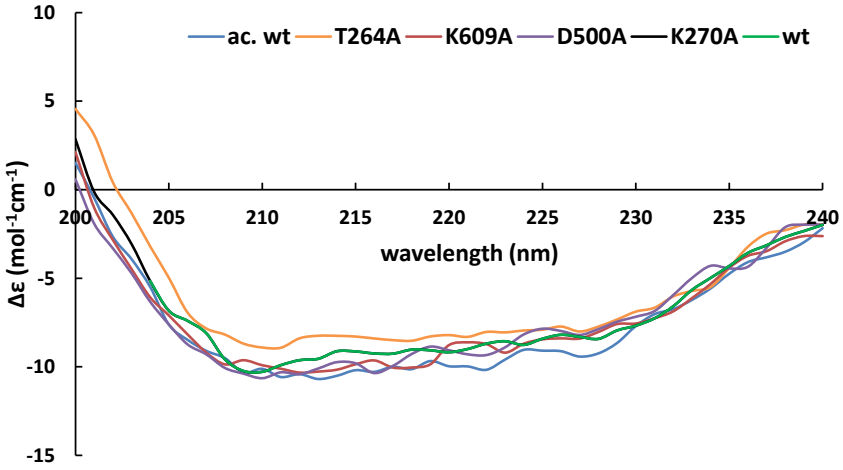

Figure 4. Conformational Acs characterization. Far UV spectra of Acs wt and mutant proteins.

Table 2. α-helical content of Acs proteins.

	wt	ac. wt	T264	K270	D500	K609
Helical content (%)	13.4	13.1	12.2	13.1	13.8	12.2

The single amino acid substitutions result in substantial Acs activity changes

To study Acs wt kinetics and how the mutations affected them, kinetics characterization was carried out for ATP and acetate substrates. Michaelis-Menten behaviors were observed for all the proteins and substrates. The kinetic graphs are shown in Figure 5 and kinetic parameters are summarized in Table 3.

Acs wt kinetics showed a K_M value of 73 and 35 µM for ATP and acetate, respectively. Moreover acetylation did not affect to the K_M values (76.32 and 41 µM for ac. wt). However K_{cat} were strongly affected by acetylation. Thus, Acs wt showed K_{cat} values of 6955.55 and 4622.00 min^{-1} for ATP and acetate, respectively, while for ac. wt the observed values were 52.23 and 38.26 min^{-1}. As regards mutant kinetic parameters, the results showed that T246A and D500A mutations affected strongly to Acs activity. The K_M and K_{cat} for both of the substrates studied were much lower than those for Acs wt. Thus, specificity constants (K_{cat}/K_M) for T264A mutant

showed a 35.68 and 42.87 fold decrease for ATP and acetate substrates, respectively, while K_{cat}/K_M D500A mutant protein showed a 3176.73 and 24915.09 fold decrease for ATP and acetate, respectively. Surprisingly, a great increase in Acs catalytic constants was observed for protein with the residue K270 mutated. Thus, while K_M values were very similar to Acs wt, K_{cat} values were much higher. K_{cat} was 8.16 times higher for ATP and 6.36 times higher for acetate substrate. Finally K609A mutant protein did not show any activity.

Table 3. Kinetic parameters for Acs and mutant proteins with ATP and acetate as substrates.

	wt	**ac. wt**	**T264**	**K270**	**D500**	**K609**
K_M ATP (µM)	73.00 ± 8	76.32 ± 10.12	336.00 ± 52	65.25 ± 3.2	270.00 ± 13	Inactive
K_{cat} ATP (min^{-1})	6955.55 ±820	52.23 ± 6.5	900.25 ± 82	56768.96 ± 1536	8.20 ± 0.35	Inactive
K_M acetate (µM)	35.00 ± 2	41.00 ± 2.35	351.42 ± 16	25.00 ± 1.5	1600 ± 82	Inactive
K_{cat} acetate (min^{-1})	4622.00 ± 582	38.26 ± 5.69	1083.06 ± 52	29437.93 ±1253	8.58 ± 0.35	Inactive
K_{cat}/K_M ATP (min^{-1} μM^{-1})	95.28	0.68	2.67	870.02	0.03	Inactive
K_{cat}/K_M acetate (min^{-1} μM^{-1})	132.05	0.93	3.08	1177.52	0.0053	Inactive

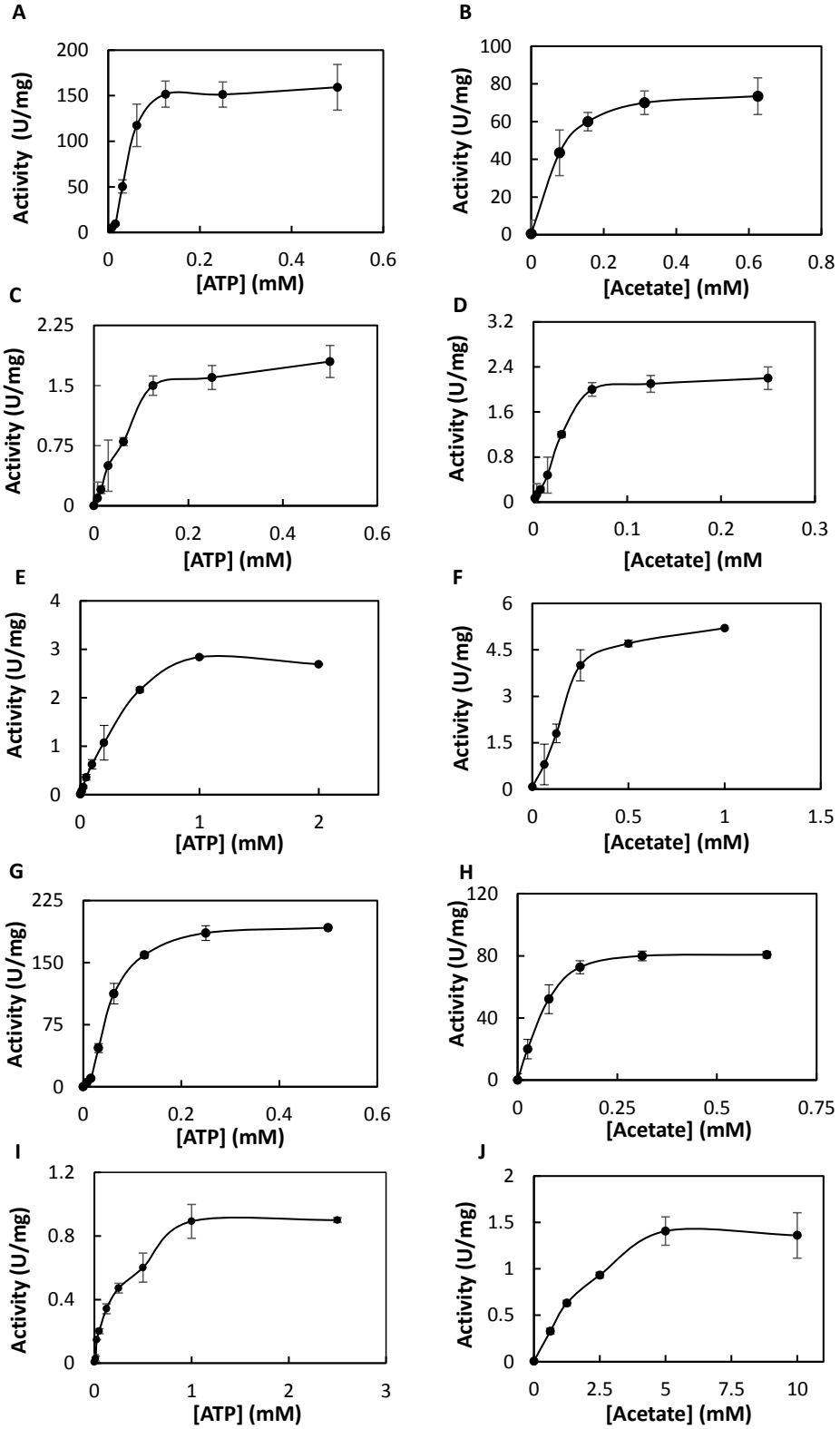

Figure 5. Substrate saturation curve of the Acs wt protein **(A)**, ac. Acs wt protein **(C)**, Acs T264A mutant protein **(E)**, Acs K270A mutant protein **(G)** and Acs D500A mutant protein **(I)** at different concentrations of ATP. Substrate saturation curve of the Acs wt protein **(B)**, ac. Acs wt protein **(D)**, Acs T264A mutant protein **(F)**, Acs K270A mutant protein **(H)** and Acs D500A mutant protein **(J)** at different concentrations of acetate.

The single amino acid substitutions result in Acs substantial ATP-binding changes

In order to study the ATP-binding parameters for Acs wt and to know whether acetylation affected it, thermodynamic assays were performed using purified Acs without CobB incubation (acetylated) and after CobB incubation (deacetylated). No-binding was observed when acetate was titrated into a sample cell containing Acs alone. This suggests that Acs binds ATP before binding its organic acid substrate. Final Acs wt ATP titrations are shown in Figure 6.

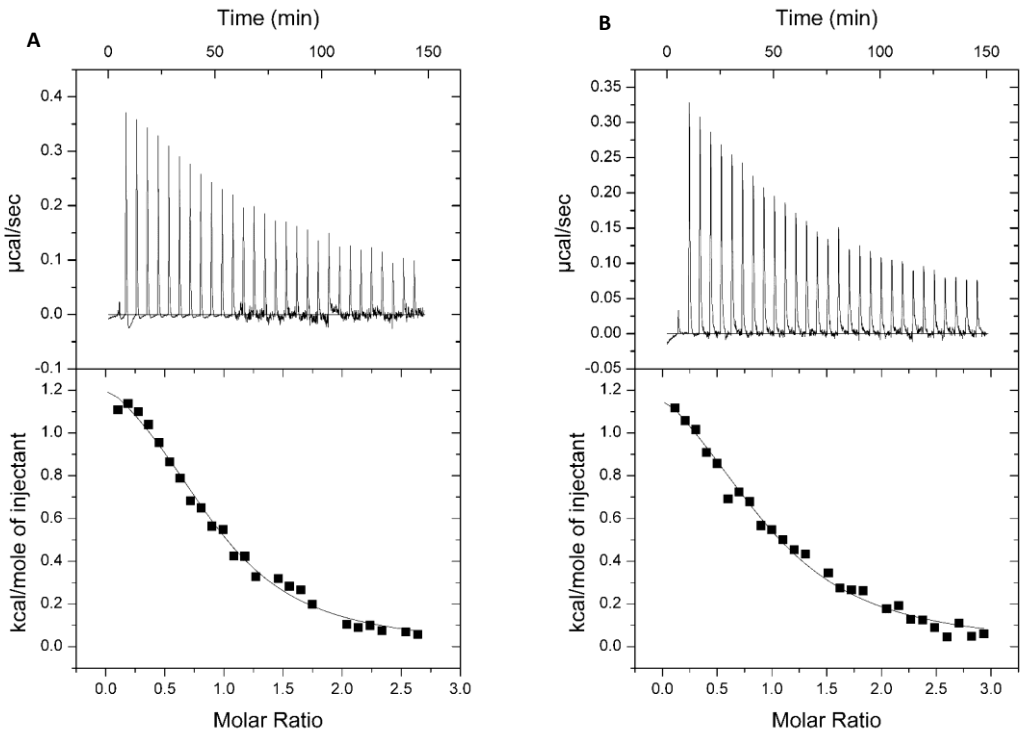

Figure 6. Isothermal titration calorimetry studies for Acs wt. A plot of energy transfer rate as a function of molar ratio (top panels) and integrated data after subtraction of the heat of dilution (bottom panels) of ATP-binding to Acs wt **(A)** and ac. Acs wt **(B)** is shown. The solid lines represent the best-fit curves to the data, using a one-site binding model.

Acs showed an endothermic ATP-binding for both acetylated and deacetylated proteins. Each ATP injection produced an endothermic heat of reaction which decreased in magnitude with subsequent injections. Acs ATP-binding showed positive enthalpy, ΔH, which reflects disruptions of the energetically favourable non-covalent interactions. Thus, ATP-binding was purely entropy-driven, ΔS. Binding stoichiometry was close to 1 (n ≈ 1) for acetylated and deacetylated Acs. The dissociation constant (Kd), ΔH and ΔS showed very similar values for both of the proteins. Thus, the Kd determined for deacetylated Acs was 14.1 µM and 17.7 µM for the

acetylated protein. Thermodynamic parameters extracted from ITC assays are summarized in Table 4.

Table 4. Thermodynamic parameters of ATP-binding for Acs wt and mutant proteins. ΔH: enthalpy change, ΔS: entropy change, ΔG: Gibbs free energy change, Ka: binding constant, n: number of sites, Kd: dissociation constant.

Protein	ΔH (cal mol^{-1})	ΔS (cal mol^{-1} K^{-1})	ΔG (cal mol^{-1})	Ka (M^{-1})	n	Kd (μm)
wt	1617 ± 235	27.6 ± 2.30	-6469.82	70850 ± 17672	0.96	14.1
ac. wt	1248 ± 165	25.8 ± 1.27	-6310.95	56550 ± 30471	0.92	17.7
K609A	3828 ± 321	37.2 ± 0.14	-7071.12	235000 ± 12560	0.85	4.2
D500A	-	-	-	-	-	-
T264A	-	-	-	-	-	-
K270A	533 ± 28	24.1 ± 0.28	-6527.56	74750 ± 7424	1.22	13.3

As regards mutant proteins ATP-binding, endothermic ligand bindings were also observed, but significant differences existed. Final mutant titrations are shown in Figure 7. Acs K609A mutant showed the tightest binding, with a Kd = 4.2 μM. Moreover, K609A mutant showed the highest value of ΔH. Acs K270A mutant showed the lowest value of ΔH, and a Kd very similar to Acs wt proteins (13.3 μM). Finally, Acs D500A and T264A mutant proteins did not show any ATP-binging under the assayed conditions. Thermodynamic mutant parameters are summarized in Table 4. Figure 8 shows kcal/mole of injectant *versus* molar ratio of ligand/protein for all titrations.

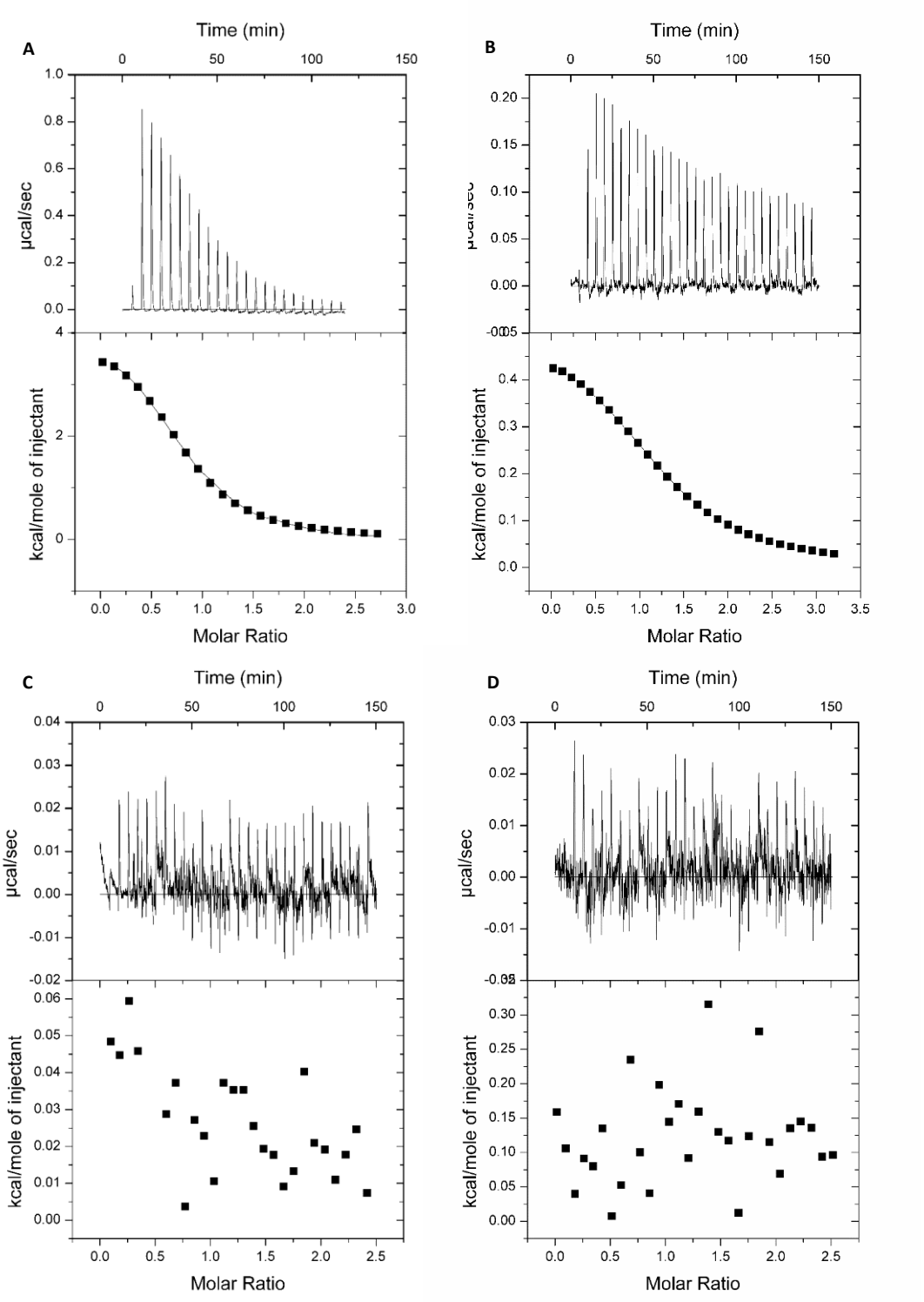

Figure 7. Isothermal titration calorimetry studies for Acs mutant proteins. A plot of energy transfer rate as a function of molar ratio (top panels) and integrated data after subtraction of the heat of dilution (bottom panels) of ATP-binding to Acs K609A **(A)**, K270A **(B),** D500A **(C)** and T264A **(D)** mutant Acs proteins is shown. The solid lines represent the best-fit curves to the data, using a one-site binding model.

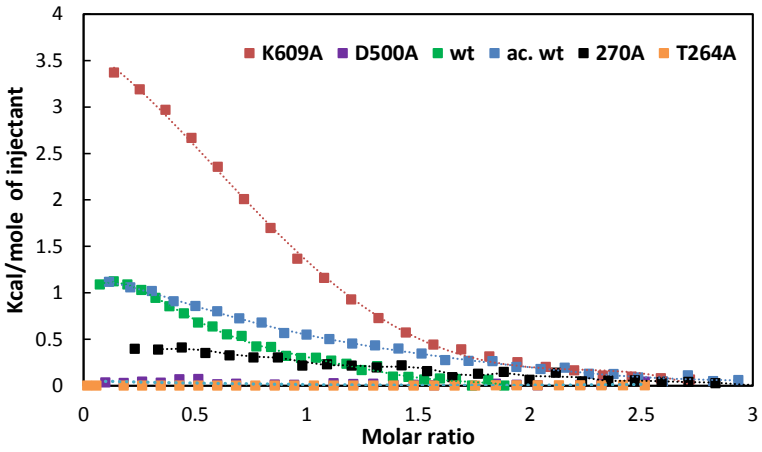

Figure 8. Isothermal titration calorimetry studies for Acs wt and mutant proteins.

Acs is competitively inhibited by cAMP

S. enterica Acs inhibition by cAMP has been recently reported [33]. In order to know if *E. coli* Acs was also inhibited by cAMP and AMP, single reactions were carried out at 1 mM cAMP or AMP concentrations. Acs inhibition by cAMP was observed, but no inhibition was observed when AMP was present (Figure 9D). To study *E. coli* Acs inhibition by cAMP, a kinetic characterization was carried out. To determine the inhibition constant (Ki), apparent K_M were determined at different cAMP concentrations from 0 to 1 mM (0, 50, 500 and 1000 µM) and apparent K_M were plotted *versus* inhibitor concentration (Figure 9A). The calculated value of Ki was approximately 232 µM. To complete the inhibition study, a double-reciprocal plot (1/v *versus* 1 / [ATP]) at different cAMP concentrations was carried out (Figure 9B). These plots suggested that the activity of the Acs is inhibited by cAMP through a competitive inhibition mechanism, as was previously described for *S. enterica* Acs [33].

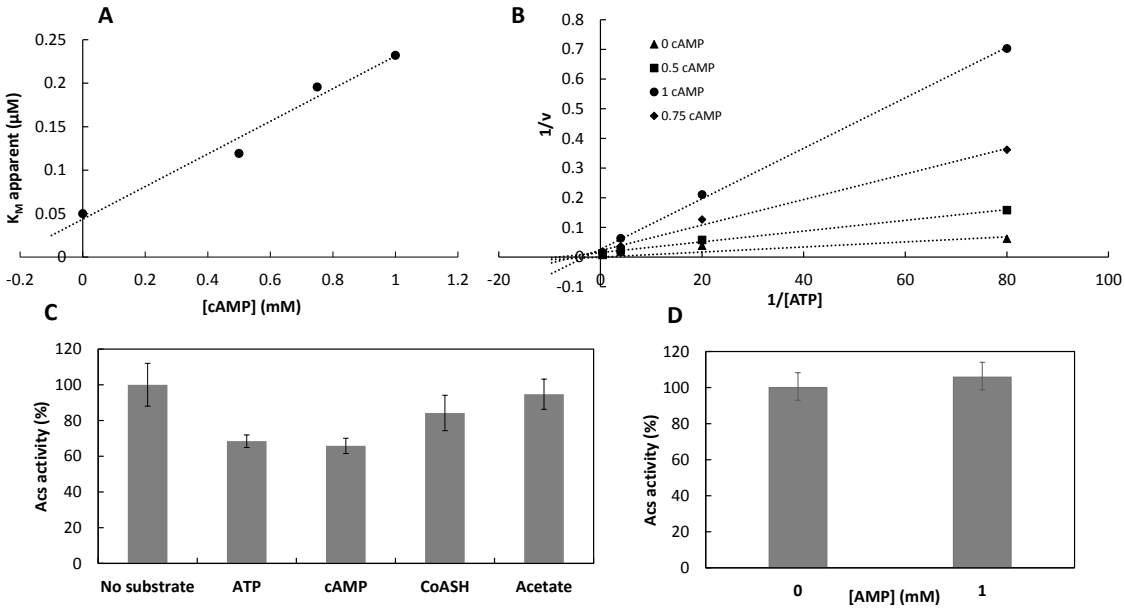

Figure 9. Analysis of Acs inhibition by cAMP. **(A)** Acs apparent K_M at different cAMP concentrations. **(B)** Double-reciprocal plot (1/v *versus* 1/ ATP]) of Acs activity at different cAMP concentrations: 0 (▲), 0.5 (■), 0.75(♦) and 1 (•) µM. **(C)** Acs activity (%) after CobB deacetylation in the absence or in the present of ATP, cAMP, CoA or acetate. **(D)** Acs activity (%) in the absence and in the presence of AMP 1mM. Presented data are average of triplicates. Standard deviations were always less than 10%.

To ascertain whether the presence of substrates or cAMP inhibitor affected Acs deacetylation by CobB, as has been described for *S. enterica* Acs, deacetylation assays using acetylated Acs as substrate were carried out in the presence of 1 mM ATP, cAMP, CoA or acetate. Acs activity was measured after deacetylation, and the activity was compared with a control assay (no substrate or inhibitor added). Results are shown in Figure 9C. Data suggest that Acs CobB-dependent deacetylation is partially inhibited in the presence of ATP and cAMP, although it is not affected by the presence of acetate or CoA.

Discussion

ANL enzymes belong to a diverse superfamily of proteins with a great importance in the metabolism from bacteria to humans. Acs protein has a principal role in *E. coli* acetate metabolism, catalysing one of the acetate uptake pathways. Moreover, *E. coli* is the most used microorganism in biotechnology, while acetate excretion is a big challenge for researchers, since extracellular acetate limits growth rates and bioprocess yields [34,35]. In this way, increasing our understanding of the acetate metabolism is essential to optimize the biotechnological systems based on *E. coli* metabolism.

ANL dynamic conformation is an atypical characteristic of this family of enzymes. Several ANL enzymes have been resolved in the thioester-forming or open conformation [36–41], but less information is available about the adenylating or closed conformation. To our knowledge, only nine proteins have been crystalized in this conformation [8–16]. In this study we decided to use these structures as templates to predict nine models of *E. coli* Acs protein in the closed conformation. The least z-score models were selected to further study Acs protein. The models were aligned with template structures and identical positions were located. Previous ANL studies and models allowed us to select four residues which were located surrounding the ATP substrate (Figure 2A1 and 2A2), two of them (T264 and K270) belonging to P-loop from A3 motif, which has a similar sequence than those from ATPases and GTPases [42] and has been found wrapping ATP pyrophosphate in several ANL structures [8–11,13,14]. Aspartic acid 500 is a 100% conserved ANL residue from the A7 motif involved in ATP-binding through ribose sugar moiety [9,11,14,16] and finally, lysine 609, the first lysine from the A10 motif is involved in adenylating catalytic step. Conserved A10 lysine has been observed in several crystal structures interacting with ATP substrate, although the interaction points are not entirely clear. Structures have been resolved with conserved lysine making hydrogen-binding contact with the α-phosphate of the ATP [11,13,16,43,44], with the β-phosphate [8,9] or with both of them [10]; even no-interaction has been observed [14]. This residue plays an essential catalytic role in adenylating reactions as was reported for propionyl-CoA synthetase from *S. enterica* for the first time [26]. The role of the conserved lysine from A10 motif has been widely studied for several ANL enzymes showing a great decrease or a null activity when this residue is mutated [7,13,25,28,41,45–47]. Moreover the acetylation of the A10 conserved lysine has been described as a regulator mechanism in many ANL enzymes [19,21,38,48,49]. Thus, in *E. coli*, Acs activity is regulated *in vivo* by acetylation/deacetylation, which constitutes an acetate metabolism regulation system [28,50]. *E. coli* Acs is acetylated by PatZ acetyltransferase (also known as Pka or YfiQ) in several lysines, although, to date, K609 is the only one responsible for Acs activity regulation. K609 acetylation induces Acs inhibition [24], which is reversed by CobB sirtuin [28]. In this study Acs kinetics were determined for the Acs wt enzyme and for the single amino acid selected mutants. As regards Acs wt kinetic parameters, K_M values were similar to those reported for other ANL enzymes, which are in the range of 20-100 μM. However, K_{cat} values were much higher than those previously reported. To our knowledge, ANL K_{cat} determined to date are between 10-2000 min^{-1}, whereas *E. coli* Acs wt K_{cat} determined in this study were 6955 and 4622 min^{-1} for ATP and acetate, respectively [6,9,12,13,15,16,26,41,45,51]. These high values could be due to protein

deacetylation after purification. Ac. Acs kinetic parameters showed that acetylation does not affect enzyme specificity (K_M), but activity (K_{cat}) was greatly reduced. This result suggests that acetylation decreases the amount of active enzyme through enzyme inhibition, although it does not affect substrates specificity. Acs deacetylation increased K_{cat} values more than a 100 fold. From these results, we conclude that protein deacetylation is essential to study correctly Acs activity and single amino acids substitutions, although, to our knowledge, this is the first kinetic study of an ANL enzyme previously deacetylated to ensure that all the protein is catalytically active.

The kinetic parameters of mutant proteins showed several differences with respect to Acs wt parameters. Acs D500A protein showed a 3.69 and 45-fold increase for ATP and acetate K_M, respectively, which indicated that this residue plays an important role in Acs substrates specificity. K_{cat} also showed a great decrease with respect to Acs wt parameters. The catalytic response of an ANL enzyme to this conserved aspartic acid mutation has been previously reported. Thus, a 75-fold and 500-fold increase in the K_M values for ATP were observed for DltA enzyme from *B. cereus* and 4CBCL from *A. faecalis,* respectively, when this residue was mutated [7,9]. The kinetic parameters of Acs T264A and K270A mutants from P-loop motif were also determined. T264 replacement by alanine induced an important change in Acs catalytic response. K_M values were 4.6 and 10 times higher than native values for ATP and acetate, respectively. A decrease in K_{cat} values was also observed. The catalytic role of T264 (first residue in P-loop) has previously been studied and similar catalytic effects were described [7,11]. K_M values for K270A mutant were very similar to those observed for native Acs; however K_{cat} values were much different. K270A mutant showed a surprising increase in the K_{cat} constants (almost 10-fold). To our knowledge, the catalytic role of this residue has not been studied to date.

The ITC results showed an endothermic ATP-binding for all the proteins assayed. ITC data allow ΔG of a binding to be determined from the ΔH and ΔS components, thus revealing the overall nature of the forces that drive the binding interaction. ΔH is a measure of the total energy of a thermodynamic system and is negative and positive in the exothermic and the endothermic processes, respectively. Thereby, ΔS is a global thermodynamic property of a system and its positive and negative signs indicates the overall increase or decrease in degrees of the freedom of the system. The protein–ligand binding processes will be driven by the decrease in the total ΔG free energy of the system [52]. In this way, ΔG was determined for all the binding assays carried out and a decrease was observed in all cases (Table 3).

Acs wt and ac. wt proteins showed very similar thermodynamic parameters, which suggests that *in vivo* Acs acetylation does not affect ATP-binding. The obtained values of Kd were 14.1 and 17.7 μM for wt and ac. wt protein, respectively. These values are similar to those determined for the *Rhodopseudomonas palustris* (*R. palustris*) malonyl-CoA synthetase (MatB) protein (5.6 μM) [12] and *Mycobacterium smegtatis* (*M. smegtatis*) FadD32 protein (35 μM) [14], but was much lower than that reported for *S. enterica* SePat (322 μM) [33]. Moreover Kd values are in the same order of magnitude as the ATP K_M determined in this study, 73 and 76.32 μM, respectively. Acs K270A mutant protein showed a Kd for ATP-binding very similar to Acs wt (13.3 μM), as was observed when ATP K_M were compared, however the ΔH was lower. The fact that K609A mutant protein showed a more energetic binding and a lower dissociation constant (4.2 μM) than Acs wt was unexpected. A similar behavior was observed by Crosby et al. (2012) for the *R. palustris* MatB protein [12], in, to our knowledge, the only previous ATP-binding study for a mutated ANL protein A10 lysine carried out to date. Thus, MatB wt protein showed a lower energetic binding and a higher dissociation constant than K488A (A10 conserved lysine) mutant [12]. This result suggests that K609 acetylation affects ATP-binding, although, surprisingly, leading to stronger ATP-binding. The role of K609 in ATP-binding will be studied more deeply in future works. Acs D500A mutant protein did not show any ATP-binding under the assayed conditions. This result demonstrates the importance of this aspartic acid to bind ATP ligand and is in agreement with the previously reported study carried out by Han et al. (2017) for the *S. enterica* Acs protein [33]. Finally, Acs protein lost the ability to bind ATP when threonine 264 was mutated. To our knowledge, the essential role of this residue to ATP-binding had not been previously reported for an ANL protein. The fact that when we titrated T264 and D500 mutant proteins, under the same conditions to wt and 270A mutant, no-binding was observed is in agreement with the high K_M and low K_{cat} determined in this study for them.

Competitive inhibition of *S. enterica* Acs by cAMP has been recently demonstrated [33], so we decided to study *E. coli* Acs inhibition. An inhibition constant of 232 μM was established. This value was very similar to those determined for *S. enterica* Acs (185 μM) and intracellular cAMP concentration calculated for *E. coli* grown in the absence of glucose [53,54]. Moreover, we found that the presence of cAMP and ATP hindered CobB deacetylation. This result was observed for *S. enterica* Acs in the presence of cAMP and the authors suggested that Acs-CobB binding could induce a different Acs conformation and the presence of cAMP might hinder the formation of this conformation. Further investigation is necessary to confirm this suggestion,

which would suppose a new level of regulation of Acs deacetylation by CobB depending on cAMP and ATP intracellular concentrations.

In conclusion, this work studies for the first time the *E. coli* Acs ATP-binding parameters and the role of four important conserved residues. Thus, the effect of K609 mutation on ATP-binding observed in this study opens a new research field for understanding how mutation induces enzyme inhibition. Finally, the essential role of T264 and D500 residues in Acs ATP-binding has been demonstrated.

References

1. Gulick AM. Conformational dynamics in the acyl-CoA synthetases, adenylation domains of non-ribosomal peptide synthetases, and firefly luciferase. ACS Chem Biol. 2009;4: 811–827. doi:10.1021/cb900156h

2. Berg P. Acyl adenylates: an enzymatic mechanism of acetate activation. J Biol Chem. 1956;222: 991–1013.

3. Farrar WW, Plowman KM. Kinetics of acetyl-CoA synthetase-I. Mode of addition of substrates. Int J Biochem. 1975;6: 537–542. doi:10.1016/0020-711X(75)90069-5

4. Tian Y, Suk D-H, Cai F, Crich D, Mesecar AD. *Bacillus anthracis* O-succinylbenzoyl-CoA synthetase: reaction kinetics and a novel inhibitor mimicking its reaction intermediate. Biochemistry. 2008;47: 12434–12447. doi:10.1016/j.neuron.2009.10.017.A

5. Kim YS, Kang SW. Steady-state kinetics of malonyl-CoA synthetase from *Bradyrhizobium japonicum* and evidence for malonyl-AMP formation in the reaction. Biochem J. 1994;297: 327–333.

6. Li H, Melton EM, Quackenbush S, DiRusso CC, Black PN. Mechanistic studies of the long chain acyl-CoA synthetase Faa1p from *Saccharomyces cerevisiae*. Biochim Biophys Acta - Mol Cell Biol Lipids. 2007;1771: 1246–1253. doi:10.1016/j.bbalip.2007.05.009

7. Wu R, Cao J, Lu X, Reger AS, Gulick AM, Dunway-Mariano D. Mechanism of 4-chlorobenzoate: Coenzyme A ligase catalysis. Biochemistry. 2008;47: 8026–8039. doi:10.1021/bi800698m

8. Kochan G, Pilka ES, von Delft F, Oppermann U, Yue WW. Structural snapshots for the conformation-dependent catalysis by human medium-chain acyl-Coenzyme A synthetase ACSM2A. J Mol Biol. 2009;388: 997–1008. doi:10.1016/j.jmb.2009.03.064

9. Osman KT, Du L, He Y, Luo Y. Crystal structure of *Bacillus cereus* D-alanyl carrier protein ligase (DltA) in complex with ATP. J Mol Biol. 2009;388: 345–355. doi:10.1016/j.jmb.2009.03.040

10. Law A, Boulanger MJ. Defining a structural and kinetic rationale for paralogous copies of phenylacetate-CoA ligases from the cystic fibrosis pathogen *Burkholderia cenocepacia* J2315. J Biol Chem. 2011;286: 15577–15585. doi:10.1074/jbc.M111.219683

11. Chen Y, Sun Y, Song H, Guo Z. Structural basis for the ATP-dependent configuration of adenylation active site in *Bacillus subtilis* O-succinylbenzoyl-Coa synthetase. J Biol Chem. 2015;290: 23971–23983. doi:10.1074/jbc.M115.676304

12. Crosby HA, Rank KC, Rayment I, Escalante-Semerena JC. Structure-guided expansion of the substrate range of methylmalonyl Coenzyme A synthetase (MatB) of *Rhodopseudomonas palustris*. Appl Environ Microbiol. 2012;78: 6619–6629. doi:10.1128/AEM.01733-12

13. Li Z, Nair SK. Structural basis for specificity and flexibility in a plant 4-coumarate:CoA ligase. Structure. 2015;23: 2032–2042. doi:10.1016/j.str.2015.08.012

14. Li W, Gu S, Fleming J, Bi L. Crystal structure of FadD32, an enzyme essential for mycolic acid biosynthesis in *Mycobacteria*. Sci Rep. 2015;5: 1–8. doi:10.1038/srep15493

15. Fan M, Xiao Y, Li M, Chang W. Crystal structures of *Arabidopsis thaliana* oxalyl-CoA synthetase essential for oxalate degradation. Mol Plant. 2016;9: 1349–1352. doi:10.1016/j.molp.2016.06.002

16. Scaglione A, Fullone MR, Montemiglio LC, Parisi G, Zamparelli C, Vallone B, et al. Structure of the adenylation domain Thr1 involved in the biosynthesis of 4-chlorothreonine in *Streptomyces sp.* OH-5093—protein flexibility and molecular bases of substrate specificity. FEBS J. 2017;284: 2981–2999. doi:10.1111/febs.14163

17. Muller M. Energy metabolism of protozoa without mitochondria. Annu Rev Microbiol. 1988;42: 465–488. doi:10.1146/annurev.mi.42.100188.002341

18. Starai VJ, Escalante-Semerena JC. Acetyl-coenzyme A synthetase (AMP forming). Cell Mol Life Sci. 2004;61: 2020–2030. doi:10.1007/s00018-004-3448-x

19. Starai VJ, Celic I, Cole RN, Boeke JD, Escalante-Semerena JC. Sir2-dependent activation of acetyl-CoA synthetase by deacetylation of active lysine. Science. 2002;298: 2390–2392. doi:10.1126/science.1077650

20. Gardner JG, Grundy FJ, Henkin TM, Escalante-Semerena JC. Control of acetyl-Coenzyme A synthetase (AcsA) activity by acetylation/deacetylation without NAD^+ involvement in *Bacillus subtilis*. J Bacteriol. 2006;188: 5460–5468. doi:10.1128/JB.00215-06

21. Crosby HA, Heiniger EK, Harwood CS, Escalante- JC. Reversible N-Lysine acetylation regulates the activity of acyl-CoA synthetases involved in anaerobic benzoate catabolism in *Rhodopseudomonas palustris*. Mol Microbiol. 2010;76: 874–888. doi:10.1111/j.1365-2958.2010.07127

22. Hayden JD, Brown LR, Gunawardena HP, Perkowski EF, Chen X, Braunstein M. Reversible acetylation regulates acetate and propionate metabolism in *Mycobacterium smegmatis*. Microbiology. 2013;159: 1986–1999. doi:10.1099/mic.0.068585-0

23. Schwer B, Bunkenborg J, Verdin RO, Andersen JS, Verdin E. Reversible lysine acetylation controls the activity of the mitochondrial enzyme acetyl-CoA synthetase 2. Proc Natl Acad Sci U S A. 2006;103: 10224–10229. doi:10.1073/pnas.0603968103

24. de Diego T, Gallego-Jara J, Castaño-Cerezo S, Bernal Sánchez V, Fernández Espín V, García de la Torre J, et al. The protein acetyltransferase PatZ from *Escherichia coli* is regulated by autoacetylation- induced oligomerization. J Biol Chem. 2015;53: 1689–1699. doi:10.1017/CBO9781107415324.004

25. Branchini BR, Murtiashaw MH, Magyar R a., Anderson SM. The role of lysine 529, a conserved residue of the acyl-adenylate- forming enzyme superfamily, in firefly luciferase. Biochemistry. 2000;39: 5433–5440. doi:10.1021/bi9928804

26. Horswill AR, Escalante-Semerena JC. Characterization of the propionyl-CoA synthetase (PrpE) enzyme of *Salmonella enterica*: Residue lys 592 is required for propionyl-AMP synthesis. Biochemistry. 2002;41: 2379–2387. doi:10.1021/bi015647q

27. Kitagawa M, Ara T, Arifuzzaman M, Ioka-Nakamichi T, Inamoto E, Toyonaga H, et al. Complete set of ORF clones of *Escherichia coli* ASKA library (a complete set of *E. coli* K-12 ORF archive): unique resources for biological research. DNA Res. 2005;12: 291–299. doi:10.1093/dnares/dsi012

28. Gallego-Jara J, Écija Conesa A, de Diego Puente T, Lozano Terol G, Cánovas Díaz M.

Characterization of CobB kinetics and inhibition by nicotinamide. PLoS One. 2017;12: e0189689. doi:10.1371/journal.pone.0189689

29. Williamson J, Corkey B. Assays of intermediates of the citric acid. In: Lowenstein J, Kaplan N, Colowick N, editors. Methods of Enzymology. Academic P. 1969. pp. 494–497.

30. Biasini M, Bienert S, Waterhouse A, Arnold K, Studer G, Schmidt T, et al. SWISS-MODEL: Modelling protein tertiary and quaternary structure using evolutionary information. Nucleic Acids Res. 2014;42: 252–258. doi:10.1093/nar/gku340

31. Benkert P, Biasini M, Schwede T. Toward the estimation of the absolute quality of individual protein structure models. Bioinformatics. 2011;27: 343–350. doi:10.1093/bioinformatics/btq662

32. Chen YH. Determination of the helix and β form of proteins in aqueous solution by circular dichroism. Biochemistry. 1974;13: 3350–3359. doi:10.1021/bi00713a027

33. Han X, Shen L, Wang Q, Cen X, Wang J, Wu M, et al. Cyclic AMP inhibits the activity and promotes the acetylation of acetyl-CoA synthetase through competitive binding to the ATP/AMP pocket. J Biol Chem. 2017;292: 1374–1384. doi:10.1074/jbc.M116.753640

34. Renilla S, Bernal V, Fuhrer T, Castaño-Cerezo S, Pastor JM, Iborra JL, et al. Acetate scavenging activity in *Escherichia coli*: interplay of acetyl-CoA synthetase and the PEP-glyoxylate cycle in chemostat cultures. Appl Microbiol Biotechnol. 2012;95: 2109–2124. doi:10.1007/s00253-011-3536-4

35. Valgepea K, Adamberg K, Vilu R. Decrease of energy spilling in *Escherichia coli* continuous cultures with rising specific growth rate and carbon wasting. BMC Syst Biol. 2011;5: 1–11. doi:10.1186/1752-0509-5-106

36. Chen Y, Jiang Y, Guo Z. Mechanistic insights from the crystal structure of *Bacillus subtilis* O-succinylbenzoyl-CoA synthetase complexed with the adenylate intermediate. Biochemistry. 2016;55: 6685–6695. doi:10.1021/acs.biochem.6b00889

37. Gulick AM, Starai VJ, Horswill AR, Homick KM, Escalante-semerena JC. The 1 . 75 Å crystal structure of acetyl-CoA synthetase bound to adenosine-5 ' -propylphosphate and Coenzyme A. Biochemistry. 2003;42: 2866–2873. doi:10.1021/bi0271603

38. Jogl G, Tong L. Crystal structure of yeast acetyl-Coenzyme A synthetase in complex with AMP. Biochemistry. 2004;43: 1425–1431. doi:10.1021/bi035911a

39. Shah MB, Ingram-smith C, Cooper LL, Qu J, Meng Y, Kerry S, et al. The 2.1Å crystal structure of an acyl-CoA Synthetase from *Methanosarcina acetivorans* reveals an alternate acyl binding pocket for small branched acyl substrates. Proteins. 2009;77: 685–698. doi:10.1002/prot.22482.

40. Sundlov J a., Fontaine DM, Southworth TL, Branchini BR, Gulick AM. Crystal structure of firefly luciferase in a second catalytic conformation supports a domain alternation mechanism. Biochemistry. 2012;51: 6493–6495. doi:10.1021/bi300934s

41. Reger AS, Carney JM, Gulick AM. Biochemical and crystallographic analysis of substrate binding and conformational changes in acetyl-CoA synthetase. Biochemistry. 2007;46: 6536–6546. doi:10.1021/bi6026506

42. Saraste M, Sibbald PR, Wittinghofer A. The P-loop — a common motif in ATP- and GTP-

binding proteins. Trends Biochem Sci. 1990;15: 430–434. doi:10.1016/0968-0004(90)90281-F

43. May JJ, Kessler N, Marahiel MA, Stubbs MT. Crystal structure of DhbE, an archetype for aryl acid activating domains of modular nonribosomal peptide synthetases. Proc Natl Acad Sci. 2002;99: 12120–12125. doi:10.1073/pnas.182156699

44. Conti E, Stachelhaus T, Marahiel MA, Brick P. Structural basis for the activation of phenylalanine in the non-ribosomal biosynthesis of gramicidin S. EMBO J. 1997;16: 4174–4183. doi:10.1093/emboj/16.14.4174

45. Lu X, Rong Z, Indrajeet S, Li X, Kumar G, Swaminathan S, et al. Stable analogues of OSB-AMP: potent inhibitors of MenE, the O- succinylbenzoate-CoA synthetase from bacterial menaquinone biosynthesis. Chembiochem. 2012;13: 129–136. doi:10.1002/cbic.201100585

46. Chang KH, Xiang H, Dunaway-Mariano D. Acyl-adenylate motif of the acyl-adenylate/thioester-forming enzyme superfamily: a site-directed mutagenesis study with the *Pseudomonas sp.* Strain CBS3 4-chlorobenzoate:coenzyme A ligase. Biochemistry. 1997;36: 15650–15659. doi:10.1021/bi971262p

47. Stuible H-P, Büttner D, Ehlting J, Hahlbrock K, Kombrink E. Mutational analysis of 4-coumarate: CoA ligase identifies functionally important amino acids and verifies its close relationship to oher adenylate-forming enzymes. FEBS Lett. 2000;467: 117–122. doi:10.1016/S0014-5793(00)01133-9

48. Starai VJ, Escalante-Semerena JC. Identification of the protein acetyltransferase (Pat) enzyme that acetylates acetyl-CoA synthetase in *Salmonella enterica*. J Mol Biol. 2004;340: 1005–1012. doi:10.1016/j.jmb.2004.05.010

49. Hallows WC, Lee S, Denu JM. Sirtuins deacetylate and activate mammalian acetyl-CoA synthetases. Proc Natl Acad Sci. 2006;103: 10230–10235. doi:10.1073/pnas.0604392103

50. Renilla S, Bernal V, Fuhrer T, Castaño-Cerezo S, Pastor JM, Iborra JL, et al. Acetate scavenging activity in *Escherichia coli*: interplay of acetyl–CoA synthetase and the PEP–glyoxylate cycle in chemostat cultures. Appl Microbiol Biotechnol. 2012;93: 2109–2124. doi:10.1007/s00253-011-3536-4

51. Mitchell AC, Tucker AC, Escalante-Semerena JC, Gulick AM. The Structure of *S. lividans* acetoacetyl-CoA synthetase shows a novel interaction between the C-terminal extension and the N- terminal domain. Proteins. 2015;83: 575–581. doi:10.1002/prot.24738.

52. Du X, Li Y, Xia Y-L, Ai S-M, Liang J, Sang P, et al. Insights into protein–ligand interactions: mechanisms, models, and methods. Int J Mol Sci. 2016;17: 1–34. doi:10.3390/ijms17020144

53. Notley-mcrobb L, Death A, Ferenci T. The relationship between external glucose concentration and cAMP levels inside. Biochem J. 2006;143: 1909–1918. doi:10.1099/00221287-143-6-1909

54. Makman RS, Sutherland EW. Adenosine 3', 5´-Phosphate in *Escherichia coli*. J Biol Chem. 1965;240: 1309–1314.

Appendix

Table S1. Strains, plasmids and primers used in this study. Restriction nuclease sites are in grey. Bold typeface indicates the modified codon during site-directed mutagenesis.

***E. coli* strain**	**Genotype**	**Source**
BL21 (DE3)	F– ompT gal dcm lon hsdSB(rB- mB-) λ(DE3)	Agilent Technologies
DH10B	F- mcrA Δ(mrr-hsdRMS-mcrBC) Φ80dlacZΔM15 ΔlacX74 endA1 recA1 deoR Δ(ara,leu)7697 araD139 galU galK nupG rpsL λ-	Invitrogen
Plasmid	**Genotype**	**Source**
ASKA*acs*	N-terminal, His6-tag overexpression vector, Cam^R. Encodes *acs* wt	ASKA collection [27]
pBAD24-*cobB*MBP	C-terminal, His6-tag-MBP overexpression vector, Kan^R. Encodes *cobB* wt.	[28]
ASKA*acs*^{T264A}	N-terminal, His6-tag overexpression vector, Cam^R. Encodes *acs* T264A	This study
ASKA*acs*^{K270A}	N-terminal, His6-tag overexpression vector, CamR. Encodes *acs* K270A	This study
ASKA*acs*^{D500A}	N-terminal, His6-tag overexpression vector, CamR. Encodes *acs* D500A	This study
ASKA*acs*^{K609A}	N-terminal, His6-tag overexpression vector, CamR. Encodes *acs* K609A	This study
Primer	**Sequence**	
ASKA*acs*^{T264A} Fwd	CTGTTTATTCTCTA**CGC**CTCCGGTTCTACC	
ASKA*acs*^{T264A} Rev	GGTAGAACCGGAG**GCG**TAGAGAATAAACAG	
ASKA*acs*^{K270A} Fwd	CCGGTTCTACCGGT**GCA**CCAAAAGGTGTGCTG	
ASKA*acs*^{K270A} Rev	CAGCACACCTTTTGG**TGC**ACCGGTAGAACCGG	
ASKA*acs*^{D500A} Fwd	GTATTTCAG**CGG**CGCCGGCGCGCGTCGC	
ASKA*acs*^{D500A} Rev	GCGACGCGCGCC**GGC**GCCGCTGAAATAC	
ASKA*acs*^{K609A} Fwd	CTAAAACCCGCTCCG**GCG**CAATTATGCGCCGTATTC	
ASKA*acs*^{K609A} Rev	GAATACGGCGCATAATTG**CGC**CGGAGCGGGTTTTAG	

Table S2. Quality parameters of the predicted Acs models constructed using Swiss-Model software. Models are ordered from highest to lowest QMEAN z-scored.

Template (PDB code)/Reference	Seq. Identity (%)	QMEAN z-score	GMQE	Coverage
3c5e/[8]	25.14	-2.45	0.56	68-620
5bsm/[13]	22.73	-2.71	0.53	74-621
4fut/[12]	22.42	-3.38	0.5	78-621
5n9x/[16]	23.8	-3.7	0.5	78-621
5d6j/[14]	17.72	-3.8	0.49	78-622
5bur/[11]	23.99	-4.22	0.49	78-616
2y27/[10]	22.05	-4.81	0.33	253-614
3fcc/[9]	18.16	-5.3	0.48	79-619
5elo/[15]	30.75	-8.79	0.47	24-494

CHAPTER 7

Influence of carbon and nitrogen source on pH homeostasis and acetate metabolism in Escherichia coli

Abstract

Escherichia coli (*E. coli*) is the most important organism in the biotechnology field, and it is essential to study its metabolism and regulation in order to optimize related bioprocesses. The carbon and nitrogen sources used by *E. coli* are two important factors that must be considered when carrying out bioprocesses. *E. coli* can use different carbon sources, although it shows a preference for glucose over other sources such as glycerol. *E. coli* can metabolize several compounds as nitrogen source, although, it shows a preference for inorganic ammonium. In this study, the acetate metabolism was evaluated for *E. coli* growing in minimal medium MM9 (ammonium nitrogen source) and TB7 complex medium (peptides nitrogen source) supplemented with glucose and glycerol. The growth rate, acetate overflow, intracellular pH homeostasis, intracellular acetyl-phosphate, acetyl-CoA and succinyl-CoA concentrations and protein lysine acetylation were studied. The results show that both the nitrogen and carbon source strongly influence the growth rate and acetate overflow. Intracellular pH was determined for the first time in *E. coli* growing in a continuous culture. The pH of glucose cultures reached values higher than 8.5 in the exponential growth phase, but glycerol cultures showed greater intracellular pH control (pH 7.5-6.5). Finally, acetyl and succinyl donor concentrations and lysine acetylation also had different profiles according to carbon and nitrogen source. The results highlight the influence of the carbon and nitrogen source on *E. coli* acetate metabolism and the link between them.

Introduction

E. coli is a model organism in the biology and biotechnology fields, and it is an important tool in recombinant proteins and other bio-products production for industry. Research into central metabolism and regulation knowledge of this bacterium is essential for the continuous optimization of all these biotechnological processes, always bearing in mind that the carbon and nitrogen sources are two important culture factors that affect metabolism fluxes and biomass yield [1]. *E. coli* can use several compounds as carbon source, and it chooses the most easily accessible which allow fastest growth. However, *E. coli* shows a preference for glucose over other carbon sources, a phenomenon known as carbon catabolite repression (CCR). Global transcription factor CRP (Catabolite Repression Protein or cAMP Receptor Protein), cAMP and the phosphoenolpyruvate carbon system (PTS System) play major roles in CCR. When glucose is present, it is transported and activated through the PTS System (PTS carbon source). However, when the glucose concentration is limited, the PTS system increases cAMP levels to promote the transcription of genes regulated by CRP, among them non-glucose carbon source utilization

genes [2]. Glycerol is a poor-carbon source (non-PTS carbon source) but can be metabolized by *E. coli.* Moreover, interest in to know how glycerol is used by *E. coli* as carbon source has greatly increased because of its biotechnological importance as a sub-product of biodiesel synthesis, whose production is expected to increase in the future [3,4].

Nitrogen is an essential element for all organisms. *E. coli* is capable of using several organic compounds containing nitrogen (such as amino acids or peptides) as nitrogen source, although inorganic ammonium is the preferred source [5]. The Glutamate dehydrogenase (Gdh), glutamine synthetase (Gs) and glutamine oxoglutarate aminotransferase (GoGat) are the main enzymes responsible for assimilating ammonium and connecting carbon-nitrogen metabolisms through α-ketoglutarate (αKG) and glutamine metabolites [6,7]. Indeed, a new link between carbon metabolism and nitrogen assimilation has been established. Thus, in nitrogen-limiting conditions (absence of ammonium), the αKG pool increases because the amino acid biosynthesis flux is reduced, which acts as a signal to repress glucose uptake and inhibit cAMP biosynthesis [8]. Due to low cAMP levels, when *E. coli* is growing with glucose as carbon source in a poor-nitrogen source the carbon/nitrogen imbalance established limits bacterial growth [9].

E. coli excretes several metabolites to the extracellular medium during cell growth to maintain cellular homeostasis. When glucose is employed as carbon source acetate is the main excreted product. However, *E. coli* can also metabolize acetate as a non-PTS carbon source. In this way, the acetate excreted is consumed and reincorporated in the metabolism (a phenomenon known as “acetate overflow”). This overflow is an important drawback for industrial bioprocesses using *E. coli*, because acetate inhibits cell growth in high density cultures, limiting yield [10]. For this reason, much effort has been put into deepening our knowledge of the acetate metabolism with the purpose of minimizing its overflow [11–13].

In this study, the *E. coli* acetate metabolism will be evaluated for *E. coli* BW25113 and five deficient strains involved: *pta* which encodes the phosphotransacetylase enzyme [14], *ackA* which encodes the acetate kinase enzyme [15], *patZ* which encodes the main *E. coli* acetyltransferase [16], c*obB* which encodes the main *E. coli* sirtuin deacetylase [17]) and ac*s* which encodes the acetyl-CoA synthetase enzyme [18,19], growing in minimal medium MM9 (ammonium nitrogen source) and TB7 complex medium (peptides nitrogen source) supplemented with glucose (PTS carbon source) and glycerol (non-PTS carbon source). Thus, growth rate, acetate overflow, intracellular pH homeostasis, intracellular acetyl-phosphate, acetyl-CoA and succinyl-CoA concentrations and protein lysine acetylation will be evaluated. A

scheme of glucose and glycerol consumption, acetate metabolism and ammonium assimilation by *E. coli* is resumed in Figure 1.

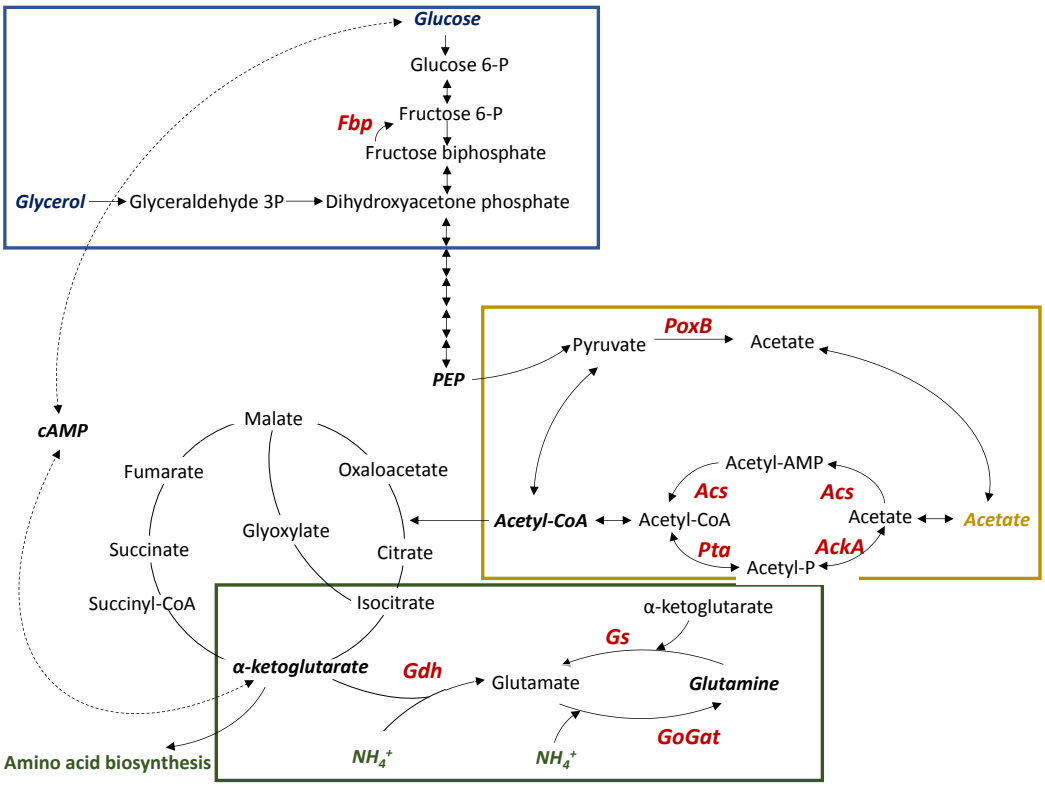

Figure 1. *E. coli* metabolism. Carbon uptake (blue box), acetate metabolism (yellow box) and nitrogen assimilation (green box). Fbp (fructose biphosphatase), PoxB (pyruvate oxidase), Acs (acetyl-CoA synthetase), Pta (phosphotransacetylase), Gdh (glutamate dehydrogenase), Gs (glutamate synthase) and GoGat (glutamine oxoglutarate aminotransferase).

Methods

Escherichia coli strains and culture conditions

E. coli BW25113 and its deletion strains [20] (Appendix Table S1) were grown in batch mode in minimal medium MM9 (10 mM $(NH_4)_2SO_4$, 8.5 mM NaCl, 40 mM Na_2HPO_4, 20 mM KH_2PO_4, 185 µM $FeCl_3$, 175 µM EDTA, 7 µM $ZnSO_4$, 7 µM $CuSO_4$, 7 µM $MnSO_4$, 7 µM $CoCl_2$, 7 µM $MgSO_4$, 0.1 mM $CaCl_2$, and 1 µM thiamine·HCl) [21] or in complex TB7 medium (10 g L^{-1} tryptone buffered at pH 7.0 with 100 mM potassium phosphate) supplemented with glucose 22 mM or glycerol 44 mM as carbon source. Strains were grown at 37 °C on a rotatory shaker at 250 rpm and cell growth was monitored spectrophotometrically by determining the optical density at 600 nm (OD_{600}). The exponential growth phase was identified and the specific growth rate was determined for all the culture of strains [22]. Kinetic and stoichiometric parameters were determined as indicated by Martinez-Gómez et al. [23].

Quantification of extracellular metabolites

To quantify extracellular metabolites, 1 mL culture samples were taken at different culture phases and harvested by centrifugation. Extracellular acetate and glycerol were analysed by an HPLC equipped with differential refractometer (Shimadzu Scientific Instruments) using an ion exclusion column (ICSep Coregel 87H3, Transgenomic). The mobile phase was 5 mM H_2SO_4 flowing at 0.6 mL min^{-1} and 55 °C. Extracellular glucose was determined by the dinitrosalicylic acid (DNS) method [24].

Intracellular and extracellular pH determination

To determine intracellular *E. coli* pH, the pGFPR01 plasmid, kindly provided by Dr. Joan Slonczewski (Department of Biology, Kenyon College, Gambier, Ohio, USA), which expresses ratiometric pHluorin from the arabinose-induced P_{BAD} promoter, was used. Thus, as pH increased, ratiometric pHluorin showed an increased in excitation at 410 nm and decreased excitation at 470 nm [25]. Intracellular pH was determined from the 410/470 fluorescence ratio.

Chemically competent *E. coli* BW25113 wt or knockout strains were transformed by heat shock at 42 °C with the pGFPR01 plasmid. Cultures were carried out in a microplate reader (Synergy H1 Hybrid Multi-Mode Reader), simultaneously monitoring growth at OD_{600} and fluorescence at two excitation wavelengths (410 and 470 nm) and 508 nm emission. 96-well plates were sterilized and prepared with 100 µL of medium at OD 0.05 and arabinose inductor, and covered with an adhesive gas-permeable sheet (Sigma Aldrich) to prevent evaporation and permit aeration. Cultures were grown in quintuplicate with double orbital shaking at 37 °C for 24 h. After reading, the fluorescence ratio was calculated and the intracellular pH was continually determined by constructing a standard curve for pH as a function of the fluorescence ratio 410/470. The calibration was carried out employing 40 mM potassium benzoate and 40 mM methylamine hydrochloride to equalize extracellular and intracellular pH as indicated by J. Slonczewski et al. [25]. Thus, overnight culture samples were inoculated to a final OD_{600} 1 in MM9 or TB7 media buffered at different pH values with potassium benzoate and methylamine hydrochloride and 410/470 fluorescence ratio was calculated as indicated by Wilks et al. [26]. Extracellular pH was determined simultaneously from parallel cultures grown in batch mode.

Intracellular metabolites quantification

To quantify intracellular metabolites, a culture volume containing 10 mg of biomass was taken at different culture growth phases (exponential OD_{600} 1 and stationary) and harvested by centrifugation at -9 °C. Cell pellets were immediately frozen with liquid N_2 and stored at -80 °C

until analysis. To determine intracellular concentrations, a cell volume of 0.7 μm^3 was taken and a viable cell number of 7.5 e^8 cells/ml per OD_{600} was estimated [27].

Acetyl-CoA and succinyl-CoA quantification

Acetyl-CoA and succinyl-CoA extraction was carried out by a freeze-thaw method with methanol [28]. Cell pellets were resuspended in 1.5 mL of pure methanol at -20 °C and put in safe-lock Eppendorf tubes. C_{13}-Malonyl-CoA was employed as internal standard at a 10 µM [29]. The suspensions were put on liquid nitrogen for 5 min to ensure total freezing, and on ice for 10 min to thaw them. This freeze-thaw procedure was repeated three times. Then, samples were centrifuged at 13000 rpm at -9 °C, and supernatants were evaporated to dryness. To quantify intracellular metabolites, samples were resuspended in 0.5 mL of HPLC-grade water.

The analyses were carried out on an HPLC-MS/MS system consisting of an Agilent 1100 Series HPLC instrument (Agilent Technologies) that was connected to an Agilent Ion Trap XCT Plus mass spectrometer (Agilent Technologies), using an electrospray (ESI) interface. Samples were injected Into an Teknokroma mediterranea^{TM} sea18 HPLC column (5 µm, 250 x 4.6 mm) and eluted at a flow rate of 700 µL min^{-1}. Mobile phase A, consisting of 50 mM ammonium acetate, and mobile phase B, consisting of acetonitrile, were used for the chromatographic separation. The elution program consisted of 100 % phase A for 5 minutes and then a gradient from 0 to 40% of mobile phase B in 10 minutes. 40 % phase B was maintained for 5 minutes and finally, 100% solvent A was maintained for 5 additional minutes. The mass spectrometer was operated in positive polarity mode with a capillary spray voltage of 3800 V and a scan speed of 22000 (m/z)/sec from 100–1000 m/z. The nebulizer gas pressure was set to 60 psi, while the drying gas was set to a flow rate of 12 L min^{-1} and the temperature was set to 350 °C. The ion chromatograms were extracted, and the peak areas were quantified using the Data Analysis program in LC/MSD Trap Version 3.2 (Bruker Daltonik). The peak area data of the compound in the standards were used to calculate the calibration curve.

Acetyl-phosphate quantification

Intracellular acetyl phosphate concentrations were determined using the method developed by Weinert et al. [27].

Western immunoblot analysis

The acetylation level was studied by western blot immunoassay. For this, 1 mL culture samples were taken at different culture growth phases and harvested by centrifugation. Cell pellets were immediately frozen with liquid N_2 and stored at -80 °C until analysis. Samples were

resuspended in 0.1 mL of lysis buffer (50 mM Tris-HCl, 150 mM NaCl, lysozyme 1 mg/mL, pH 8) and incubated at 25 °C with shaking for 40 minutes. Samples were centrifuged at 10000 rpm at 4 °C. Lysed protein loading was normalized after the amount of protein was determined. Samples were separated on 10 % acrylamide SDS-PAGE and transferred to polyvinylidene fluoride (PVDF) membranes using a semidry transfer unit (Trans-Blot® SD Semi-Dry Transfer Cell, Bio-Rad). The membranes were blocked with 1 % (w/v) bovine serum albumin (BSA) in TBST (10 mM Tris-HCl, 0.15 M NaCl, 0.05% Tween-20, pH 7.5) for 1 hour. The blot was then incubated with primary rabbit monoclonal anti-acetyl Lys antibody at a 1:500 dilution (InmuneChem) overnight at 4 °C. The membrane was washed 3 times for 10 minutes each with TBST and then incubated with HRP-conjugated goat anti-rabbit secondary antibody (Santa Cruz Biotechnology) at a 1:15000 dilution for 1 hour at room temperature. The blot was washed 6 times for 5 minutes each with TBST. Finally, the membrane was incubated for 10 min with SuperSignal™ West Pico Chemiluminescent Substrate (Thermo Scientific) and reveled with a chemiluminescence Amersham Imager 600 (GE Healthcare).

Results

Specific growth rate and acetate overflow depend on the carbon and nitrogen source in *Escherichia coli*

Specific maximum growth rate (μ_{max}), biomass yield (Yx/s), specific carbon consumption rate (qs) and acetate excretion were evaluated for *E. coli* wt and the deletion strains Δ*pta*, Δ*ackA*, Δ*patZ*, Δ*cobB* and Δ*acs* growing in minimal medium MM9 (ammonium nitrogen source) or complex medium TB7 (amino acids nitrogen source) supplemented with glucose 22 mM (PTS carbon source) or glycerol 44 mM (non-PTS carbon source). In Figure 2 cell growth, acetate, glucose and glycerol extracellular concentrations for *E. coli* wt strain growing in MM9 or TB7 supplemented with glucose or glycerol as carbon sources are shown. All knockout strains graphs are shown in Appendix Figures S1-S5. All μ_{max} are resumed in Table 1, and the stoichiometric parameters biomass yield (Yx/s) and specific carbon consumption rate (qs) are shown in Table 2.

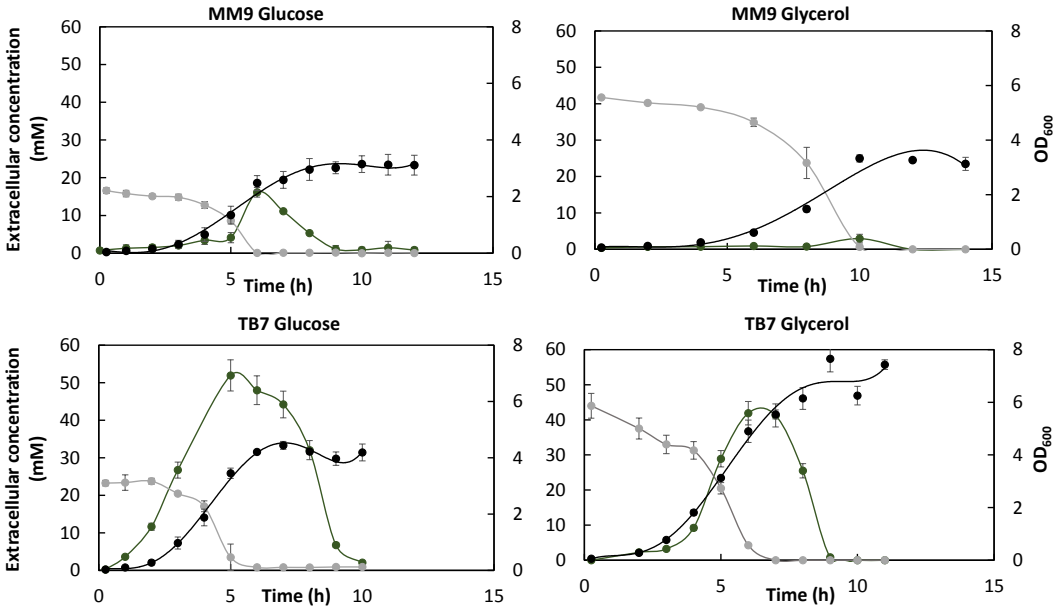

Figure 2. *E. coli* wt strain growth (black), glucose or glycerol extracellular concentration (grey) and acetate extracellular concentration (green) growing in MM9 or TB7 supplemented with glucose or glycerol as carbon sources.

Table 1. Specific maximum rates for *E. coli* wt and Δ*pta*, Δ*ackA*, Δ*patZ*, Δ*cobB* and Δ*acs* knockouts growing in MM9 or TB7 supplemented with glucose or glycerol as carbon sources.

	μ_{max} (h^{-1})			
	MM9 Glucose	**MM9 Glycerol**	**TB7 Glucose**	**TB7 Glycerol**
wt	0.73 ± 0.02	0.49 ± 0.01	1.19 ± 0.06	0.93 ± 0.04
Δ*pta*	0.75 ± 0.04	0.45 ± 0.02	1.19 ± 0.03	0.75 ± 0.04
Δ*ackA*	0.66 ± 0.05	0.48 ± 0.02	1.18 ± 0.21	0.75 ± 0.06
Δ*patZ*	0.69 ± 0.07	0.41 ± 0.03	1.14 ± 0.02	0.91 ± 0.04
Δ*cobB*	0.60 ± 0.03	0.48 ± 0.01	1.07 ± 0.05	0.85 ± 0.06
Δ*acs*	0.52 ± 0.02	0.41 ± 0.01	0.92 ± 0.07	0.81 ± 0.1

E. coli wt showed a higher μ_{max} in cultures supplemented with glucose than with glycerol. Thus, for MM9, the wt strain showed a μ_{max} of 0.73 h^{-1} and 0.49 h^{-1} for glucose and glycerol, respectively, while the corresponding values for TB7 medium were of 1.19 h^{-1} and 0.93 h^{-1} for glucose and glycerol, respectively. So, although μ_{max} was lower for glycerol in both media, the decrease was more pronounced in minimal medium (μ_{max} decrease of 43 % in MM9 and 21 % in TB7). Similarly to the wt strain, all knockouts showed a higher μ_{max} in cultures supplemented with glucose than with glycerol. The *patZ* deletion strain showed a μ_{max} very similar to wt in all cultures. Similar μ_{max} values to the wt were achieved for *pta* and *ackA* knockouts, except for glycerol TB7 cultures. Finally, Δ*cobB* and Δ*acs* strains showed a lower μ_{max} than wt in all the conditions assayed except in MM9 glycerol.

Table 2. Stoichiometric parameters of *E. coli* wt and Δ*pta*, Δ*ackA*, Δ*patZ*, Δc*obB* and Δ*acs* knockouts growing in MM9 or TB7 supplemented with glucose or glycerol as carbon sources.

	Yx/s (g/mmol)			
	MM9 Glucose	**MM9 Glycerol**	**TB7 Glucose**	**TB7 Glycerol**
wt	0.056	0.030	0.058	0.051
Δ*pta*	0.059	0.026	0.069	0.042
Δ*ackA*	0.067	0.023	0.063	0.030
Δ*patZ*	0.065	0.025	0.066	0.053
Δ*cobB*	0.034	0.020	0.050	0.036
Δ*acs*	0.039	0.019	0.053	0.038
	qs (mmol/g h)			
	MM9 Glucose	**MM9 Glycerol**	**TB7 Glucose**	**TB7 Glycerol**
wt	12.160	13.510	20.510	18.780
Δ*pta*	12.560	17.510	17.240	18.000
Δ*ackA*	9.830	20.640	18.550	24.830
Δ*patZ*	10.560	16.390	17.350	17.160
Δ*cobB*	17.640	23.460	21.180	23.480
Δ*acs*	13.300	21.070	17.350	21.140

As regards extracellular metabolites, several differences were observed depending on the culture medium and strains. Yx/s was higher for glucose than glycerol for all cultures, while qs showed a less defined profile. The *cobB* and *acs* deletion strains showed the least similar behaviour to wt in all cases, showing a very low Yx/s and a high qs. This behaviour was more pronounced in glycerol cultures.

Extracellular acetate was detected in all cultures. *E. coli* wt strain showed the highest extracellular acetate concentration in the TB7 glucose culture (51.92 mM) [30], while in minimal medium supplemented with glucose the concentration of extracellular acetate was lower (16.16 mM). Glycerol supplemented media showed lower acetate concentrations than glucose, 41.88 mM in complex medium and only 0.93 mM in MM9. The *patZ* deletion strain showed a degree of acetate overflow very similar to that observed for wt in all conditions. Meanwhile acetate concentrations of *cobB* and *acs* knockouts were slightly higher and acetate took longer to be reincorporated into the cell than wt (Appendix Figures S4 an S5). In *pta* and *ackA* deletion strains acetate overflow was very low in all cultures. The maximum extracellular concentrations detected are shown in Figure 3.

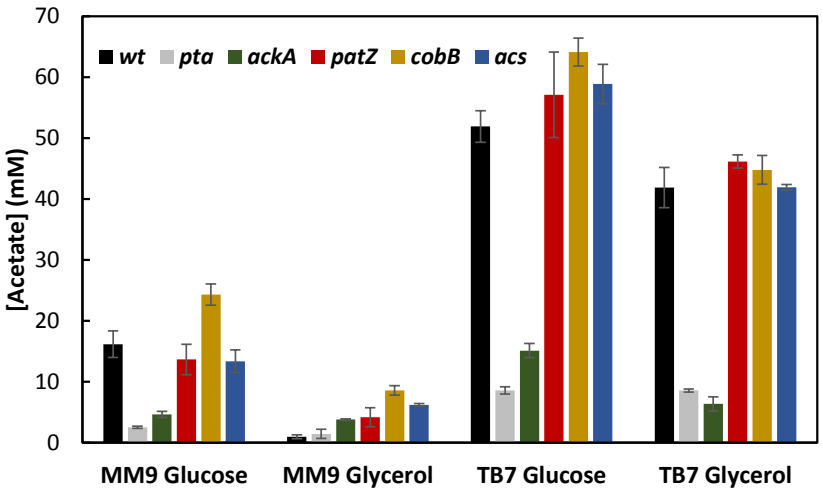

Figure 3. Maximum acetate concentrations detected for *E. coli* wt and Δ*pta*, Δ*ackA*, Δ*patZ*, Δ*cobB* and Δ*acs* knockouts growing in MM9 or TB7 supplemented with glucose or glycerol as carbon sources.

Intracellular pH of *Escherichia coli* increased up to 8 with glucose as carbon source

In this study the intracellular *E. coli* pH was determined in a continuous bacterial culture growing in MM9 and TB7 supplemented with glucose or glycerol as carbon sources. Moreover, differences in intracellular pH between wt and knockout strains were evaluated. To our knowledge, this is the first study about bacterial intracellular pH growing in a culture.

A standard curve was obtained to relate the 410/470 fluorescence ratio with intracellular pH (see Materials section). The relation was lineal from pH 5.5 to 9. The resultant calibration curve is shown in Figure 4.

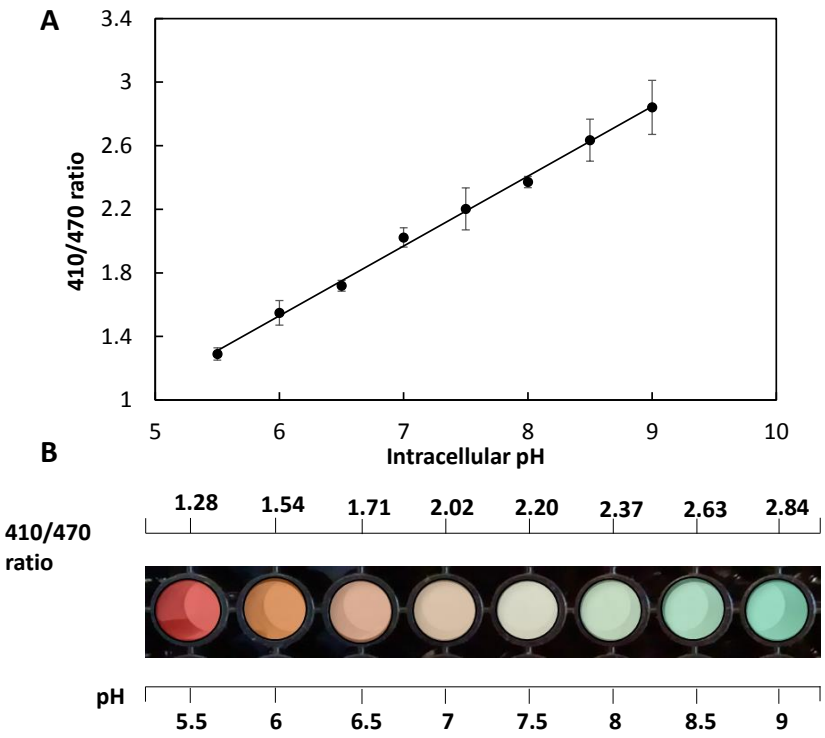

Figure 4. (A) Standard curve relating intracellular pH and 410/470 fluorescence ratio. **(B)** Image of the calibration wells with a false-colour scale as a function of the 410/470 fluorescence ratio.

Profiles of intracellular pH in the knockout strains were similar to the wt for all conditions tested. Strains growing in glucose showed high pH values at the beginning of culture (maximum pH value at OD_{600} 0.25), which then decreased to 6.5. This behaviour was accentuated when a complex medium was used. However, the pH did not increase when glycerol was used as carbon source (Figure 6).

The intracellular and extracellular pH values as a function of OD_{600} for *E. coli* wt strain are shown in Figure 5. In *E. coli* cultures grown with glucose as carbon source intracellular pH reached values higher than 8.5 during the exponential growth phase. In the mid-exponential growth phase, the intracellular pH reached 8.5 (glucose MM9) or even 9 (glucose TB7). Then, the pH gradually decreased to 6.5- 6.8 in both, minimal and complex medium. However, in glycerol cultures intracellular pH showed a very different profile, increasing pH very slightly in the exponential growth phase and decreasing (also slightly) to 6.6-6.8 values. As regards extracellular pH, in minimal medium it decreased during the exponential growth phase to 6.7-6.8 and then remained constant at around 6.5-6.8, equilibrating with the intracellular values.

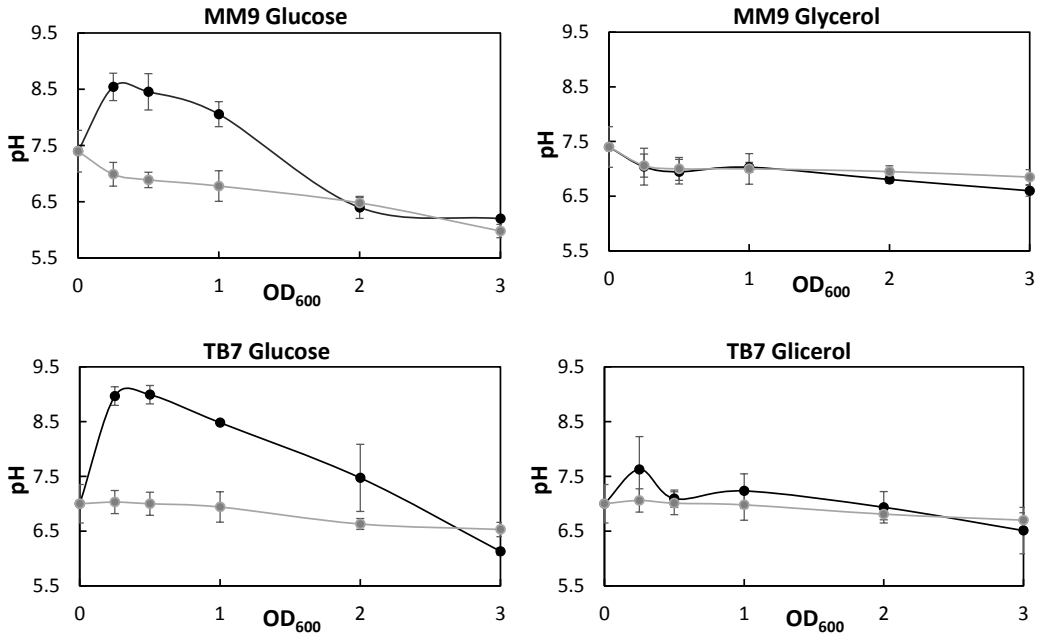

Figure 5. *E. coli* wt strain intracellular (black) and extracellular (grey) pH growing in MM9 or TB7 supplemented with glucose or glycerol as carbon sources.

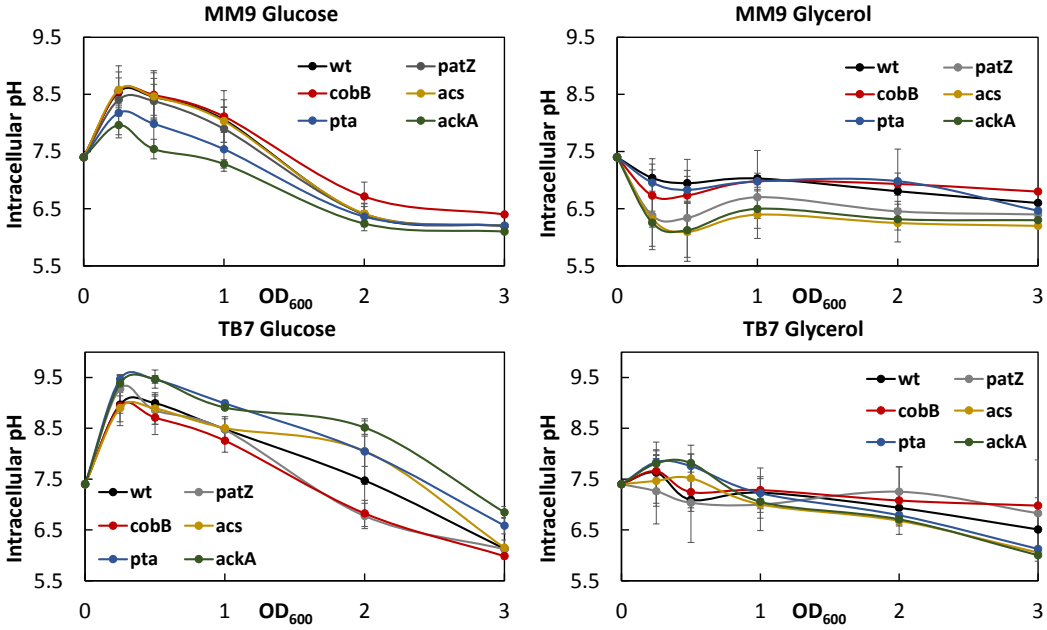

Figure 6. Intracellular pH of *E. coli* knockout strains grown in MM9 or TB7 supplemented with glucose or glycerol as carbon sources.

Intracellular acetyl-phosphate, acetyl-CoA and succinyl-CoA concentrations

Acetyl-phosphate concentrations were determined for *E. coli* wt and Δ*pta*, Δ*ackA*, Δ*patZ*, Δ*cobB* and Δ*acs* knockouts growing on MM9 and TB7 supplemented with glucose 22 mM, in the exponential growth phase (OD_{600} 1) and stationary growth phase. *E. coli* wt absolute concentrations during both growth phases and *E. coli* wt and knockouts concentrations

expressed as a percentage of wt strain in the exponential growth phase are resumed in Figure 7.

E. coli wt concentrations were much higher in minimal than in complex medium. Acetyl-phosphate concentrations were very similar in the exponential and stationary growth phases for *E. coli* growing in minimal medium supplemented with glucose. However, for complex TB7 medium, the concentration of acetyl-phosphate was much higher in the stationary growth phase than in the exponential phase.

As regards acetyl-phosphate concentrations in knockout strains, no significant differences between exponential and stationary growth phases were observed in MM9, as in the case of wt strain. The *patZ*, *cobB* and *acs* deletion strains showed similar concentrations to the wt strain, while *pta* and *ackA* knockouts showed much lower acetyl-phosphate concentrations. In the TB7 complex medium the profile of acetyl-phosphate concentrations was very different from that observed in minimal medium. Exponential concentrations were very low, but increased greatly in the stationary growth phase. Surprisingly, the Δ*ackA* strain showed a very low acetyl-phosphate concentration in minimal medium, while the highest exponential acetyl-phosphate concentration was observed in this same knockout growing in complex medium.

Acetyl-CoA and succinyl-CoA concentrations were determined for *E. coli* wt and Δ*pta*, Δ*ackA*, Δ*patZ*, Δ*cobB* and Δ*acs* knockouts growing on MM9 and TB7 supplemented with glucose 22 mM, in the exponential growth phase (OD_{600} 1) and stationary growth phase. The absolute concentrations of *E. coli* wt and concentrations in *E. coli* wt and knockouts expressed as a percentage of wt strain concentration in the exponential growth phase are resumed in Figure 8.

E. coli wt acetyl-CoA concentrations were higher at exponential growth phase than stationary, and at minimal medium than complex medium. Succinyl-CoA showed a similar profile than acetyl-CoA, although concentrations were lower.

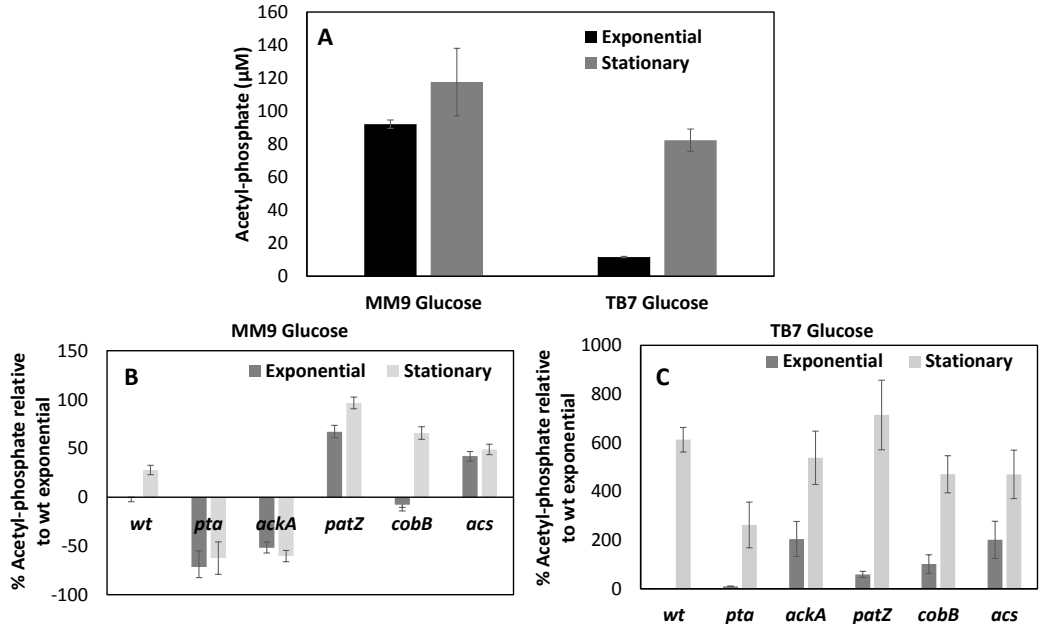

Figure 7. Intracellular acetyl-phosphate concentrations. **(A)** *E. coli* wt intracellular acetyl-phosphate concentrations in exponential and stationary growth phases in minimal and complex TB7 medium growing with glucose as carbon source. **(B)** wt and knockout minimal medium acetyl-phosphate concentrations expressed as a percentage of wt strain concentration in the exponential growth phase. **(C)** wt and knockouts complex TB7 medium acetyl-phosphate concentrations expressed as a percentage of wt strain concentration in the exponential growth phase.

Regarding to knockout strains acetyl-CoA concentrations, the highest concentrations were observed for Δ*pta* and Δ*ackA* strains at exponential growth phase in minimal and complex medium. Δ*cobB* and Δ*acs* strains also showed high acetyl-CoA concentrations in minimal MM9 medium, but not in TB7. Finally, *patZ* deletion strain showed a similar behaviour than wt. Succinyl-CoA concentrations profile was very different. In minimal medium, all knockouts strains showed a similar behaviour than wt, however, very low succinyl-CoA concentrations were observed in TB7 complex medium for *pta* and *ackA* deletion strains.

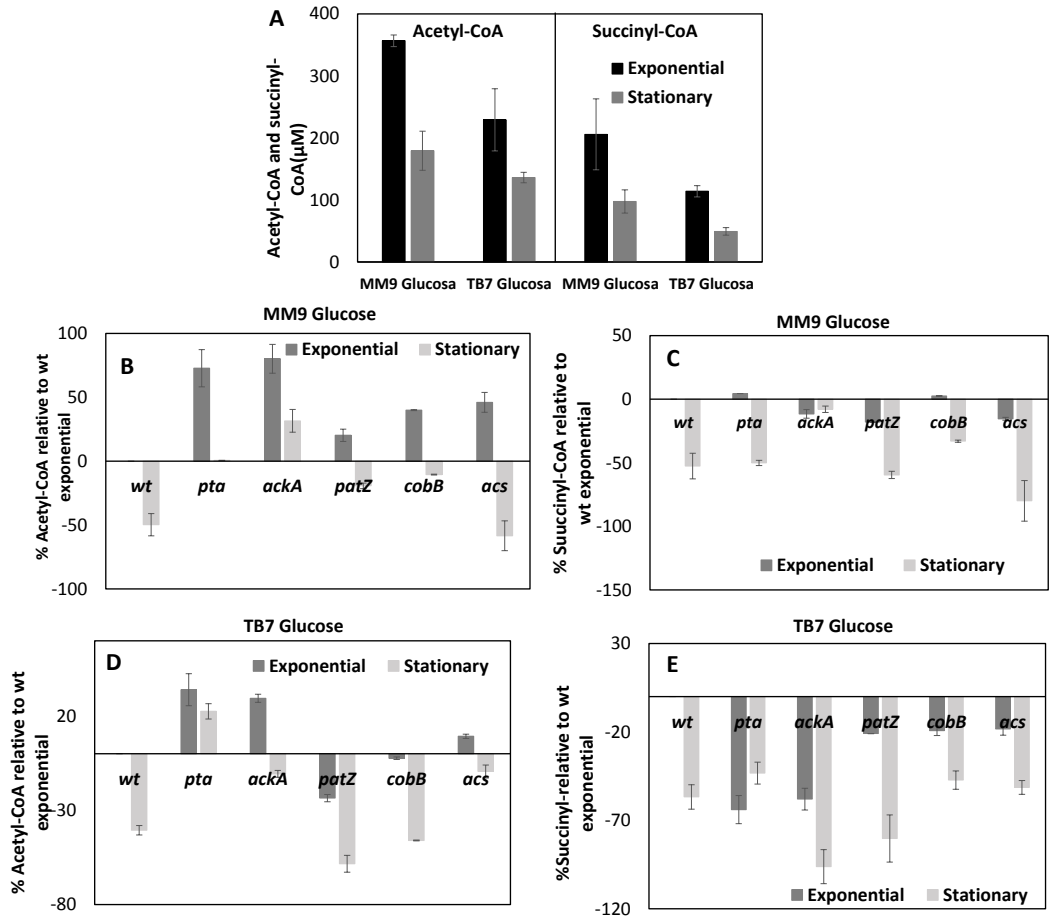

Figure 8. Intracellular acetyl-CoA and succinyl-CoA concentrations. **(A)** *E. coli* wt intracellular acetyl-CoA and succinyl-CoA concentrations in exponential and stationary phases grown in minimal and complex TB7 medium supplemented with glucose as carbon source. **(B)** Acetyl-CoA contrentration in wt and knockout grown in minimal medium was expressed as a percentage of wt strain concentration in the exponential growth phase. **(C)** Succinyl-CoA contrentration in wt and knockout grown in minimal medium was expressed as a percentage of wt strain concentration in the exponential growth phase. **(D)** Acetyl-CoA contrentration in wt and knockout grown in complex TB7 medium was expressed as a percentage of wt strain concentration in the exponential growth phase. **(E)** Succinyl-CoA contrentration in wt and knockout grown in complex TB7 medium was expressed as a percentage of wt strain concentration in the exponential growth phase.

Lysine acetylation is not directly related with intracellular pH in *Escherichia coli*

To test protein lysine acetylation in the studied strains growing in the different conditions used, western blot assays were carried out employing an anti-acetyl Lys antibody. The western blots are depicted in Figure 9. *E. coli* wt strain showed a higher degree of acetylation growing in minimal medium than in TB7 complex medium with a predominant band at approximately 70 kDa. Moreover, acetylation was more intense in cultures supplemented with glycerol than in those containing glucose. No differences were observed between the exponential and stationary growth phases. Δ*patZ*, Δ*cobB* and Δ*acs* showed a similar profile to

wt, with a higher degree of acetylation in minimal medium, although *cobB* and *acs* deletion strains showed a more intense predominant band. However, a different profile was observed for the western blots of *pta* and *ackA* knockouts western blots. Thus, while Δ*pta* showed a very low degree of acetylation in all the cultures, Δ*ackA* showed a similar acetylation profile to wt in minimal medium, but a higher acetylation level in TB7.

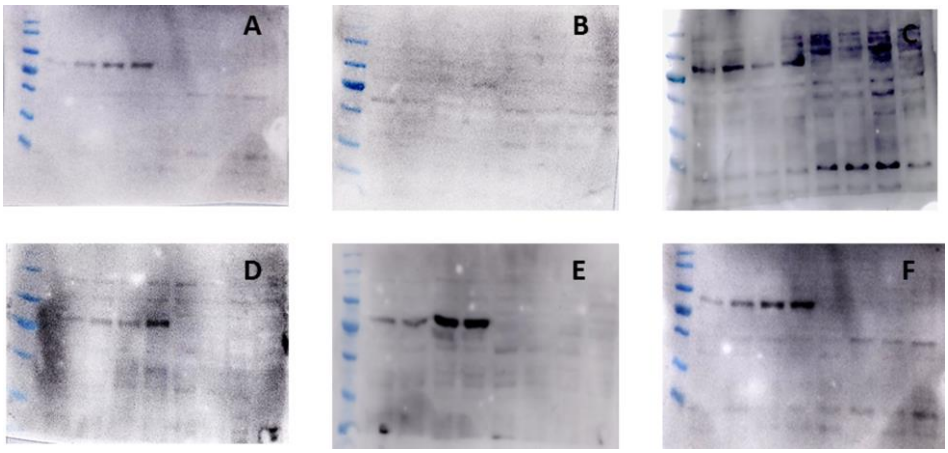

Figure 9. Anti-acetyl Lys immunoblot of wt **(A)**, Δ*pta* **(B)**, Δ*ackA* **(C)**, Δ*patZ* **(D)**, Δ*cobB* and **(E)** Δ*acs* **(F)**. Lane 1: molecular weight marker. Lanes 2 and 3: MM9 supplemented with glucose in exponential and stationary growth phases, respectively. Lanes 4 and 5: MM9 supplemented with glycerol in exponential and stationary growth phase, respectively. Lanes 6 and 7: TB7 supplemented with glucose in exponential and stationary growth phase, respectively, lane 8 and 9: TB7 supplemented with glycerol in exponential and stationary growth phase, respectively.

Discussion

Acetate metabolism has been widely studied in *E. coli* due to the biotechnological importance of acetate overflow and the link between acetate metabolism and post-translational lysine acetylation [10,13,27,31–33]. The relation between carbon flux and acetylation in *E. coli* has been studied recently [34,35], revealing that acetyl-phosphate-dependent acetylation is a response to carbon flux in glucose-supplemented cultures. However, the influence of carbon and nitrogen source on acetate overflow, intracellular pH and acetyl donor concentration, the major players in non-enzymatic lysine acetylation, had not been studied previously. Here, we present a complete study about how carbon and nitrogen sources affect acetate metabolism in *E. coli*.

E. coli wt and Δ*pta*, Δ*ackA*, Δ*patZ*, Δ*cobB* and Δacs knockouts were physiologically characterized growing in minimal medium MM9 (ammonium as nitrogen source) and TB7 complex medium (peptide as nitrogen source) supplemented with glucose (PTS carbon source) and glycerol (non-PTS carbon source). As expected, wt strain showed a higher μ_{max} growing in

the presence of glucose than with glycerol as carbon source (Table 1). The main drawback of using glycerol as carbon source in *E. coli* biotechnological processes is the lower growth rate than glucose cultures [36]. Due to the great interest shown in using glycerol as a carbon source, several authors have tried to solve this low growth rate [37,38]. In the present study, the decreased in glycerol μ_{max} in minimal medium (ammonium as nitrogen source) was about 43 % and only about a 21 % in TB7 complex medium (peptides as nitrogen source). This result suggests that glucose is a better carbon source when ammonium is the source of nitrogen than when a non-ammonium source is used, in agreement with a recently study reported by Bren et al. [9]. The authors suggested an alteration in cAMP concentrations for peptide-based media that hinders glucose consumption. Regarding knockouts μ_{max}, glycerol cultures showed lower growth rate than glucose, as in the case of wt strain (Table 1). The maximal growth rate was higher for complex medium than minimal medium in all cultures. The high growth rate observed for TB7 cultures was surprising since the preferred nitrogen source of *E. coli* is inorganic ammonium. However, biomass yield ($Y_{x/s}$) was not higher in TB7 than in MM9 medium and the carbon consumption rate was much higher (Table 2). These results suggest that *E. coli* grown with peptides as nitrogen source consumes the carbon source faster than with inorganic ammonium, but this carbon consumption is not reflected in biomass yield. This increase in glucose consumption rate in TB7 has been recently reported [35]. The high extracellular acetate levels detected in all TB7 cultures suggest a loss of carbon and energy through acetate overflow, which would explain the low biomass yield of *E. coli* cultures growing in peptide-based media. Of particular interest was the behaviour of Δ*cobB* and Δ*acs* knockouts in which μ_{max}, $Y_{x/s}$ and qs differed greatly from the values observed in wt. These differences were even more evident in glycerol cultures, which suggest the particular relevance of these enzymes in this carbon source. The similar behaviour observed for *acs* and *cobB* deletion strains is in agreement with Acs regulation by CobB sirtuin. Thus, in the absence of CobB, Acs will be totally or partially inhibited, so strain physiology will be similar to Δ*acs* knockout [39].

E. coli cells excrete acetic acid as an extracellular co-product of aerobic fermentations. So, the acetate concentration will be directly related with the cell growth rate and carbon consumption rate. However, extracellular acetate is undesirable because it retards cell growth, inhibits protein formation and represents a loss of carbon and energy that might otherwise could be invested generating biomass [33]. An extracellular acetate concentration of 16.6 mM was detected for *E. coli* wt strain growing in minimal medium supplemented with glucose (Figure 3). This acetate was reincorporated in the intracellular medium when the glucose had been consumed. However, acetate overflow was nearly null growing in minimal medium with glycerol

(Figure 2). This low level of acetate production when glycerol was the only carbon source has previously been reported by other authors [23,40], who suggested that low or no acetate production may be due to an overexpression of *poxB* and *acs* genes. Thus, Acs overexpression would prevent acetate accumulation *via* PoxB (pyruvate oxidase). Moreover, some glyoxylate genes have also been reported to be overexpressed in these conditions, which may induce the rapid consumption of acetate by glyoxylate enzymes [23,41]. When grown in complex TB7 medium, *E. coli* wt showed a high extracellular acetate concentration, although acetate accumulation was lower in glycerol than in glucose, again perhaps due to *acs* and *poxB* overexpression. For their part, *pta* and *ackA* knockout strains showed lower acetate concentrations than wt in all conditions assayed, demonstrating the important role of the Pta-AckA pathway in acetate overflow [42]. The *acs* and *cobB* deletion strains showed a similar acetate concentration to wt in glucose minimal medium and in complex TB7 medium, which suggests the little importance of this acetate assimilation route in *E. coli* under these conditions (Figure 3). However a higher acetate concentration was observed in Δ*acs* and Δ*cobB* derivative strain grown in minimal medium supplemented with glycerol, which is in agreement with the above mentioned suggesting an overexpression of *acs* [23,40].

Intracellular pH homeostasis is a crucial factor in the regulation of cell function maintaining an optimal pH, which is necessary for a variety of cellular functions including proteins. *E. coli* is a neutralophile bacterium that can grow at external pH values of ~ 5.5–9.0, while the intracellular pH values must be in a narrow range of ~ 7.5–7.7 [43,44]. Several studies have revealed how *E. coli* is able to quickly recover cytoplasmic pH homeostasis after an acid or basic stress [25,26,45,46]. However, to our knowledge, there has been no study that monitored-continuously the intracellular pH during the growth of *E. coli* in a culture. In this study, the intracellular *E. coli* pH was determined in cultures growing in MM9 or TB7 supplemented with glucose or glycerol as carbon source. The results showed a surprisingly high intracellular pH for glucose cultures, which reached values of 8.5-9 in the exponential growth phase. However, glycerol cultures had a stronger regulation of intracellular pH, keeping the values at 6.5-7.5 (Figure 5). This result demonstrates the metabolic dependence between carbon source and pH homeostasis in *E. coli*, which had not been described previously. *E. coli* pH homeostasis is carried out by different molecular mechanisms, the major strategy being the use of transporters that catalyse active proton transport, such as primary proton pumps and secondary active transporters (cation/proton antiporters) [47–49]. The second most important pH homeostasis system involves metabolic readjustments such as increased transcription of hydrogenases, decarboxylases and deaminases enzymes [50–55]. Due to the diversity of such strategies to

maintain pH homeostasis in *E. coli*, their regulation is complex. RpoS/σS is the alternative sigma factor, a subunit of RNA polymerase, which acts as the master regulator of the general stress response in *E. coli.* RpoS regulates the transcription of a significant fraction of genes related to sugar metabolism and polyamine metabolism in response to cellular stresses, and it also has an important role in nucleic acid synthesis [56]. Some important factors for pH homeostasis have been reported to be regulated by RpoS, such as glutamate descarboxylase (GadA and GadB) and the regulator GadX, and some proton transport systems [57–59]. Thus, under stress conditions, such as the limited availability of carbon, RpoS and the signal molecule cAMP are the major players in the regulation of transcription [58]. The overexpression of *rpoS* in *E. coli* growing in minimal medium supplemented with glycerol as the only carbon source has been reported [23,57,58,60]. Thus, under these conditions some members of RpoS regulon will be also overexpressed, such as some pH control systems, which agrees with the high intracellular pH homeostasis observed in this study for *E. coli* growing with glycerol as carbon source in both minimal and complex medium (Figure 5).

Non-enzymatic lysine acetylation is a non-catalysed protein modification system that is directly dependent on lysine deprotonation. The pka for a lysine N-ε residue is about 10.5, so a high pH will facilitate lysine acetylation in a non-enzymatic way. This has been studied in the case of mitochondrial proteins [61,62], which mitochondrial pH (pH 8) has been demonstrated to be sufficient to cause mitochondrial proteins acetylation and succinylation [63]. To evaluate whether the high intracellular pH reported for *E. coli* bacteria growing with glucose as carbon source influenced lysine acylation, the acetyl-phosphate, acetyl-CoA and succinyl-CoA concentrations were determined, and lysine acetylation was evaluated by western blot.

Acetyl-phosphate concentrations were higher in minimal medium than in complex TB7 medium (7.5 times higher for wt in the exponential growth phase) (Figure 7). Moreover, acetyl-phosphate concentrations were very similar for all cultures in minimal medium (similar concentration in exponential and stationary growth phases), while in TB7, concentrations were very low in the exponential growth phase (7 times higher concentration in the exponential phase than in wt stationary growth phase). This result highlights the metabolic differences that exist according to the nitrogen carbon source. In minimal medium, the low acetyl-phosphate concentrations detected in *ackA* and *pta* deletion strains may be due to the AckA-Pta blockage pathway, in agreement with the low extracellular acetate level detected. The low level of acetyl-phosphate quantified in exponential TB7 samples may be due to the high level of acetate excreted in all cultures which would avoid acetyl-phosphate accumulation. Thus, in the stationary growth phase, when acetate is reincorporated, acetyl-phosphate concentrations are

higher. Some previous studies have reported intracellular acetyl-phosphate concentrations in *E. coli* [27,64–67] with different conclusions. Thus, acetyl-phosphate concentrations were reported for the first time in 1994 for *E. coli* wt and for *pta* and *ackA* deletion strains. The authors observed a concentration of about 0.3 mM for wt strain in TB complex medium. Δ*ackA* showed a concentration similar to that of wt, while Δ*pta* showed lower acetyl-phosphate concentrations [64]. Higher acetyl-phosphate concentrations (3 mM) were reported for *E. coli* wt by Klein et al. (2007) [65]. Weinert et al. (2013), observed high *ackA* acetyl-phosphate concentrations compared to wt and acetyl-phosphate accumulation in growth-arrested cells [27].

Similar to acetyl-phosphate, acetyl-CoA and succinyl-CoA concentrations were higher in minimal than in complex medium (Figure 8). However, unlike in the case of acetyl-phosphate, the acetyl-CoA and succinyl-CoA concentrations were higher in the exponential growth phase. Finally, succinyl-CoA concentrations were lower than those of acetyl-CoA. The *pta* and *ackA* deletion strains showed high acetyl-CoA concentrations in both minimal and complex medium. This result, together with the low acetyl-phosphate concentrations observed in MM9, suggests that AckA-Pta pathway blockage triggers acetyl-CoA accumulation. *E. coli* acetyl-CoA and succinyl-CoA concentrations have been poorly studied [64,67], although previous reported concentrations (300-600 µM for acetyl-CoA and 200 µM for succinyl-CoA) in agreement with those reported in this study.

Western blot were carried out to evaluate the acetylation level of *E. coli* wt and Δ*pta*, Δ*ackA*, Δ*patZ*, Δ*cobB* and Δacs knockouts growing in MM9 or TB7 supplemented with glucose or glycerol (Figure 9). *E. coli* wt, *ackA*, *patZ*, *cobB* and *acs* deletions strains showed a similar acetylation profile in MM9 medium, with a higher level of lysine acetylation in glycerol than glucose as carbon source. A~70 kDa acetylated protein band was observed in all cases. Although acetyl-CoA and acetyl-phosphate concentrations were not determined for the glycerol cultures, the higher degree of acetylation observed might be a consequence of higher acetyl donor concentrations, which could be explained by the low acetate concentration detected in the extracellular medium (Figure 3). However, Δ*pta* strain showed a very low acetylation level, in agreement with the low acetyl-phosphate concentrations detected in this strain. For the all strains acetylation was lower in TB7 complex medium than in minimal MM9, similar to the lower acetyl-CoA and acetyl-phosphate concentrations, except in the case of *ackA* deletion strain. Δ*ackA* showed a high degree of acetylation in TB7 medium in agreement with the high acetyl-phosphate detected. High Δ*ackA* and low Δ*pta* acetylation levels have been previously reported by other authors [31,68]. No-relation between intracellular pH and acetylation level was found

in this study, which suggests that non-enzymatic acetylation is not directly related with intracellular pH in *E. coli*.

The results presented in this study demonstrate the influence of the carbon and nitrogen source on *E. coli* metabolism and the link between carbon uptake and nitrogen assimilation. Nitrogen and carbon sources are directly related with the acetate metabolism in *E. coli.* Reflecting this, acetate excretion was higher with glucose PTS carbon source than with glycerol, and the use of peptides as nitrogen source induced higher growth rate and carbon consumption rate but not an increase in biomass yield. This breakdown may be due to an increase in the acetate overflow flux, which would provoke a loss of energy in the cell. Intracellular pH during *E. coli* growth with different carbon and nitrogen sources was evaluated in this work for the first time. We conclude that pH homeostasis is strongly influenced by carbon source. The surprisingly high intracellular pH change observed in glucose cultures which contrast with glycerol intracellular pH control, confirms glycerol as an ideal carbon source for cultures carried out with acid or alkaline pH. Finally, lysine acetylation in *E. coli* also is influenced by components of the medium, although intracellular pH does not seem play a large part in this respect.

References

1. Lowry OH, Carter J, Ward JB, Glaser L. The effect of carbon and nitrogen sources on the level of metabolic intermediates in *Escherichia coli*. J Biol Chem. 1971;246: 6511–6521. doi:10.1007/s13213-011-0241-6

2. Görke B, Stülke J. Carbon catabolite repression in bacteria: many ways to make the most out of nutrients. Nat Rev Microbiol. 2008;6: 613–624. doi:10.1038/nrmicro1932

3. Vasudevan PT, Briggs M. Biodiesel production—current state of the art and challenges. J Ind Microbiol Biotechnol. 2008;35: 421–430. doi:10.1007/s10295-008-0312-2

4. Clomburg JM, Gonzalez R. Anaerobic fermentation of glycerol: a platform for renewable fuels and chemicals. Trends Biotechnol. 2013;31: 20–28. doi:10.1016/j.tibtech.2012.10.006

5. Reitzer L. Nitrogen assimilation and global regulation in *Escherichia coli*. Annu Rev Microbiol. 2003;57: 155–176. doi:10.1146/annurev.micro.57.030502.090820

6. Commichau FM, Forchhammer K, Stülke J. Regulatory links between carbon and nitrogen metabolism. Curr Opin Microbiol. 2006;9: 167–172. doi:10.1016/j.mib.2006.01.001

7. Magasanik B. The regulation of nitrogen utilization in enteric bacteria. J Cell Biochem. 1993;51: 34–40. doi:10.1002/jcb.240510108

8. Doucette CD, Schwab DJ, Wingreen NS, Rabinowitz JD. α-ketoglutarate coordinates carbon and nitrogen utilization *via* enzyme I inhibition. Nat Chem Biol. 2012;7: 894–901. doi:10.1038/nchembio.685

9. Bren A, Park JO, Towbin BD, Dekel E, Rabinowitz JD, Alon U. Glucose becomes one of the worst carbon sources for *E. coli* on poor nitrogen sources due to suboptimal levels of cAMP. Sci Rep. 2016;6: 2–11. doi:10.1038/srep24834

10. Bernal V, Castaño-Cerezo S, Cánovas M. Acetate metabolism regulation in *Escherichia coli*: carbon overflow, pathogenicity, and beyond. Appl Microbiol Biotechnol. 2016;100: 8985–9001. doi:10.1007/s00253-016-7832-x

11. De Mey M, De Maeseneire S, Soetaert W, Vandamme E. Minimizing acetate formation in *E. coli* fermentations. J Ind Microbiol Biotechnol. 2007;34: 689–700. doi:10.1007/s10295-007-0244-2

12. Hädicke O, Bettenbrock K, Klamt S. Enforced ATP futile cycling increases specific productivity and yield of anaerobic lactate production in *Escherichia coli*. Biotechnol Bioeng. 2015;112: 2195–2199. doi:10.1002/bit.25623

13. Castaño-Cerezo S, Bernal V, Röhrig T, Termeer S, Cánovas M. Regulation of acetate metabolism in *Escherichia coli* BL21 by protein N-lysine acetylation. Appl Microbiol Biotechnol. 2015;99: 3533–3545. doi:10.1007/s00253-014-6280-8

14. Castaño-Cerezo S, Pastor JM, Renilla S, Bernal V, Iborra JL, Cánovas M. An insight into the role of phosphotransacetylase (pta) and the acetate/acetyl-CoA node in *Escherichia coli*. Microb Cell Fact. 2009;8: 2109–2124. doi:10.1186/1475-2859-8-54

15. Kakuda H, Hosono K, Ichihara S. Identification and characterization of the *ackA* (acetate kinase a)-*pta* (phosphotransacetylase) operon and complementation analysis of acetate utilization by an *ackA*-*pta* deletion mutant of *Escherichia coli*. J Biochem. 1994;116: 916–922. doi:10.1093/oxfordjournals.jbchem.a124616

16. de Diego T, Gallego-Jara J, Castaño-Cerezo S, Bernal Sánchez V, Fernández Espín V, García de la Torre J, et al. The protein acetyltransferase PatZ from *Escherichia coli* is regulated by autoacetylation- induced oligomerization. J Biol Chem. 2015;53: 1689–1699. doi:10.1017/CBO9781107415324.004

17. Zhao K, Chai X, Marmorstein R. Structure and substrate binding properties of CobB, a Sir2 homolog protein deacetylase from *Escherichia coli*. J Mol Biol. 2004;337: 731–741. doi:10.1016/j.jmb.2004.01.060

18. Kumari S, Tishel R, Eisenbach M, Wolfe AJ. Cloning, characterization, and functional expression of *acs*, the gene which encodes acetyl Coenzyme A synthetase in *Escherichia coli*. J Bacteriol. 1995;177: 2878–2886.

19. Starai VJ, Celic I, Cole RN, Boeke JD, Escalante-Semerena JC. Sir2-dependent activation of acetyl-CoA synthetase by deacetylation of active lysine. Science. 2002;298: 2390–2392. doi:10.1126/science.1077650

20. Baba T, Ara T, Hasegawa M, Takai Y, Okumura Y, Baba M, et al. Construction of *Escherichia coli* K-12 in-frame, single-gene knockout mutants: the Keio collection. Mol Syst Biol. 2006;2: 1–11. doi:10.1038/msb4100050

21. Castaño-Cerezo S, Bernal V, Blanco-Catalá J, Iborra JL, Cánovas M. cAMP-CRP coordinates the expression of the protein acetylation pathway with central metabolism in *Escherichia coli*. Mol Microbiol. 2011;82: 1110–1128. doi:10.1111/j.1365-2958.2011.07873.x

22. Sauer UWE, Lasko DR, Fiaux J, Hochuli M, Glaser R, Bailey JE, et al. Metabolic flux ratio analysis of genetic and environmental modulations of *Escherichia coli* central carbon metabolism. J Bacteriol. 1999;181: 6679–6688.

23. Martínez-Gómez K, Flores N, Castañeda HM, Martínez-Batallar G, Hernández-Chávez G, Ramírez OT, et al. New insights into *Escherichia coli* metabolism: Carbon scavenging, acetate metabolism and carbon recycling responses during growth on glycerol. Microb Cell Fact. 2012;11: 1–21. doi:10.1186/1475-2859-11-46

24. Miller Lorenz G. Use of dinitrosalicylic acid reagent for determination of reducing sugar. Anal Chem. 1959;31: 426–428.

25. Martinez K a., Kitko RD, Mershon JP, Adcox HE, Malek K a., Berkmen MB, et al. Cytoplasmic pH response to acid stress in individual cells of *Escherichia coli* and *Bacillus subtilis* observed by fluorescence ratio imaging microscopy. Appl Environ Microbiol. 2012;78: 3706–3714. doi:10.1128/AEM.00354-12

26. Wilks JC, Slonczewski JL. pH of the cytoplasm and periplasm of *Escherichia coli*: Rapid measurement by green fluorescent protein fluorimetry. J Bacteriol. 2007;189: 5601–5607. doi:10.1128/JB.00615-07

27. Weinert BT, Iesmantavicius V, Wagner SA, Schölz C, Gummesson B, Beli P, et al. Acetyl-phosphate is a critical determinant of lysine acetylation in *E. coli*. Mol Cell. 2013;51: 265–272. doi:10.1016/j.molcel.2013.06.003

28. Duportet X, Bastos R, Aggio M, Granato S. The biological interpretation of metabolomic data can be misled by the extraction method used. Metabolomics. 2012;8: 410–421. doi:10.1007/s11306-011-0324-1

29. Neubauer S, Chu DB, Marx H, Sauer M, Hann S, Koellensperger G. LC-MS/MS-based analysis of Coenzyme A and short-chain acyl-Coenzyme A thioesters. Anal Bioanal Chem. 2015;407: 6681–6688. doi:10.1007/s00216-015-8825-9

30. Shiloach J, Fass R. Growing *E. coli* to high cell density,a historical perspective on method development. Biotechnol Adv. 2005;23: 345–357. doi:10.1016/j.biotechadv.2005.04.004

31. Kuhn ML, Zemaitaitis B, Hu LI, Sahu A, Sorensen D, Minasov G, et al. Structural, kinetic and proteomic characterization of acetyl phosphate-dependent bacterial protein acetylation. PLoS One. 2014;9: e94816. doi:10.1371/journal.pone.0094816

32. Castaño-Cerezo S, Bernal V, Post H, Fuhrer T, Cappadona S, Sánchez-Díaz NC, et al. Protein acetylation affects acetate metabolism, motility and acid stress response in *Escherichia coli*. Mol Syst Biol. 2014;10: 1–16. doi:10.15252/msb.20145227

33. Eiteman MA, Altman E. Overcoming acetate in *Escherichia coli* recombinant protein fermentations. Trends Biotechnol. 2006;24: 530–536. doi:10.1016/j.tibtech.2006.09.001

34. Schilling B, Christensen D, Davis R, Sahu AK, Hu LI, Walker-Peddakotla A, et al. Protein acetylation dynamics in response to carbon overflow in *Escherichia coli*. Mol Microbiol. 2015;98: 847–863. doi:10.1111/mmi.13161

35. Christensen DG, Orr JS, Rao C V, Wolfe J. Increasing growth yield and decreasing acetylation in *Escherichia coli* by optimizing the carbon-to-magnesium ratio in peptide-based media. Appl Environ Microbiol. 2017;83: 1–13. doi:10.1128/AEM.03034-16

36. Lin ECC. Glycerol dissimilation and its regulation in bacteria. Annu Rev Microbiol. 1976;30: 535–578. doi:10.1146/annurev.mi.30.100176.002535

37. Applebee MK, Joyce AR, Conrad TM, Pettigrew DW, Palsson B. Functional and metabolic effects of adaptive glycerol kinase (GLPK) mutants in *Escherichia coli*. J Biol Chem. 2011;286: 23150–23159. doi:10.1074/jbc.M110.195305

38. Yao R, Xiong D, Hu H, Wakayama M, Yu W, Zhang X, et al. Elucidation of the co-metabolism of glycerol and glucose in *Escherichia coli* by genetic engineering, transcription profiling, and ^{13}C metabolic flux analysis. Biotechnol Biofuels. BioMed Central; 2016;9: 1–14. doi:10.1186/s13068-016-0591-1

39. Gallego-Jara J, Écija Conesa A, de Diego Puente T, Lozano Terol G, Cánovas Díaz M. Characterization of CobB kinetics and inhibition by nicotinamide. PLoS One. 2017;12: e0189689. doi:10.1371/journal.pone.0189689

40. Peng L, Shimizu K. Global metabolic regulation analysis for *Escherichia coli* K12 based on protein expression by 2-dimensional electrophoresis and enzyme activity measurement. Appl Microbiol Biotechnol. 2003;61: 163–178. doi:10.1007/s00253-002-1202-6

41. Hardiman T, Lemuth K, Keller M a., Reuss M, Siemann-Herzberg M. Topology of the global regulatory network of carbon limitation in *Escherichia coli*. J Biotechnol. 2007;132: 359–374. doi:10.1016/j.jbiotec.2007.08.029

42. Renilla S, Bernal V, Fuhrer T, Castaño-Cerezo S, Pastor JM, Iborra JL, et al. An insight into the role of phosphotransacetylase (pta) and the acetate/acetyl-CoA node in *Escherichia coli*. Microb Cell Fact. 2009;8: 2109–2124. doi:10.1007/s00253-011-3536-4

43. Slonczewski JL, Rosen BP, Alger JR, Macnab RM. pH homeostasis in *Escherichia coli*: measurement by ^{31}P nuclear magnetic resonance of methylphosphonate and phosphate. Proc Natl Acad Sci. 1981;78: 6271–6275. doi:10.1073/pnas.78.10.6271

44. Zilberstein D, Agmon V, Schuldiner S, Padan E. *Escherichia coli* intracellular pH, membrane potential, and cell growth. J Bacteriol. 1984;158: 246–252.

45. Slonczewski JL, Fujisawa M, Dopson M, Krulwich TA. Cytoplasmic pH measurement and

homeostasis in bacteria and archaea. Adv Microb Physiol. 2009;55: 1–79. doi:10.1016/S0065-2911(09)05501-5

46. Etana Padan, Eitan Bibi, Masahiro Ito T a. K. Alkaline pH homeostasis in bacteria : new insights. Biochim Biophys Acta. 2005;1717: 67–88. doi:10.1016/j.bbamem.2005.09.010

47. Taglicht D, Padan E, Schuldiner S. Proton-sodium stoichiometry of NhaA, an electrogenic antiporter from *Escherichia coli*. J Biol Chem. 1993;268: 5382–5387.

48. Mesbah NM, Cook GM, Wiegel J. The halophilic alkalithermophile *Natranaerobius thermophilus* adapts to multiple environmental extremes using a large repertoire of $Na^+(K^+)/H^+$ antiporters. Mol Microbiol. 2009;74: 270–281. doi:10.1111/j.1365-2958.2009.06845.x

49. Kakinuma Y. Inorganic cation transport and energy transduction in *Enterococcus hirae* and other streptococci. Microbiol Mol Biol Rev. 1998;62: 1021–1045.

50. Blankenhorn D, Phillips J, Slonczewski JL. Acid- and base-induced proteins during aerobic and anaerobic growth of *Escherichia coli* revealed by two-dimensional gel electrophoresis. J Bacteriol. 1999;181: 2209–2216.

51. Yohannes E, Barnhart DM, Slonczewski JL. pH-dependent catabolic protein expression during anaerobic growth of *Escherichia coli* K-12. J Bacteriol. 2004;186: 192–199. doi:10.1128/JB.186.1.192

52. Maurer LM, Yohannes E, Bondurant SS, Radmacher M, Slonczewski JL. pH regulates genes for flagellar motility , catabolism , and oxidative stress in *Escherichia coli* K-12. J Bacteriol. 2005;187: 304–319. doi:10.1128/JB.187.1.304

53. Kanjee U, Houry W a. Mechanisms of acid resistance in *Escherichia coli*. Annu Rev Microbiol. 2013;67: 65–81. doi:10.1146/annurev-micro-092412-155708

54. Ave H, Angeles L. Molecular aspects of bacterial pH sensing and homeostasis. Nat rev Microbiol. 2011;9: 330–343. doi:10.1038/nrmicro2549

55. Noguchi K, Riggins DP, Eldahan KC, Kitko RD, Slonczewski JL. Hydrogenase-3 contributes to anaerobic acid resistance of *Escherichia coli*. PLoS One. 2010;5: e10132. doi:10.1371/journal.pone.0010132

56. Maciag A, Peano C, Pietrelli A, Egli T, De Bellis G, Landini P. *In vitro* transcription profiling of the σS subunit of bacterial RNA polymerase: re-definition of the σS regulon and identification of σS-specific promoter sequence elements. Nucleic Acids Res. 2011;39: 5338–55. doi:10.1093/nar/gkr129

57. Patten CL, Kirchhof MG, Schertzberg MR, Morton R a., Schellhorn HE. Microarray analysis of RpoS-mediated gene expression in *Escherichia coli* K-12. Mol Genet Genomics. 2004;272: 580–591. doi:10.1007/s00438-004-1089-2

58. Franchini AG, Ihssen J, Egli T. Effect of global regulators RpoS and cyclic-AMP/CRP on the catabolome and transcriptome of *Escherichia coli* K12 during carbon- and energy-limited growth. PLoS One. 2015;10: e0133793. doi:10.1371/journal.pone.0133793

59. Dong T, Kirchhof MG, Schellhorn HE. RpoS regulation of gene expression during exponential growth of *Escherichia coli* K12. Mol Genet Genomics. 2008;279: 267–277. doi:10.1007/s00438-007-0311-4

60. Dong T, Schellhorn HE. Control of RpoS in global gene expression of *Escherichia coli* in minimal media. Mol Genet Genomics. 2009;281: 19–33. doi:10.1007/s00438-008-0389-

3

61. Llopis J, McCaffery JM, Miyawaki A, Farquhar MG, Tsien RY. Measurement of cytosolic, mitochondrial, and Golgi pH in single living cells with green fluorescent proteins. Proc Natl Acad Sci. 1998;95: 6803–6808. doi:10.1073/pnas.95.12.6803

62. Cano Abad MF, Di Benedetto G, Magalhães PJ, Filippin L, Pozzan T. Mitochondrial pH monitored by a new engineered green fluorescent protein mutant. J Biol Chem. 2004;279: 11521–11529. doi:10.1074/jbc.M306766200

63. Wagner GR, Payne RM. Widespread and enzyme-independent Nε-acetylation and Nε-succinylation of proteins in the chemical conditions of the mitochondrial matrix. J Biol Chem. 2013;288: 29036–29045. doi:10.1074/jbc.M113.486753

64. Prüβ BM, Wolfe AJ. Regulation of acetyl phosphate synthesis and degradation, and the control of flagellar expression in *Escherichia coli*. Mol Microbiol. 1994;12: 973–984. doi:10.1111/j.1365-2958.1994.tb01085.x

65. Klein AH, Shulla A, Reimann S a, Keating DH, Wolfe AJ. The intracellular concentration of acetyl phosphate in *Escherichia coli* is sufficient for direct phosphorylation of two-component response regulators. J Bacteriol. 2007;189: 5574–81. doi:10.1128/JB.00564-07

66. Keating DH, Shulla A, Klein AH, Wolfe AJ. Optimized two-dimensional thin layer chromatography to monitor the intracellular concentration of acetyl phosphate and other small phosphorylated molecules. Biol Proced Online. 2008;10: 36–46. doi:10.1251/bpo141

67. Bennett BD, Kimball EH, Gao M, Osterhout R, Van SJ, Rabinowitz JD. Absolute metabolite concentrations and implied enzyme active site occupancy in *Escherichia coli*. Nat Chem Biol. 2010;5: 593–599. doi:10.1038/nchembio.186

68. Schilling B, Christensen D, Davis R, Sahu AK, Hu LI, Walker-Peddakotla A, et al. Protein acetylation dynamics in response to carbon overflow in *Escherichia coli*. Mol Microbiol. 2015;98: 847–863. doi:10.1111/mmi.13161

Appendix

Table S1. Strains used in this study.

E. coli strain	Genotype	Source
BW25113	*lacI* q *rrnB*T14 D*lacZ*WJ16 *hsdR*514 D(*araBAD*)AH33 D(*rhaBAD*)LD78	Keio collection [20]
BW25113 Δ*pta*	[BW25113] *pta:kan*	Keio collection [20]
BW25113 Δ*ackA*	[BW25113] *ackA:kan*	Keio collection [20]
BW25113 Δ*patZ*	[BW25113] *patZ:kan*	Keio collection [20]
BW25113 Δ*cobB*	[BW25113] *cobB:kan*	Keio collection [20]
BW25113 Δ*acs*	[BW25113] *acs:kan*	Keio collection [20]

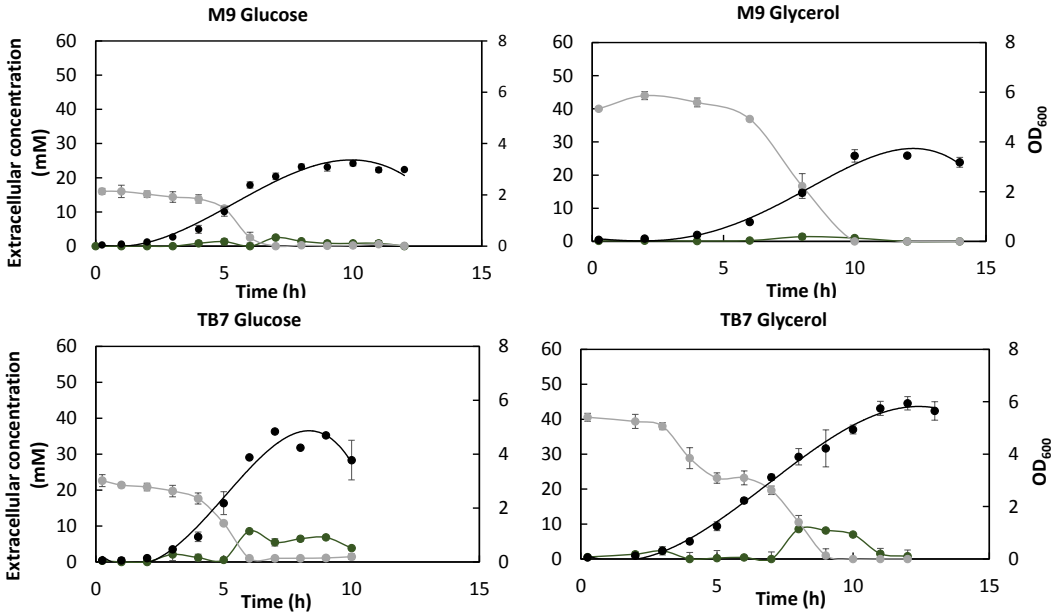

Figure S1. *E. coli pta* deletion strain growth (black), extracellular acetate (green) and glucose or glycerol consumption (grey) graphs.

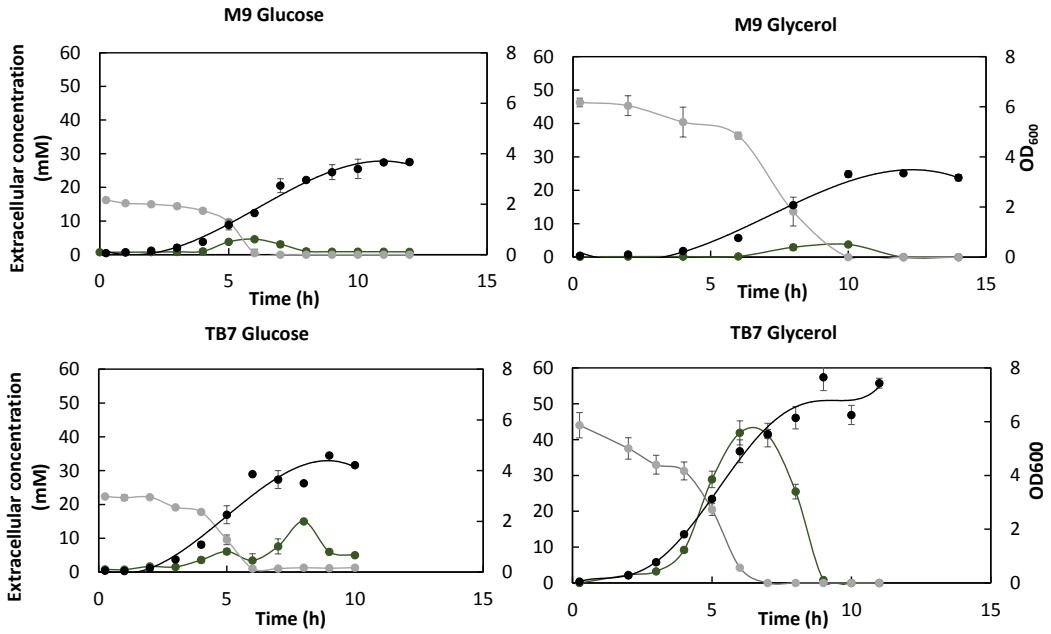

Figure S2. *E. coli ackA* deletion strain growth (black), extracellular acetate (green) and glucose or glycerol consumption (grey) graphs.

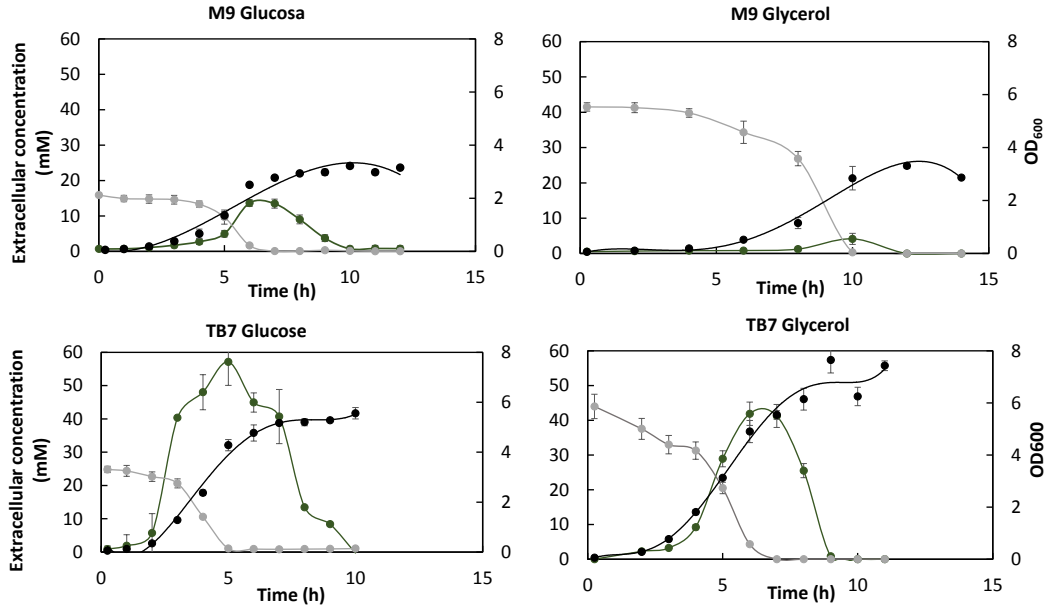

Figure S3. *E. coli patZ* deletion strain growth (black), extracellular acetate (green) and glucose or glycerol consumption (grey) graphs.

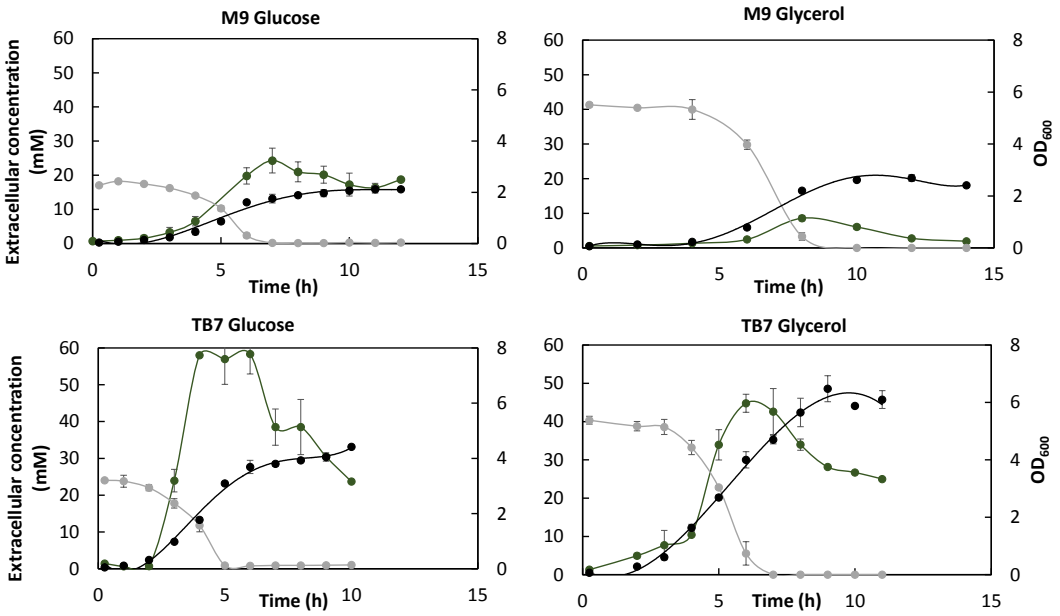

Figure S4. *E. coli cobB* deletion strain growth (black), extracellular acetate (green) and glucose or glycerol consumption (grey) graphs.

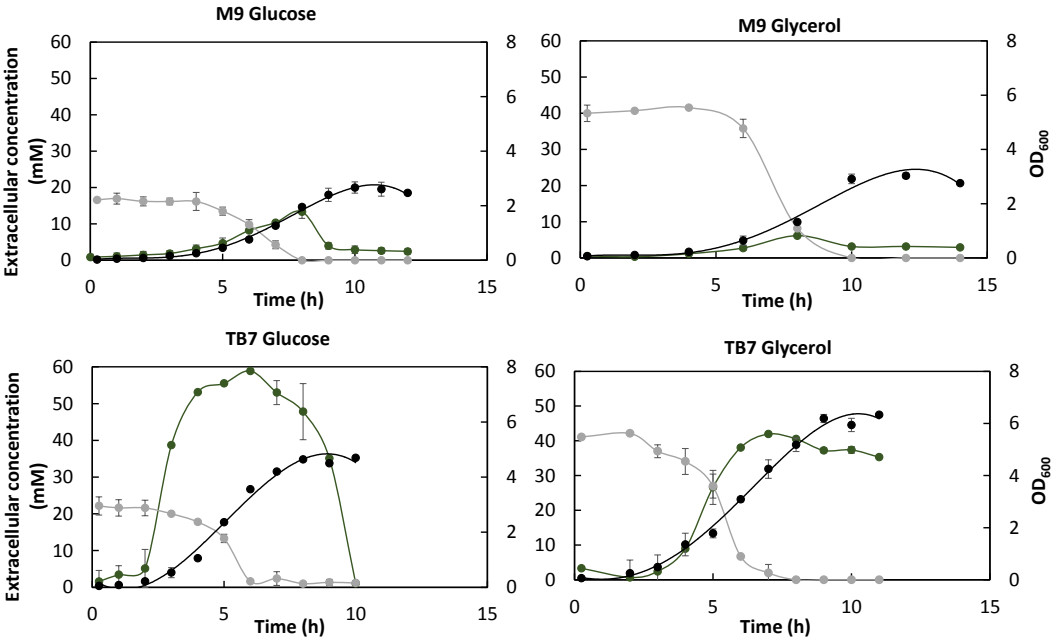

Figure S5. *E. coli acs* deletion strain growth (black), extracellular acetate (green) and glucose or glycerol consumption (grey) graphs.

CHAPTER 8

Final discussion and conclusions

Final discussion

The main aim of this PhD thesis has been to increase our understanding of acetate metabolism in *Escherichia coli* (*E. coli*). *E. coli* acetate metabolism regulation is very important for obtaining an optimized biotechnological strain. In chapters 4 and 5, biochemical characterization of PatZ (also known PkA ad YfiQ) and CobB enzymes was carried out. These enzymes are the most studied acetyltransferase and deacetylase from *E. coli*, respectively, and are responsible for regulating the acetyl-CoA synthetase (Acs) activity. Acs catalyses one of the pathways responsible for acetate reincorporation in *E. coli* and its importance has been widely demonstrated in the physiological characterization of the strain lacking *acs* gene (chapters 5 and 7). Acs has also been biochemically studied and important insights into the catalytic mechanism and acetylation/deacetylation regulation have been achieved (chapter 6). Finally, the influence of carbon and nitrogen source on acetate metabolism and lysine acetylation was analysed. Glucose and glycerol as carbon sources and ammonium and peptides as nitrogen sources were compared and several differences in acetate overflow, intracellular pH and lysine acetylation were observed (chapter 7). Results have been widely discussed in previous chapters, however, to get a global vision of all them, a final discussion is presented below.

Bacteria are ideal models for studying many fundamental aspects of biochemistry and molecular biology. In biotechnology *E. coli* is considered the most important model organism because of its simplicity, extensive knowledge of its metabolism, great adaptability and catabolic flexibility in different culture conditions (carbon source, nitrogen source, oxygen availability, and temperature) and fast growth rate. Moreover, the development of modern molecular biology tools has made it possible to produce the recombinant proteins and other bio-products in *E. coli* that are essential for industry today. For example, terpenoids are high-value compounds with many applications as flavoring agents, fragrances, disinfectants, agrochemicals, pharmaceuticals, and nutraceuticals [1]. Lycopene is a tetraterpenoid with several applications in pharmacology [2–7]. However, in spite of its great importance, most lycopene is obtained from tomato, and no competitive biotechnological process exists for its production. In chapter 3 of this PhD thesis an *in situ* semi-continuous lycopene extraction method using *E. coli* has been developed. The aim of this chapter was to develop a competitive lycopene production model and to illustrate the potential role of *E. coli* as a model system for obtaining high-value products. Genetic engineering strategies to construct an *E. coli* strain that overproduces lycopene were carried out. Plasmid combination, isopropyl β-D-1-thiogalactopyranoside (IPTG) concentration

and carbon source were optimized and a maximum and specific lycopene production of 37.56 ± 1.41 mg L^{-1} and 25.34 ±1.2 mg g $cell^{-1}$ were obtained. Using glycerol as carbon source cell growth was lower and lycopene production was higher. The improvements observed with glycerol compared with glucose were more deeply studied in chapter 7, where *E. coli* growing with glycerol as carbon source led to a lower level of carbon waste probably due to the minimized acetate overflow. One of the main limitations for biotechnological lycopene production is the limit to lycopene storage in the bacterial membrane [8,9]. For this reason an *in situ* extraction to prevent accumulation in the cell membrane was developed. To achieve this objective, a two-phase culture system was used with octane as organic phase, reaching a lycopene production of 74.71 ± 3.74 mg L^{-1} or 49.70 ± 2.48 mg g $cell^{-1}$, which is much higher than that obtained from tomato, 0.42 mg g^{-1}, suggesting that this is a promising strategy for its industrial production [10]. The high potential to increase production through genetic engineering and the need to increase our understanding of *E. coli* metabolism and the means to control it have been demonstrated.

Acetate overflow is a great drawback for industrial bioprocesses using *E. coli*, because acetate inhibits cell growth in high density cultures and leads to a loss of metabolic energy and carbon wastage, limiting the yield [11,12]. The acetate metabolism and lysine acetylation are closely related through acetyl-phosphate and acetyl-CoA pools. Moreover, Acs, the protein responsible, together with Pta (phosphotransacetylase) and AcKa (acetate kinase), for acetate reincorporation and conversion into acetyl-CoA, is regulated by acetylation/deacetylation in *E. coli* [13,14]. Chapters 4, 5 and 6 of this dissertation focused on Acs regulation by acetylation.

PatZ is the main acetyltransferase in *E. coli* and its kinetics for Acs acetylation are characterized for the first time in chapter 4. Kinetic analysis showed the positive cooperativity of PatZ towards its substrate acetyl-CoA with a Hill coefficient close to 8 and a Michaelis-Menten behavior in response to Acs concentration. Sixteen acetylated lysines were identified for Acs and a gradual decrease in Acs catalytic activity was observed. *E. coli* acetyl-CoA concentrations were determined in chapter 7 for *E. coli* cultures grown with glucose as carbon source. The results showed that acetyl-CoA concentrations are higher in the exponential than in the stationary growth phase. Moreover, the concentrations (approximately 0.35 mM exponential and 0.15 mM stationary) were around PatZ $K_{0.5}$ (0.185 mM) for acetyl-CoA determined in chapter 4. Therefore, acetyl-CoA intracellular concentrations could regulate Acs activity *in vivo*. These results suggest a mechanism for linking the physiological state of the cell to the acetylation state and activity of Acs. Acs regulation by K609 acetylation/deacetylation was first described in *Salmonella enterica*

(*S. enterica)* in 2002 [14]. In chapter 5 of this dissertation CobB kinetics for Acs deacetylation were characterized. This is the first kinetic characterization of a sirtuin deacetylating a whole native acetylated protein. We demonstrated that Acs was deacetylated by CobB in several acetylated lysines with monophasic kinetics. Moreover, acetylated K609 was not a requirement for CobB recognition, so the results suggest that structural protein components are the main determinants of sirtuin specificity and not acetylated peptide sequence, as previously suggested other researchers [15,16]. Thus, one of the biggest challenges in sirtuin research is to determine how specificity is determined in natively folded substrate proteins, and the study described in this PhD thesis represent an important starting point for such investigations. K609 Acs acetylation leads to a loss of Acs activity, as demonstrated in chapters 4, 5 and 6 of this thesis. Several proteins belonging to the ANL superfamily of adenylating enzymes, as Acs, have been reported to be regulated by acetylation/deacetylation of the A10 motif conserved lysine. Conserved A10 lysine has been observed in several crystal structures interacting with ATP substrate, although the interaction points are not entirely clear. Structures have been resolved with conserved lysine making hydrogen-binding contact with the α-phosphate of the ATP [17–21], with the β-phosphate [22,23] or with both of them [24]; even no-interaction has been observed [25]. In chapter 6, thermodynamic experiments were carried out in order to compare the ATP-binding parameters of deacetylated Acs wt protein with the acetylated Acs wt (ac. wt) protein and K609A Acs mutant protein parameters. Acs wt and ac. wt proteins showed a similar behavior when ATP-binding was studied by isothermal titration calorimetry (ITC). Dissociation constants (Kd) were 14.1 and 17.7 μM for the deacetylated and acetylated proteins, respectively. Specificity constants also were very similar for ATP and acetate substrates. These results suggest that Acs *in vivo* acetylation does not affect specificity and affinity parameters, however, catalytic activity showed a great decrease when Acs was acetylated. When Acs protein with K609 mutated was studied a higher ATP-affinity was observed. The Kd determined was 4.2 μM, 3.3 times lower than wt Kd. This result demonstrates that K609 residue has an important role in ATP-binding and that mutation leads to a different and higher ATP-binding. A similar result was observed for MatB protein from *Rhodopseudomonas palustris* [26]. The fact that K609 mutant shows a higher affinity for ATP than wt might drive us to think that it should have a higher activity, but kinetics characterization for A10 mutated lysine *E. coli* Acs and other ANL proteins has demonstrated that this mutation leads to a loss of activity [20,27–33]. Thus, the observed ATP-binding suggests that this mutant binds ATP in a different way with respect to wt protein, which inhibits the catalytic reaction. The Acs K609A mutant protein ATP-binding will be

studied more deeply in future works to clarify the role of this residue in the adenylating catalytic step. Moreover, the fact that ac. wt protein and K609A mutant showed a different behavior when ATP-binding was studied suggests that alanine mutation does not mimic lysine acetylation correctly. In this way different mutations will be evaluated in order to get a greater protein model to mimic an Acs acetylated protein.

An important part of this PhD thesis has focused on biochemical protein characterization, carrying out structural, kinetic and calorimetric analysis in order to improve our knowledge of PatZ, CobB and Acs enzymes.

In chapter 4 of this dissertation a complete PatZ biochemical characterization has been carried out. PatZ belongs to the GNAT acetytransferases superfamily. Several GNATs have been demonstrated to carry out catalytic activities through conserved glutamic acid activity. In this chapter the role of the PatZ conserved E809 was analysed, concluding that this residue is not relevant for PatZ acetyltransferase activity, as has been demonstrated for other GNATs [34–37]. These results suggest a non-conserved catalytic mechanism for the GNATs superfamily of adenylating enzymes. As regards structural regulation, oligomeric studies showed that PatZ is a stable tetramer in solution and is transformed to its octameric form when acetyl-CoA is present. Native western blot showed that the octameric PatZ structure was acetylated. PatZ autoacetylation kinetics were studied and PatZ octamerization from the tetramer was demonstrated. Moreover, PatZ autoacetylation was reversed by CobB deacetylase *in vitro*, establishing a new substrate for this sirtuin. The reversible autoacetylation of other acetyltransferases has been described previously (46–49), but this study demonstrates, for the first time, the structural regulation of an acetyltransferase by autoacetylation. Finally, an *in silico* structural model for the tetrameric PatZ conformation was developed using bioinformatic tools. This model was validated with the experimental data obtained from PatZ biophysical characterization.

CobB is the most studied lysine deacetylase from *E. coli*. Nowadays, there is a great interest in sirtuins as targets for the treatment of metabolic diseases [38,39] and several studies have addressed the regulation and inhibition of these enzymes. Nicotinamide (NAM), a product of the sirtuin catalytic reaction, is a potent inhibitor for all of these enzymes. CobB inhibition by NAM was studied in chapter 5 of this dissertation. A non-competitive inhibition was established and the inhibitory parameters were determined. Intracellular concentrations of NAM, an intermediate from the *E. coli* NAD^+ salvage pathway, were determined for *E. coli* growing under different conditions. These are, to our knowledge, the first NAM intracellular concentrations

determined in a bacterial organism, and the values detected were high enough to regulate CobB *in vivo*. NAM is synthetized by NMN nucleosidase enzyme and consumed by nicotinamidase (PncA), so we measured nicotinamide concentrations in an *E. coli* strain lacking the *pncA* gene to check whether NAM concentrations were higher. Several physiological aspects of *E. coli* are known to be regulated by CobB, such as acetate overflow through Acs and flagella expression through RcsB deacetylation [13,40–42]. We compared extracellular acetate, flagella expression and migration of *E. coli* wt with the *cobB* and *pncA* deletion strains. The behaviour observed for the mutant strains was very similar, with a higher extracellular acetate concentration and a higher degree of migration and flagella expression than the observed in wt strain. These results suggest that *in vivo* CobB activity depends on NAM concentrations. Due to the high number of enzymes which consume NAD^+, it is necessary to recycle the releasing molecules. The NAD^+ salvage pathway recycles the internally degraded NAD^+ products such as nicotinamide D-ribonucleotide and NAM, and it is used for the assimilation of exogenous NAD^+. CobB, as all sirtuin proteins, consumes NAD^+ as a co-substrate, releasing NAM as a product. Therefore, lysine deacetylation in *E. coli* is closely related to this route, since it allows recycling of the produced nicotinamide, preventing it from accumulating, and allowing the formation of new NAD^+ molecules. The efficacy in the degradation of nicotinamide will depend on the kinetic characteristics of PncA enzyme, which were characterized in this dissertation for the first time in a bacterial organism. The presented results highlight the importance of PncA as a regulator enzyme and a new important metabolic role that prevents NAM accumulation to avoid CobB inhibition. Several questions remain unanswered and a new field of study is opened up concerning the PncA and NAD^+ salvage pathway regulatory role in lysine acetylation in *E. coli*.

In chapter 6 of this PhD thesis Acs protein has been studied. Enzyme kinetics for ATP and acetate substrates and thermodynamics parameters for ATP-binding have been determined. Acs wt parameters were established and compared with Acs mutant proteins parameters. Results showed that D500 and T264 ANL conserved residues are essential for ATP-binding and catalysis. The mutation of these residues led to a great decrease in enzyme specificity, catalytic activity and ATP-affinity. The K270 mutation study showed that this residue has not an important role in specificity and ATP-affinity, although the substitution of this lysine to alanine led to a higher Acs catalytic activity, which might be due to the loss of lysine positive charge. Moreover, the important role of lysine 270 in catalysis but not in substrate binding had not been studied previously.

Chapter 7 of this monograph was designed to study the influence of carbon and nitrogen source on the *E. coli* acetate metabolism. Glycerol is a biodiesel by-product, which has become an easily available and low cost carbon source. Nitrogen source is a poorly-studied but important factor in a bacterial culture. Many bioprocesses use complex or rich media for bacterial cultures. Complex media are undefined media composed of tryptone and/or yeast extracts, so nitrogen source is based on peptides or amino acids. To our knowledge, although several processes use glycerol as carbon source and/or peptides as nitrogen source, little is known about how they affect the *E. coli* physiology. The maximum growth rate, stoichiometric parameters and acetate overflow revealed interesting differences. Thus, although maximum growth and carbon consumption rates were always higher for complex than minimal medium, biomass yield and acetate overflow revealed a loss of carbon and energy through acetate overflow in complex medium cultures. Acetate excretion was more than four times higher in complex medium than in minimal medium, while biomass yields were similar. These results suggest a great biotechnological inefficiency of complex medium probably due to high acetate overflow. Glycerol showed a lower growth rate and biomass yield than glucose, although acetate overflow was greatly minimized, becoming almost null in minimal medium. The reduced extracellular acetate detected in minimal medium supplemented with glycerol confirmed glycerol as an ideal carbon source for biotechnological processes based on *E. coli*, since the limitations of growth inhibition and energy loss would be eliminated. As previously mentioned, in chapter 3 of this dissertation a lycopene overproduction system using *E. coli* was developed, and lycopene production with glucose and glycerol as carbon sources was compared. Glucose showed higher growth rates and biomass production, although glycerol showed the highest lycopene production. The results of chapter 3 corroborates the conclusions extracted from chapter 7 and both studies show the importance and suitability of glycerol as carbon source in biotechnological processes based on *E. coli*.

Intracellular pH homeostasis is a crucial factor in the regulation of cell function and is carried out by different molecular mechanisms, the main strategy involving the use of transporters that catalyse active proton transport. In chapter 7 of this thesis, the intracellular *E. coli* pH was determined in cultures growing in minimal medium MM9 or complex medium TB7 supplemented with glucose or glycerol as carbon source. The results showed a surprising increase in intracellular pH for *E. coli* growing with glucose as carbon source in the exponential growth phase. However, this increase was not detected for glycerol cultures. This increase suggests a disorder in pH homeostasis control which must be studied more deeply. Moreover,

the differences observed between glucose and glycerol highlight the metabolic influence of the carbon source used. Previous works have demonstrated that the greatest part of lysine acetylation occurs in a non-enzymatic way in *E. coli* [40,41,43]. Non-enzymatic acetylation is acetyl-phosphate dependent and specific, with the specificity determined by the accessibility, reactivity and three-dimensional microenvironment of the target lysine. Intracellular pH seems to play a crucial role in lysine acetylation, because of the necessary lysine deprotonation. In 2013, Wagner and Payne demonstrated that the high pH reached in mitochondria and acetyl-CoA concentrations were sufficient to cause enzyme-independent acetylation of mitochondrial and non-mitochondrial proteins *in vitro* [44]. In this way, the intracellular pH determined in chapter 7 of this dissertation could suggest a suitable microenvironment for lysine acetylation in glucose cultures. To ascertain whether intracellular pH is a determinant in *E. coli* non-enzymatic lysine acetylation, we decided to measure intracellular concentrations of acetyl-CoA and acetyl-phosphate for *E. coli* growing in minimal and complex medium supplemented with glucose. Acetyl-phosphate concentrations were not very high (around 0.1 mM) for minimal medium although they are similar to that determined previously by other researchers [41,45]. Acetyl-CoA concentrations were higher than acetyl-phosphate (0.35 mM) in the exponential growth phase for minimal medium cultures. When lysine acetylation was studied by western blot using an anti-acetyl Lys antibody, the results showed that acetylation is higher in minimal than complex medium for all the strains. However, lysine acetylation in glucose cultures was not greater than when supplemented with glycerol. Therefore, intracellular pH did not seem play a large part in *E. coli* non-enzymatic lysine acetylation. The fact that intracellular pH is not an essential actor in lysine acetylation could indicate that other mechanisms are involved in non-enzymatic acetylation. For example, new mechanisms, such as that recently reported by James et al., [46] (in which an acetyl-cysteine intermediate facilitate acetylation) should be studied in greater depth.

Summarizing, in this PhD thesis the role of *E. coli* as an essential tool for biotechnological processes has been confirmed and a great advance in our understanding of the *E. coli* acetate metabolism has been achieved. The increased knowledge of the PatZ, CobB and Acs mechanism and regulation represents an important step forward in *E. coli* lysine acetylation research. The study of the influence of culture medium on acetate overflow revealed how bacterial physiology and intracellular pH homeostasis are widely dependent on carbon and nitrogen sources in *E. coli*. Finally, this dissertation opens up new ways to continue investigating lysine acetylation as an essential post-translational modification for *E. coli* metabolism.

Conclusions

The main aim of this PhD thesis was to increase our knowledge of acetate metabolism regulation in *E. coli*. The results have been discussed in previous chapters. Finally, the main conclusions reached are summarized below:

1- A semi-continuous lycopene overproduction and *in situ* extraction system using a metabolically engineered *E. coli* strain was optimized for the first time with an aqueous-organic culture system. Overproduction and extraction conditions were optimized, achieving a final production of 74.71 ± 3.74 mg L^{-1} or 49.70 ± 2.48 mg g $cell^{-1}$. The development of this bioprocess confirms the potential role of *E. coli* in the biotechnology field.

2- The acetyltransferase PatZ acetylates Acs and shows positive cooperativity in response to acetyl-CoA substrate with a Hill coefficient close to 8. Acs activity is regulated by the acetylation level and sixteen acetylated lysines have been identified in the protein. Moreover, the conserved glutamic acid E809 is not relevant for Acs acetylation. This result suggests a non-conserved catalytic mechanism for the GNATs superfamily of adenylating enzymes.

3- PatZ is *in vitro* autoacetylated and deacetylated by the sirtuin CobB. Kinetic parameters were determined and six acetylated lysines were identified. PatZ autoacetylation induces its octamerization from the stable tetramer. Finally, an *in silico* protein–protein docking was carried out to construct a model for the PatZ tetrameric structure. The model has been validated by comparing the biophysical parameters determined experimentally with those obtained computationally using HIDROPRO.

4- Acs is deacetylated by CobB in several lysines with monophasic kinetics. The kinetic of the deacetylation of a whole native protein was studied for the first time. Moreover, acetylation of lysine 609 is not necessary for CobB recognition. The results suggest that structural protein components are the main determinants of sirtuin specificity and not acetylated peptide sequence.

5- CobB is non-competitively inhibited by NAM with a Ki of approximately 108 µM. NAM intracellular concentrations have been determined for a bacterial organism for the first time and the detected concentrations are sufficient to promote *in vivo* CobB regulation. Acetate overflow, cell migration and flagella expression are regulated by *pncA* expression and nicotinamide concentrations. The results highlight the importance of PncA as a regulator enzyme with a new important metabolic role in preventing nicotinamide accumulation to avoid CobB inhibition.

6- *In vivo* Acs acetylation affects to enzyme catalytic efficiency but not to substrates specificity and ATP-binding.

7- K609 Acs conserved residue has an important role in ATP-binding. Acs K609A mutant protein showed higher affinity for ATP substrate than Acs wt enzyme. D500 and T264 conserved residues are essential for Acs ATP-binding, substrates specificity and catalysis. K270 mutation study showed that this residue has not an important role in Acs specificity and ATP-affinity, although the substitution of this lysine to alanine led to a higher Acs catalytic activity.

8- Carbon and nitrogen sources have a great influence on bacterial physiology. Complex media are less efficient than minimal media due to a high carbon wastage through acetate overflow. *E. coli* cultures supplemented with glycerol as carbon source show a lower acetate overflow than those supplemented with glucose, which is a great advantage for its use in biotechnology.

9- Carbon and nitrogen sources are determinant for intracellular pH homeostasis. Intracellular pH was determined for the first time for *E. coli* in a continuous culture. The results show that glycerol cultures maintain a high intracellular pH control, while glucose cultures show a great increase in intracellular pH in the early exponential growth phase. However, this intracellular pH increase does not seem to affect protein lysine acetylation.

References

1. Ajikumar PK, Tyo K, Carlsen S, Mucha O, Phon TH, Stephanopoulos G. Terpenoids: opportunities for biosynthesis of natural product drugs using engineered microorganisms. Mol Pharm. 2008;5: 167–190. doi:10.1021/mp700151b

2. Chasse G, Mak ML, Deretey E, Farkas I, Torday LL, Papp JG, et al. An *ab initio* computational study on selected lycopene isomers. J Mol Struct THEOCHEM. 2001;571: 27–37. doi:10.1016/S0166-1280(01)00424-9

3. Rabi T, Gupta S. Dietary terpenoids and prostate cancer chemoprevention. Front Biosci. 2008;13: 3457–3469. doi:10.2741/2940

4. Rao A. Lycopene, tomatoes, and the prevention of coronary heart disease. Exp Biol Med. 2002;227: 908–913. doi:10.1177/153537020222701011

5. Kitade Y, Watanabe S, Masaki T, Nishioka M, Nishino H. Inhibition of liver fibrosis in LEC rats by a carotenoid, lycopene, or a herbal medicine, Sho-saiko-to. Hepatol Res. 2002;22: 196–205. doi:10.1016/S1386-6346(01)00132-2

6. Sedjo RL, Roe DJ, Abrahamsen M, Harris RB, Craft N, Baldwin S, et al. Vitamin A, carotenoids and risk of persistent oncogenic human Papillomavirus Infection. Cancer Epidem Biomarkers Prev. 2002. pp. 876–884.

7. Giovannucci E, Rimm EB, Liu Y, Stampfer MJ, Willett WC. A prospective study of tomato products, lycopene, and prostate cancer risk. J Natl Cancer Inst. 2002;94: 391–398. doi:10.1093/jnci/94.5.391

8. Albrecht M, Misawa N, Sandmann G. Metabolic engineering of the terpenoid biosynthetic pathway of *Escherichia coli* for production of the carotenoids beta-carotene and zeaxanthin. Biotechnol Lett. 1999;21: 791–795. doi:10.1023/A:1005547827380

9. Sandmann G. Carotenoid biosynthesis and biotechnological application. Arch Biochem Biophys. 2001;385: 4–12. doi:10.1006/abbi.2000.2170

10. Sharma SK, Le Maguer M. Kinetics of lycopene degradation in tomato pulp solids under different processing and storage conditions. Food Res Int. 1996;29: 309–315. doi:10.1016/0963-9969(96)00029-4

11. Bernal V, Castaño-Cerezo S, Cánovas M. Acetate metabolism regulation in *Escherichia coli*: carbon overflow, pathogenicity, and beyond. Appl Microbiol Biotechnol. 2016;100: 8985–9001. doi:10.1007/s00253-016-7832-x

12. Valgepea K, Adamberg K, Vilu R. Decrease of energy spilling in *Escherichia coli* continuous cultures with rising specific growth rate and carbon wasting. BMC Syst Biol. 2011;5: 1–11. doi:10.1186/1752-0509-5-106

13. Castaño-Cerezo S, Bernal V, Blanco-Catalá J, Iborra JL, Cánovas M. cAMP-CRP coordinates the expression of the protein acetylation pathway with central metabolism in *Escherichia coli*. Mol Microbiol. 2011;82: 1110–1128. doi:10.1111/j.1365-2958.2011.07873.x

14. Starai VJ, Celic I, Cole RN, Boeke JD, Escalante-Semerena JC. Sir2-dependent activation of acetyl-CoA synthetase by deacetylation of active lysine. Science. 2002;298: 2390–2392. doi:10.1126/science.1077650

15. AbouElfetouh A, Kuhn ML, Hu LI, Scholle MD, Sorensen DJ, Sahu AK, et al. The *E. coli* sirtuin CobB shows no preference for enzymatic and nonenzymatic lysine acetylation

substrate sites. Microbiol Open. 2014;4: 66–83. doi:10.1002/mbo3.223

16. Knyphausen P, De Boor S, Kuhlmann N, Scislowski L, Extra A, Baldus L, et al. Insights into lysine deacetylation of natively folded substrate proteins by sirtuins. J Biol Chem. 2016;291: 14677–14694. doi:10.1074/jbc.M116.726307

17. May JJ, Kessler N, Marahiel MA, Stubbs MT. Crystal structure of DhbE, an archetype for aryl acid activating domains of modular nonribosomal peptide synthetases. Proc Natl Acad Sci. 2002;99: 12120–12125. doi:10.1073/pnas.182156699

18. Conti E, Stachelhaus T, Marahiel MA, Brick P. Structural basis for the activation of phenylalanine in the non-ribosomal biosynthesis of gramicidin S. EMBO J. 1997;16: 4174–4183. doi:10.1093/emboj/16.14.4174

19. Chen Y, Sun Y, Song H, Guo Z. Structural basis for the ATP-dependent configuration of adenylation active site in *Bacillus subtilis* O-succinylbenzoyl-Coa synthetase. J Biol Chem. 2015;290: 23971–23983. doi:10.1074/jbc.M115.676304

20. Li Z, Nair SK. Structural basis for specificity and flexibility in a plant 4-coumarate:CoA ligase. Structure. 2015;23: 2032–2042. doi:10.1016/j.str.2015.08.012

21. Scaglione A, Fullone MR, Montemiglio LC, Parisi G, Zamparelli C, Vallone B, et al. Structure of the adenylation domain Thr1 involved in the biosynthesis of 4-chlorothreonine in *Streptomyces sp.* OH-5093—protein flexibility and molecular bases of substrate specificity. FEBS J. 2017;284: 2981–2999. doi:10.1111/febs.14163

22. Kochan G, Pilka ES, von Delft F, Oppermann U, Yue WW. Structural snapshots for the conformation-dependent catalysis by human medium-chain acyl-Coenzyme A synthetase ACSM2A. J Mol Biol. 2009;388: 997–1008. doi:10.1016/j.jmb.2009.03.064

23. Osman KT, Du L, He Y, Luo Y. Crystal structure of *Bacillus cereus* D-alanyl carrier protein ligase (DltA) in complex with ATP. J Mol Biol. 2009;388: 345–355. doi:10.1016/j.jmb.2009.03.040

24. Law A, Boulanger MJ. Defining a structural and kinetic rationale for paralogous copies of phenylacetate-CoA ligases from the cystic fibrosis pathogen *Burkholderia cenocepacia* J2315. J Biol Chem. 2011;286: 15577–15585. doi:10.1074/jbc.M111.219683

25. Li W, Gu S, Fleming J, Bi L. Crystal structure of FadD32, an enzyme essential for mycolic acid biosynthesis in *Mycobacteria*. Sci Rep. 2015;5: 1–8. doi:10.1038/srep15493

26. Crosby HA, Rank KC, Rayment I, Escalante-Semerena JC. Structure-guided expansion of the substrate range of methylmalonyl Coenzyme A synthetase (MatB) of *Rhodopseudomonas palustris*. Appl Environ Microbiol. 2012;78: 6619–6629. doi:10.1128/AEM.01733-12

27. Wu R, Cao J, Lu X, Reger AS, Gulick AM, Dunway-Mariano D. Mechanism of 4-chlorobenzoate: Coenzyme A ligase catalysis. Biochemistry. 2008;47: 8026–8039. doi:10.1021/bi800698m

28. Branchini BR, Murtiashaw MH, Magyar R a., Anderson SM. The role of lysine 529, a conserved residue of the acyl-adenylate- forming enzyme superfamily, in firefly luciferase. Biochemistry. 2000;39: 5433–5440. doi:10.1021/bi9928804

29. Horswill AR, Escalante-Semerena JC. Characterization of the propionyl-CoA synthetase (PrpE) enzyme of *Salmonella enterica*: Residue lys 592 is required for propionyl-AMP synthesis. Biochemistry. 2002;41: 2379–2387. doi:10.1021/bi015647q

30. Gallego-Jara J, Écija Conesa A, de Diego Puente T, Lozano Terol G, Cánovas Díaz M. Characterization of CobB kinetics and inhibition by nicotinamide. PLoS One. 2017;12: e0189689. doi:10.1371/journal.pone.0189689

31. Reger AS, Carney JM, Gulick AM. Biochemical and crystallographic analysis of substrate binding and conformational changes in acetyl-CoA synthetase. Biochemistry. 2007;46: 6536–6546. doi:10.1021/bi6026506

32. Lu X, Rong Z, Indrajeet S, Li X, Kumar G, Swaminathan S, et al. Stable analogues of OSB-AMP: potent inhibitors of MenE, the O- succinylbenzoate-CoA synthetase from bacterial menaquinone biosynthesis. Chembiochem. 2012;13: 129–136. doi:10.1002/cbic.201100585

33. Chang KH, Xiang H, Dunaway-Mariano D. Acyl-adenylate motif of the acyl-adenylate/thioester-forming enzyme superfamily: a site-directed mutagenesis study with the *Pseudomonas sp.* Strain CBS3 4-chlorobenzoate:coenzyme A ligase. Biochemistry. 1997;36: 15650–15659. doi:10.1021/bi971262p

34. Yuan H, Rossetto D, Mellert H, Dang W, Srinivasan M, Johnson J, et al. MYST protein acetyltransferase activity requires active site lysine autoacetylation. EMBO J. 2012;31: 58–70. doi:10.1038/emboj.2011.382

35. Creaven M, Hans F, Mutskov V, Col E, Caron C, Dimitrov S, et al. Control of the histone-acetyltransferase activity of Tip60 by the HIV-1 transactivator protein, Tat. Biochemistry. 1999;38: 8826–8830. doi:10.1021/bi9907274

36. Thompson PR, Wang D, Wang L, Fulco M, Pediconi N, Zhang D, et al. Regulation of the p300 HAT domain via a novel activation loop. Nat Struct Mol Biol. 2004;11: 308–315. doi:10.1038/nsmb740

37. Angus-Hill ML, Dutnall RN, Trafrov ST, Sternglanz R, Ramakrishnan V. Crystal structure of the histone acetyltransferase Hpa2 : a tetrameric member of the Gcn5-related N-acetyltransferase superfamily. J Mol Biol. 1999;294: 1311–1325.

38. Guarente L. Sirtuins in aging and diseases. In: Walker JM, editor. Methods in Molecular Biology. Humana Press; 2013. pp. 3–10. doi:10.1007/978-1-62703-637-5_1

39. Sebastián C, Satterstrom FK, Haigis MC, Mostoslavsky R. From sirtuin biology to human diseases: an update. J Biol Chem. 2012;287: 42444–42452. doi:10.1074/jbc.R112.402768

40. Castaño-Cerezo S, Bernal V, Post H, Fuhrer T, Cappadona S, Sánchez-Díaz NC, et al. Protein acetylation affects acetate metabolism, motility and acid stress response in *Escherichia coli*. Mol Syst Biol. 2014;10: 1–16. doi:10.15252/msb.20145227

41. Kuhn ML, Zemaitaitis B, Hu LI, Sahu A, Sorensen D, Minasov G, et al. Structural, kinetic and proteomic characterization of acetyl phosphate-dependent bacterial protein acetylation. PLoS One. 2014;9: e94816. doi:10.1371/journal.pone.0094816

42. Hu LI, Chi BK, Kuhn ML, Filippova E V, Walker-Peddakotla AJ, Bäsell K, et al. Acetylation of the response regulator RcsB controls transcription from a small RNA promoter. J Bacteriol. 2013;195: 4174–4186. doi:10.1128/JB.00383-13

43. Weinert BT, Iesmantavicius V, Wagner SA, Schölz C, Gummesson B, Beli P, et al. Acetyl-phosphate is a critical determinant of lysine acetylation in *E. coli*. Mol Cell. 2013;51: 265–272. doi:10.1016/j.molcel.2013.06.003

44. Wagner GR, Payne RM. Widespread and enzyme-independent Nε-acetylation and Nε-

succinylation of proteins in the chemical conditions of the mitochondrial matrix. J Biol Chem. 2013;288: 29036–29045. doi:10.1074/jbc.M113.486753

45. Prüβ BM, Wolfe AJ. Regulation of acetyl phosphate synthesis and degradation, and the control of flagellar expression in *Escherichia coli*. Mol Microbiol. 1994;12: 973–984. doi:10.1111/j.1365-2958.1994.tb01085.x

46. James AM, Hoogewijs K, Logan A, Hall AR, Ding S, Fearnley IM, et al. Non-enzymatic N-acetylation of lysine residues by acetyl-CoA often occurs *via* a proximal S-acetylated thiol intermediate sensitive to glyoxalase II. Cell Rep. 2017;18: 2105–2112. doi:10.1016/j.celrep.2017.02.018